Comprehensive Mapping of Paediatric High Grade Glioma by Oligo Array Comparative Genomic Hybridisation

Jennifer Barrow

Thesis presented for the degree of

Doctor of Philosophy

The University of Nottingham

May 2011

This thesis is dedicated to all the children and their families whose lives have been affected by brain tumours.

ABSTRACT

Overall paediatric high grade glioma (pHGG) has a poor prognosis, in part due to the lack of understanding of the underlying biology. We therefore used high resolution 244K oligo array comparative genomic hybridisation (oligo aCGH) (Agilent Technologies) to analyse DNA from 38 formalin-fixed paraffin embedded pHGG samples, including 13 DIPG. The pattern of gains and losses were distinct from those seen in HGG arising in adults. In particular we found 1q gain in 21% of our cohort compared to 9% in adults. Homozygous loss at 8p12 was seen in 6/38 (15%) of pHGG. This deletion has not been previously reported in adult or paediatric high grade gliomas. The minimal deleted region is of the gene *ADAM3A* and homozygous deletion of *ADAM3A* was confirmed by quantitative real time PCR (qPCR). This novel homozygous deletion of *ADAM3A* in pHGG merits further study. Amplification of the 4q11-13 region was detected in 8% of cases and included *PDGFRA* and *KIT* and subsequent qPCR analysis was consistent with amplification of *PDGFRA*. *MYCN* amplification was seen in 2/38 samples (5%) and was shown to be significantly associated with anaplastic astrocytomas (p=0.03). Loss of *CDKN2A/B* was seen in 4/38 (10%) samples by oligo a CGH, confirmed by FISH on TMAs, and was restricted to supratentorial tumours. ~50% of supratentorial tumours were positive for CDKN2B expression by IHC, whilst ~75% of brainstem gliomas were positive for CDKN2B expression (p = 0.03). Overall DIPG shared a similar spectrum of changes to supratentorial HGG with some notable differences including high frequency of 17p loss and 14q loss, low occurrence of 10q loss and lack of *CDKN2A/B* deletion.

ACKNOWLEDGMENTS

I would like to thank the many people who have and supported me throughout my PhD. Firstly I would like to thank my supervisor Professor Richard Grundy for giving me the opportunity to do my PhD and for his encouragement and guidance. I am also extremely grateful to Dr Martyna Adamowicz-Brice for her patience and constant support especially when I first started in the lab.

I am especially grateful to the Molecular Biology Services lab at Warwick University for letting me use their lab and equipment, and for their help and assistance during the running of my arrays.

I would like to thank the entire CBTRC team; I think everyone in the lab has helped me at some point along the way and I am extremely grateful to all of you. Finally, I want to thank my family and friends for their love and support throughout my PhD, especially my fiancé Richard.

A special thank you is reserved for The Samantha Dickson Brain Tumour Trust for funding my PhD.

LIST OF FIGURES

LIST OF TABLES

LIST OF ABBREVIATIONS

aCGH	Array comparative genomic hybridisation
AA	Anaplastic astrocytoma
AO	Anaplastic oligodendroglioma
BAC	Bacterial artificial chromosome
BBB	Blood brain barrier
bp	Basepair
BSG	Brainstem glioma
CBTRC	Children's brain tumour research centre
CGH	Comparative genomic hybridisation
CNS	Central nervous system
CNS PNET	Central nervous system primitive neuroectodermal tumour
Ct	Threshold cycle
CT	Chemotherapy
DAB	3,3-diaminobenzidine
DAPI	4',6-diamidino-2-phenylindole
DIPG	Diffuse intrinsic pontine glioma
DNA	Deoxyribonucleic acid
dNTP	Deoxyribonucleotide triphosphate
DPX	Depex-polystyrene dissolved in Xylene
FAP	Familial adenomatous polypopsis

FFPE	Formalin fixed paraffin embedded
FISH	Fluoresence in situ hybridisation
GBM	Glioblastoma multiforme
GFAP	Glial fibrillary acidic protein
H and E	Haematoxylin and eosin
HNPCC	Hereditary nonpolyposis colorectal cancer
IHC	Immunohistochemistry
LOH	Loss of heterozygosity
Mb	Megabase
MRI	Magnetic resonance imaging
mRNA	Messenger RNA
µg	Microgram
ng	Nanogram
p	short arm of chromosome
PAC	P1 artificial chromosome
PBS	Phosphate buffered saline
PCR	Polymerase chain reaction
PNET	Primitive neuroectodermal tumour
Q	Short arm of chromosome
QC	Quality control
Rb	Retinoblastoma
RT	Radiotherapy
SHH	Sonic hedgehog

SNP	Single nucleotide polymorphism
SPSS	Statistical package for the social sciences
TMA	Tissue microarray
UKCCSG/CCLG	United kingdom children's cancer study group/children's cancer and leukaemia group
WHO	World health organisation

CHAPTER 1

INTRODUCTION

1.1 Paediatric Brain Tumours

1.1.1 Background

Paediatric brain tumours are the most common solid tumours in children and have the highest mortality rate of all paediatric cancers (Wong, Tsang et al. 2006). Tumours of the brain and spinal cord account for up to 25% of all childhood cancers (Stiller 2004). Over the past 20 years the reported incidence of paediatric primary nervous system tumours has risen to 35%. During this time no obvious advances in treatment have been discovered (Packer 1999). Whilst research has led to knowledge of genetic alterations of other childhood cancers such as leukaemia, paediatric brain tumours still lag behind. As a result 80% of leukaemia incidences are successfully treated compared to a survival rate of around 60% for all paediatric brain tumours (Stiller 2004). However, over the past decade more attention has been directed towards brain tumour research in both adults and children with the hope that gaining information about the genetics of these tumours will facilitate new treatments, as in other cancers. Of those children that survive brain tumours around 60% will suffer long term deficits due to damage to the normal brain tissue caused by the tumour itself, surgery, intensive radiotherapy and some chemotherapeutic agents. Radiotherapy is preferably only given to children over three but damage can still be done in these children leading to decrease in IQ and other neurological problems (Mulhern, Merchant et al. 2004).

Paediatric cancers, including brain tumours, vary at the histological level which makes tumour classification difficult and treating these tumours complex (Stiller 2004). Increased knowledge of the genetics of paediatric brain tumours will hopefully lead to treatment based on an understanding of the underlying biology of the tumour rather than the treatment program currently used.

1.1.2 Neural Development

During neural development cells have properties that are similar to that of cancer cells; the ability to divide, self-renew and migrate. Paediatric brain tumours are termed ‘embryonal tumours’ as they are thought to originate from immature tissues as the result of abnormal development due to defects in key developmental pathways (Scotting, Walker et al. 2005).

The nervous system consists of the peripheral nervous system (PNS) and the central nervous system (CNS). The central nervous system is made up of the brain and spinal cord. Around 90% of cells in the CNS are glial cells. There are six major catagories of glial cell; astrocytes, oligodendrocytes, ependymal cells, Schwann cells, migroglia and satellite cells. The most abundant of these glial cells types are astrocytes. Astrocytes act as a scaffold which hold the neurons in the appropriate place and act as a guide during fetal brain development to migrating neurons. Astrocytes play an important role in the maintenance of the blood brain barrier (BBB) and the repair of damage to the brain. Oligodendrocytes are responsible for the formation of myelin sheaths around the axons of neurons in the CNS. Schwann cells are the myelin producing cells in the PNS. Ependymal cells form the lining of the ventricles of the brain and have a role in the production of cerebrospinal fluid.

Glial cells, unlike neurons, do not lose the ability to divide and more than half of paediatric brain tumours are of glial origin (Packer 1999). The most common type of glioma is the astrocytoma. 7.7% of all childhood cancers are astrocytomas (Rickert, Strater et al. 2001).

1.1.3 Cancer Stem Cells

Stem cells are characterised by their ability to self renew and differentiate into a wide range of cell types. Embryonic stem cells are pluripotent meaning they are able to become any type of cell. In adult humans there are still stem cells present in certain areas of the body such as bone marrow, blood vessels, colon, and heart and in the brain.

Until recently it was thought that there was very rarely, if ever, cell division occurring in the brain. A series of studies in the early 90s showed that neurogenesis was present in the brains of birds, mice and eventually humans (Hemmati, Nakano et al. 2003; Vescovi, Galli et al. 2006). If neurogenesis is occurring in the mature brain then this indicates that there is a population of undifferentiated stem cells which are actively proliferating. If there are proliferating cells present in the brain capable of differentiating into a range of cell types then it is logical to hypothesise that these cells could undergo transformation into cancer causing stem cells. The sub ventricular zone has been identified as the area of the brain where most neurogenesis occurs (Vescovi, Galli et al. 2006). Cells from the sub ventricular zone which express Glial Fibrillary Acidic Protein (GFAP), an astrocytic marker, have been shown to be neural stem cells. Many gliomas develop in areas adjacent or close to the sub ventricular zone indicating that transformed neural stem cells may be the source of these tumours.

Most tumour cells are differentiated cells that individually are incapable of tumorigenesis. A number of groups have now shown that tumours, particularly GBM and medulloblastoma, contain a fraction of cells that can form neurospheres in culture and have the ability to differentiate into an array of different cell types. This stem cell – like behaviour of a small fraction of cells was first seen in leukaemia and has led to the 'cancer stem cell' theory (Singh and Dirks 2007). Small numbers of cells from leukaemia, and more recently multiple myeloma and breast cancer, have be shown to have the ability to self renew in the long term and to initiate tumours. Expression of CD133, Sox2, BMI1 and nestin is seen in both normal stem cells and the tumour derived progenitors with self renewal ability (Singh and Dirks 2007).

The term 'cancer stem cell' implies that these tumour initiating cells are derived from normal stem cells, and whilst this may be the case it could also be that cancer stem cells are a results of de-differentiation of mature brain cells.

1.2 Classification of astrocytic tumours

The vast majority of high grade gliomas in children are high grade astrocytomas. Gliomas that are either non-astrocytic or mixed are rare in children (Broniscer and Gajjar 2004). Astrocytomas fall into two major categories; low grade (World Health Organisation (WHO) grade I and II) and high grade (WHO grade III and IV) (Louis, Ohgaki et al. 2007).

Astrocytic Tumours

'Astrocytic tumours' describes a range of tumours spanning all four WHO grades.

1.2.1 Grade I Astrocytomas.

Pilocytic astrocytomas are the most common gliomas of childhood, comprising 21% of CNS tumours between 0-14 years. They most commonly occur in the cerebellum but also arise in the brainstem, spinal cord and supratentorially. Pilocytic tumours are usually slow growing tumours that appear well circumscribed on scans and rarely infiltrate surrounding tissues. The histopathological characteristics of pilocytic astrocytomas are compacted bipolar cells, rare mitoses and Rosenthal fibres (See fig. 1.1) (Louis, Ohgaki et al. 2007).

It is rare for juvenile pilocytic astrocytomas to progress to a higher grade tumour and most tumours remain as grade I for many years. Prognosis is usually good for pilocytic tumours, although pilocytic tumours of the brainstem often result in death. Pilocytic astrocytomas are the tumours most associated with neurofibromatosis 1 (NF1), and NF1 pilocytic tumours have a better prognosis than non-NF1 tumours (see section 1.3.1) (Rosenfeld, Listernick et al. 2009).

1.2.2 Grade II Astrocytomas.

Grade II astrocytomas describes a range of tumour types with varying histology. Diffuse astrocytomas are infiltrating tumours that most frequently occur supratentorially. Whilst these tumours are slow growing, there is high cellular differentiation and the ability to progress into high grade tumours which distinguish diffuse astrocytomas from pilocytic astrocytomas. The term 'diffuse astrocytoma'

actually covers three different tumours types according to the 2007 WHO CNS tumour classification book; fibrillary astrocytoma, gemistocytic astrocytoma and protoplasmic astrocytoma (Louis, Ohgaki et al. 2007).

- Fibrillary astrocytomas are the most common grade II astrocytoma. Histologically, fibrillary tumours consist of fibrillary neoplastic astrocytes with nuclear aytpia. Cell density is higher than grade I tumours but still only moderate, and the nuclei can appear 'naked' due to the lack of cytoplasm. GFAP is expressed but not in all cells.
- Gemistocytic astrocytomas are characterised, as the name suggests, by the presence of gemistocytes. Gemistocytes are large astrocytes with abundant cytoplasm that highly express GFAP. For a grade II tumour to be classified as a gemistocytic astrocytoma more than 20% of cells should be gemistocytes.
- Protoplasmic astrocytomas have a similar histological appearance to pilocytic astrocytomas with low cellularity, lack of mitoses and low GFAP. Formation of microcysts and mucoid degeneration are the defining features of this tumour sub-type.

Diffuse astrocytomas with gemistocytes are likely to progress to higher grade tumours more rapidly than those without gemistocytes. Survival of patients with diffuse astrocytomas varies widely, with the average survival time post- surgery of 6-8 years. The variation in survival is dependent on many factors including extent of resection of the original tumour, tumour progression to a higher grade, size of the tumour and patient age (Louis, Ohgaki et al. 2007).

Pleomorphic xanthoastrocytomas are also grade II tumours usually occurring in the cerebral hemispheres with a good prognosis. Histologically varied, these tumours are characterised by large, neoplastic astrocytic cells with atypical nuclei. These tumours are GFAP positive (Louis, Ohgaki et al. 2007).

1.2.3 High grade astrocytomas (WHO Grade III and IV)

High grade astrocytomas are highly vascular and frequently rapidly advancing tumours with a poor prognosis in both children and adults. Very young children

(children under 3 at diagnosis) with high grade astrocytomas fare better than older children, which suggests different underlying genetic causes (Duffner, Krischer et al. 1996). There are also thought to be differences in the genetic causes of adult and paediatric gliomas. 70% of adult gliomas occur supratentorially whilst up to 60% of paediatric glioma occur infratentorially. Whilst high grade astrocytomas are the most common type of brain tumour in adults only 6-12% of primary paediatric brain tumours are supratentorial high grade astrocytomas (Broniscer and Gajjar 2004). High grade astrocytomas are aggressive tumours that can invade adjacent tissues (Rutka, Murakami et al. 1997). Prognosis varies depending on the location of the tumour within the brain, the degree of resection and the treatment possibilities. The majority of astrocytomas develop in the frontal lobe, the area of the brain responsible for many functions including thought, behaviour, and judgement.

Grade III astrocytomas

Grade III astrocytomas are also called anaplastic astrocytomas (AA). AAs are malignant tumours with mitotic activity, infiltration of surrounding tissue, high cellularity and nuclear atypia (See fig. 1.1). AAs are most frequently seen in the cerebral hemispheres and can arise as a progression from a grade II diffuse astrocytoma in adults (Louis, Ohgaki et al. 2007). AAs are thought to arise from immature astrocytic cells although the mechanism has not been well characterised. AAs can, and often do, progress to grade IV (glioblastoma multiforme).

Grade IV Astrocytoma

Grade IV astrocytoma, also known as glioblastoma multiforme (GBM), is the most common primary brain tumour in adults but is relatively rare in children. GBM is an aggressive tumour with high cellularity, high levels of mitoses, neovascularisation, nuclear atypia and necrosis (See fig. 1.1) (Louis, Ohgaki et al. 2007). Necrosis is caused by poor oxygen supply leading to cell lysis. It is a complex process that is not only associated with cell death but also cell proliferation and tumour growth (King 2000).

GBMs are highly infiltrative and invade neighbouring tissues. Histopathology can vary between tumours and within a single tumour, leading to difficulty in diagnosis from small biopsies (Nalin Gupta 2004).

1.2.4 GBM Sub-types

Small cell GBMs are a subtype of GBM characterised by small, round, densely packed cells with high levels of mitosis and low GFAP. These tumours can look similar in appearance to anaplastic oligodendroglioma.

Giant cell GBMs are GBMs with giant, multinuclear cells which make up 5% of GBM occurrences. Giant cell GBM shares histopathological features with ordinary GBM but has variable expression of GFAP. Some studies have indicated that giant cell GBM may have a better prognosis than normal GBM, possibly due to the less infiltrative nature of giant cell GBM.

Gliosarcoma describes a sub-type of GBM with a mixture of glial and sarcoma –like areas of tumours in a biphasic pattern. It is thought that both parts of the tumour arise from neoplastic glial cells (Louis, Ohgaki et al. 2007).

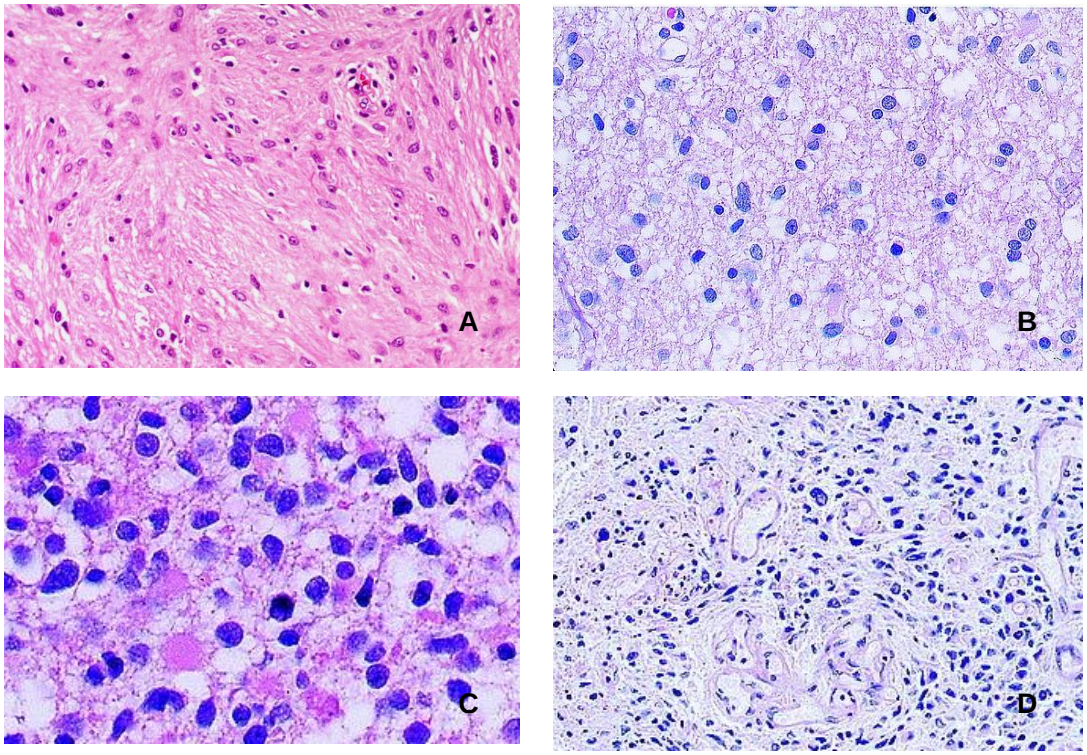

Figure 1.1. Haematoxylin and eosin (H&E) stained sections of a brain tumour showing major features typical for a particular tumour. Haematoxylin stains nuclei purple and eosin stain cytoplasm pink: A. Pilocytic astrocytomas are slow growing tumours with rare mitoses and Rosenthal fibres. B. Diffuse astrocytomas are slow growing but have high cellular differentiation. C. Anaplastic astrocytomas have high cellularity, mitotic cells and nuclear atypia. D. Glioblastoma multiforme is a highly cellular tumour with mitoses, neovascularisation, nuclear atypia and necrosis.

1.2.5 Oligodendrogliomas

Oligodendrogliomas are thought to develop either from transformation of mature oligodendrocyte cells or from glial precursor cells, and are more common in adults although they do rarely occur in children (Louis, Ohgaki et al. 2007). Only 1% of paediatric brain tumours are oligodendrogliomas (Nalin Gupta 2004). Oligodendrogliomas are classified as either grade II or grade III tumours depending on the levels of cellularity and cell proliferation and the presence of features associated with other higher grade glioma tumours.

Grade II oligodendrogliomas are diffuse tumours with well differentiated cells resembling oligodendroglial cells. Histologically, these tumours are characterised by small, uniformly round nuclei surrounded by a 'halo' of cytoplasm (Nalin Gupta 2004). Cellularity is moderate and there is infrequent mitosis. In adults, loss of 1p and 19q is seen in more than 80% of oligodendrogliomas and is associated with increased survival (Louis, Ohgaki et al. 2007). Grade II oligodendrogliomas can progress to grade III tumours, but this usually takes a number of years (Louis, Ohgaki et al. 2007).

Anaplastic oligodendrogliomas are grade III tumours which share the diffuse, infiltrative ability of grade II oligodendrogliomas. However, the grade III tumours have additional features such as high levels of mitosis, increased cellularity, necrosis and neovascularisation that are associated with more malignant tumours (Louis, Ohgaki et al. 2007).

Oligoastrocytomas are grade II glial tumours with components from two separate glial cell origins; oligodendroglial and astrocytic. These tumours usually occur in the cerebral hemispheres and share the histological features of grade II oligodendrogliomas and grade II astrocytomas. Anaplastic oligoastrocytomas are grade III tumours that have all the characteristics of grade II oligoastrocytomas with additional features associated with malignancy (Louis, Ohgaki et al. 2007).

1.2.6 Brainstem Glioma

Brainstem gliomas account for up to 20% of paediatric CNS tumours, with a mean age of diagnosis of 7-9 years old (Jallo, Biser-Rohrbaugh et al. 2004). Brainstem gliomas are considered surgically inaccessible due to their anatomical location. The brainstem describes an area of the brain encompassing the midbrain, pons and medulla oblongata (see fig. 1.2) (Jallo, Biser-Rohrbaugh et al. 2004).

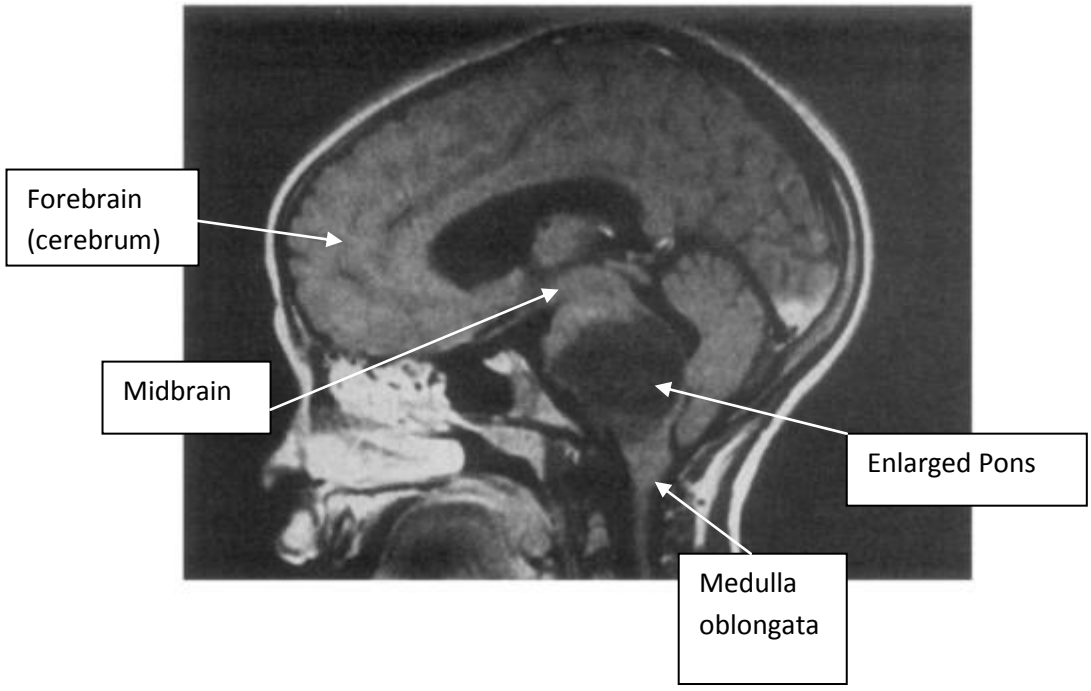

Figure 1.2. MRI Image of the brain in which the areas of the brain described as being part of the brainstem (midbrain, pons, medulla oblongata) are highlighted.

Around 20% of brainstem gliomas are low grade astrocytomas and the remaining 80% are diffuse tumours involving the pons (Hargrave, Bartels et al. 2006). Diffuse pontine gliomas differ from all other brainstem gliomas and are characterised by infiltration of the brainstem which in turn causes swelling. The majority are classified as high grade gliomas, at least in terms of behaviour but also frequently in terms of histology (Jallo, Biser-Rohrbaugh et al. 2004). Only 3-9% of all paediatric brain tumours are diffuse brainstem gliomas and more than 90% of children die within two years of diagnosis (Hargrave, Bartels et al. 2006). Due to the infiltrative

nature of diffuse brainstem gliomas surgical resection is not an option. Neurofibromatosis-linked diffuse pontine gliomas have an improved prognosis compared to those diffuse pontine gliomas not linked to neurofibromatosis, as they are less aggressive tumours. Further studies are required to determine the prognostic and genetic differences between these two subtypes of diffuse pontine glioma (Jallo, Biser-Rohrbaugh et al. 2004).

Diffuse pontine gliomas are only one subtype of brainstem glioma. The first classification of brainstem glioma subtypes was by Epstein in 1985 which divided the tumours into three groups; intrinsic tumour, exophytic tumours and disseminated tumours (Epstein 1985). The most recent classification by Choux in 2000 divided brainstem gliomas into four subtypes; diffuse, focal, exophytic and cervicomedullary (Choux 2000).

Table 1.1 Classification of brainstem gliomas.

Brain Stem Tumour Type	**Approximate Frequency (%)**	**Imaging Characteristics**	**Pathology**
Diffuse Intrinsic	75-86	Pontine enlargement	Astrocytoma (grade II-IV)
Focal midbrain	5-10	Small, well defined	Low grade astrocytoma.
Dorsally exophytic	10-20	Arise from the floor of the fourth ventricle	Pilocytic astrocytoma, grade II astrocytoma.
Cervicomedullary	5-10	Causes a characteristic bulge in the medulla towards the fourth ventricle	Low grade astrocytoma.

Focal tumours are small tumours with well-defined borders that most frequently occur in the midbrain and medulla. Focal tumours are low grade and so lack

infiltrative ability and can be treated with surgery (Mauffrey 2006). Exophytic tumours grow up from the floor of the fourth ventricle, often nearly filling the fourth ventricle. Exophytic tumours are usually low grade and so there is minimal invasion of the brainstem and surgery is often the preferred treatment (Freeman and Farmer 1998). Cervicomedullary tumours arise either in the medulla or in the spinal cord and cause a characteristic bulge in the medulla towards the fourth ventricle. Cervicomedullary tumours are mostly low grade tumours and so can be treated with surgery as there is little infiltration of the brainstem.

Symptoms of brainstem gliomas include diplopia, irregular eye movement, dysphagia, dysarthria and muscle weakness in the face. Other possible symptoms are ataxia, headache and vomiting and mood/behavioural changes. Radiotherapy is the most common treatment with up to 70% of children showing neurological improvement and a visible response to radiotherapy on the MRI, although this response is short lived. Diffuse pontine gliomas tend to be more resistant to radiotherapy than other brainstem tumours. No chemotherapy agents have so far been shown to significantly increase survival. Drug access to the brain is problematic due to the blood brain barrier (BBB) but many trials are ongoing. In this case drug resistance is problematic as drugs that can cross the BBB are ineffective.

The location of brainstem gliomas means surgery is usually not an option making little tissue available for research, and if there is tissue available it is often from a needle biopsy and so is minimal. The ability to perform stereotactic biopsy on brainstem tumours has been around since 1978, but has always been controversial as there is no significant improvement in prognosis. Epstein's 1985 paper argued that biopsying brainstem tumours was a risk that gave no benefit to the patient, and this view was supported by Stroink in 1986 (Epstein 1985; Stroink, Hoffman et al. 1986). However, in recent years with the evolution of new biologically analysis techniques and genetically tailored treatments for cancers such as leukaemia, the question of biopsy has arisen again. In 2003 a meta-analysis of brainstem biopsies was carried out by Samadini *et al* and the need for biopsy stressed (Samadani and Judy 2003).

Currently, brainstem gliomas are biopsied if there is an atypical MRI, the clinical presentation is unusual or to allow the patient to enter a clinical trial that requires biopsy. However, MRI predicts tumour grade correctly in only two thirds of cases

and recent studies have found none of the negative effects of biopsy which were previously reported. With recent advances in high throughput genetic techniques which can determine the genetic signatures of tumours and the success of tailored treatments based on these genetic findings it is important to have brainstem tissue available for research if the treatment of these tumours is to improve.

Understanding the genetic causes and underlying biology of these tumours is the key to future treatments. Many adult brainstem gliomas have mutation or loss of heterozygosity of the well characterised tumour suppressor *p53*, over expression of the growth factor EGFR protein and loss of the tumour suppressor *PTEN* (TCGA 2008). Further research will uncover more potential targets for therapy but the tissue available to carry out this research is still frustratingly scarce.

1.2.7 Treatment of high grade glioma

Low grade gliomas can often be completely resected and chemotherapy and radiotherapy are only used if the resection is incomplete (Wong, Tsang et al. 2006). Therefore these tumours have a high cure rate and low therapy related damage. Patients with high grade glioma have a much graver prognosis. Surgery is often the first stage in the treatment of supratentorial high grade glioma. The extent of resection depends on a number of factors; the patient's age, the patient's condition and most importantly the anatomical location of the tumour. For paediatric high grade glioma as extensive a surgical resection as is possible should be performed to give the best prognosis for the patient (Kramm, Wagner et al. 2006). By the time patients become symptomatic the tumour may have reached a considerable size and this in turn can limit the degree of surgical resection that can be achieved. Following surgery radiotherapy is given, with the dose depending on the location of the tumour and the age of the patient. Radiotherapy is predominantly used to stabilize the tumour and increase progression free survival in high grade glioma patients.

Chemotherapy in children following radiation treatment has been shown in a number of studies to increase progression-free survival, especially in patients with GBM. However, chemotherapy only provides a slight improvement in survival time at present. A recent study in adult patients with GBM showed promising results with

the drug temozolomide in addition to radiotherapy but only by months (Martens, Laabs et al. 2008).

Clinical trials of a number of chemotherapeutic agents have been carried out in adult GBM. EGFR overexpression is associated with tumour growth, migration, invasion, progression and resistance to radiotherapy in vitro. EGFR inhibitors, such as Erlotinib and Gefitinib, have been trialled due to the frequent overexpression of EGFR in adult GBM (40%) (Halatsch, Schmidt et al. 2006). These low molecular weight tyrosine kinase inhibitors are particular attractive for brain tumours as they should be able to cross the blood brain barrier. In a trial by Halatsch et al there was no significant clinical response with Gefitinib or Erlotinib compared with standard chemotherapy treatment (Halatsch, Schmidt et al. 2006).

Monoclonal antibodies, such as the EGFR inhibitor Cetuximab have a high molecular weight so crossing the blood brain barrier is an issue. However, Cetuximab has been shown to increase apoptosis and decrease rate of growth in a xenograft model of GBM (Martens, Laabs et al. 2008).

A recent trial by the Canadian Paediatric Brain Tumour Consortium (CPBTC) looked at the effect of Imatinib which inhibits subclass III receptor tyrosine kinases including PDGFRA and B, KIT and VEGF (Baruchel, Sharp et al. 2009). PDGFRA, KIT and VEGF proteins are seen overexpressed in both adult and paediatric high grade gliomas. Patients were aged between 2-18 years with a tumour of the CNS. Unfortunately no clinical response was seen in the tumours with Imatinib, possibly due to the poor penetration of the blood brain barrier by Imatinib (Baruchel, Sharp et al. 2009).

O^6-methylguanine-DNA methyltransferase (MGMT) is a gene located on 10q26 that encodes a DNA repair protein (Hegi, Diserens et al. 2005). MGMT removes alkyl groups from the O^6 position on guanine bases and so prevents the cross linking of double stranded DNA which can trigger apoptosis (Esteller, Garcia-Foncillas et al. 2000). MGMT expression has been negatively linked with survival in high grade gliomas as MGMT is able to undo some of the damage done by alkylating agents used as chemotherapeutic drugs, such as temozolomide (Hegi, Diserens et al. 2005). In patients where the promoter region of MGMT is methylated, and so MGMT is not expressed, survival is increased as the tumours are more susceptible to temozolomide

treatment as there is reduced DNA repair activity (Esteller, Garcia-Foncillas et al. 2000; Hegi, Diserens et al. 2005). MGMT is a possible drug target in pHGG as inhibiting the activity of MGMT in tumours with high levels of MGMT expression would theoretically increase the tumour's sensitivity to alkylating chemotherapeutic agents (Esteller, Garcia-Foncillas et al. 2000).

The BBB is an obstacle to all therapeutic agents directed towards brain tumours (Schinkel 1999). An intracranial approach to drug delivery has been used in adults, e.g. Gliadel wafers following GBM resection. However, it is unknown how far the drug is distributed throughout the surrounding tissue especially with high molecular weight drugs (Perry, Chambers et al. 2007).

1.3 Syndromes associated with High Grade Glioma

1.3.1 Neurofibromatosis

There are two major categories of neurofibromatosis; type 1 (NF1) and type 2 (NF2). Both NF1 and NF2 are nervous system disorders that involve the growth of nerve tumours.

NF1 is more common than NF2, affecting around 1 in 3500 people (Boyd, Korf et al. 2009). Approximately 50% of cases of NF1 are cause by sporadic mutations in the NF1 gene, with the other 50% caused by inherited mutation. NF1 is an autosomal dominant disease with penetrance reaching almost 100% by the age of 20. Even though the penetrance is high the severity of symptoms can vary dramatically even between family members. NF1 symptoms include nerve tumours, bone abnormalities and cafe-au-lait spots on the skin. It is common for a first degree relative to also be affected (Rosenfeld, Listernick et al. 2009).

Mutations to *NF1* that cause the NF1 disorder include deletions, insertions and stop mutations and in some cases the entire gene is deleted. *NF1* produces the protein neurofibromin, a tumour suppressor. Neurofibromin is normally expressed in neurons and glial and Schwann cells and is a cell cycle regulator that inhibits Ras signalling, which in turn inhibits the action of mTOR. Deregulation of Ras leads to

uncontrolled cell proliferation (Boyd, Korf et al. 2009; McGillicuddy, Fromm et al. 2009) .

Sufferers of NF1 are susceptible to benign and malignant tumours, with dermal neurofibromas being the most common benign tumour occurring in 40% of children with NF1. 20% of children with NF1 will develop tumours of the CNS with optic pathways tumours being the most common (Rosenfeld, Listernick et al. 2009). Brainstem gliomas in individuals with NF1 are almost always low grade tumours that are slow growing and have a better prognosis than brainstem tumours in individuals without NF1 (Rosenfeld, Listernick et al. 2009).

NF2 is an autosomal dominant disorder caused by mutations in the *NF2* gene. The NF2 protein, merlin, is involved in cell-cell interactions and adhesion and has been implicated as a tumour suppressor. NF2 is characterised by the formation of schwannomas, meningiomas and ependymomas with neurofibromas actually rare. NF2 is particularly associated with bilateral vestibular schwannomas (Evans 2009). The incidence of NF2 may be as high as 1/25,000 with the majority of cases presenting with hearing loss caused by vestibular schwannomas (Evans 2009).

1.3.2 Turcot Syndrome

Turcot syndrome describes a disorder with multiple colon tumours and a primary brain tumour, and was first described by Turcot in 1959. Turcot syndrome is the overall name for two separate conditions caused by different genes but with very similar symptoms (Hamilton, Liu et al. 1995).

Brain tumour polyposis 1 (BTP1) affects mainly children and young adults under the age of 20. Symptoms of BTP1 include astrocytomas, small numbers of intestinal polyps, and coffee coloured spots on the skin. It is thought BTP1 is linked to Hereditary Non-Polyposis Colorectal Carcinoma (HNPCC). HNPCC is caused by an inherited defect in the mismatch repair pathway (Chan, Yuen et al. 1999).

Brain tumour polyposis 2 (BTP2) can affect any age group. BTP2 is characterised by large numbers of intestinal polyps and is associated with medulloblastoma. There is often a family history of colorectal polyps and it is thought BTP2 is closely related to

Familial Adenomatous Polyposis (FAP). FAP is associated with mutations in the APC gene which acts as a tumour suppressor gene (Hamilton, Liu et al. 1995; Chan, Yuen et al. 1999). FAP is an autosomal dominant condition with an incidence of 1 in 10000 people.

1.3.3 Li-Fraumani Syndrome

Li-Fraumeni syndrome is a rare, autosomal dominant disorder that is usually caused by a germ line *TP53* gene mutation. *TP53* is a well characterised tumour suppressor gene and deregulation of *TP53* can lead to uncontrolled cell proliferation (King 2000). Almost 400 different mutations have been described in Li-Fraumeni families and sufferers. People suffering from Li-Fraumeni syndrome have an increased risk of tumours such as sarcomas, breast cancer, brain tumours and leukaemia (Rieber, Remke et al. 2009). The overall lifetime cancer risk for sufferers of Li-Fraumeni is 85%.

1.3.4 Tuberous sclerosis

Tuberous sclerosis (TS) is a rare genetic disorder which affects multiple systems. TS causes the growth of benign tumours predominantly in the CNS but also in other vital organs. TS gets its name from the characteristic tuberous growths in the brain. Common symptoms of TS include seizures, developmental problems, behavioural problems and kidney disease. The incidence of TS is approximately 1 in every 6000 births and TS is found in all ethnic groups and both males and females.

TS is caused by mutation of one of two possible genes; *tuberous sclerosis 1* (*TSC1*) or *tuberous sclerosis 2* (*TSC2)* (Napolioni and Curatolo 2008). Only one of these genes needs to be deregulated for TS to occur. *TSC1* and *TSC2* encode the proteins hamartin and tubulin respectively. Both these proteins are involved in a complex that acts to inhibit mTOR (Napolioni and Curatolo 2008).

TS is an autosomal dominant disorder, although most cases are caused by sporadic mutations. Three types of brain tumour are associated with TS, including giant cell astrocytomas. Tumours are rarely malignant, but high grade tumours can occur.

1.4 Genetics of Cancer

Cancer is a genetic disease of somatic cells. All cancers have some underlying genetic cause that affects the control of the cell cycle (Tamarin 2002). The two main categories of genes that play a major role in carcinogenesis are oncogenes and tumour suppressor genes.

1.4.1 Oncogenes and Tumour Suppressors

Oncogenes (cancer genes) are genes which are activated by mutation or gain of copy number and cause the over proliferation of cells seen in tumours. Oncogenes are present in a non-mutated form in normal cells and are here referred to as proto-oncogenes to distinguish the non-mutated genes from the mutated form. Oncogenes are dominant at the cellular level (King 2000).

There are three different mechanisms by which a proto-oncogene can be transformed into an oncogene.

1. A mutation which causes a change in amino acid in the expressed protein can induce an oncogene. Mutations associated with cancer are usually missense mutations that disrupt the DNA binding domain.
2. Translocations which move a proto-oncogene into a region with a strong promoter can cause over expression of the gene, inducing oncogenic activity.
3. Amplification of the area of the genome where the proto-oncogene is located causes an increase in copy number of the proto-oncogene, and therefore over-expression of the gene (Tamarin 2002). Gene amplification is often seen in advanced, aggressive cancers possibly due to increased chromosome instability.

Tumour Suppressors

A big step in understanding the genetic mechanism of cancer came with Knudson's two hit hypothesis. This hypothesis, formulated in 1971 by Alfred Knudson, was based on his observation of Retinoblastoma patients. Retinoblastoma can be unilateral or bilateral and Knudson observed that the bilateral form occurred most frequently in children under the age of two (90% cases). Knudson hypothesised that the difference between the age of incidence could be explained by the number of hits, or mutations, that it takes for retinoblastoma to occur (King 2000).

Normally cells have two wild type copies of the retinoblastoma gene (*Rb*). In bilateral retinoblastoma the first 'hit' is inherited and so only one functional *Rb* allele remains. This means only one 'hit' is required for the formation of a tumour. In sporadic cases, the individual has two copies of the wild type *Rb* allele to start with so two 'hits' are required to make both alleles non functional. Whilst the probability of the first mutation is low, the first mutation leads to DNA instability meaning the probability of the second hit is much higher. This explains the earlier age at which bilateral retinoblastoma occurs as the carrier is already born with one mutated *Rb* allele. *Rb* was the first tumour suppressor gene to be described. In reality, most cancers are much more complex than this hypothesis suggests with multiple hits being required in both tumour suppressor genes and oncogenes to trigger carcinogenesis (King 2000).

Tumour suppressor genes are genes that have inhibitory functions in cell cycle progression (Tamarin 2002). The loss of a tumour suppressor gene due to mutation or deletion leads to a deregulation of the cell cycle and unrestricted cell proliferation. Tumour suppressor genes are recessive at the cellular level and so both copies of the gene must carry an inactivating mutation or be deleted for carcinogenesis to occur in reality.

Variation in copy number of regions of the human genome has been highlighted recently as being important in the study of human disease. Around 12% of the human genome is covered by copy number variable regions (CNVRs), although changes to copy number often occur preferentially away from genes (Redon, Ishikawa et al. 2006). Genes that have been identified as containing copy number

variation include genes involved in cell-cell adhesion and response to intercellular chemical signals (Redon, Ishikawa et al. 2006).

Mutation of genes is a common event in cancer. There are various types of mutation, with missense mutations being the most common in cancer. Dominant negative mutations are mutations where the mutated gene product in some way inhibits the wild type product, most frequently by dimerisation.

1.4.2 Loss of Heterozygosity

Loss of heterozygosity (LOH) describes an event where one allele at a particular locus is lost leaving one allele present. If the remaining allele contains a recessive mutation then the mutant phenotype will now be seen. LOH can occur via a number of mechanisms; deletion, gene conversion, mitotic recombination, chromosome loss (fig. 1.3 and fig. 1.4) (Tamarin 2002).

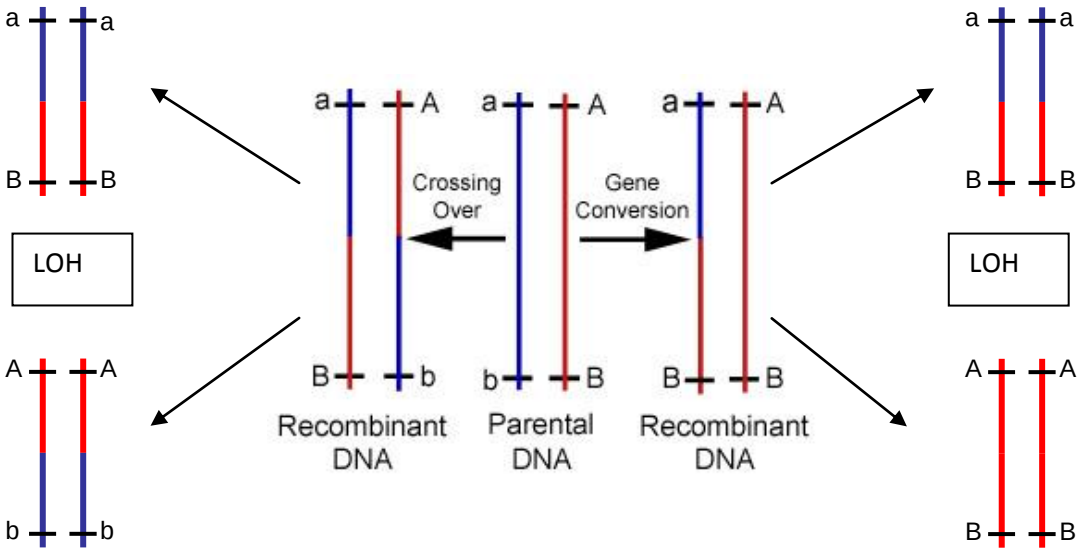

Figure 1.3: Gene Conversion and Mitotic Recombination leading to loss of heterozygosity (LOH).

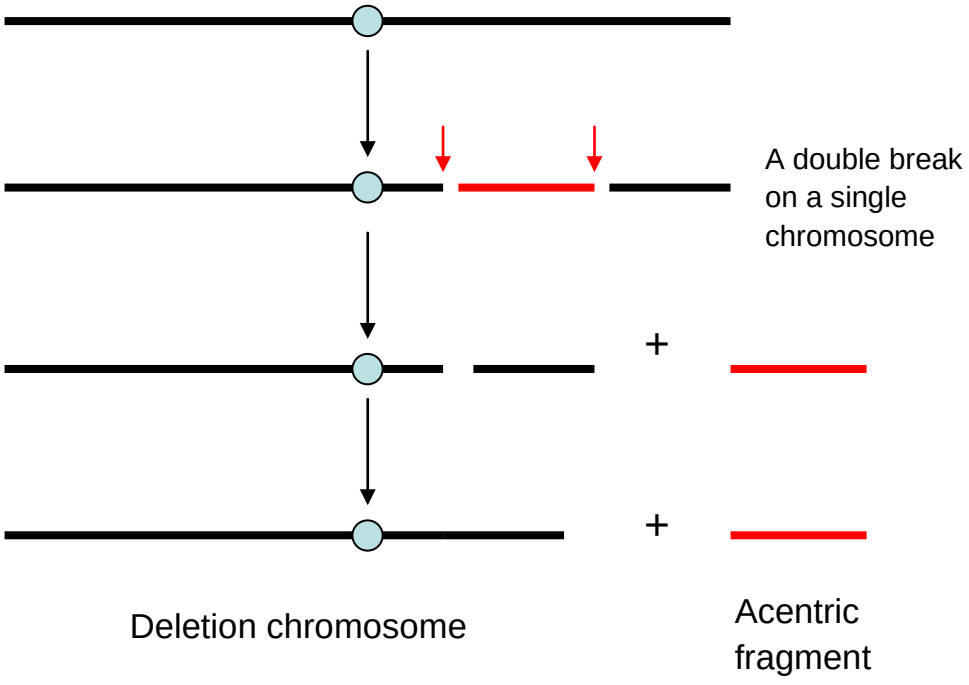

Figure 1.4: Double strand break on a single chromosome leading to a deletion of a region of the chromosome and hence LOH of the deleted region.

1.4.3 Epigenetics

Epigenetics describes changes to the DNA that do not involve alteration of the bases that make up the DNA but can affect the expression of genes. Methylation is the most frequent epigenetic alteration in humans. Around 80% of cytosines in CpG islands in the human genome are methylated. Methylation is associated with the silencing of genes. If the promoter region of a gene is methylated the DNA transcriptases cannot bind and so the gene is not expressed. The methylation of tumour suppressor genes halts expression and can lead to uncontrolled cell proliferation, e.g. aberrant methylation of the *APC* gene in colorectal carcinoma and *BRCA1* in breast cancer (Magdinier, Ribieras et al. 1998; Catteau, Harris et al. 1999; Iwama 2001).

Genes can be methylated at certain stages of development and so not expressed, but then de-methylated at other stages of development and so expressed (Jones and Takai 2001). Loss of methylation (hypomethylation) is thought to play an important role in cancer. Hypomethylation can allow the aberrant expression of oncogenes that promote cell division. It is thought abnormal methylation of genes may play a key role in cancer (Garinis, Patrinos et al. 2002).

Imprinting is inherited methylation where alleles of certain genes from each parent are silenced by methylation. Loss of imprinting leads to aberrant gene expression and has been shown to play a role in carcinogenesis. The first example of loss of imprinting in cancer was in Wilms' tumours. The gene *IGF-2* (11p15) is usually imprinted so that the maternally inherited *IGF-2* allele is methylated whilst the paternal allele is un-methylated and so expressed. In many Wilms' tumours loss of imprinting leads to expression of the maternal *IGF-2* allele in addition to the paternal, leading to overexpression of *IGF-2*. As *IGF-2* is a growth factor, over-expression may give cells a growth advantage (Brown, Power et al. 2008).

Uniparental disomy (UPD) describes a situation where both alleles of a gene are from the same parent. There are several known disorders in human caused by UPD where there is a recessive mutation in the affected genomic region or imprinting

patterns are disrupted. There are a number of mechanism by which UPD can occur (see fig. 1.5).

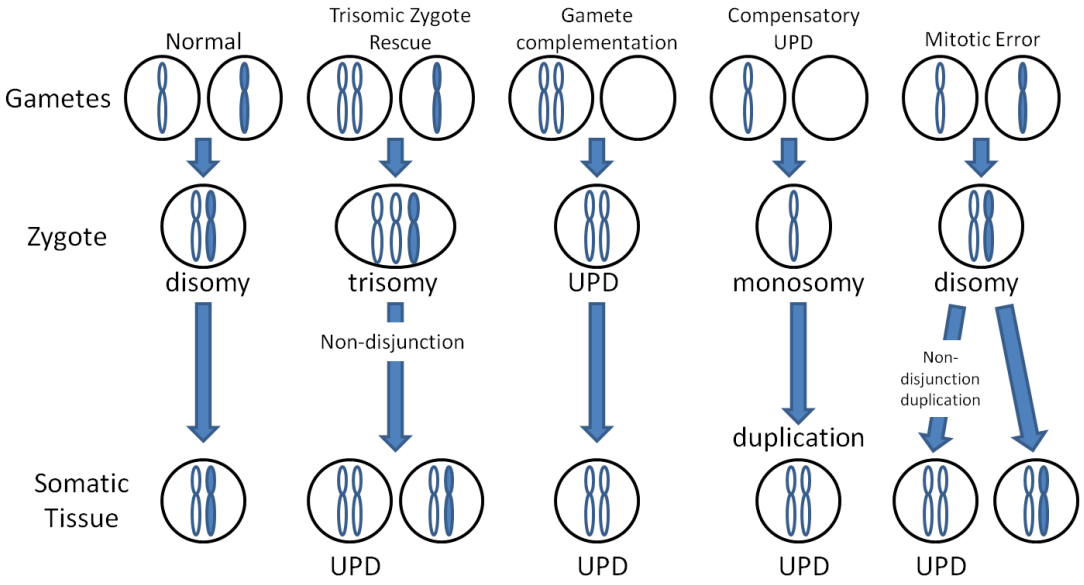

Figure 1.5: Mechanisms of uniparental disomy (UPD).

1.4.4 Genetics of paediatric high grade glioma

A small number of single nucleotide polymorphism (SNP) and CGH studies have been carried out on paediatric high grade gliomas. Wong et al carried out a study of 28 paediatric gliomas (14 high grade and 14 low grade) which were analysed by Affymetrix 10K SNP array (Wong, Tsang et al. 2006). A major difference between the high grade and low grade tumours was the lack of LOH in the low grade gliomas compared to wide spread LOH in the high grade gliomas. There is very little detectable LOH in low grade gliomas, and if LOH does occur in low grade tumours it is often only one arm of the chromosome that is affected. In contrast high grade gliomas are characterised by multiple copy number aberrations and LOH is a common event. It is most common on chromosome arms 4q, 6q, 9p, 10q, 11p, 12, 13q, 14q, 17, 18p and 19q.

Amplification of epidermal growth factor receptor (*EGFR)* and platelet derived growth factor receptor type alpha (*PDGFRA)* were seen in a small number of the high grade tumours (4/13). *EGFR* is the most commonly amplified gene in primary glioblastoma in adults but amplification of *EGFR* is rarely seen in paediatric

glioblastoma (Maher, Furnari et al. 2001). *EGFR* amplification is associated with a loss of chromosome 10 in glioblastoma and with a loss of the $p14^{ARF}$ locus on chromosome arm 9p (Godard, Getz et al. 2003; Ohgaki 2005).

In some cases, the amplification of *EGFR* was shown to have occurred even though the *EGFR* locus was located in a chromosomal region affected by loss of heterozygosity. This means the amplification of *EGFR* was of the one remaining *EGFR* allele only. This mechanism of allele-specific amplification where LOH has occurred had not been previously reported. In a study by Niskizaki et al amplification of 7p12 (*EGFR*) occurred exclusively in tumours with loss of 10q. The well characterised tumour suppressor *PTEN*, located on 10q is frequently lost in anaplastic astrocytomas (Maher, Furnari et al. 2001). Loss of the 10q 23-25 locus is more common in primary astrocytoma than secondary astrocytoma which correlates with the observed loss of *PTEN* (Rickert, Strater et al. 2001).

The same mechanism of loss of one allele and then amplification of the remaining allele was also seen at the *PDGFRA* locus (Wong, Tsang et al. 2006). *PDGFRA* is located on chromosome arm 4q, a region frequently lost in paediatric high grade glioma. *PDGFRA* is highly expressed in glial cell progenitors but expression is down-regulated in infancy, and so may play a role in the differentiation and migration of neurons (Maher, Furnari et al. 2001).

Chromosome arm 12q has been shown to be gained in glioblastoma in a number of studies and appears to be associated with glioblastoma tumourigenesis. 12q is the location of *MDM2*, an oncogene which negatively regulates the activity of tumour suppressor *p53* through binding with $p14^{ARF}$. 12q is also the site of *CDK4*, a cyclin-dependent kinase important for cell cycle progression. *MDM2* and *CDK4* are frequently seen amplified together, although the amplifications are thought to be independent events (Suzuki, Maruno et al. 2004).

Loss of chromosome arm 17p is frequently seen in both paediatric and adult glioblastoma, specifically loss of heterozygosity at 17p13.1 (Rickert, Strater et al. 2001). This locus is the position of the tumour suppressor gene *TP53*. There is a significantly higher occurrence of *TP53* mutation in secondary glioblastoma compared with primary glioblastoma (Ohgaki 2005). Loss of 17p has been observed in low grade gliomas as well as high grade gliomas, although less frequently.

Many other gains and losses of chromosomal regions have been reported in paediatric high grade glioma although few studies have been done and not all the results correlate between studies. This is lack of correlation is probably due to poor histological review of the samples involved in these studies. A frequent loss that has been reported in a number of papers is loss of chromosome arm 9p. The 9p21 locus is the site of three candidate genes for glioblastoma neogenesis; *CDKN2B*, *CDKN2A* and *ELAVL2* (Hu, Pang et al. 2002; Wong, Tsang et al. 2006). *CDKN2A* is an important tumour suppressor gene and has been implicated in tumourigenesis in a variety of cancers. *CDKN2B* lies adjacent to *CDKN2A* and is involved in the control of cell growth and proliferation by the inhibition of cyclin dependant kinases (Simon, Koster et al. 1999). *ELAVL2* has recently been shown to be lost in some glioblastoma multiforme samples (Wong, Tsang et al. 2006). *ELAVL2* has a role in the post-transcriptional regulation of *p21* mRNA and therefore is involved in controlling neural differentiation. *p21* is a tumour suppressor gene encoding a protein that is expressed at very low levels in normal glial cells but found over expressed in a high number of glioma. The *p21* gene is located at 6p21.2, but no copy number variation at this locus or at any other region of 6p has been reported so far. High grade tumours with expression of p21 have a shorter disease-free survival than those without (Korkolopoulou, Kouzelis et al. 1998).

The *CCND3* gene, located adjacent to the *p21* gene at 6p21, is a member of the cyclin family which regulates cyclin dependent kinase activity. *CCND3* forms a complex with *CDK4* and *CDK6*, a process required for cell cycle progression from G1 to S phase. *CCND3* is involved in the phosphorylation of pRb. The gene *RB1* is located at 13q14.2 and encodes pRb, a well known regulator of the cell cycle. Chromosome arm 13q is a common region of loss of heterozygosity in paediatric high grade glioma and is associated with malignant transformation from low grade to high grade glioma in adults (Wong, Tsang et al. 2006). Disruption of the pRb pathway is thought to be associated with the dramatic increase in cell proliferation seen in the transformation from low grade to high grade glioma (Ohgaki 2005).

1.4.5 Adult vs Paediatric High Grade Glioma

Primary GBM is the most common glioma in adult patients and arises *de novo* from the glial cells, whilst in paediatrics low grade gliomas are much more common than high grade tumours. Paediatric low grade gliomas (grade II) can progress to high grade tumours although this is uncommon. A number of studies have looked at the genetics of adult GBM with disruption of the RB, p53 and Ras/PI3K pathways seen in most tumours.

Rickert et al performed metaphase CGH on 23 paediatric high grade astrocytomas (Rickert, Strater et al. 2001). There were wide spread chromosome imbalances with high level gains on 1q, 2q, 7q, 3q, 9, 17q, 4q, 8q, 18 and 20q. The findings were compared with adult high grade glioma data. Gain of 1p, 2q and 21q and loss of 6q, 11q and 16q seem to be more common in the paediatric tumours compared with the adult (Rickert, Strater et al. 2001).

Paediatric high grade gliomas have had much less research attention compared with adult tumours. Mutations in *p53* and loss of the *INK4A/ARF* locus have been shown in adult and paediatric high grade glioma. *EGFR* amplification, the most common amplification in adult GBM, is much less common in children (Sung, Miller et al. 2000). *PDGFRA* is the most common focal amplification in paediatric tumours but is seen much less frequently in adult tumours (Wong, Tsang et al. 2006).

In paediatric tumours gain of 1q has been identified as the most common whole arm gain whereas in adults gain of 1q is much less frequent. Chromosome arms 10q, 13q and 14q are lost in both adult and childhood tumours (Wong, Tsang et al. 2006). The level of loss of 13q and 14q is similar in adults and paediatrics but gain of 10q is less common in paediatric tumours.

Age seems to be an important factor in survival with children under three having a better survival rate than children over three. *TP53* mutation is much less frequent in children under three than children over three and adults, indicating a distinct tumour mechanism in very young children (Pollack, Finkelstein et al. 2001).

Oligodendrogliomas in adults frequently have loss of 1p and 19q, and this is associated with increased survival compared to other high grade glial tumours (Cairncross, Ueki et al. 1998; Kreiger, Okada et al. 2005). Paediatric

oligodendrogliomas do not tend to have the characteristic loss of 1p and 19q and survival does not seem to be affected. Whilst adult and paediatric high grade glioma clearly share similar aberrations it is the frequency of these aberrations which separates adult and paediatric high grade gliomas into two separate entities.

Similarities between the genetic profiles of secondary adult high grade gliomas and paediatric high grade gliomas have been noticed. For example, amplification and subsequent overexpression of *PDGFRA* is seen in adult secondary GBM and paediatric GBM, but not in adult primary GBM. *EGFR* amplification is seen in adult primary GBM, but not in adult primary GBM or paediatric GBM (Faury, Nantel et al. 2007). Other focal aberrations found in paediatric GBM, e.g. *MYCN* amplification, are also seen in adult secondary GBM.

Microsatellite instability is seen in 25% of pHGG but is rarely seen in adult tumours. Microsatellite instability is caused by defects in the mismatch repair pathways, often due to mutations in mismatch repair genes, e.g. *MLH1*, *MSH6, PMS1, PMS2 (Abdel-Rahman 2008)).* Microsatellites are small repeating sequences that are prone to replication errors by DNA polymerase. If there are defects in the mismatch repair pathway then these errors are not fixed resulting in mutations (Boland and Goel 2010).

Table 1.2: Summary of genetic aberrations found in adult and paediatric high grade glioma

Adult high grade glioma	**Paediatric high grade glioma**
Amplification of *EGFR* is the most common genetic aberration.	Overexpression of EGFR is common but gene amplification is rare.
Loss of *p53* is common in adult tumours.	Loss of *p53* is common in children diagnosed over the age of 4, rarer in children diagnosed under the age of 4.
Rb pathway commonly disrupted.	*Rb* pathway in children is not well characterised.
Deletion of *p16* seen in 50-70% patients	Deletion of *p16* only in 9% of patients.
Microsatellite instabilty rarely seen in adults.	Microsatellite instability found in around 25% of paediatric tumours. (caused by a disruption in the MMR pathway)
PTEN mutations common in primary adult glioblastomas.	*PTEN* mutations rarely seen in paediatric secondary glioblastomas.

(Pollack, Finkelstein et al. 2001; Rickert, Strater et al. 2001; Broniscer and Gajjar 2004; TCGA 2008)

1.4.6 Mouse Models

Mouse models of tumours are vital tools in studying the behaviour and progression of tumours and the effect of genetic alterations to tumours. Mouse models are also important in the development of therapies to treat human tumours. Mouse models of gliomas have had limited successful with tumours demonstrating low penetrance and minimal progression (Reilly, Loisel et al. 2000). Whilst single gene knockouts of gene such as *Cdkn2a*, *Nf1* and *Trp53* have resulted in the formation of low grade tumours, no high grade tumours are seen. Reilly et al demonstrated that a double

knockout of one copy of *Nf1* and Tr*p53* enabled the development of low and high grade gliomas (Reilly, Loisel et al. 2000).

Further studies have shown that overexpression of activated EGFR in *Cdkn2a* deficient mice can give rise to low and high grade tumours if targeted to specific nestin expressing cells in the developing brain. High and low grade tumours also arise when *ras* and activated *Akt1* are targeted to nestin positive cells highlighting the importance of the disruption of specific pathways in the development of high grade gliomas (Holland, Hively et al. 1998). More recently, it has been shown that inactivation of tumour suppressor genes, e.g. *Nf1*, *Trp53*, *Pten*, in nestin-expressing neural stem cells can result in high grade astrocytoma formation (Alcantara Llaguno, Chen et al. 2009).

1.5 Signalling Pathways

1.5.1 Growth Factors

Growth factors are thought to have an important role in primary and secondary GBM. EGF and PDGF are two growth factors that have been widely implicated in GBM development. PDGF is expressed by neuron and astrocytes during neural development. Glial progenitors and neurons express PDGFRA during development, but expression is down regulated as the glial progenitors differentiate. PDGF expression is still present in the adult brain in neurons and astrocytes, whilst PDGFRA expression is only seen in the sub-ventricular zone. This suggests it is the neural stem cells that are expressing PDGFRA, and so PDGFRA may have a vital role in neural stem cell differentiation and migration.

A study by Toepoel et al has suggested that expression levels of PDGFRA, as determined by promoter haplotype, may pre-dispose individuals to gliomas (Toepoel, Joosten et al. 2008). Five distinct promoter haplotypes have been identified for PDGFRA. Haplotype H1, associated with lower PDGFRA expression, is found at high frequencies in patients with neural tube defects whilst patients with GBMs have a lower frequency of the H1 haplotype (Toepoel, Joosten et al. 2008). This suggests high PDGFRA expression pre-disposes patients to gliomagenesis. PDGFRA is an interesting target for drug development. Imatinib, a tyrosine kinase

inhibitor, targets the tyrosine kinase site of PDGFRA, decreasing the function of PDGFRA. Imatinib is commonly used in the treatment of chronic myeloid leukaemia and gastrointestinal tumours (Waller 2010).

The most common gene amplification in adult GBM is the amplification of *EGFR*. *EGFR* is the activator of the EGFR/PTEN/Akt/mTOR pathway that is thought to be key in the development of primary GBM in adults (Ohgaki and Kleihues 2007).

1.5.2 RTK/Ras/PI3K pathway

A recent study by The Cancer Genome Atlas (TGCA) identified three key pathways frequently disrupted in adult GBM; the RTK/Ras/PI3K pathway, the p53 pathway and the RB pathway (TCGA 2008).

The Ras family of proteins are key cell cycle regulators. Ras proteins are activated when growth factor ligands, e.g. EGF, bind to extra-cellular membrane bound growth factor receptors, e.g. EGFR. This binding leads to activation of downstream target such as Raf and PI3K. When Ras binds with GTP it recruits Raf to the cell membrane where Raf becomes active either by phosphorylation or another process. When Raf is active it phosphorylates MEK, which in turn phosphorylates ERK1 and ERK2. When ERK1 and 2 are phosphorylated they become active and phosphorylate a variety of targets. Some of these targets are transcription factors and so are involved in cell proliferation.

Loss of control of cell proliferation in many cancers is thought to be down to deregulation of the Ras/Raf/MEK/ERK signalling pathway. Although mutation of *Ras* in brain tumours is rare, around 30% of adult high grade gliomas have overexpression of EGFR, which is known to activate the Ras pathway (Fanton, McMahon et al. 2001).

Ras activation of PI3K leads to the activation of Akt which then phosphorylates the pro-apoptotic protein Bad. The phosphorylation of Bad means that Bad can no longer bind to Bcl2, an anti-apoptotic protein. When Bad is phosphorylated, Bcl2 is released in an active form and apoptosis is inhibited (King 2000). Another downstream target of Akt is mTOR, a kinase that mediates cell response to stress.

mTOR controls expression of p21 which halts the cell cycle in response to damage. Inhibition of mTOR leads to decreased expression of p21 and increases the cell's susceptibility to DNA damage and so the cell's susceptibility to chemotherapeutics that use a DNA damage mechanism. mTOR also promotes angiogenesis by promoting the expression of hypoxia-inducible factor (HIF) which controls the expression of a variety of genes involved in angiogenesis.

The *NF1* protein neurofibromin converts Ras from its active form to an inactive form and so stops cell proliferation. When NF1 function is lost the Ras mechanism of cell cycle control is lost (Boyd, Korf et al. 2009).

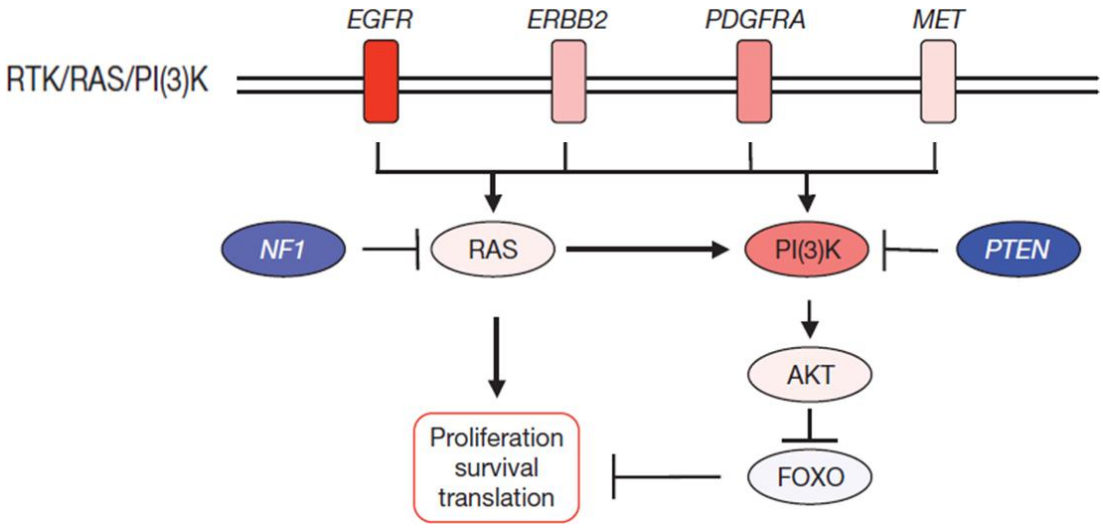

Figure 1.6: RTK/Ras/PI3K signalling pathway, adapted from TCGA (TCGA 2008).

Loss of 10q is the most common chromosome arm loss in high grade glioma. *PTEN*, located at 10q23, dephosphorylates PIP3 and PIP2 which blocks PI3K activity and so negatively regulates the cell cycle at G1. If *PTEN* is lost, then PI3K activates Akt which in turn can activate downstream targets including BCL2 (via Bad) and mTOR. *PTEN* is mutated in up to 40% of adult GBM but mutations are rarely seen in secondary GBM.

1.5.3 RB Pathway and p53 Pathway

RB1 is a tumour suppressor gene that controls the cell cycle at the point of transition from G1 to S phase by inhibiting E2F1 (see fig. 1.7). A complex composed of CDK4 and CCND1 phosphorylates RB1 which leads to the release of E2F1. E2F1 then activates genes required for the transition from G1 to S phase. If the CDK4/CCND1 complex is inhibited by p16INK4A binding to CDK4 then the complex cannot phosphorylate RB1 and so the cell cycle is stopped. Mutations in *RB1* that cause inactivation can lead to uncontrolled cell proliferation. Disruption of the RB pathway is seen in the majority of adult GBM. Disruption is usually due to loss of *RB1*, loss of *p16INK4A*, or amplification of *CDK4*.

p53 is the most commonly aberrant gene in human cancer. Around half of grade II astrocytomas and anaplastic astrocytomas have no wild type *p53* allele. p53 is a transcription factor which halts the cell cycle in response to stress, eg. DNA double strand breaks, to allow DNA repair enzymes to work or to induce apoptosis. p14ARF binds to and stabilizes p53. p53 is degraded by the MDM2, a gene which is amplified in around 10% of adult GBM.

p16INK4A and p14ARF are both produced from the *INK4a/ARF* locus at 9p21 due to alternative splicing so if this locus is lost both the RB1 and p53 pathways are deregulated. In adult GBM, even if the INK4a/ARF locus is intact tumours usually have disruption of the RB1 and p53 pathways by some other mechanism (Kanu et al).

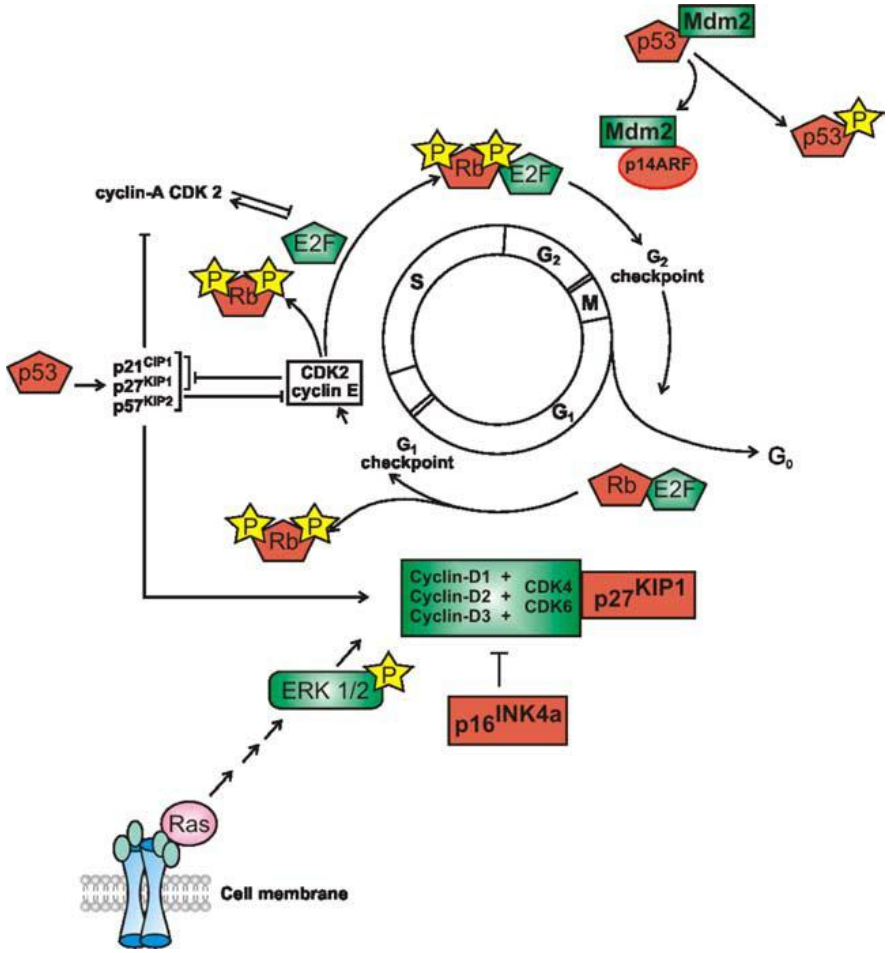

Figure 1.7: RB/p53 signalling pathway (Soni, King et al. 2005).

1.6 Research Methods

1.6.1 Formalin-Fixed Paraffin Embedded and Fresh Frozen Tissue Samples

Formalin-fixation has been the most common soft tissue preservation method for clinical studies for decades. Tissue is fixed in formalin and then embedded in a paraffin block for storage and for histopathological review. Paraffin sections are used in the histopathological diagnosis of tumours. Unfortunately DNA from formalin-fixed paraffin embedded tissue (FFPE tissue) shows some degradation due to the extensive cross-links formed between nucleic acids and proteins within cells by the formalin-fixation method. The crosslinks formed in the fixation process can be broken by treatment of the fixed tissue with protease, although it is likely that some

crosslinks will remain. DNA isolated from FFPE samples tends to have a broad range of fragment sizes and so will appear as a smear on an electrophoresis gel. Only a few studies have looked at the possibility of using DNA isolated from FFPE tissue for whole genome molecular analysis and the results have been varied, although some success has been reported where the isolated DNA has been of a reasonable integrity. The variation in success when using FFPE tissue for molecular analysis is probably due to a number of factors including the age of the sample, the time taken to fix the sample when originally extracted from the patient, and whether buffered formalin was used in the fixation process. Array CGH can be used with FFPE tissue with good results although the quality of the aCGH does depend on the integrity of the test DNA. The lack of quality of DNA extracted from FFPE tissue presents a real problem for genomic analysis of these samples, especially as FFPE tissue is often the only available material for research.

The gold standard is flash frozen tissue where the tissue is frozen in liquid nitrogen immediately following surgery. This preserves the DNA and RNA and does not cause any chemical alteration of nucleic acid. Therefore, DNA and RNA isolated from frozen material is usually of a high quality unlike DNA isolated from formalin fixed tissue.

1.6.2 Comparative Genomic Hybridisation

Comparative Genomic Hybridization (CGH) is a technique that was developed to detect gains and losses in copy number in DNA. Traditional CGH uses fluorescent dyes to label the genomic DNA; test DNA samples are labeled red and control DNA samples labeled green (Figure 1.8). Control DNA can be DNA isolated from an unaffected tissue in the case of a tumour or a DNA pool from healthy individuals. The ratio of red to green signals is measured on metaphase chromosomes with deleted regions appearing red and amplified regions green. Regions of the chromosome with no difference in copy number between the test and the control DNA appear yellow. This method of labeling metaphase chromosomes only provides limited resolution of the areas of copy number change (Inazawa, Inoue et al. 2004).

It is assumed that any reference sample will have a diploid genome although there may be some local areas of gain or loss due to variation within the population.

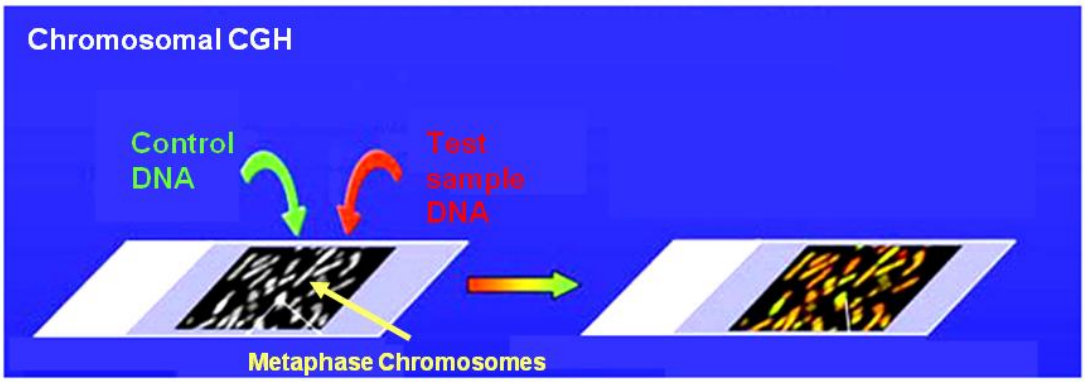

Figure 1.8: Metaphase CGH.

Array CGH (aCGH) uses a series of genomic clones, spotted onto a glass slide, that span the genome. The clones are bacterial artificial chromosomes (BACs), P1-derived artificial chromosomes (PACs) or yeast artificial chromosomes (YACs) and each BAC or PAC contains an insert between 100-300bp in size (Cowell, Matsui et al. 2004). The clones spotted on the slide are termed the probes and are therefore the hybridization target for the sample DNA. The test and reference DNA compete for binding to the probes on the array and therefore the ratio of red to green dye represents the differences in copy number between the two samples (Warr, Ward et al. 2001). The resolution of aCGH is determined by three factors; the size of the probes, the distance between the probes and the number of probes on the slide (Johnson, Hamoudi et al. 2006). Arrays contain on average around 6000 BACs and can have a resolution of up to 1Mb (Cowell, Matsui et al. 2004).

Array CGH allows for the screening of chromosomal gains and losses and so can indicate changes in copy number when there is a change in the net amount of chromosomal material. However, because aCGH works by detecting gains and losses in copy number, changes in the DNA where there is no overall loss or gain of chromosomal material cannot be detected. In the same way, when loss of heterozygosity (LOH) occurs without a net loss of genomic material or in an area with no probe coverage, no change will be detected by aCGH. This may occur due to a duplication of the corresponding area of the intact chromosome (Cowell, Matsui et al. 2004).

Array CGH can be used with formalin-fixed paraffin embedded (FFPE) tissue with good results although the quality of the aCGH does depend on the integrity of the sample DNA (Johnson, Hamoudi et al. 2006).

The newest advance in comparative genomic hybridization is oligo array CGH (oligo aCGH). Oligo aCGH uses short DNA sequences called oligonucleotides as probes rather than BAC or PAC clones. Oligo arrays have several advantages over BAC arrays; oligonucleotides are easier to design and create and their production is less time consuming and cheaper than BAC clone production. Oligo aCGH can have a resolution as high as 6.4 Kb. As a result of the increased resolution, oligo aCGH is able to detect single copy number amplifications and deletions and gives a more informative genomic profile than aCGH (Carvalho, Ouwerkerk et al. 2004).

There are three main stages to the oligo aCGH protocol; digestion, labelling and hybridization. The digestion stage involves the addition of restriction enzymes to the DNA sample to produce DNA fragments of an appropriate length for labeling and hybridization. Labeling involves the binding of fluorescent dyes to the digested DNA, either cyanine 3 (Cy-3) or cyanine 5 (Cy-5). The test sample is labelled with Cy-3 and the control sample with Cy-5, or vice versa. Hybridisation is the process of applying the labelled test DNA and control DNA to the oligo aCGH microarray slide and incubating the array at a certain temperature for a specific amount of time (see fig. 1.9). After incubation the microarray slides are washed and scanned to generate an image that can be transferred into an analytical program for analysis.

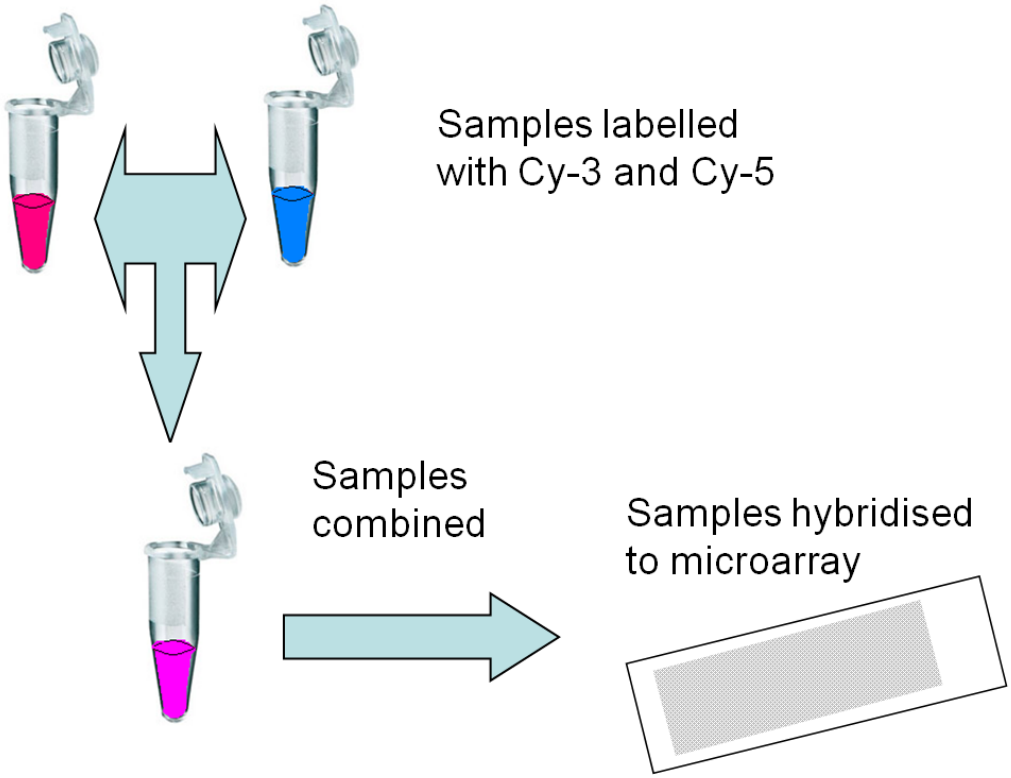

Figure 1.9: Combination of Cy-3 and Cy-5 labeled samples for hybridization to aCGH microarray.

Copy number aberrations are extremely common in cancer cells and aCGH is helping not only to identify the numerical abnormalities but also to associate these variations with diagnostic factors. Copy number aberrations leading to diseases are often the result of recombination between regions rich in low copy number repeats (Mendrzyk, Korshunov et al. 2006). This is a potential problem for aCGH because these regions of low copy number repeats have a tendency to cross hybridize. This will therefore lead to a misrepresentation of copy number as probes will not be able to bind to cross hybridized DNA (Fellermann, Stange et al. 2006).

1.6.3 Single Nucleotide Polymorphism (SNP) arrays

Array CGH and oligo array CGH allow for the identification of areas of chromosomal gain and loss but do not have a high enough resolution to identify single base pair changes within the genomic material (Herr, Grutzmann et al. 2005). Having the resolution to detect single base pair changes means that genotyping arrays such as SNP arrays have the ability to detect copy neutral events e.g. mitotic recombination, gene conversion, uniparental disomy (Zhao, Li et al. 2004). Single

nucleotide polymorphisms (SNPs) are the most common form of genetic variation in the human genome with more than 10^6 SNP loci thought to be present (Dong, Wang et al. 2001). SNP arrays or oligonucleotide arrays consist of a series of oligonucleotides arranged on a glass chip. The oligonucleotides, which are the probes on the array, are approximately 25bp in length and contain known SNPs. The high resolution of SNP arrays has made them a standard method for detecting complex genetic aberrations within DNA samples in cancer research. There are a number of biotech companies that produce SNP chips commercially including NimbleGen and Affymetrix. Affymetrix, the market leader in SNP array manufacturing, produces SNP arrays called GeneChips which use pairs of perfect match (PM) probes and mismatch (MM) probes (Affymetrix 2006). The mismatch probes act as an internal control by detecting levels of non-specific hybridization that may occur. High density arrays contain thousands of oligonucleotides with Affymetrix GeneChips containing up to 500,000 probes (Affymetrix 2006).

Affymetrix GeneChip

Figure 1.10: Affymetrix GeneChip.

The first step in SNP analysis is the extraction of DNA from the cells of the sample tissue. The DNA is then amplified, ligated and labeled with fluorescent dye before it is hybridized to the oligonucleotide probes on the surface of the chip array (fig. 1.11) (Primrose 2001). Any test DNA displaying variation at a SNP site cannot hybridize to the complementary oligonucleotide probe on the chip, as just one base difference is enough to prevent annealing. The reagents used in the SNP chip protocol make non-specific binding very unlikely but if it were to occur then this hybridization would be detected by the MM probes and the non-specific binding compensated for.

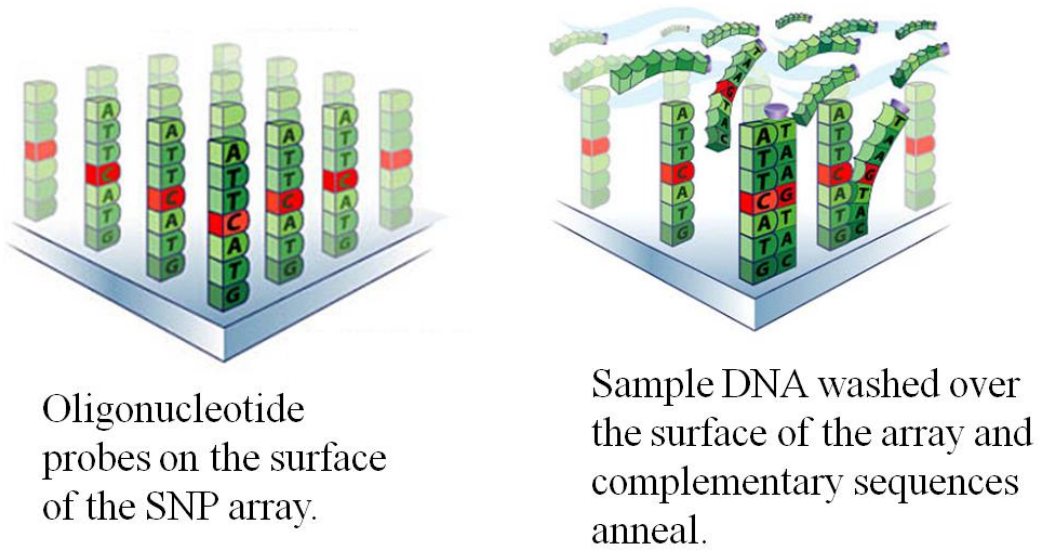

Figure 1.11: Hybridisation of DNA to SNP array (Affymetrix 2006).

When hybridization is complete the chip is washed to remove any un-hybridized material before the chip is scanned and the data produced is interpreted by a computer. There is a range of computer software available to aid the analysis of the vast amounts of data generated from SNP chip array analyses. The DNA required for analysis on a SNP chip has to be of a good quality to generate data with the minimum amount of background noise.

The problem when designing SNP chip arrays is that the vast majority of SNPs fall outside genes due to selective pressure away from coding regions of the genome. This poses the question of whether to select for SNPs within genes or distribute the SNPs throughout the genome.

1.7 Hypotheses and Aims

The objective of this study is to use high through-put genetic techniques to facilitate the identification of diagnostic and prognostic markers in paediatric high grade glioma using FFPE samples, and hence identify novel therapy targets.

Having conducted the literature review the hypotheses of this study were:

- Paediatric and adult high grade glioma have different genetic causes.
- High grade glioma occurring in the brainstem are genetically distinct from high grade glioma in the cerebrum.
- High grade glioma occurring in children over 3 years old are genetically distinct from those tumours occurring in children under 3 years old.

CHAPTER 2

MATERIALS AND METHODS

The aim of this study was to use high through-put genetic techniques to analyse FFPE pHGG samples. The following techniques and methods were used during this study.

2.1 DNA Isolation

2.1.1 DNA isolation from FFPE tissue

All the samples for this oligo aCGH project are fixed in formalin and embedded in paraffin blocks. 10 cores or scrolls were taken from each tumour sample to be used for DNA isolation. 10 cores should correspond to approximately 30 mg of tissue. The cores were placed in an Eppendorf tube on dry ice and then crushed into a very fine powder. Throughout the crushing process the cores were kept on dry ice so they remained frozen and were easier to crush. Once the cores were reduced to a powder, 1 ml of 100% xylene was added to break down the paraffin and the tube was incubated at 50˚C for 10 min. It is very important that the cores were been sufficiently crushed to allow as large a surface area as possible to be exposed to the xylene.

After incubation, each tube was centrifuged for 2 min to produce a tissue pellet and the xylene carefully removed and discarded. 1 ml of 100% ethanol was added at room temperature and the tube was vortexed then centrifuged for 2 min. The ethanol was carefully removed and discarded to leave a pellet. This wash with ethanol was then repeated before the tube was quickly centrifuged again to remove as much ethanol as possible. The tube was left with the lid open to air dry for 10-15 min until there was no visible liquid remaining in the tube.

RecoverAll Total Nucleic Acid Kit for FFPE (Ambion, Applied Biosystems, Warrington) was used for DNA extraction. 400 µl of digestion buffer plus 4 µl of protease was added to each tube to allow protease digestion of tissue. The protease was added to remove the cross-links between primary amino groups in proteins with other nearby nitrogen atoms in protein or DNA through a $-CH_2-$ linkage formed during the formalin fixation process. The tube was gently agitated to ensure all the

tissue is immersed. The tubes were then placed at 50 ˚C for 48 h to allow the digestion process to occur.

After the 48 h incubation 480 µl of isolation additive was added to each tube and the tube vortexed. The resulting solution has a milky white appearance. 1.1 ml 100% ethanol was added to each sample making sure the sample solution was well mixed by pipetting up and down. A collection tube was prepared for each sample by placing a filter in the top of the collection tube. 700 µl of each sample was then applied to the filters in the corresponding tubes and the lids firmly shut. The collection tubes were centrifuged at 10,000 xg for 1 min to allow the sample solution to pass through the filter cartridge. The flow through was discarded and the filter replaced into the same collection tube. This centrifuge step was repeated until all the sample had passed through the filter. 700 µl of wash 1 was applied to the centre of the filter and the collection tubes centrifuged at 10,000 xg for 30 s. The flow-through was discarded and the filter replaced into the same collection tube. 500 µl of wash 2/3 from the RecoverAll kit was applied to the centre of the filter and the collection tube centrifuged at 10,000 xg for 30 s. Again, the flow-through was discarded and the filter replaced into the same collection.

The final stage in the DNA isolation process was nuclease digestion and final purification. An RNase mix was prepared;

	per sample
RNase A	10 µl
Nuclease free water	50 µl

60 µl of RNase mix was added to the centre of each filter and the tube incubated at 37 ˚C for 30 min. After incubation, 700 µl of wash 1 was added to the centre of the filter cartridge. The tubes were then left for 1 min at room temperature before centrifuging at 10,000 xg for 30 s. The flow-through was discarded and the filter cartridge replaced into the correct collection tube. 500µl of wash 2/3 from the RecoverAll kit was applied to each filter and the collection tubes centrifuged at

10,000 xg for 30 s. The flow-through was discarded and the wash 2/3 step repeated. The collection tubes were centrifuged at 10,000 xg for one min to remove as much liquid as possible for the filter.

The filter was then removed from the collection tube and placed into a new collection tube. 30 µl of nuclease-free water or elution solution, which had been heated to 95˚C, was applied to each filter and left to rest at room temperature for one min. The tubes were then spun at maximum xg for one min. An additional 30 µl of nuclease-free water or elution solution was added to each filter and the following steps repeated. This produced a final volume of approximately 60 µl in each tube.

The DNA samples were then stored at -20˚C.

2.1.2 Multiplex PCR Quality Control Step

It has been shown that DNA concentration alone is not a definitive predictor of success of oligo aCGH. Multiplex PCR is a quality control method which better illustrates the integrity of the DNA. Multiple sets of primers are used in a single PCR reaction to generate products of differing length. The multiplex PCR used in this study is taken from van Beers 2005 paper and was designed for the purpose of measuring the integrity of DNA isolated from FFPE tissue.(van Beers, Joosse et al. 2006) This reaction involves four sets of primers that produce a 100 base pair (bp), 200 bp, 300 bp and 400 bp product from the GAPDH gene.

Table 2.1. Primer sequences used for multiplex PCR (van Beers, *et al* 2006).

Primer	Primer Sequence
100 F	GTTCCAATATGATTCCACCC
100 R	CTCCTGGAAGATGGTGATGG
200 F	AGGTGGAGCGAGGCTAGC
200 R	TTTTGCGGTGGAAATGTCCT
300 F	AGGTGAGACATTCTTGCTGG
300 R	TCCACTAACCAGTCAGCGTC
400 F	ACAGTCCATGCCATCACTGC
400 R	GCTTGACAAAGTGGTCGTTG

PCR Mastermix

Reagent	Volume
BioMix Red	7.5 µl
H_2O	3.5 µl
Primers (x8)	1.5 µl

100 ng of sample DNA was added to 23 µl of PCR mastermix in a PCR tube. Tubes were placed into PCR machine and the following programme run:

Cycles	Temperature (^oC)	Time (min)
1	94	4
35	94	1
	56	1
	72	3
1	72	7
Hold	15	

PCR products were run on a 1.5% agarose gel (1.5 g agarose in 100 ml TAE buffer) stained with ethidium bromide alongside 100 bp ladder.

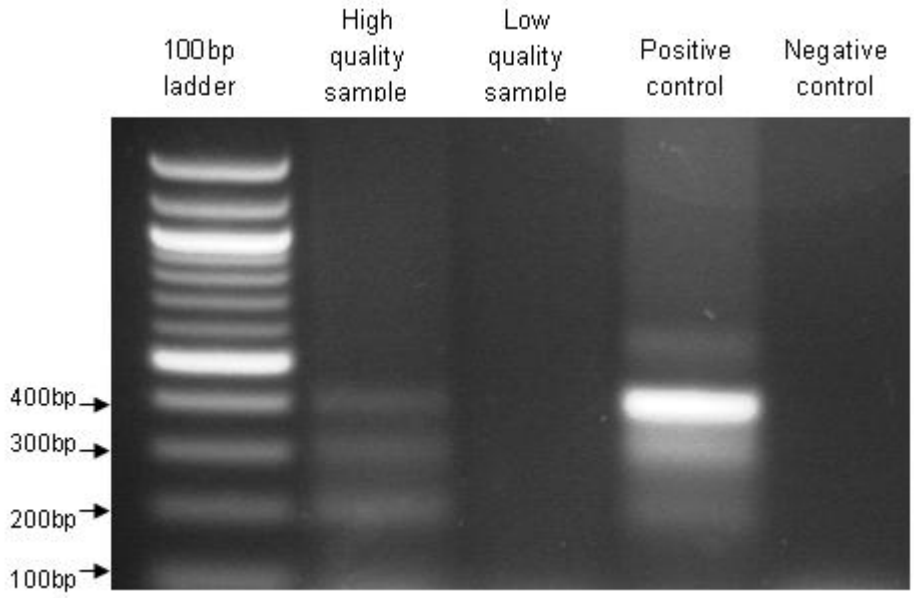

Figure 2.1: Products from multiplex PCR run on an agarose gel.

The high quality samples produced all four bands as the DNA is less fragmented than the poor quality samples which produce no bands. DNA samples which produced a 200 bp band or longer were used for oligo aCGH.

2.2 Oligo array Comparative Genomic Hybridisation (aCGH)

2.2.1 Agilent Oligo aCGH Protocol Overview (Agilent Technologies, Berkshire)

Agilent's oligonucleotide array based comparative genomic hybridisation is designed to detect copy number aberrations using 60-mer oligonucleotides in a microarray format.

There are two methods of sample preparation depending on the quantity of sample DNA available. If 0.5 µg or more of sample DNA is available then the 'direct method' of preparation can be followed. If less than 0.5 µg of sample DNA is available for analysis, whole genome amplification must be carried out to create enough template DNA for the digestion and labelling stages.

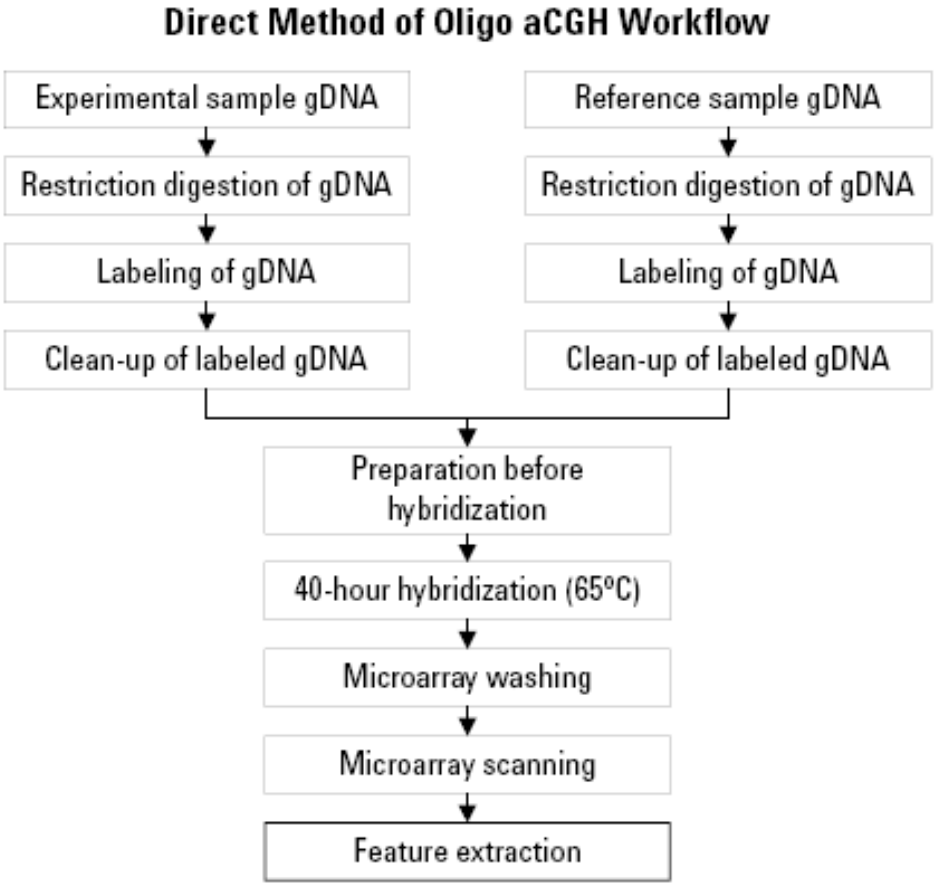

Figure 1 Direct workflow for sample preparation and microarray processing. Minimum of 0.5 µg starting gDNA per sample is required.

Figure 2.2: Oligo aCGH protocol (Agilent Technologies).

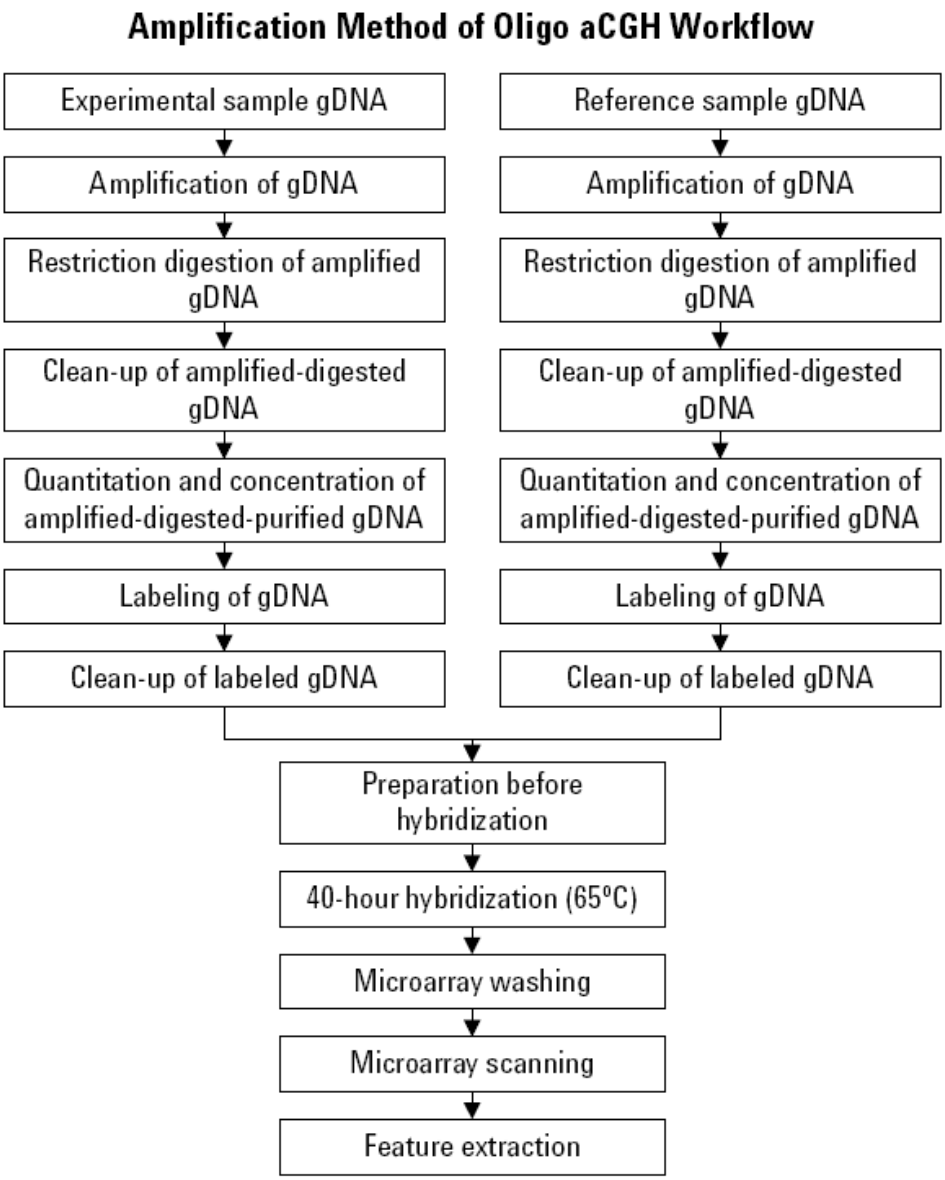

Figure 2 Amplification workflow for sample preparation and microarray processing. Minimum of 0.1µg starting gDNA per sample is required.

Figure 2.3: Oligo aCGH protocol for amplified DNA (Agilent Technologies).

Agilent aCGH Protocol (Agilent Technologies)

2.2.2 DNA digestion

For 244K Agilent oligo arrays only 0.5 µg of input DNA is required, however 1 µg of DNA was used due to the poor quality of DNA isolated from formalin fixed tissue to ensure there are enough long fragments of DNA in the solution. Nuclease-free water was added to the input DNA to give a volume of 20.2 µl. The DNA was digested by two restriction enzymes; Alu1 and Rsa1.

Digestion Master Mix

Component	**per reaction (µl)**
nuclease-free water	2.0
10X Buffer C	2.6
Acetylated BSA (10µg/µl)	0.2
Alu I (10U/µl)	0.5
Rsa I (10U/µl)	0.5
Final Volume	**5.8**

5.8 µl of digestion mix was added to each genomic DNA sample to make a total volume of 26 µl. The samples were incubated at 37˚C, the optimal temperature for enzyme activity, for 2 h and then moved to 65C˚ for 20 min to denature the enzymes and deactivate them. At this point 2 µl of each sample can be run on a gel to ensure the digestion has been successful. Fragments should ideally be between 200-500bp in length, although when using DNA isolated from FFPE tissue the fragments may be shorter due to degradation.

2.2.3 DNA labelling

Oligo array CGH uses the principle of a competitive binding process between two samples; the test sample and the control sample. Each sample was labelled with one of two dyes, Cy-3 or Cy-5. The experimental sample was labelled with one dye and the control DNA is labelled with the other.

5 µl of random primers were added to each DNA sample, and samples were incubated at 95 ˚C for 3 min then placed on ice for 5 min.

Labelling Master Mix

Component	per reaction (µl)
nuclease-free water	2.0
5X buffer	10.0
10XdNTP	5.0
cyanine-3-dUTP or cyanine-5-dUTP	3.0
Exo-klenow fragment	1.0
Final Volume	**21.0**

21 µl of master mix was added to each sample, and then the samples were incubated for 2 h at 37 ˚C followed by 10 min at 65 ˚C to denature the enzyme.

After labelling, a series of steps were performed to clean up the labelled DNA before hybridisation of the samples to the arrays. 430 ml of 1xTE buffer was added to each sample before the sample was loaded into a Microcon YM-30 filter (Millipore, Watford) and spun at 8000 xg for ten min. After discarding the flow-through, a

further 480 µl of 1xTE was added to each filter and each sample was again spun at 8000xg for ten min. After discarding the flow through the filters are inverted into fresh tubes and spun at 8000 xg for one min to collect the purified DNA from the filter into the tube.

Samples are analysed on the Nanodrop photospectrometer (Thermo Fisher Scientific, Leicestershire) to determine the DNA yield and the amount of dye activity. The specific activity of the labelled DNA can be determined by using the following equation:

$$\text{Specific activity} = \frac{\text{(pmol per µl dye)}}{\text{(µg per µl genomic DNA)}}$$

(specific activity is measured in pmol dyes per µg genomic DNA)

Table 2.2: Recommended specific activity values for labelled DNA

Input DNA (µg)	Yield (µg)	Specific activity of cyanine-3 labelled sample (pmol/µg)	Specific activity of cyanine-5 labelled sample (pmol/µg)
0.5	5 to 7	25 to 40	20 to 35

At this point if the DNA has labelled appropriately (see Table 2.2) the correct Cy-3 and Cy-5 labelled samples should be combined to give a final volume of 79 µl.

2.2.4 Hybridisation

The labelled samples are prepared for hybridisation to the arrays by the addition of Human Cot-1 DNA (Invitrogen, Paisley, UK), blocking agent and hybridisation buffer.

Component	Volume (µl) per hybridisation
Cy-3 and Cy-5 labelled gDNA mixture	79
Cot-1 DNA (1.0 mg/µl)	25
Agilent 10X Blocking Agent	26
Agilent 2X Hybridisation Buffer	130
Final Hybridisation Sample Volume	**260**

After being briefly spun down the samples were incubated for 3 min at 95 ˚C and then for 30 min at 37 ˚C. After incubation the samples are spun at 79000 xg for one min. The samples are now prepared for hybridisation to the arrays.

Agilent oligo aCGH microarrays

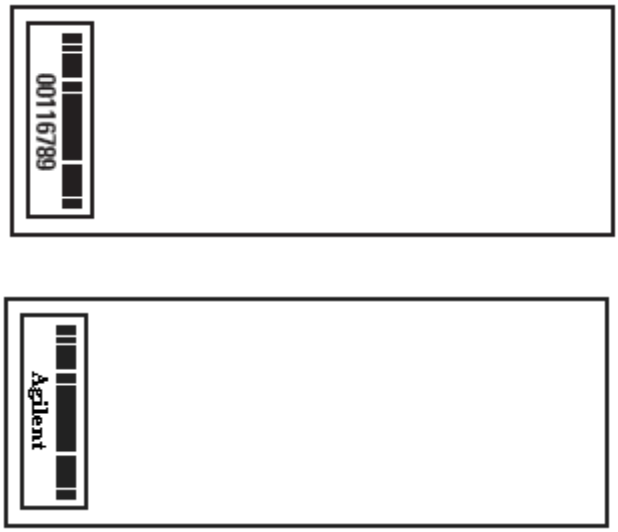

The microarray slides have a barcode on either side. The side with the numerical barcode is the back of the slide and the side with the Agilent barcode is the side with the array on (the active side).

Figure 2.4: Agilent microarray slides.

For the 244K Agilent arrays there is one array on the active side of the slide (Figure 2.4). The hybridisation sample was not applied directly to the array slide but instead to a gasket slide.

The gasket slide has a defined region (well) with rubber boundaries which correspond to the position of the array on the active side of the array slide.

Figure 2.5: Agilent gasket slide.

A gasket slide was placed into an Agilent SureHyb chamber with the Agilent barcode facing upwards (Figure 2.5). 490 µl of sample was dispensed into the well on the gasket slide.

The microarray slide was placed on top of the gasket slide with the numerical barcode facing upwards and the active side in contact with the gasket slide. The top of the hybridisation chamber was placed carefully on top of the slide 'sandwich' and clamped into place by sliding on the clamp and tightening the screw.

Assembled SureHyb Chamber

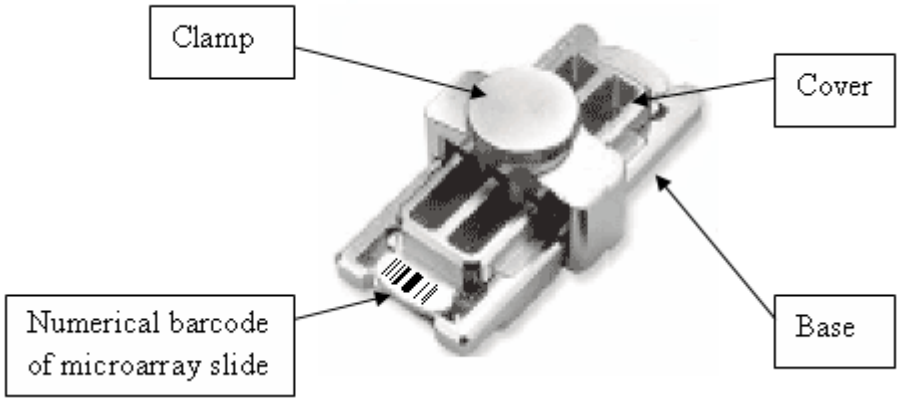

Figure 2.6: Diagram of Agilent SureHyb chamber.

After the chamber is assembled (Figure 2.6), it is important to rotate the chamber to wet the surface of the arrays and to make sure there are no stationary bubbles which could cause a mark on the array. The assembled chambers were placed into the hybridisation oven and hybridised at 65 ˚C for 40 h.

2.2.5 Washing and Scanning

Table 2.3: Summary of washes used for oligo aCGH

	Dish	**Wash Buffer**	**Temperature**	**Time**
Disassembly	1	Oligo aCGH Wash Buffer 1	Room temperature	
1st Wash	2	Oligo aCGH Wash Buffer 1	Room temperature	5 min
2nd Wash	3	Oligo aCGH Wash Buffer 2	37˚C	1 min
Acetonitrile Wash	4	Acetonitrile	Room temperature	1 min
3rd Wash	5	Stabilization and Drying Solution	Room temperature	30 s

A hybridisation chamber was removed from the hybridisation oven and rotated to check there were no stationary bubbles that could cause anomalies on the array

images. The chamber was placed on a flat surface, and the clamp screw loosened and the clamp removed. The slide sandwich was carefully taken out and both slides immersed into dish 1 filled with wash buffer 1. One of the flat ends of the plastic tweezers was carefully slid between the slides and twisted to break the slides apart. Leaving the gasket slide in the container the array slide was removed, being careful not to touch the active surface, and placed into the slide holder in dish 2. The slide is now ready for the washing process.

When all hybridised slides have been released from their gasket slides and are in dish 2 containing wash buffer 1, the magnetic stirrer was activated and left for 5 min. The slides were then transferred to dish 3 containing wash buffer 2 at 37 ˚C and left for 1 min with a magnetic stirrer. The slides were next placed in acetonitrile for 1 min with a magnetic stirrer and finally into Stabilisation and Drying solution (Agilent Technologies) for 30 s. The slides should be removed from the Stabilisation and Drying solution slowly and carefully to prevent drops on the slides which could mark the arrays. The array slides are now prepared for scanning and should be scanned immediately to prevent oxidation of the dyes which will affect signal intensities.

Scanning arrays

To scan the arrays in an Agilent scanner, the arrays slides were placed into slide holders with the active side of the slide protected by the lid of the slide holder and the back of the array slide exposed (Figure 2.7).

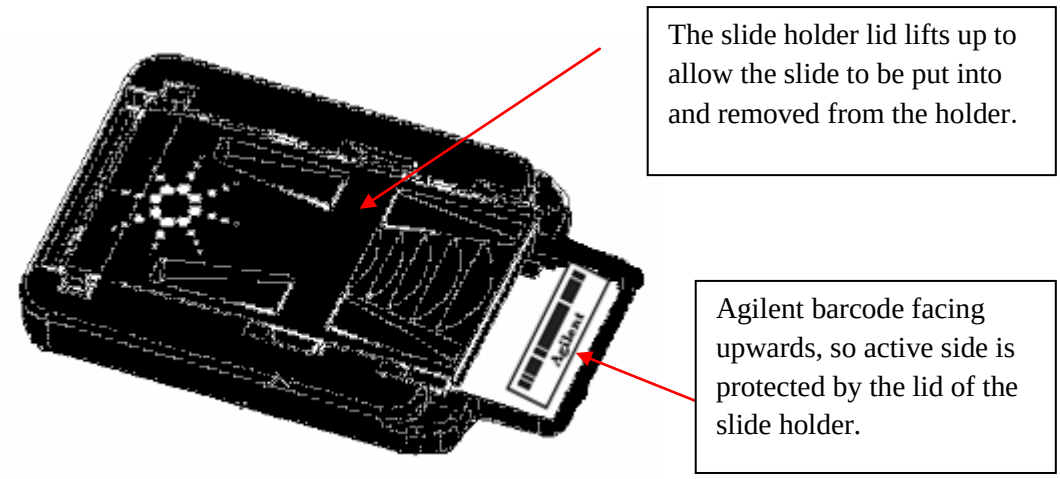

Figure 2.7: Slide holder for scanning of microarrays.

The slide carousel was removed from the scanner and slides loaded into the appropriate slots being careful to leave the 'Home' position in the carousel empty. The lid was placed onto the carousel making sure it clicks into place. The carousel was replaced inside the scanner and the scanner lid closed.

The Agilent scanner used the software program Agilent Scanner Control software v7.0. When the Agilent Scanner Control Program was opened the lid of the scanner automatically locked.

Table 2.4: Default settings for scanning 244K Agilent oligo aCGH microarrays;

Scan Region	Scan Area (61x21.6 mm)
Scan Resolution (µm)	5
Dye Channel	Red & Green
Green PMT	100%
Red PMT	100%

If any changes were made to the settings (Table 2.4) ‘set values’ was clicked to apply the changes. When the scanner had warmed up and was ready to scan a green light was displayed and Scanner Control displayed the option to scan, e.g. ‘scan slot 1 to 6’. To begin the scan the ‘scan slot a to b’ option was clicked. Each 244K array slide took about 15 min to scan at a resolution of 5 µm.

2.2.6 Processing of oligo aCGH data

The Agilent Scanner Control Program creates Tif images of the scanned arrays These Tif images require processing before they can be imported into a program for data analysis. The Agilent Feature Extraction Software version 9.1 was used in the study to process the array Tif files.

Feature Extraction

The Tif files were imported into Feature Extraction by clicking ‘Add new extraction sets’ icon on the toolbar at the top of the screen. When the files were imported they were automatically assigned a grid template, which was an .xml design file. If the correct grid template was not already incorporated into the program it was downloaded from the Agilent website.

Once the Tif files had been successfully imported the tab labelled ‘Project Properties’ was clicked. The majority of the default settings were appropriate in this study with the following exceptions: The outputs MAGE and JPEG were set to ‘None’ and the TEXT output package was set to ‘Compact’, as instructed in the Agilent oligo aCGH protocol.

The ‘Extraction Set Configuration’ tab was selected and each file was checked to make sure there was a grid template, and that the Protocol Name column was displaying the correct protocol. For this study the protocol was CGH-v4_91. If the correct protocol was not available in the software it was downloaded from the Agilent website.

The project was saved in an appropriate location (File>Save As) and then the extraction process was started by selecting ‘Project’ then ‘Start Extracting’. The extraction proceeded automatically and generated QC summary reports for each

separate array. The QC report allows you to determine if the hybridisation has been uniform across the array, to look at the level of background noise on the array, and to make sure that Feature Extraction correctly aligned the grid template onto the Tif image of the scanned array.

Feature Extraction generated .txt files from the processing of the Tif images which were imported into Agilent's data analysis software. In this study CGH Analytics version 3.4.1 was used for the majority of data analysis. Updated versions of the CGH Analytic program, DNA Analytics and Genomics Workbench were also used to produce figures.

CGH Analytics

To import the .txt files produced by Feature Extraction into CGH Analytics 'Data' in the toolbar at the top of the screen was clicked on and 'Import>FE Files' selected. The files to be imported were located and selected. CGH Analytics then gave the option to 'flip' a file which is important when dye swaps have been performed. In this study all dye swap arrays were 'flipped' so that the dye swaps and their corresponding array could be combined to give one single profile.

CGH Analytics recognised the type of Agilent array that has produced the txt file and automatically assigned a design file. The design files are GEML files that contain information on probe location, sequence and identification and are vital to the data analysis. If the appropriate design file is not already present in the software then it was downloaded from Agilent's eArray. A genome build was automatically assigned to each array. Genome build Hg17 was used for the initial analysis in this study, with Hg18 being used in the updated versions of CGH Analytics used for later analysis and to create figures.

To visualise data in CGH Analytics, the array files have to be put into 'experiments'. To create an experiment right click on the experiments folder in the left task pane and select 'new experiment'. The new experiment was renamed accordingly. Array files from the data node were selected and dragged into the desired experiment. To

activate an experiment, the experiment was selected by right clicking on the experiment node and then ‘select experiment’ clicked.

In this study every array that was hybridised with DNA isolated from FFPE tissue had a corresponding dye swap. In order for every dye swap pair to be viewed as a single profile ‘Intra Array’ was selected in the ‘Combine’ section of the task bar at the top of the screen before the experiment is selected. This causes the 2 array files to be combined and an average log2ratio for every probe on the array is calculated from the values of the 2 arrays. By creating an average profile from 2 separate arrays the noise seen on each individual array and any dye bias is reduced giving a cleaner combined profile.

Centralization

The centralization algorithm shifts the data so that the zero point reflects the most common copy number seen across the data. Centralization is active as a default in CGH Analytics and is very important when analysing noisy data as in this study. If centralization is for any reason turned off it can be turned on again by selecting ‘Tools>User Preferences’ and then selecting the ‘Miscellaneous’ tab. In the Centralization section of the tab click ‘Apply’ to turn on Centralization.

QC Metrics

The QC Metrics were viewed in a table by selecting ‘Tools>QC Metrics’. The QC Metrics include values for signal intensity of the dyes used and the derivative log ration spread (DLR Spread) which is a measure of noise. DLR spread estimates the log ratio noise by calculating the spread of log ratio differences between consecutive probes along all chromosomes. The values are grouped into excellent, good and poor determined by the QC thresholds. The QC metrics give an indication of the quality of the array and can also show why a particular array has given an unexpected result, e.g. if the signal intensity of the dyes is significantly lower than the other.

Algorithms

ADM-1 and ADM-2

The ADM algorithms work by identifying all aberrant regions within a sample with higher or lower aberrant regions based on statistical scores. ADM-1 and 2 are very similar with ADM-s including quality information on each probe value for a more stringent aberration calculation.

Z-score

Z-score assesses genomic regions with higher or lower numbers of probes with $\log_2$ratios that deviate significantly from zero. There are two stages to the z score calculation. Firstly, the number of probes with log ratios that are significantly different from a normal sample, where log ratios are zero, is calculated. Secondly, regions within the sample with higher or lower proportions of significantly aberrant probes than in the sample overall are identified as aberrant. The z score algorithm uses a sliding window of fixed size making it good for 'noisy' data. The Z score threshold can be adjusted to the correct level based on a visual analysis of gains and losses within a data set. Therefore, z-score was used as the algorithm during the data analysis in the study. Visual analysis of the data combined with initial qPCR results helped to determine the Z-score threshold. A Z-score threshold of 3.5 was used for the majority of samples, with a threshold of 4.0 being used for the noisiest samples.

Data Analysis in CGH Analytics

CGH Analytics has three panels showing three different views of the data (Figure 2.8). The first panel is the genome view which gives an overall indication of aberrations across all chromosomes. By clicking on a particular chromosome, you can then view that chromosome in greater detail in the second panel, the chromosome view.

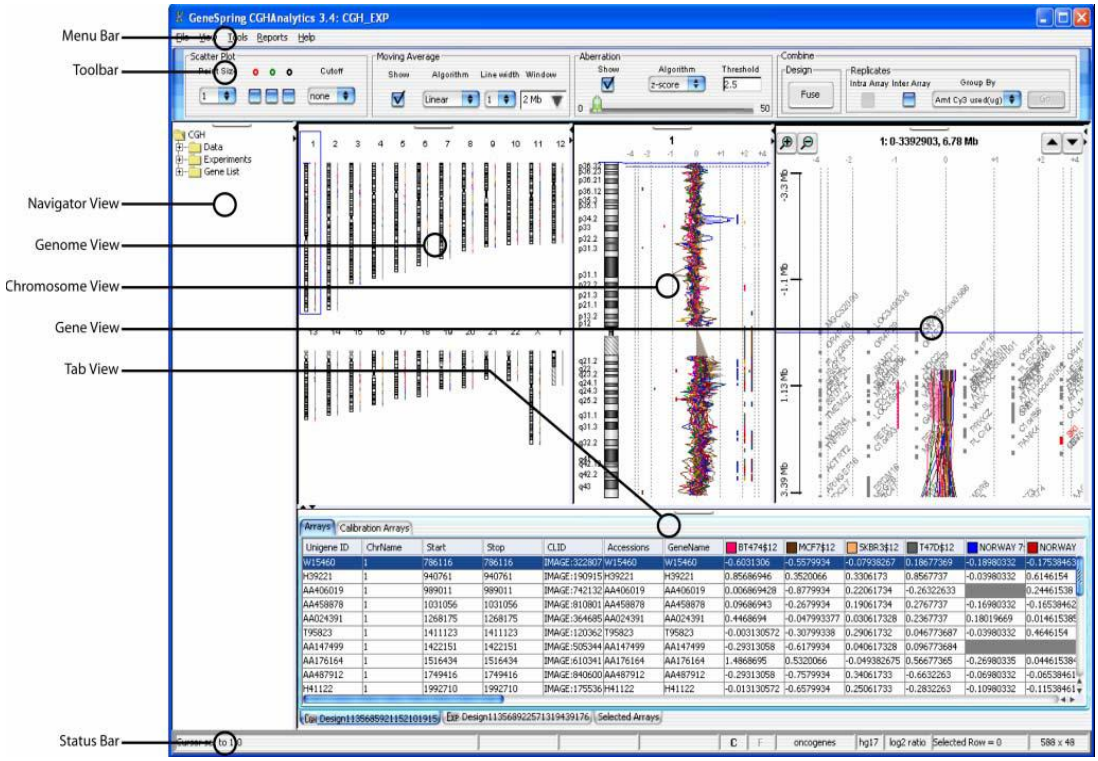

Figure 2.8: Screenshot of CGH Analytics.

The chromosome view shows one chromosome at a time and aberrations can be viewed more clearly. There are several viewing options in the chromosome view. The moving average line shows the average $\log_2$ratio of the probes along the chromosome displayed as a continuous line. Aberrant regions were highlighted in a number of ways including shading the aberrant area, which was the preferred method in this analysis. The distribution of the probes along the chromosome can be viewed, with each probe represented by a dot. This is a quick way of visually determining the noise level as the more scattered the probes are away from the zero line, the noisier the chromosome. The data display options can be changed by right clicking in the appropriate view panel and selecting 'Properties', which then displays the preference window (Figure 2.9).

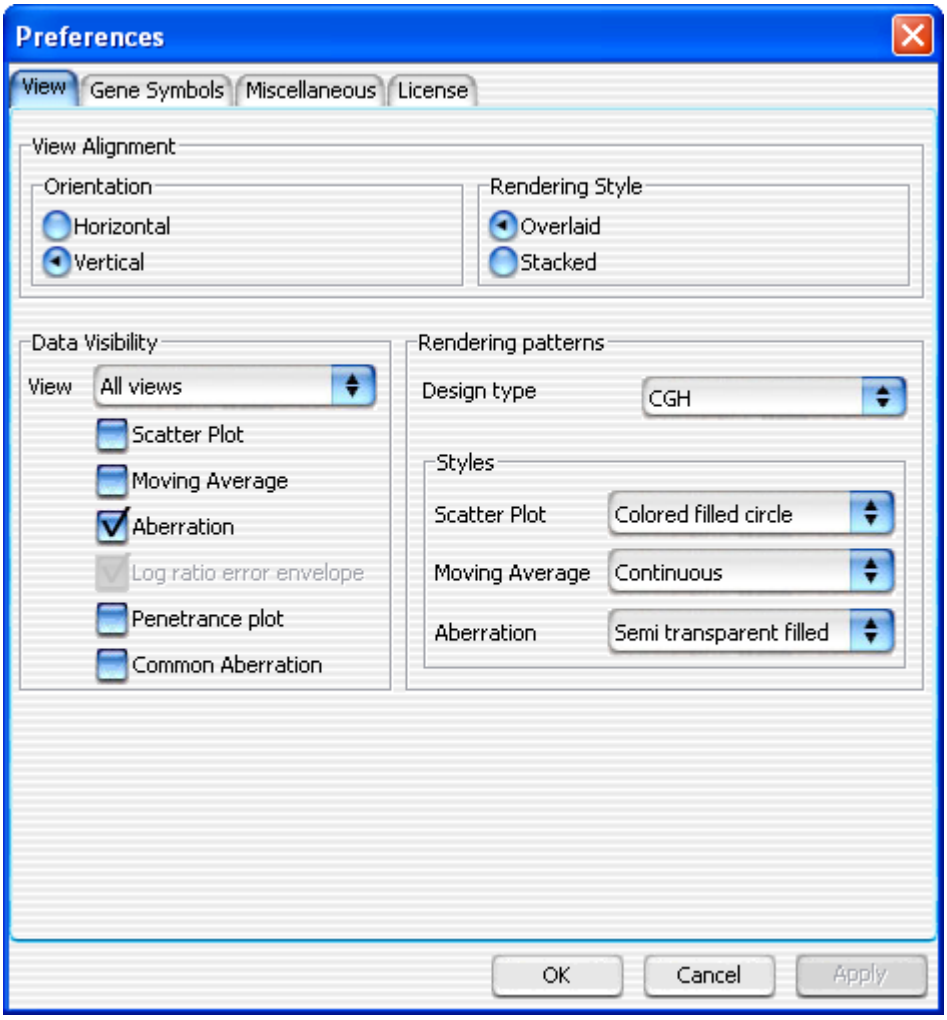

Figure 2.9: Preferences for visualising data in CGH Analytics.

By highlighting a particular region of the chromosome in the chromosome view panel, particular regions were looked at in greater detail in the third view panel, the gene view. The gene view allowed the viewing of individual probes, again represented by coloured dots, and each probe was labelled with the gene that it is located in. The smaller the highlighted region in the chromosome view, the greater the detail seen in the gene view. These three views make a visual analysis of the data simple to carry out.

Aberration Filters

The aberration filters allow the user to reduce the number of regions that the program calls as 'aberrant' by setting certain parameters for aberrations. The 'Minimum Number of Probes' value defines the minimum number of probes that must be present in an aberrant region before that region is called as aberrant. The 'Minimum

Number of Probes' value was determined by a visual analysis of the data combined with initial qPCR results to try and filter out false aberrations due to noise but maintain the true aberrations. The 'Minimum Number of Aberrant Regions' determines how many aberrant regions the program will show across the genome, and will remove the least significant aberrant regions. This is important in noisy data, as in this study, as it with display only the most significant aberrations and remove false aberrations.

Reports

CGH analytics produced a variety of lists and reports from the data. There are two types of aberration summary displayed in a graphical manner; the graphical aberration summary and the graphical common aberration summary. The graphical aberration summary (Figure 2.10) displays the aberrations for one chromosome and can be used for multiple samples to give a heat map –like figure.

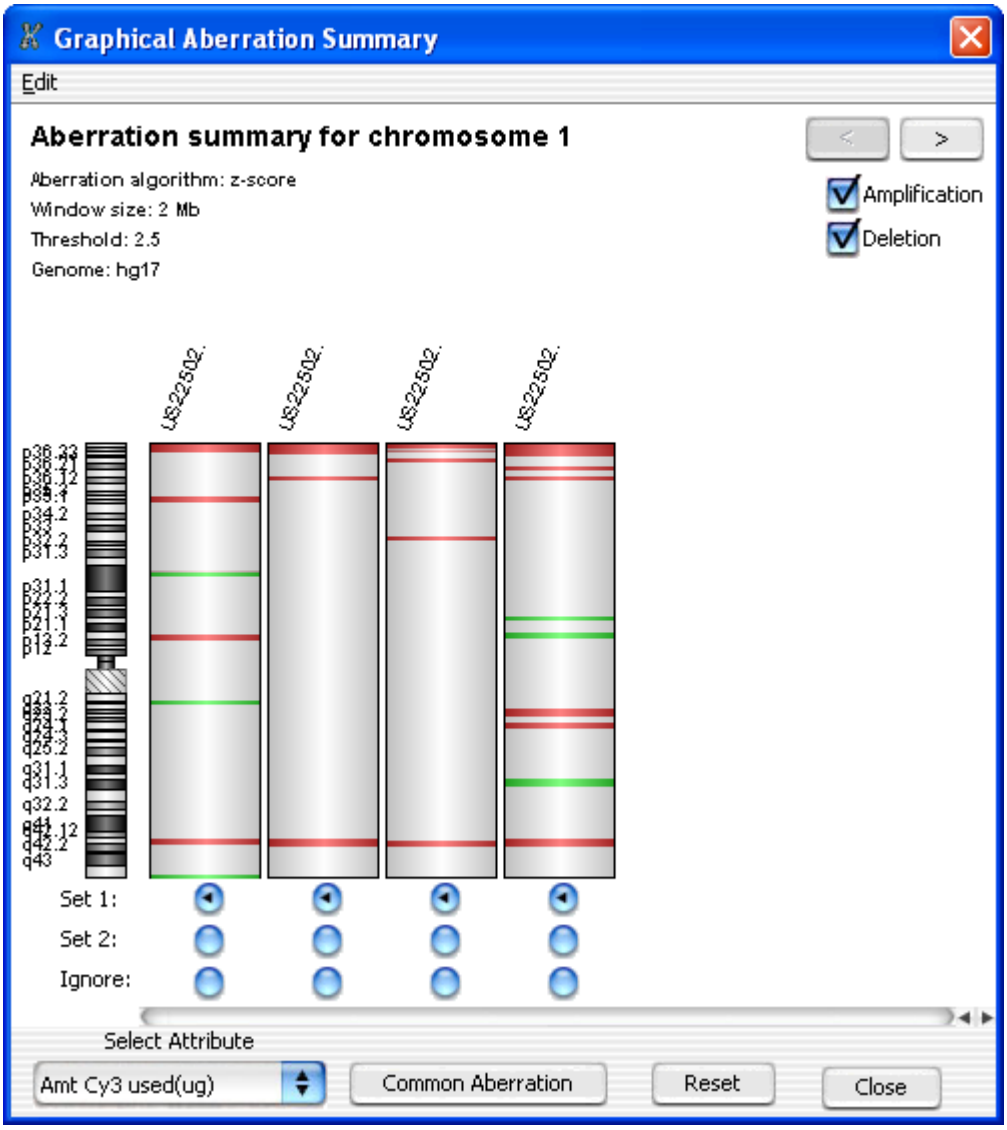

Figure 2.10: Graphical aberration summary.

The graphical penetrance summary (Figure 2.11) combines the data from all selected arrays to give a representation of the areas with the most common aberrations. All chromosomes can be viewed at once, or smaller groups of chromosomes can be selected.

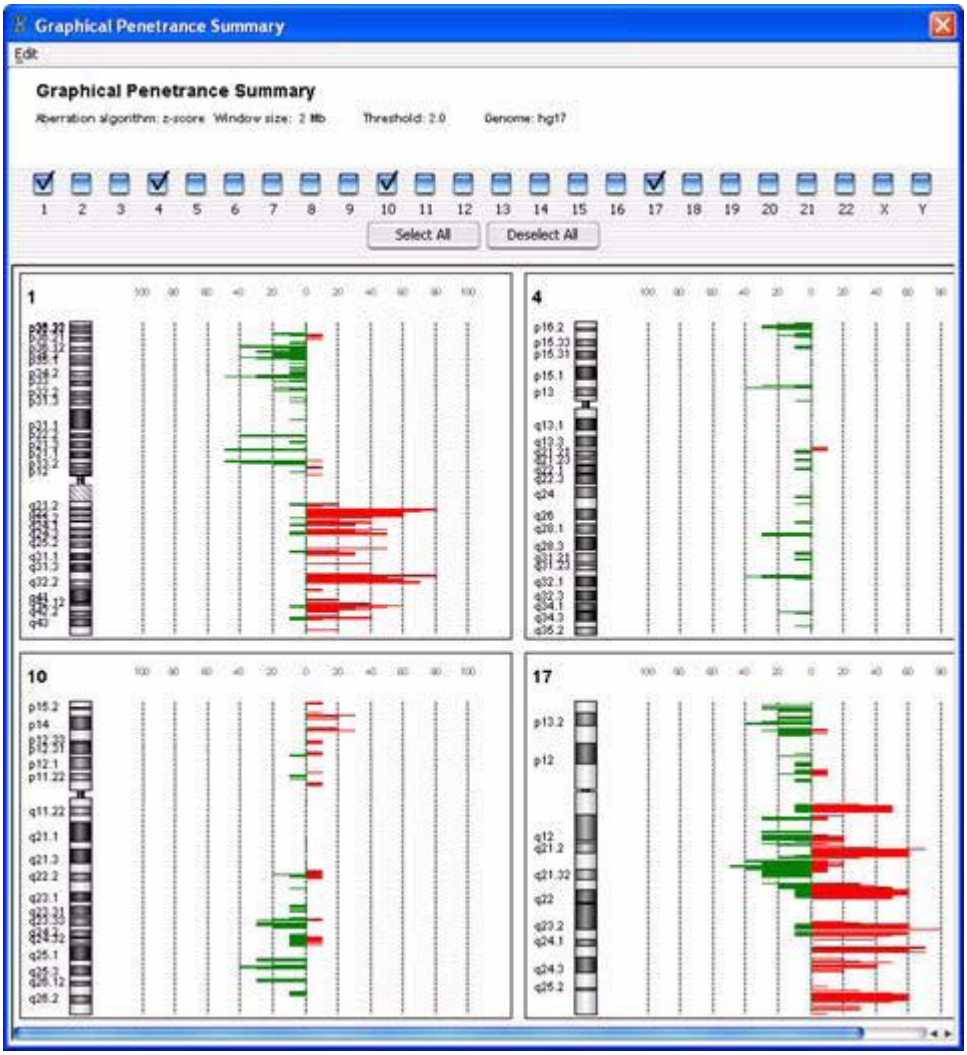

Figure 2.11: Graphical penetrance summary.

Text aberration summaries were generated and were based on probe values or intervals or a combination of probe values and intervals. The reports were exported from CGH Analytics and were view in Microsoft Excel.

Gene lists for aberrant regions were created by right clicking on an aberrant region in the gene view panel and selecting 'Create gene list.' The user can then specify if the gene list should include all genes in the current gene view or just the genes in the aberrant region below the cursor. The gene list was then saved as a node in the task pane on the left side of the screen and viewed when required. The gene lists were also exported to Microsoft Excel. The creation of gene lists of aberrant regions was important in this study.

2.3 Immunohistochemistry

Immunohistochemistry was performed on 5 µm paraffin sections on glass slides using Real Envision Detection System with Peroxidase/DAB+ (Dako, Cambridgeshire).

2.3.1 De-paraffinisation

Slides were placed in a metal rack and submerged in xylene for 15 min. The slides were removed from xylene, drained briefly, then placed in 100% ethanol for 5 min. Finally the slides were washed in 95% ethanol for 5 min then washed in running water. If the water runs clear then the process has been successful and if not the de-paraffinisation process can be repeated.

2.3.2 Antigen Retrieval

A pressure cooker was filled approximately half full with sodium citrate buffer (10.5g citric acid monohydrate added to 5 l of distilled water, adjusted to pH6 with approx 65 ml 2 M NaOH). The rack of slides was placed into the pressure cooker, submerged in sodium citrate buffer, and left for 1 min at full pressure. The cooker is then de-pressurised and the whole cooker cooled in cold water for 20 min, with the slides remaining in the citrate buffer. After 20 min the slides were removed from the citrate buffer and placed into a coplin jar with PBS (phosphate buffered saline) buffer for 5 min.

After 5 min slides were removed from PBS and dried briefly. 100ul of peroxidise blocking solution (Dako) is applied to each section for 5 min. Slides are then washed in PBS for 5 min. After the slides were dried briefly, 100 µl of primary antibody was applied to the sections. Antibodies used in this study were MYCN monoclonal mouse (NCM II 100) antibody (Abcam, Cambridgeshire; 1:100) and CDKN2B/p15INK4b mouse monoclonal antibody (ab4068, Abcam; 1:50). FFPE sections from an sPNET with a validated amplification of *MYCN* were used as a

positive control for MYCN IHC. FFPE tonsil sections were used as a positive control for CDKN2B IHC.

Slides were incubated overnight at 4^{o}C.

Slides washed in PBS for 5 min then dried briefly. 100ul secondary antibody applied to sections and slides incubated at room temperature for 30 min. Slides washed in PBS for 5 min then briefly dried. 100 µl 3,3'-Diaminobenzidine (DAB) (20 µl DAB in 1 ml substrate buffer) (Dako) applied to each section for 5 min. Slides washed in PBS for 5 min.

2.3.3 Counterstain

Slides placed in rack and washed in Harris Haematoxylin (Surgipath, Cambridgeshire) for 10 s, then briefly in running water until the water run clear. Slides placed in lithium carbonate for 10 s then in running water. Slides drained well then washed briefly in 95% ethanol followed by 100% ethanol and xylene.

2.3.4 Mounting

Slides removed from xylene and left briefly for any remaining xylene to evaporate. A small amount of Dibutyl Phthalate; Xylene (DePeX) mounting medium (Surigipath) was placed onto a coverslip and the slide placed gently on top, allowing the coverslip to attach to the slide by capillary action. Slides were allowed to dry before viewing on an Olympus BX41 light microscope with an Olympus DP25 camera and CellB Imaging Software (Olympus) at x40 magnification.

2.4 PDGFRA Immunohistochemistry

PDGFRA IHC was performed at the Institute of Cancer Research, Surrey.

De-paraffinisation

Slides incubated at 60oC for 30 min. Slides then deparaffinised in xylene (2 x 5 min) and washed in 100% ethanol (5 min), 90% ethanol (5 min) and 70% ethanol (5 min). Slides then rinsed for 5 min in running tap water. Peroxidase (DAKO) applied to sections for 5 min and slides then washed in TBST (5 min).

Antigen retrieval

Slides placed in pressure cooker with 10 mM citrate buffer for 15 min and then allowed to cool for 20 min. Slides washed in TBST and Protein block (Dako) applied for 10 min. Primary antibody diluted in TBST and applied to section for 1 h. The primary antibody used was PDGFRA rabbit monoclonal antibody (D1E7E, Cell Signalling) at a dilution of 1:4000). Slides washed in TBST (4 x 3 min) then secondary antibody (Dako) applied for 30 min. Slides washed in TBST (4 x 3 min). ABC Elite Reagent (Vectastain) applied for 30 min then slides washed in TBST (4 x 3 min). DAB (1 drop chromogen in 1 ml buffer) applied to sections for 5 min then slides washed in TBST (2 x 3 min) then rinsed in running tap water.

Counterstain

Slides stained in Mayer's haematoxylin for approximately 1 min then washed in running tap water. Sections dehydrated by washing in 70% ethanol (3 min), 90% ethanol (3 min), 100% ethanol (2 x 3 min) and xylene (2 x 5 min). Slides then mounted, as previously described in section 2.4.4.

2.5 Sigma GenomePlex Whole Genome Amplification

To perform whole genome amplification a Sigma GenomePlex Kit was used (Sigma-Aldrich, Dorset). 1 µl of 10 X fragmentation buffer added to 10 ng template DNA (1 ng/ul) in a PCR tube. Tubes placed in thermal cycler at 95^{o}C for 4 min. Tubes cooled on ice. 1 µl 1 X library preparation buffer added to each tube followed by 1 µl library stabilisation solution. Tubes vortexed and placed in thermal cycler for 2 min at 95^{o}C. Tubes cooled on ice. 1 µl library preparation enzyme added to each sample and tubes vortexed and briefly spun down. Tubes incubated in thermal cycler with the following programme;

16^{o}C of 20 min

24^{o}C for 20 min

37^{o}C for 20 min

75^{o}C for 5 min

4^{o}C hold

Tubes briefly centrifuged and the following master mix was prepared and added to each sample; 7.5 µl 10X amplification master mix

47.5 µl Nuclease-free water

5 µl WGA DNA polymerase

Tubes vortexed, briefly centrifuged and then placed in a thermal cycler with the following programme;

Initial denaturation: 95^{o}C for 3 min

14 cycles of;

Denature: 94^{o}C for 15 s

Anneal/extend: 65^{o}C for 5 min

Samples were stored at -20^{o}C. DNA quality was checked by loading ~5 µl of amplified DNA on a 1.5% agarose gel. Mean DNA fragment size was ~400 bp.

2.6 Fluorescence In Situ Hybridisation (FISH)

FISH was performed on 3 µm paraffin sections on glass slides. Slides were baked in an oven overnight at 60^{o}C. Tonsil sections were used as positive controls for all FISH experiments performed.

Day 1

Slides were placed in a rack then put in xylene for 3 x 5 min then 3 x 5 min in 100% ethanol. Slides were then put in a coplin jar with formalin fixative (10% phosphate buffered formalin, Sigma) for 1 h to fix the tissue. Whilst the slides were in formalin, the steamer was filled with distilled water and the slide container with citrate buffer and switched on to heat the citrate buffer.

After an hour the slides were removed from the formalin fixative and washed in warm running water for 5 min. Slides were placed into the citrate buffer in the steamer for 1 h. After an hour the slides were removed and washed in warm running tap water for 5 minutes. Slides were placed into a coplin with Pepsin (Dako 8 mg/ml, 320 mg in 40 ml 0.1 HCl) for 30 min then washed slides in cold running tap water for 5 min. Slides were rinsed in distilled water then air dried.

Slides were placed in a coplin with Carnoy mild fixative (3 parts 100% methanol to 1 part glacial acetic acid) for 30 min then air dried. 10ul of commercial FISH probe applied and covered with a coverslip. FISH probes used in this study; Vysis 1q25 SpectrumGreen probe and 1p36 SpectrumOrange control probe (Abbott Molecular, Maidenhead, UK), Kreatech *MYCN* (2p24) specific PlatinumBright550 probe plus *LAF* (2q11) PlatinumBright495 control probe (Stretton Scientific, Stretton, UK), Kreatech *p16* (9p21) PlatinumBright550 probe and 9q21 PlatinumBright495 control probe (Stretton Scientific). Slides placed in StatSpin Hybridiser (Dako) at 90^{o}C for 12 min then 37^{o}C overnight.

Day 2

Slides placed in coplin with 2 x SSC for 30 min. Coverslips were removed gently taking care not to disturb the tissue. Slides placed into a coplin jar containing 4 M urea (4 M urea in 2 x SSC) for 2 min then returned to 2 x SSC for 1 min. Slides washed in distilled water for 1 min then air dried. 1 drop of DAPI mounting medium

(Vector Laboratories, Peterborough, UK) applied to a coverslip and the slide placed on top gently. Paint around coverslip with nail varnish to seal in DAPI mounting agent. Slides viewed and photographed on a Leica DMRB microscope with a Nikon camera using NIS Elements (Nikon) software at x100 magnification.

Advice on scoring FISH, particularly in relation to 1q FISH, was given by the Cytogenetics Department at Nottingham City Hospital.

2.7 Quantitative Real Time PCR

Primers for quantitative real time PCR (qPCR) designed using Primer-BLAST, a tool developed by NCBI which uses Primer3 to design primers and then performs a BLAST search to avoid primer set that produce more than just the intended product.

2.7.1 Primer optimisation

A temperature gradient PCR was performed to determine the optimal annealing temperature for primers. A control DNA was used in the PCR with the following master mix:

Reagent	Volume (µl)
Stratagene Brilliant SYBR Green qPCR Master Mix (Agilent Technologies)	12.5
Forward Primer (1 µM)	2.5
Reverse Primer (1 µM)	2.5
H_2O	6.125
DNA (10ng)	1
Reference Dye (1:500) (Agilent Technologies)	0.385

Master mix placed in a PCR tube then put into thermal cycler with the following PCR programme:

Number of Cycles	Time	Temperature (^{o}C)
1	10 min	95
40	30 s	95
	1 min	56-62
1	1 min	72

PCR results were visualised on a 2% agarose gel. The annealing temperature which gives the brightest band on the gel, and therefore the most product, is the optimal temperature for the primers.

Quantitative PCR uses a control gene with a normal copy number (2) in all the tumour samples in the study which is used as a normal to compare the gene of interest to. A normal control DNA is always run alongside tumour DNA to normalise the real time reaction.

2.7.2 Primer Efficiencies

The efficiencies of the primer sets need to be known as two sets of primers, one set for the control gene and one set for the gene of interest, are used in each experiment. To calculate primer efficiency, a serial dilution was set up for each primer set using a range of control DNA concentrations. All experiments were performed in triplicate and the average taken. The same master mix was used as for the temperature gradient PCR.

Table 2.5: Tube set up for qPCR.

	1	**2**	**3**
A	10 ng	10 ng	10 ng
B	5 ng	5 ng	5 ng
C	2.5 ng	2.5 ng	2.5 ng
D	1.25 ng	1.25 ng	1.25 ng
E	0.625 ng	0.625 ng	0.625 ng
F	negative	Negative	negative

With each cycle of PCR SYBR green dye is incorporated into the DNA product and therefore fluorescence can be used to determine the amount of product generated in the reaction.

The results of the efficiency PCR were viewed as an amplification plot (below). Ct values for each dilution were taken from the amplification graph at the point where the amplification curve crossed the fluorescent threshold of 250 Dr.

The average Ct values for each dilution were plotted on an efficiency graph in the program and an efficiency value was calculated (Efficiency=10(-1/gradient of slope)-1).

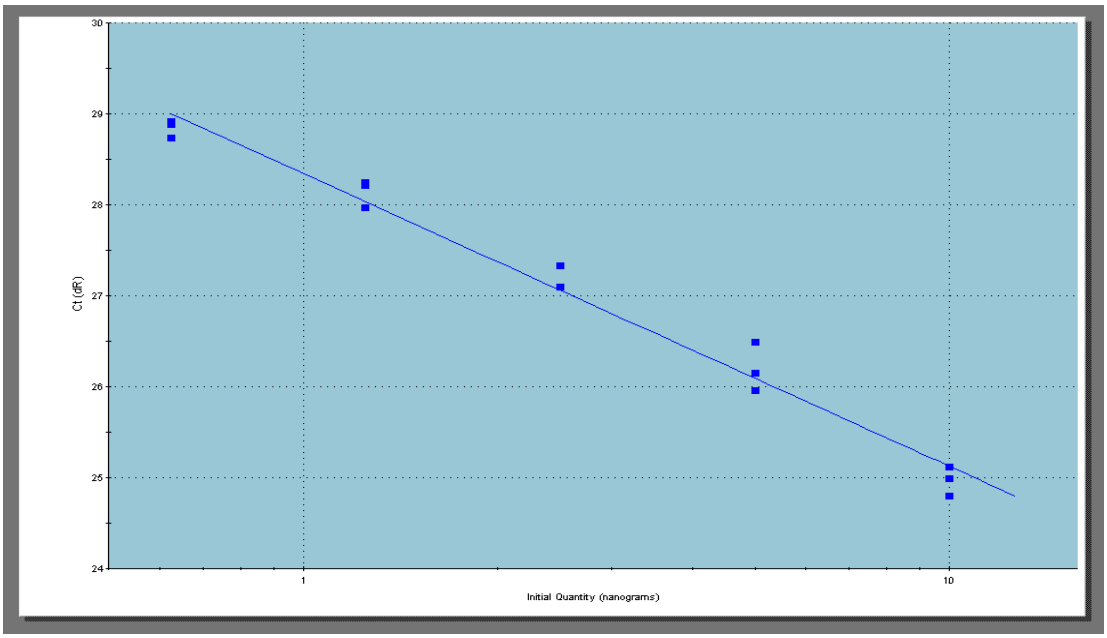

Efficiency Graph

Figure 2.12: qPCR primer efficiency graph.

2.7.3 The Pfaffl equation

The efficiency values are used to calculate fold change of copy number in tumour samples using the Pfaffl equation. The Pfaffl equation is used rather than the more commonly used deltaCt equation as it takes into account primer efficiencies, so primer sets with different efficiencies can be used in the same reaction. For primer efficiencies to be used in the Pfaffl equation, add 1 to the efficiency value.

Pfaffl Equation

$$\text{Fold Change} = \frac{\text{Efficiency target gene}^{(\text{(Ct target gene, control DNA) - (Ct target gene, tumour DNA)})}}{\text{Efficiency control gene}^{(\text{(Ct control gene, control DNA) - (Ct control gene, tumour DNA)})}}$$

The value for fold change was multiplied by two to give a derived copy number for the target gene.

CHAPTER 3

PILOT STUDIES

3.1 SNP array analysis of FFPE DNA

Affymetrix SNP array analysis was carried out on DNA isolated from an FFPE sample. There are many samples in this study that only have formalin-fixed tissue available for molecular analysis. SNP arrays provide the highest resolution molecular analysis and are routinely used with high quality DNA from frozen tissue. To determine if DNA isolated from FFPE tissue would be of sufficient quality for SNP analysis, DNA was isolated from an FFPE CNS PNET sample using Ambion's RecoverAll Total Nucleic Acid Kit for FFPE. The DNA was hybridised to an Affymetrix 100K SNP chip (Affymetrix, Buckinghamshire, UK).

The Affymetrix SNP array protocol involves digestion and ligation of the sample DNA followed by a PCR step. Following the PCR step the DNA concentration is measured using a spectrophotometer. The DNA concentration after the PCR step needs to be 900 ng/µl.

The DNA concentrations after PCR for the DNA isolated from the FFPE sample were;

- FFPE Xba1 sample = 376.43 ng/µl
- FFPE HindIII sample = 355.4 ng/µl

This is well below the required concentration. Two further PCR reactions were needed to reach the required concentration which used up expensive reagents and took a substantial amount of time.

The DNA is then purified and fragmented and then can be run on a gel to check that the fragmentation has been successful.

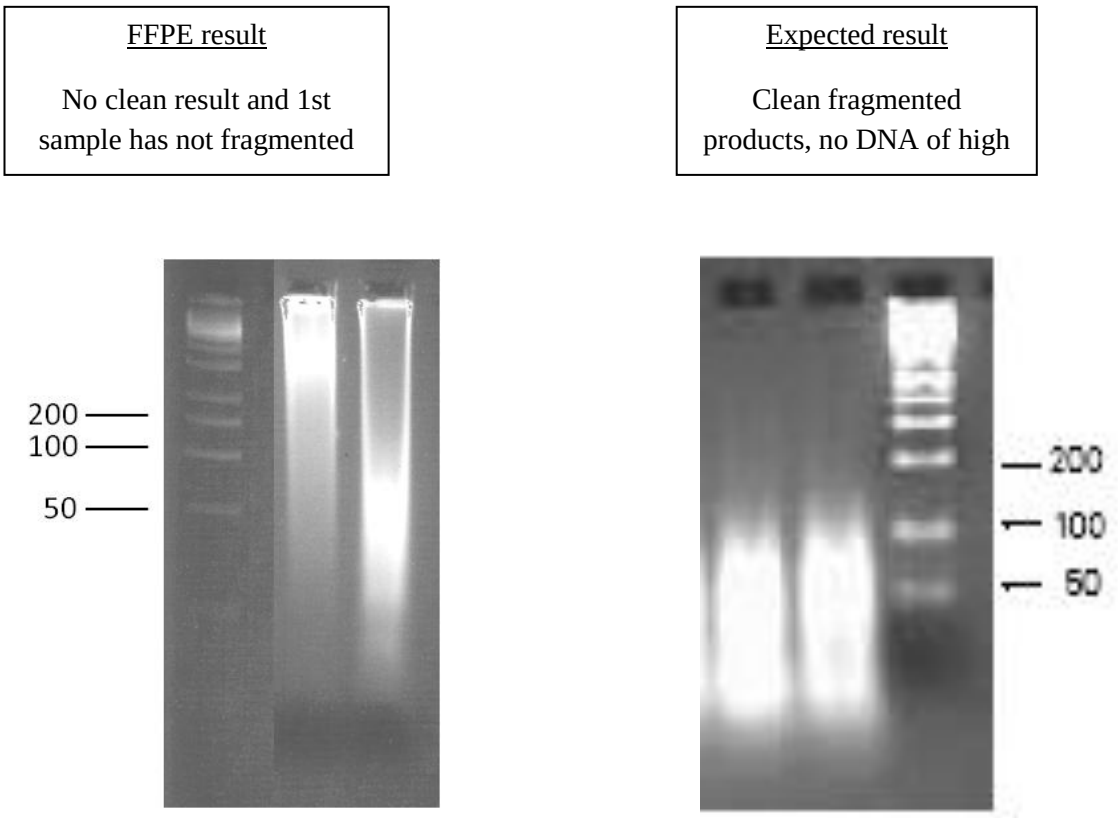

Figure 3.1: Fragmentation gels of FFPE and frozen DNA.

Although the FFPE DNA sample was not passing the QC steps the decision was made to complete the hybridisation and get a final result. The DNA was hybridised to a 100K Affymetrix SNP chip and scanned. The results of the hybridisation were;

1. FFPE HindIII sample = 24.69% SNP call rate.
2. FFPE Xba1 sample = 24.53% SNP call rate.

The SNP call rate (the number of probes with intensity values that can be detected) should be 92% or higher and so no useful information could be determined about the

sample from this result. It was therefore concluded that DNA isolated from FFPE samples was too degraded to be successfully analysed by SNP arrays.

3.2 Pre-Pilot Study

The pre-pilot study was designed to test the quality of results from Agilent's oligo aCGH platform when using DNA isolated from FFPE samples compared to DNA isolated from frozen samples. The purpose of this pre-pilot study was purely to confirm that DNA isolated from a 10 year old FFPE sample would be of sufficient integrity to use for oligo aCGH. The pre-pilot study used four Agilent 44K oligo arrays with the following sample combinations;

Array	Cy3		Cy5
1	Frozen Test Sample DNA	vs.	FFPE Test Sample DNA
2	FFPE Test Sample DNA	vs.	Frozen Test Sample DNA
3	Wilms' tumour pooled blood	vs.	CNS PNET pooled blood
4	CNS PNET pooled blood	vs.	Wilm's tumour pooled blood

The test sample is a CNS PNET tumour that had been hybridised to Affymetrix SNP arrays in a previous study. Using this sample meant that it would be possible to compare the oligo aCGH results with the SNP array results and check that the data corresponded. On arrays 1 and 2 frozen DNA is hybridised against FFPE DNA. There should be no differences between the both samples as DNA was isolated from the same tumour. Therefore any differences can be assumed to be caused by degradation of the DNA isolated from the FFPE sample. Wilms' tumour blood and CNS PNET pooled blood control samples were hybridised on arrays 3 and 4 because many of the HGG samples do not have matched blood and so a pooled blood control would be used. The blood from Wilms' tumour patients and CNS PNET patients

should both be normal (diploid) and so there should be no significant differences between the two blood samples.

On each array there should be no differences between the two samples being hybridised. This means there should be equal binding of each sample to the probes on the array and therefore equal Cy3 and Cy5 signals detected by the scanner. When put into Agilent CGH Analytics Software the visual representation of aberrations should therefore be a straight line.

The figure below shows the oligo aCGH profile of 'frozen vs fixed DNA' (left) and 'blood vs blood' (right). Both profiles are the combined results of dye swaps.

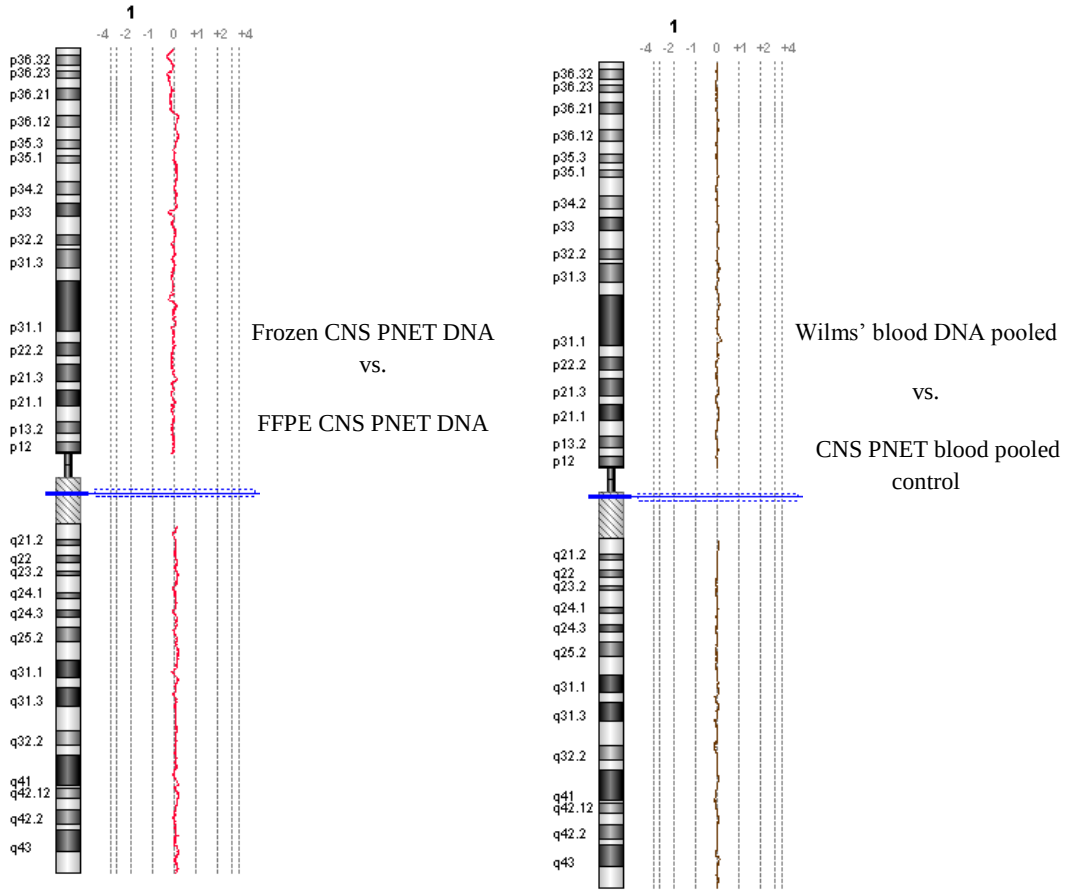

Figure 3.2: aCGH profiles of frozen DNA vs FFPE DNA and Wilms' blood pooled DNA vs CNS PNET pooled blood DNA.

The profile for the 'frozen vs. fixed DNA' is slightly less straight than the 'blood vs. blood profile' and this is probably due to DNA degradation of the DNA from the FFPE sample. However, the profile does not vary considerably from the zero line

which represents a diploid genome and so it was concluded that the FFPE DNA had worked sufficiently well to go ahead with a trial study.

3.3 The Pilot Study

The pilot study was designed to answer a number of questions;

- Are the oligo aCGH results with 'Frozen DNA vs. CNS PNET pooled blood' comparable with 'FFPE DNA vs. CNS PNET pooled blood'?
- Will whole genome amplification of DNA isolated from FFPE samples affect the oligo aCGH results?
- If whole genome amplification is carried out on the sample DNA should it also be performed on the blood control DNA?
- Are the results of oligo aCGH reproducible when using FFPE samples?
- Are the results from oligo aCGH with FFPE tissue comparable with the results from SNP chip analysis with frozen tissue from the same tumour?

To answer these questions the pilot study was designed as below;

Array	**Cy3**		**Cy5**
1	Frozen CNS PNET DNA	vs.	CNS PNET pooled blood
2	CNS PNET pooled blood	vs.	Frozen CNS PNET DNA
3	FFPE CNS PNET DNA	vs.	CNS PNET pooled blood
4	CNS PNET pooled blood	vs.	FFPE CNS PNET DNA
5	WGA FFPE CNS PNET DNA	vs.	CNS PNET pooled blood
6	CNS PNET pooled blood	vs.	WGA FFPE CNS PNET DNA
7	WGA FFPE CNS PNET DNA	vs.	WGA CNS PNET pooled blood
8	WGA CNS PNET pooled blood	vs.	WGA FFPE CNS PNET DNA
9	WGA FFPE CNS PNET DNA	vs.	WGA CNS PNET pooled blood
10	WGA CNS PNET pooled blood	vs.	WGA FFPE CNS PNET DNA

The pilot study was performed on Agilent 105K oligo aCGH arrays, which have a lower resolution (15 Kb) than the 244K arrays that were used in the actual HGG study (6.4 Kb), but a higher resolution than the 44K arrays used in the pre-pilot study (35 Kb). Arrays 1, 2, 3 and 4 addressed the question as to whether profiles produced using FFPE DNA are of a reasonable quality when compared to profiles produced using frozen DNA. Array 5 and 6 showed the affect of whole genome amplification of the sample DNA on the oligo aCGH results. Arrays 7, 8, 9 and 10 showed the effect on the oligo aCGH results of carrying out whole genome amplification on the sample DNA and the control DNA, and also showed how reproducible the results are when using FFPE samples.

Are the oligo aCGH results with 'Frozen DNA vs. s PNET pooled blood' comparable with 'FFPE DNA vs. sPNET pooled blood'?

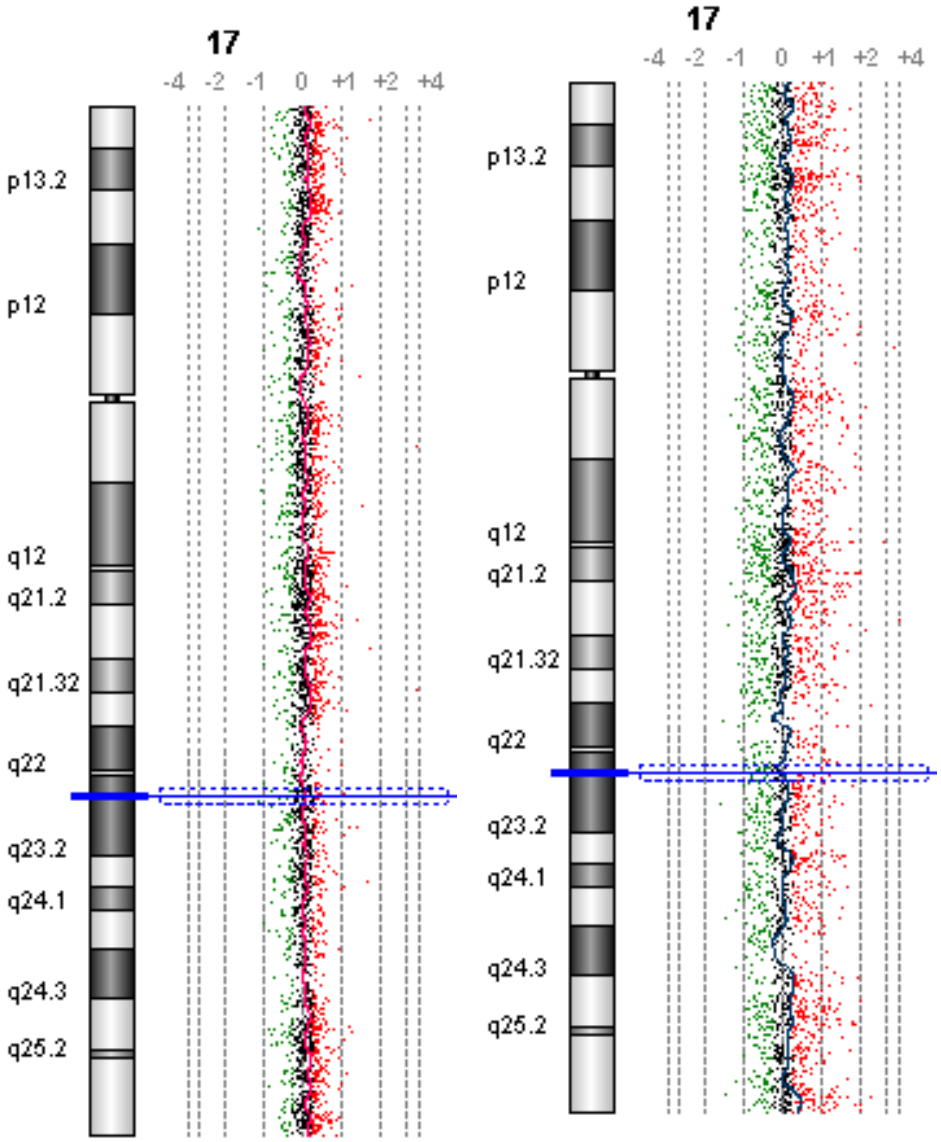

Frozen DNA vs Pooled Blood Control

FFPE DNA vs Pooled Blood Control

Figure 3.3: Comparison between frozen DNA and FFPE DNA profiles.

These two oligo aCGH profiles illustrate the increased noise introduced when using FFPE DNA. However, there are no significant false aberrations on the FFPE DNA profile and so the data are still useful and informative.

Will whole genome amplification of DNA isolated from FFPE samples affect the oligo aCGH results?

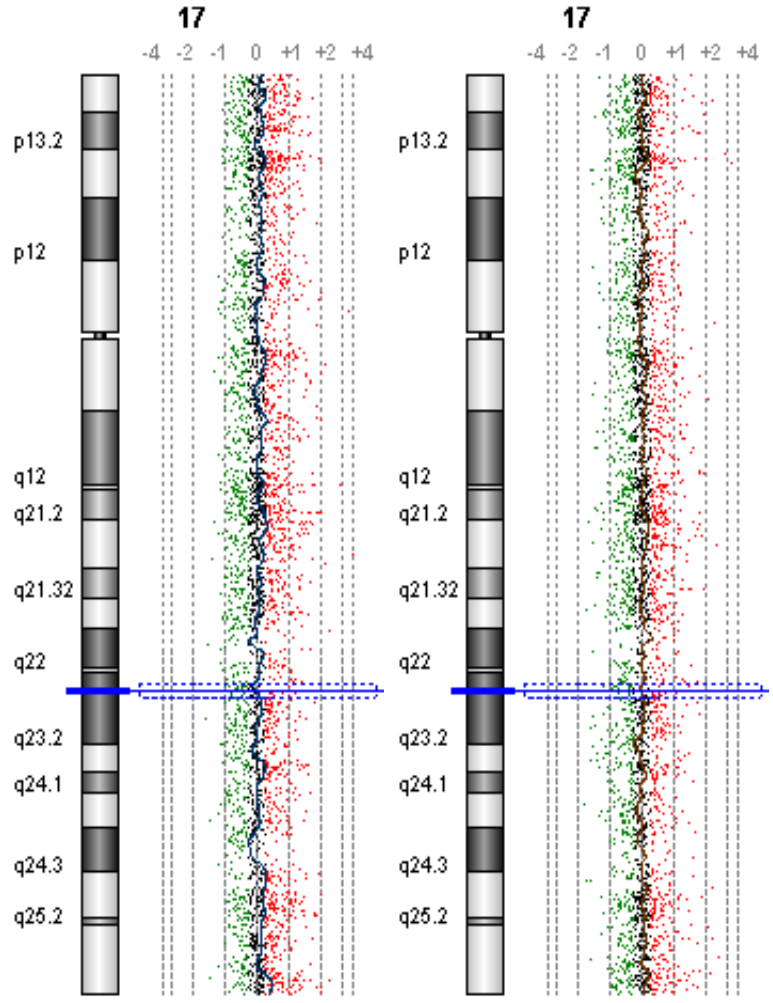

FFPE DNA vs. Pooled blood control

WGA FFPE DNA vs. Pooled blood control

Figure 3.4: The effect of DNA amplification on aCGH profiles.

The profile on the left is non-amplified FFPE DNA and the profile on the right is amplified FFPE DNA. There is hardly any visible difference between the 2 profiles although the noise on the WGA arrays was higher than the non-amplified. However, the 2 profiles are of a comparable quality so where WGA is necessary due to insufficient DNA, oligo aCGH will still generate useful results.

If whole genome amplification is carried out on the sample DNA should it also be performed on the blood control DNA?

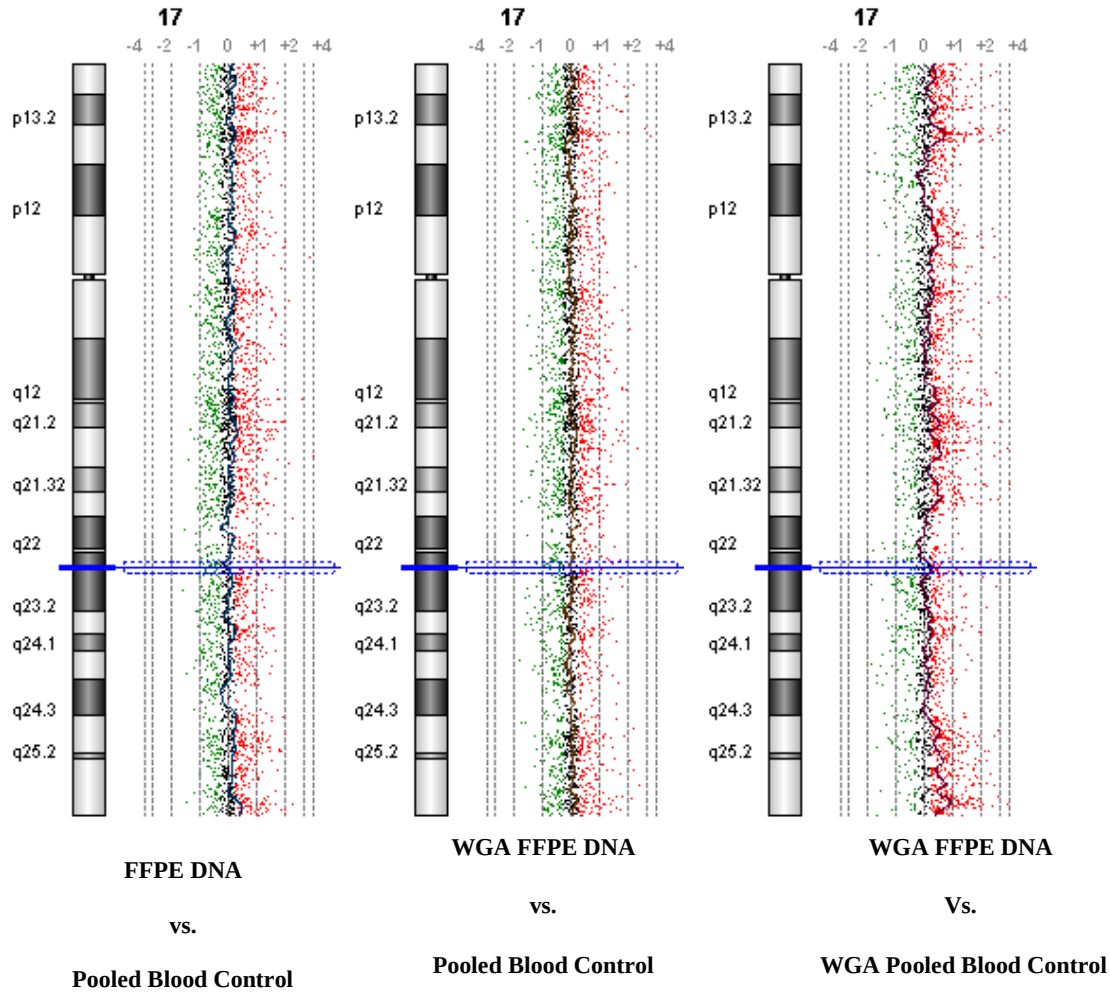

Figure 3.5: The effect of DNA amplification on noise in aCGH.

The array profile on the left had no amplification, the centre array had amplification of the sample DNA, and the array on the right had amplification of both the sample DNA and the control DNA. The 'WGA FFPE DNA vs. WGA pooled blood control' array is visibly noisier than the other 2 profiles, which is the expected outcome as the more amplification the more noise would be predicted. The array profiles for 'FFPE DNA vs. Pooled Blood Control' and 'WGA FFPE DNA vs. Pooled Blood Control' are very similar whilst the 'WGA FFPE DNA vs. WGA pooled blood control' array profile is considerably noisier. Therefore, if there is insufficient sample DNA then

whole genome amplification will be carried out on the sample DNA but not on the blood control DNA to keep noise to a minimum.

Are the results of oligo aCGH reproducible when using FFPE samples?

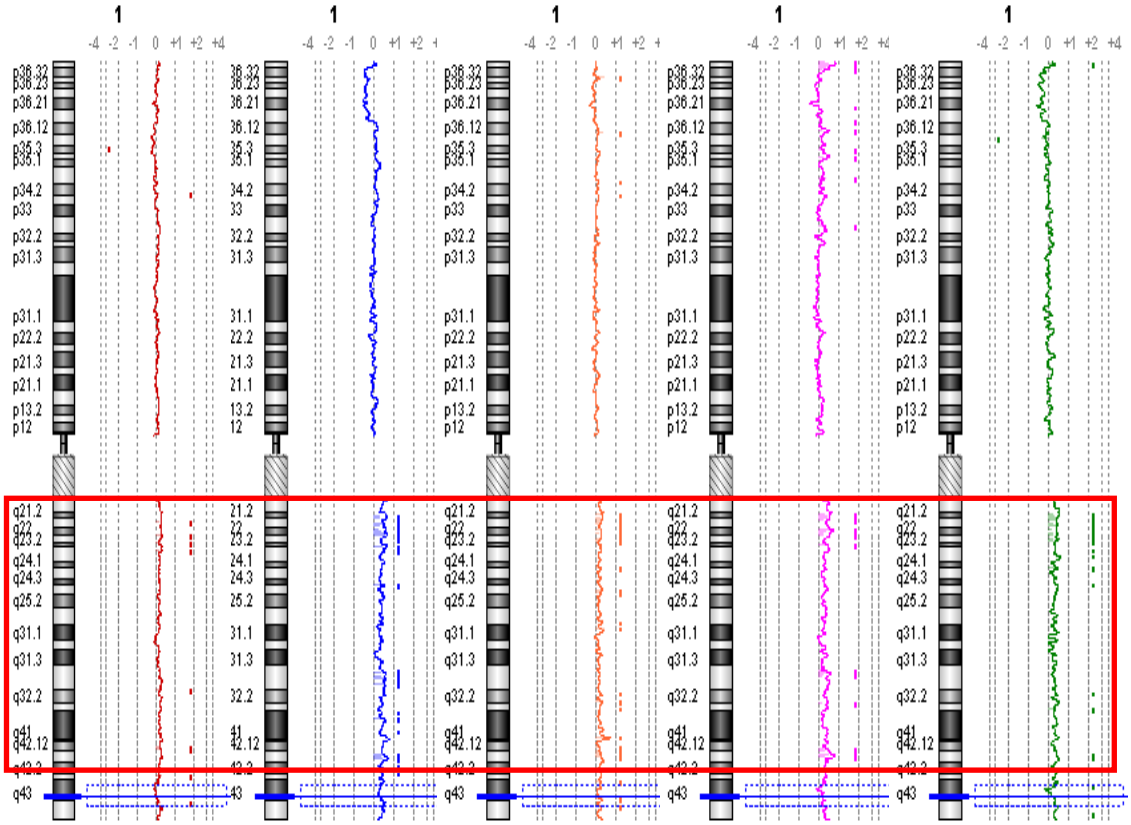

Figure 3.6: The reproducibility of aCGH using FFPE DNA.

The array profiles above show small aberrations on chromosome 1q which have been accurately reproduced on each array run in the pilot study. WGA DNA was used as there was an abundance of WGA DNA available to run on three arrays. Although there is clearly more noise in the FFPE arrays than the frozen array, this figure shows that results of oligo aCGH when using FFPE are highly reproducible.

Are the results from oligo aCGH with FFPE tissue comparable with the results from SNP chip analysis with frozen tissue from the same tumour?

The reasons for completing the pilot study were to establish that DNA isolated from FFPE of considerable age, e.g. 10 years old, would be of sufficient quality for oligo aCGH on Agilent 105K arrays, but also to optimise the oligo aCGH protocol. The results of the pilot study were compared with a list of aberrations generated by SNP array analysis of DNA from a frozen sample from the same tumour. Overall the two methods had identified similar aberrations even though some aberrations seen in the SNP array analysis were not seen in the oligo aCGH analysis. This is to be expected, however, as the resolution of oligo aCGH on 105K arrays is less than SNP 100K arrays and of course poorer quality DNA isolated from FFPE tissue was used as opposed to DNA isolated from frozen tissue.

Conclusion

The pilot study has shown that DNA isolated from FFPE tissue can be of sufficient quality to be used for Agilent oligo array CGH and the results obtained from FFPE DNA are comparable with the ones generated using DNA isolated from frozen material.

CHAPTER 4

SAMPLES

4.1 FFPE samples for oligo aCGH

Primary and recurrent paediatric brain tumour samples were identified for entry into this study from the Children's Cancer and Leukaemia Group (CCLG) and the pathology archives at Birmingham Children's Hospital and the Queen's Medical Centre, Nottingham. All cases were centrally reviewed to determine histological diagnosis according to the 2000 WHO classification. Only cases of WHO grade III and IV gliomas were included in this study.

DNA was isolated from ~80 FFPE high grade glioma samples. Those samples which produced enough DNA for aCGH underwent multiplex PCR, with only those samples producing at least the 200 bp band deemed high enough quality for aCGH. Several brainstem glioma samples were including despite failing the multiplex PCR QC step due to the rarity of these tumours. 38 FFPE samples were analysed by aCGH (Table 4.1).

Table 4.1: 38 FFPE high grade glioma samples were run on Agilent 244K oligo arrays.

Sample	Sex	Age at Diagnosis (yrs)	Location	Resection Status	Sample taken pre/post treatment	Reviewed Diagnosis	Treatment	Survival (Months)
HGG1	M	5.8	Cerebral	Complete	Pre-treatment	GBM	CT+RT	5
HGG2	M	7.3	Cerebral	Complete	Post-treatment	GBM	RT	6
HGG3	M	4	Cerebral	Subtotal	Pre-treatment	GBM	CT	3
HGG4	M	6	Cerebral	Complete	Post-treatment	GBM	RT+CT	12
HGG5	M	1	Cerebral	Biopsy	Pre-treatment	GBM	CT	27
HGG6	F	1.2	Posterior fossa	Subtotal	Pre-treatment	GBM	CT	>168
HGG7	M	14.1	DIPG	Biopsy	Pre-treatment	GBM	-	-
HGG8	F	6.7	Cerebral	Subtotal	Post-treatment	GBM	RT	24
HGG9	M	17.3	DIPG	Biopsy	Pre-treatment	LGA	-	127
HGG10	M	-	Cerebral	Subtotal	Post-treatment	GBM	CT	-
HGG11	F	7.8	DIPG	Post mortem	Post-treatment	GBM	CT+RT	5
HGG12	M	8.8	Cerebral	Complete	Pre-treatment	AA	RT	>108
HGG13	M	8.1	DIPG	Biopsy	Pre-	GBM	RT	9

					treatment			
HGG14	M	16.1	DIPG	Biopsy	Pre-treatment	GBM	-	35
HGG15	M	-	Cerebral	Subtotal	Pre-treatment	AA	CT+RT	-
HGG16	M	3.1	-	-	Post-treatment	AO	-	21
HGG17	M	18.9	Frontal lobe	Subtotal	Pre-treatment	GBM	CT+RT	21
HGG18	M	12	Parietal lobe	Subtotal	Pre-treatment	GBM	CT+RT	>78
HGG19	F	3.8	DIPG	Biopsy	Pre-treatment	GBM	RT	15
HGG20	M	12.5	DIPG	Biopsy	Pre-treatment	GBM	-	1
HGG21	M	12.6	DIPG	Biopsy	Pre-treatment	GBM	CT+RT	16
HGG22	M	-	Frontal	Biopsy	Pre-treatment	GBM	CT	1
HGG23	F	5.8	Chiasm	Subtotal	Pre-treatment	GBM	CT	>70
HGG24	F	2.4	Frontal lobe	Subtotal	Pre-treatment	AA	CT	>88
HGG25	M	16.7	Parietal lobe	Complete	Pre-treatment	GBM	RT	>34
HGG26	M	2.7	Frontal lobe	Subtotal	Pre-treatment	AO	CT+RT	>46
HGG27	F	7.3	Posterior Fossa	Biopsy	Pre-treatment	AO	-	-
HGG28	M	7.3	DIPG	Biopsy	Pre-treatment	GBM	CT+RT	10
HGG29	M	0.1	Cerebral	Subtotal	Pre-treatment	GBM	-	4
HGG30	M	12.8	Thalamus	Subtotal	Pre-treatment	GBM	CT+RT	48
HGG31	F	4.5	Frontal lobe	Complete	Pre-treatment	GBM	CT+RT	20
HGG32	F	4.5	Frontal lobe	Complete	Post-treatment	GBM	CT+RT	20
HGG33	M	2.9	Frontal lobe	Complete	Post-treatment	GBM	RT	15
HGG34	M	10.1	Cerebral	Subtotal	Pre-treatment	GBM	CT+RT	11
HGG35	F	5.6	DIPG	Biopsy	Pre-treatment	GBM	CT	11
HGG36	M	12.3	DIPG	Biopsy	Pre-treatment	GBM	RT	8
HGG37	M	4.5	DIPG	Post mortem	Post-treatment	GBM	CT+RT	5
HGG38	M	13.3	DIPG	Post mortem	Post-treatment	GBM	CT+RT	7

GBM= glioblastoma, AA= anaplastic astrocytoma, AO= anaplastic oligodendroglioma, LGA=low grade astrocytoma, DIPG = diffuse intrinsic pontine glioma.

The samples used for the aCGH study were 19 GBMs, three AO, three AA and 13 brainstem gliomas. aCGH data for the 38 FFPE samples is publically available from NCBI's GenBank database, accession number GSE21420

The results were analysed using Agilent CGH Analytics Software version 3.1.14 (Agilent Technologies). As expected DNA isolated from FFPE samples was of poorer quality than freshly extracted DNA due to the extensive cross-links formed between nucleic acids and proteins within cells by the formalin-fixation method. Pilot studies have shown that DNA isolated from FFPE tissue can be of sufficient quality to produce reliable, reproducible data that is comparable with results generated using DNA isolated from frozen tissue, using Agilent Oligo Array CGH. A multiplex PCR was used as a quality control (QC) step to make sure DNA samples were of sufficient quality for oligo array comparative genomic hybridisation (aCGH).

The majority of the samples analysed by aCGH had passed the QC PCR step and so had produced a PCR product of 200bp or greater. However, a number of samples that were brainstem tumours were analysed by aCGH without having passed this QC step because of the rarity of these samples.

CGH Analytics has a number of in-built QC measures. The most important QC measure for low quality DNA is the Derivative Log Ratio spread (DLR spread). The DLR spread calculates the differences between the log2 ratio values of adjacent probes, and so gives a measure of noise. The DLR spreads for the combined dye swaps of all the FFPE samples run are displayed in the table below.

Table 4.2: Multiplex PCR results and DLR Spreads of 38 HGG Samples.

Sample	Multiplex PCR	DLR Spread
HGG1	400bp	0.61
HGG2	200bp	0.56
HGG3	400bp	0.37
HGG4	400bp	0.30
HGG5	200bp	0.82
HGG6	200bp	0.63
HGG7	400bp	0.32
HGG8	300bp	0.39
HGG9	300bp	0.50

HGG10	400bp	0.36
HGG11	400bp	0.70
HGG12	300bp	0.57
HGG13	no pcr	0.90
HGG14	no pcr	0.91
HGG15	no pcr	1.03
HGG16	400bp	0.54
HGG17	400bp	0.47
HGG18	400bp	0.70
HGG19	no bands	0.61
HGG20	300bp	0.51
HGG21	300bp	0.43
HGG22	200bp	0.39
HGG23	200bp	0.35
HGG24	400bp	0.33
HGG25	200bp	0.41
HGG26	400bp	0.43
HGG27	300bp	0.62
HGG28	400bp	0.34
HGG29	200bp	0.71
HGG30	200bp	0.46
HGG31	400bp	0.47
HGG32	300bp	0.38
HGG33	400bp	0.63
HGG34	400bp	0.40
HGG35	200bp	0.61
HGG36	no pcr	1.02
HGG37	no pcr	0.54

HGG38	no pcr	0.80

As expected, the DLR spread values vary widely between samples. The samples which, on average, gave the best results in the QC PCR step have the lower DLR spreads, i.e. have the lowest level of noise. Agilent guidelines suggest that good quality FFPE samples should give a DLR spread of <0.4. Most of the samples fall within or just outside the acceptable DLR spread range according to the Agilent protocol, however a number of samples do not. These very noisy samples were carefully analysed to determine whether there was any usable data. CGH Analytics uses various filters and algorithms to filter out 'noise' in a variety of ways. For noisy data, such as the data in the study from degraded DNA samples, the z-score algorithm is the most appropriate.

Due to the wide range in DLR spread across the samples in this study, the samples were divided into three groups depending of their DLR spread value with group 1 being the cleanest and group 3 being the noisiest. The settings for the noise filters and z-score algorithm were altered slightly for each group meaning the noisiest samples could have more stringent noise filtering than the good quality samples. This also meant that small aberrations in the clean samples were not lost by applying overly stringent filters to those samples.

Table 4.3: Groups based on DLR spread

Group	Z-score Threshold	Minimum number of aberrant probes	Minimum number of aberrant regions
1	3.5	3	100
2	3.5	4	100
3	4.0	4	100

4.2: Tissue MicroArrays (TMAs)

The high grade glioma TMAs were constructed from 152 FFPE samples. Areas of viable and representative tumour following review of paraffin blocks were marked by the reviewing pathologist before inclusion into the TMA. 3 x 0.6mm cores were included for each tumour. TMAs are an efficient way to screen large numbers of FFPE tumour samples for specific aberrations in copy number and expression levels. The TMAs were used in this study for FISH and IHC experiments.

Table 4.4 TMA samples clinical information

Sample	Sex	Age at Diagnosis (yrs)	Tumour Site	Resection Partial/Complete	Reviewed diagnosis	Primary/ Recurrence	Treatment	Survival Time (Months)
1	M	2.3	Parietal Lobe	Subtotal	GBM	Primary	CT	3
2	-	-	-	-	GBM	Primary	-	-
3	F	8.1	Frontal Lobe	Subtotal	SC GBM	Post ALL	-	3
4	F	14.3	Parietal Lobe	Subtotal	GBM	Primary	CT+RT	20
5	F	4.3	Temporal Lobe	Complete	GBM	Primary	CT+RT	24
6	F	9.2	Frontal lobe	Biopsy	GBM	Post ALL (post radiation)	CT+RT	29
7	F	4.3	Parietal Lobe	Subtotal	GBM	Primary	RT	30
8	M	1.1	Parietal Lobe	Subtotal	GBM	Primary	-	
9	M	4.7	Occipital Lobe	Subtotal	GBM	Primary	CT+RT	4
10	M	9.3	Frontal lobe	Complete	GBM	Primary	CT+RT	29
11	M	-	-	Subtotal	GBM	1st recurrence	-	-
12	M	10.2	Temporal Lobe	Complete	GBM	Primary	CT+RT	7
13	M	2.9	Frontal lobe	Total	GBM	Primary	CT	15
14	F	3.6	Frontal lobe	Subtotal	GC GBM	Primary	CT	-
15	M	7.3	Thalamus	Subtotal	GBM	Primary	RT	-
16	M	9.8	Frontal lobe	Subtotal	GBM	Primary	CT+RT	12
17	M	6.7	Frontal lobe	Subtotal	AA	Primary	RT	7
18	M	8.4	Brain Stem/Pons	Biopsy	GBM	Primary		2
19	M	10.9	Frontal lobe	Complete	GBM	Primary	CT+RT	4
20	M	-	Frontal lobe	Subtotal	AA	Primary		3
21	M	4.8	Brain Stem/Pons	Biopsy	GBM	Primary	RT	6
22	M	10.1	Cerebral	Subtotal	GBM	Primary	CT+RT	-
23	M	-	-	-	GBM	-	-	-
24	M	-	-	-	GBM	-	-	-
25	F	8.5	Thalamus	Biopsy	AA	Primary	CT+RT	15
26	F	4.5	Frontal lobe	Complete	GBM	Primary	CT+RT	20
27	F	-	Frontal lobe	Complete	GBM	1st recurrence	-	-

28	F	3.3	Temporal Lobe	Subtotal	HGG	Primary	-	3
29	M	12.3	Brain Stem/Pons	Biopsy	GBM	Primary	RT	8
30	F	7.6	Thalamus	-	AA	Primary	-	0
31	F	-	Parietal Lobe	-	GBM	Primary	-	0
32	F	4.3	Temporal Lobe	Complete	GBM	Primary	CT+RT	24
33	M	7.7	Pineal Gland	Biopsy	GBM	Primary	CT	5
34	M		Pineal Gland	Subtotal	GBM	1st recurrence	-	-
35	M	12.8	Thalamus	Subtotal	GBM	Primary	CT+RT	-
36	M	-	-	-	GBM	1st recurrence	-	-
37	M	7.3	Brain Stem/Pons	Biopsy	GBM	Primary	CT+RT	10
38	M	-	Frontal lobe	Complete	GBM	1st recurrence	RT	-
39	M	-	Frontal lobe	-	GBM	-	-	-
40	F	-	Frontal lobe	Subtotal	GC GBM	Primary second op	-	-
41	M	9.0	Temporal Lobe	-	AA	Primary	-	-
42	M	-	Temporal Lobe	Complete	AA	1st recurrence	CT	-
43	M	0.1	Cerebral	Subtotal	GBM	Primary	-	4
44	F	5.6	Brain Stem/Pons	Biopsy	GBM	Primary	CT	11
45	F	5.7	Brain Stem/Pons	Subtotal	GBM	Primary	-	5
46	M	14.1	Cerebral	Subtotal	GBM	Primary	RT	-
47	-	-	Cerebral	Subtotal	GBM	1st recurrence	CT	-
48	M	1.0	Cerebral	Biopsy	GBM	Primary	CT	27
49	M	2.4	Cerebral	Complete	GBM	1st recurrence	CT	10
50	M	2.5	Cerebral	Complete	GBM	-	CT	9
51	M	2.8	Cerebral	Complete	AA	Primary	CT	-
52	F	2.0	Cerebral	Subtotal	AA	Primary	CT	-
53	M	5.8	Cerebral	Complete	GBM	Primary	CT+RT	5
54	M	5.8	Cerebral	Complete	GBM	Primary	CT+RT	5
55	M	7.3	Cerebrum	Complete	GBM	post ALL (post radiation)	CT+RT	6
56	M	3.8	Cerebral	Biopsy	GBM	Primary	CT	5
57	M	4.3	Brain	Biopsy	Gliomatosis cerebri grade III	Primary	CT	16
58	F	8.1	Cerebral	-	GBM	-	-	-
59	M	13.1	Cerebral	-	Gliomatosis cerebri grade III	-	-	-
60	M	1.8	Brain	Biopsy	GBM	Primary	CT	3
61	M	4.0	Cerebral	Subtotal	GBM	Primary	CT	3
62	M	0.5	Cerebral	Biopsy	GBM	Primary	-	-
63	M	6.5	Cerebral	Complete	GBM	1st recurrence	CT+RT	12
64	F	12.3	Brain	Biopsy	AA	Primary	CT+RT	-
65	F	16.3	Brain	Biopsy	GBM	Primary	CT+RT	15
66	F	14.1	Cerebral	Complete	GBM	Primary	CT+RT	8
67	F	0.7	Brain stem	Biopsy	AA	Primary	CT+RT	89
68	F	1.2	Posterior fossa	Subtotal	GBM	Primary	CT	-
69	F	10.6	Brain stem	Biopsy	AA	Primary	CT+RT	18

70	F	15.3	-	-	GBM	-	-	-
71	F	4.6	-	Biopsy	small cell GBM	Primary	-	-
72	M	10.1	Brain	Biopsy	AA	Primary	CT+RT	10
73	M	4.3	Spine	Complete	GBM	Primary	CT+RT	-
74	F	18.8	Cerebral	Subtotal	AA	Primary	-	-
75	M	0.0	Brain	Biopsy	AA	Primary	CT	-
76	F	6.7	Cerebral	Subtotal	GBM	1st recurrence	RT	24
77	M	-	right occipital lobe	Subtotal	GBM	-	CT	-
78	M	-	right parietal	Complete	small cell GBM	Primary	RT	-
79	F	-	temporal parietal lobe	Biopsy	GBM	Post C. ALL (1986)	RT	-
80	M	16.6	cerebellum	Complete	GBM	Primary	CT	-
81		0.0	-	Complete	GBM	Primary	-	-
82	F	-	hypothalamic	Subtotal	GBM	Primary	CT	-
83	M	-	brainstem	Complete	GBM	Primary	RT	-
84	M	-	Temporal Lobe	Complete	AA	1st recurrence	CT	-
85	M	6.7	Frontal lobe	Subtotal	GBM	Primary	RT	7
86	M	-	cerebellum	Biopsy	AA	Primary	RT	-
87	F	-	right thalamus/midbrain	Biopsy	AA	Primary	RT	-
88	M	-	spinal cord	Complete	GBM	Primary	RT	-
89	M	10.7	left parietal	Complete	AA	Primary	CT+RT	-
90	M	-	Brain stem	Biopsy	LGA	Primary	-	-
91	F	-	Brainstem	Biopsy	BSG	Primary	CT+RT	-
92	M	-	brainstem	Biopsy	AO	Primary	-	-
93	M	-	Brain stem	Subtotal	BSG	Primary	At LRI	-
94	M	-	Cerebral	Subtotal	AA	Primary	CT+RT	-
95	F	-	Brain stem	Biopsy	BSG	Primary	-	-
96	M	-	cerebellum	Complete	BSG	Primary	-	-
97	F	-	Brain stem	Biopsy	BSG	Primary	RT	-
98	M	-	-	Subtotal	BSG	Primary	-	-
99	M	-	cerebral	Complete	AA	Primary	RT	-
100	F	-	Brain stem	Biopsy	LGA	Primary	-	-
101	M	0.7	Brain stem	-	BSG	Primary	CT	-
102	F	-	Brain stem	Biopsy	LGA	Primary	CT+RT	-
103	F	-	cerebral	Complete	AO	Primary	CT	-
104	-	-	-	Complete	LGA	Recurrence	-	-
105	M	7.0	Cerebral	Complete	Anaplastic pleomorphic xantroastrocytoma	Primary	RT	-
106	F	14.0	R Parieto-occipital	Subtotal	AO	Primary	CT+RT	-
107	M	17.1	L Basal Ganglia	Biopsy	AA	Primary	CT	-
108	M	18.9	R Frontal lobe	Subtotal	GBM	Primary	CT+RT	-
109	M	12.0	L Parietal lobe	Subtotal	GBM	Primary	CT+RT	-
110	M	12.5	Brain stem	Biopsy	BSG		-	-
111	M	13.0	Brain stem	Biopsy	BSG	Primary	RT	-

112	M	19.6	Brain stem	Biopsy	BSG	Primary	CT+RT	-
113	M	12.6	Brain stem/cerebellum	Biopsy	BSG	Primary	CT+RT	-
114	F	3.8	Brain stem	Biopsy	BSG	Primary	RT	-
115	M	3.3	Brain stem	Subtotal	BSG	Primary	RT	-
116	F	5.8	Chiasm	Subtotal	GBM	primary	CT	>70
117	-	0.0	-	-	GBM	-	-	-
118	M	2.7	Frontal	Subtotal	AO	primary	CT+RT	>46
119	M	0.6	Frontal	Biopsy	GBM	primary	CT	1
120	-	0.0	-	-	Gliomatosis cerebri III	-	-	-
121	F	2.4	Frontal	Subtotal	AA	primary	CT	>88
122	-	0.0	-	-	AO	-	-	-
123	M	16.7	Parietal	Complete	GBM	primary	RT	>34
124	M	5.2	Suprasellar	Biopsy	AA	Primary	-	-
125	F	5.5	Suprasellar	Complete	AA	Primary	-	-
126	M	10.3	Frontal lobe	Biopsy	GBM	Recurrence	-	-
127	M	17.3	Frontal lobe	Biopsy	AO	Primary	-	-
128	F	7.3	Posterior Fossa	Biopsy	AO	Primary	-	-
129	M	8.4	Brain Stem/Pons	Biopsy	GBM	Primary	-	2
130	F	5.7	Brain Stem/Pons	Subtotal	GBM	Primary	-	5
131	M	7.3	Brain Stem/Pons	Biopsy	GBM	Primary	CT+RT	10
132	M	9.8	Suprasellar (corpus callosum)	Biopsy	AA	Primary	CT	-
133	F	15.7	Diffuse right frontal lobe	Biopsy	AA	Primary	CT	-
134	-	0.0	-	-	GBM	-	-	-
135	-	0.0	-	-	GBM	Primary	-	-
136	-	0.0	-	-	AO	-	-	-
137	M	1.6	right fronto-temporal lobe	-	AO	Primary	-	-
138	-	2.6	-	-	AO	1st recurrence	-	-
139	-	3.1	-	-	AO	-	-	-
140	-		-	-	DIPG	-	-	-

GBM=glioblastoma, AA=anaplastic astrocytoma, AO=anaplastic oligodendroglioma, DIPG=diffuse intrinsic pontine glioma, BSG=brainstem glioma, LGA=low grade astrocytoma, - = information unknown.

The majority of samples used for the aCGH analysis were included in the TMA (35/38). The table below lists the FFPE samples included in the aCGH study alongside the corresponding location of the samples on the TMA.

Table 4.5: Location of aCGH Samples on the TMAs.

FFPE Sample for aCGH	Location on TMA
HGG1	TMA 53
HGG2	TMA 55
HGG3	TMA 61
HGG4	TMA 63
HGG5	TMA 48
HGG6	TMA 68
HGG7	TMA 96
HGG8	TMA 76
HGG9	TMA 90
HGG10	TMA 47
HGG11	TMA 140
HGG12	TMA 99
HGG13	not on TMA
HGG14	TMA 93
HGG15	TMA 94
HGG16	TMA 139
HGG17	TMA 108
HGG18	TMA 109
HGG19	TMA 114
HGG20	TMA 110
HGG21	TMA 113
HGG22	TMA 119
HGG23	TMA 116
HGG24	TMA 121
HGG25	TMA 123
HGG26	TMA 118
HGG27	TMA 128
HGG28	TMA 131
HGG29	TMA 43
HGG30	TMA 35
HGG31	TMA 26
HGG32	TMA 27
HGG33	TMA 38
HGG34	TMA 22
HGG35	TMA 44
HGG36	TMA 29
HGG37	not on TMA
HGG38	not on TMA

CHAPTER 5

GENOME WIDE ANALYSIS

5.1 Excel analysis of chromosome arm aberrations

A summary of chromosome arm gains and losses was compiled using the original text files generated by the Agilent software 'Feature Extraction' version 9.5.3.1. Text files were modified in Microsoft Excel and then split into separate chromosome files. Each probe on the array is given a $\log_2$ ratio value by the Feature Extraction software. A gain of one copy of a gene has a $\log_2$ ratio of 0.58 (3/2 ratio), a gain of two copies has a $\log_2$ ratio of 1 (4/2 ratio), etc. Because the data are from FFPE DNA there is a level of noise which has to be taken into account. The samples are split into 3 groups depended on the DLR spread, which is basically a measure of noise. Group 1 samples are the least noisy samples and group 3 the noisiest.

Table 5.1: Cut Off Levels for Probe Gains and Losses;

	Loss cut off (log2ratio)	Gain cut off (log2ratio)
Group 1	< -0.51	> 0.3
Group 2 & 3	< -0.6	> 0.25

Excel work-flow

- Values in original txt file generated by Feature Extraction are log10.

Convert log10 to log2; log10 to linear: 10^x

In excel: =POWER(10,REF)

Linear to log2: $\frac{\ln(n)}{\ln 2 = \log 2}$

In excel: =LOG(REF,2)

- Dye swap txt files (log2 ratios) combined: =((REF1+(-REF2))/2)

To summarise arm gains and losses;

- Log2 ratios copied into an excel worksheet matched with probes and chromosomal location.

FORMULAS; (using group1 values)

Probes on **whole** chromosome: COUNTA(REF1:REFEND)

Probes on **p** arm: COUNTA(REF1:REFp)

Probes on **q** arm: COUNTA(REFq:REFEND)

% Probes lost on whole chromosome:
COUNTIF(REF1:REFEND,<”0.51”)/**whole***100

% Probes lost on p arm: COUNTIF(REF1:REFp,<”0.51”)/**p***100

% Probes lost on q arm: COUNTIF(REFq:REFEND,<”0.51”)/**q***100

% Probes gained on whole chromosome:
COUNTIF(REF1:REFEND,>”0.3”)/**whole***100

% Probes gained on p arm: COUNTIF(REF1:REFp,>”0.3”)/**p***100

% Probes gained on q arm: COUNTIF(REFq:REFEND,>”0.3”)/**q***100

A cut-off level of 50% was used to determine arm gain or loss, i.e. 50% or more of the probes on a chromosome arm would have to show gain for the whole arm to be classed as gained. Chromosome arm gain and loss in the 38 FFPE samples is displayed in table 5.2.

Table 5.2: Chromosome arm gain and losses from Excel analysis.

Chromosome Arm	Gain (%)	Loss (%)
1p	0	8
1q	21	0
2p	3	0
2q	3	0
3p	0	3
3q	3	3
4p	0	3
4q	3	8
5p	8	3
5q	3	5
6p	0	3
6q	3	5
7p	3	0
7q	3	0
8p	0	3
8q	3	3
9p	5	5
9q	5	0
10p	0	5
10q	0	10
11p	0	0

11q	0	0
12p	5	3
12q	5	0
13q	3	10
14q	0	5
15q	3	0
16p	3	5
16q	0	8
17p	8	3
17q	8	0
18p	0	8
18q	3	3
19p	15	0
19q	8	0
20p	0	3
20q	3	0
21p	10	8
21q	0	5
22q	3	3

Chromosome 1q is gained in 21% of samples, and has been shown to be gained in other paediatric brain tumours. Other noticeable gains are 19p (15%), 17p and q (8%), 21p (10%). Noticeable losses are 1p (8%), 10q (10%), 13q (10%). It is worth noting that chromosomes 19, 20, 21 and 22 have higher noise levels in the array CGH data compared to the other chromosomes, which may account for the high values for these chromosome arm gains and losses. Noise levels can vary from chromosome to chromosome due to the location of the probes within the chromosomes and the probe design.

5.2 CGH Analytics analysis of chromosome arm aberrations

Calculating arm gain/loss in Microsoft Excel had the advantage of having definite numerical cut off values for gain or loss of individual probes and so for chromosome arms. However, in excel there are no noise filters and no way of centralising the data as in CGH Analytics. Because of this a visual analysis of chromosome arm gain and loss was looked at in CGH Analytics.

The samples were separated into three groups based on their DLR spread and appropriate probe filters and z-score level applied (previously described). Every chromosome for each sample was looked at individually and if it appeared that over half the arm was lost or gained then it was noted as a whole arm loss or gain.

There are various ways of viewing chromosome arms in CGH Analytics. The ‘chromosome view’ shows an individual chromosome for one or a number of samples.

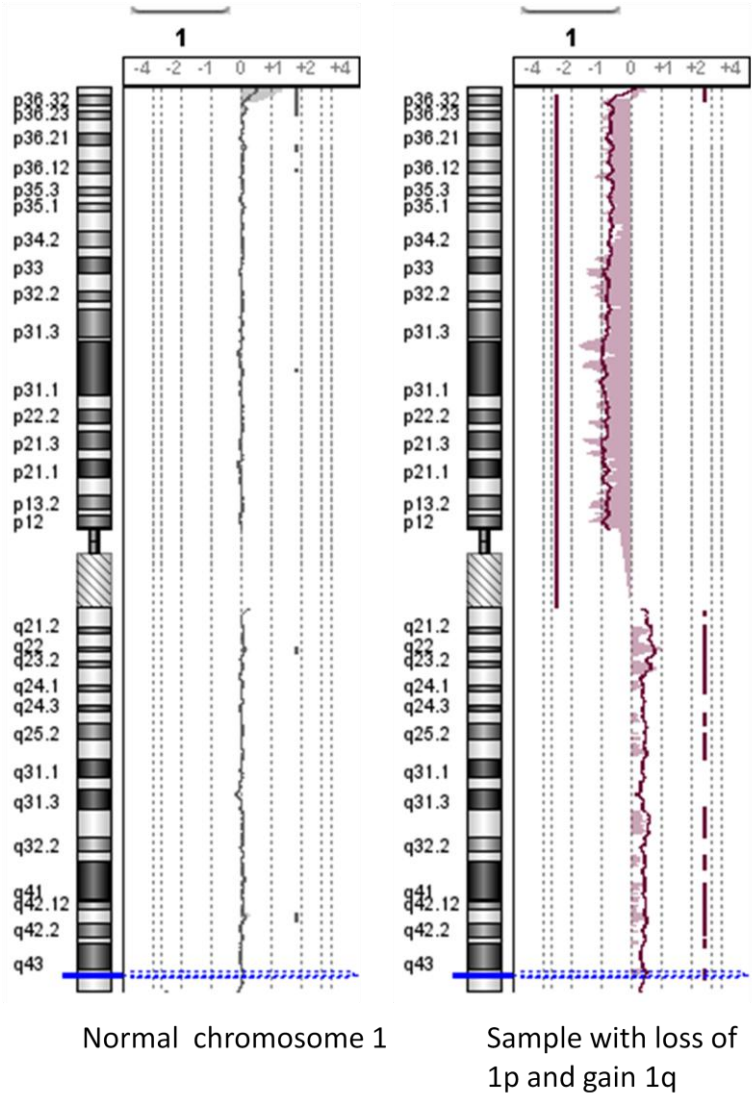

Figure 5.1: Chromosome view showing normal and aberrant chromosome 1.

The continuous wavy line represents the 'moving average' of the log2ratio values of the probes on the array. On the chromosome view showing the normal, balanced chromosome 1 (copy number 2), the moving average follows the '0' line meaning that there is no difference between the tumour sample and the control sample. On the right hand chromosome view, the moving average line moves away from the 0 line into the negative values on 1p and then into positive values on 1q. This represents a loss of 1p and gain of 1q. The shaded areas beneath the moving average line and the solid straight lines alongside the moving average line show the aberrant regions, as defined by the filters applied by the user.

CGH analytics can generate heat maps of individual chromosomes for a selected group of samples, e.g. chromosome 1 below: (red is gain, green is loss)

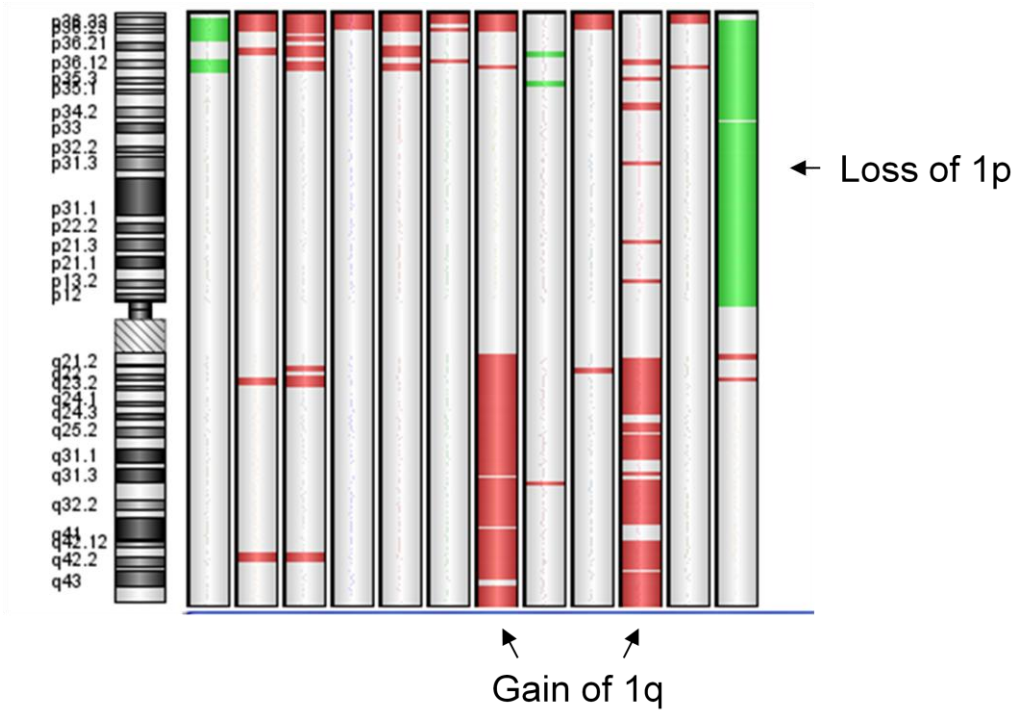

Figure 5.2: Heatmap of chromosome 1.

Having the ability to look at the data visually is useful for noisy data as it is often obvious where an aberration is 'real' or is due to a handful of probes in a noisy region.

Using both the chromosome view and heat maps generated by CGH Analytics a summary of chromosome arm gain/loss in the 38 FFPE samples was generated.

Table 5.3: Chromosome arm gains and losses from CGH Analytics analysis.

Chromosome Arm	Gain (%)	Loss (%)
1p		8
1q	22	
2p	3	
2q	3	3
3p	3	
3q		3
4p		3
4q		8
5p	11	3
5q	3	5
6p	8	3
6q	5	11
7p	5	
7q	8	
8p		5
8q	3	
9p	8	
9q	5	
10p		5
10q		18
11p		3
11q		3
12p	5	3
12q	3	3
13p		
13q		11

14q		13
15q	3	8
16p	5	11
16q		13
17p	8	13
17q	11	5
18p		8
18q		3
19p	3	11
19q	3	11
20p	5	3
20q	5	3
21p		
21q		3
22p		
22q	5	13

5.3 Excel vs CGH Analytics

Overall, both methods of determining chromosome arm gain/loss have given very similar results for the majority of chromosome arms. Gain of 1q is the most common chromosome aberration in both cases, with loss of 10q being the second most common. Where there are discrepancies between the two methods, they are minor for most chromosomes. However, results for 6p, 19p, 19q, 21p and 22q are different for the two methods.

By CGH Analytics analysis, three samples had gain of 6p but by the Excel calculation no samples had gain of 6p. The gains of 6p seen in CGH Analytics were not of the whole arm, but the majority of the arm. As 50% of the probes had to be gained in the excel calculations to call the arm as ‘gained’, even though more than

half the arm was shown to be gained in CGH Analytics the noise in the data may have led to less than 50% of the probes on the arm having log2ratio values above the 'gain' cut off.

Chromosome 19 was the noisiest chromosome in this study. This was predicted by Agilent, the company who produce the oligo arrays used in this study, as designing probes for chromosome 19 is notoriously difficult. The discrepancy between the results for chromosome 19 arm gains/losses by CGH Analytics and Excel can be explained by the noise on this chromosome. The same is true for chromosome arm 21p, but to a lesser extent. The excel calculations showed 10% samples having gain of 21p and 8% having loss, whilst CGH Analytics showed no gain or loss for 21p. The noise filters and centralisation algorithms that can be applied to the data in CGH Analytics can remove noise that may lead to false gains/losses, as shown on 21p.

Loss of 22q was seen in 13% samples in CGH Analytics, but only 3% samples in Excel. In many cases, the majority but not all of 22q was lost and as with 6p and so the cut off for chromosome arm loss in Excel may have been too stringent to call the arm as lost.

The CGH Analytics analysis gives a more accurate representation of chromosome arm gain/loss as it is able to take into account noise and more importantly, can centralise the data by finding the most common log2ratio and so remove the false chromosome loss seen in the Excel analysis. Therefore, the CGH Analytics data will be used in further discussion and analyses.

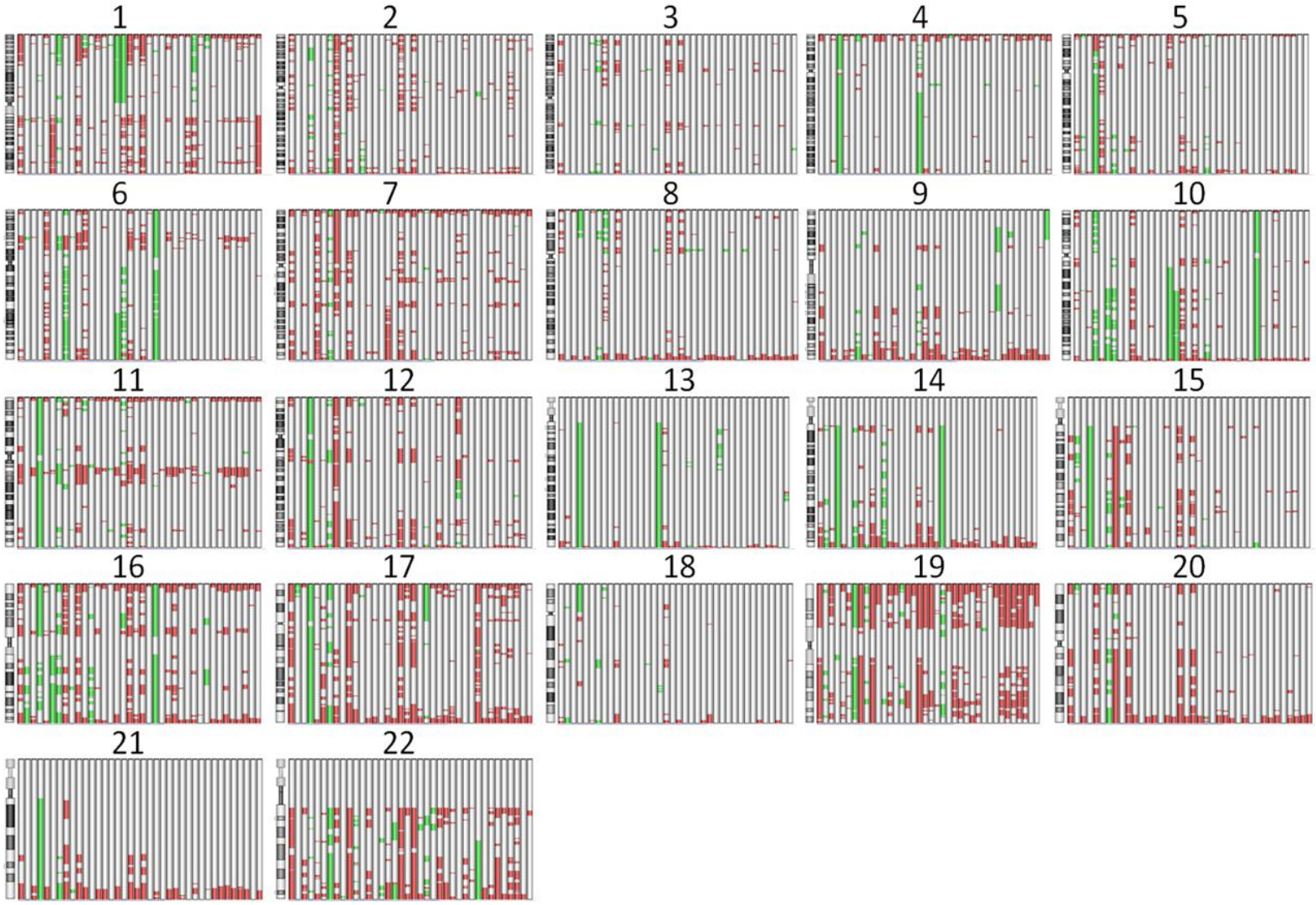

Figure 5.3: Ideogram of the 38 FFPE samples analysed by aCGH. Regions of loss are highlighted in green and regions of gain highlighted in red.

Chromosome arm gains and loss were seen across the genome (Figure 5.3). Some samples had numerous whole arm aberrations whilst other samples showed none (Table 5.4).

Table 5.4: Chromosome arm gain and loss in 38 HGG samples.

Sample	Gain	Loss
HGG1	17p, 17q	
HGG2	1q, 12p	13q
HGG3		
HGG4	17p, 17q	9p, 10p, 10q, 22q
HGG5		
HGG6		
HGG7	5p, 5q, 6p, 6q, 7p, 7q, 20p, 20q	
HGG8		
HGG9		
HGG10	1q	9p
HGG11	17p	14q
HGG12		
HGG13	1q	14q, 16p, 16q, 17p
HGG14		
HGG15		
HGG16	1q, 17q	10q, 16q
HGG17	1q, 9q	4q, 9p, 3q, 10q
HGG18	22q	
HGG19		
HGG20	1q	1p, 4q, 6q, 10q, 13q
HGG21		
HGG22	5p, 7q	1p, 6q, 10q
HGG23		
HGG24	16p, 16q	
HGG25	2p, 2q, 3p, 5p, 6p, 7p, 7q, 8q, 12p, 12q, 15q, 16p, 16q, 17q, 19p, 19q, 20p, 20q	6q, 8p,
HGG26	6p, 6q	22q
HGG27	1q	
HGG28		6p, 6q, 14q, 16p, 16q, 17p, 19p, 19q, 22q
HGG29	22q	
HGG30	5p	4p, 4q, 5q, 8p, 10p, 10q, 11p, 11q, 12p, 12q, 13q, 14q, 15q, 16p, 17p, 17q, 18p, 19p, 19q, 21q, 22q
HGG31		

HGG32		
HGG33		
HGG34		
HGG35	1q	1p
HGG36		16p, 16q, 17p, 17q, 19p, 19q, 20q, 22q
HGG37		5p, 5q, 13q, 14q, 15q, 16q, 17p, 18p, 18q, 19p, 19q, 20p
HGG38	9q	5q, 18p

p = the short arm of the chromosome, q = the long arm of the chromosome.

Overall, loss was more common than gain with 82 chromosome arms lost compared to 52 gained.15/38 samples showed no chromosome arm gains or losses, whilst three samples showed 10 or more chromosome arm aberrations. It has been previously reported that tumours occurring in younger children have less genomic copy number aberrations than those in older children. 12/15 samples with no chromosome arm aberrations had 'age at diagnosis' data available, and 5/12 (42%) samples were in children under five years. Of the 23 samples with chromosome arm aberrations 22 had 'age at diagnosis' data available and 6/22 (27%) samples were from children under five.

There is one primary/recurrent pair within the data set; samples HGG31 (primary) and HGG32 (recurrence). Both the primary and recurrent tumour had no chromosome arm aberrations.

5.4 Chromosome arm aberrations in brainstem gliomas

Chromosome arm aberrations in brainstem gliomas are displayed in Table 5.5.

Table 5.5: Chromosome arm gain and loss in 13 brainstem tumours.

Sample	Gain	Loss
HGG7	5p,5q,6p,6q,7p,7q,20p,20q	
HGG9		
HGG11	17p	14q
HGG13	1q	14q,16p,16q,17p
HGG14		
HGG19		
HGG20	1q	1p,4q,6q,10q,13q
HGG21		
HGG28		6p,6q,14q,16p,16q,17p,19p,19q,22q
HGG35	1q	1p
HGG36		16p,16q,17p,17q,19p,19q,20q,22q
HGG37		5p,5q,13q,14q,15q,16q,17p,18p,18q,19p,19q,20p
HGG38	9q	5q,18p

p = the short arm of the chromosome, q = the long arm of the chromosome.

As with the other high grade gliomas, there is a wide variety in frequency of chromosome arm gain/loss in the brainstem tumours. Four of the 13 brainstem tumours show no chromosome arm aberrations whilst one sample shows more than ten arm aberrations. There a number of notable differences between the frequencies of chromosome arm aberrations in brainstem gliomas and non-brainstem high grade gliomas. 10q, which is frequently lost in adult high grade gliomas, is lost in 18% of all high grade tumours but only 1/13 (8%) brainstem gliomas. Across all the samples in this study there are five losses of 17p with four of those losses occurring in brainstem gliomas. Therefore, 4/13 (31%) of the brainstem gliomas samples have loss of 17p compared to 1/25 (4%) in the rest of the high grade glioma cohort (see

Figure 5.4). 14q is lost in four of the 13 brainstem gliomas (31%) but only one of the non-brainstem tumours.

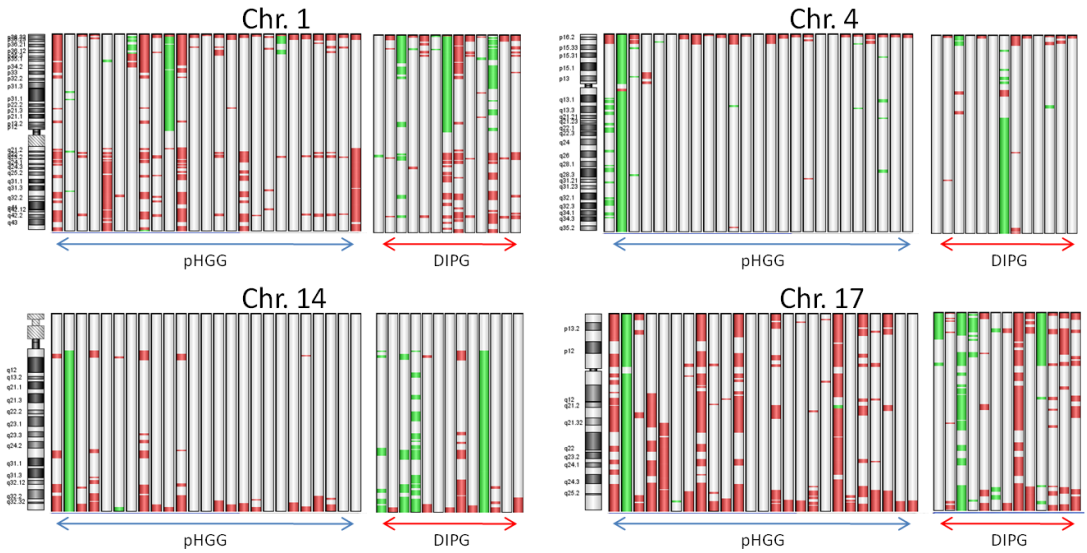

Figure 5.4: Ideogram showing all areas of gain and loss on chromosomes 1, 4, 14 and 17 in 25 high grade glioma samples and 13 DIPG. Red indicates regions of gain and green indicates regions of loss.

5.5 Discussion

High resolution aCGH analysis of pHGG samples has identified widespread chromosome arm gains and losses. This study includes the largest cohort of brainstem gliomas to date (13) plus 25 non-brainstem high grade gliomas. By comparing brainstem and non-brainstem HGG some site related differences in chromosome arm aberrations were found. Overall, 39% of chromosome arm aberrations were gains and 61% were losses. The higher frequency of chromosome arm losses suggests that the mechanism of oncogenesis in these tumours is most commonly loss of tumour suppressor genes. However, aCGH only shows copy number alterations, and recent studies have shown mutations and epigenetics alterations to be important in oncogenesis. Therefore, the mechanisms of oncogenesis in these tumours can not be completely determined from aCGH data.

Gain of 1q has been previously reported as the most common whole chromosome arm abnormality in paediatric high grade glioma, as seen in this study. Gain of 1q is commonly seen in paediatric brain tumours including CNS PNETs, ependymoma and high grade glioma (Dyer, Prebble et al. 2002; Pfister, Remke et al. 2007; Paugh, Qu et al. 2010). In this study 22% of high grade gliomas demonstrated gain of 1q whilst only 9% of adult high grade gliomas have been reported to have gain 1q (TCGA 2008). A similar pattern of high frequency of 1q gain in children compared to adult tumours is seen in ependymoma (Dyer, Prebble et al. 2002). 23% of brainstem tumours in this study have gain of 1q which is comparable to the level of gain seen in other paediatric high grade glioma. Why 1q gain is seen so frequently in paediatric tumours is unknown although certain genes have been implicated as being the oncogenic culprits. The gene *MUC1* (1q21) has been suggested as a potentially important oncogene in CNS PNETs, and gain of MUC1 was shown to be associated with poor prognosis in these tumours (Pomeroy, Tamayo et al. 2002). Gain of 1q has been associated with poorer outcome in other paediatric brain tumours (Dyer, Prebble et al. 2002; Mendrzyk, Korshunov et al. 2006).

Loss of 10q is seen in 18% of all high grade glioma samples in this study (5/25 (20%) non-brainstem gliomas and 1/13 (8%) brainstem gliomas), which is notably lower than 35% loss of 10q previously reported in paediatric high grade glioma (Paugh, Qu et al. 2010). Loss of 10q is the most common whole arm aberration in adult GBM (80%) which includes loss of *PTEN* (10q23). The difference between the frequency of 10q loss in pHGG in this study (6/38) compared to adult HGG (152/189) is statistically significant ($p = 0.0001$). *PTEN* is a tumour suppressor which negatively regulates the Akt signalling pathway and *PTEN* loss or mutation is seen in many cancers (Maher, Furnari et al. 2001). The differential lack of 10q loss in this cohort, and particularly in the brainstem tumours, may indicate a different mechanism of loss or that different pathways are involved in these paediatric tumours and this has implications for therapy. However, aCGH does not allow for LOH analysis so it is possible that LOH of 10q is present in some samples. The quality of the FFPE DNA used in this study may also account for minor differences in the frequency of aberrations seen in this study compared to SNP array studies using DNA from frozen samples.

17p loss was seen in 13% tumours overall. Loss of 17p is seen in many tumours and 17p13.1 is the location of the well characterised tumour suppressor gene *p53*, which has been widely implicated in cancer. (King 2000) Mutation of *p53* has been reported in adult high grade glioma but less so in paediatric high grade glioma, especially in children under three, indicating that there is another mechanism of loss of function of *p53* in paediatric tumours (Pollack, Finkelstein et al. 2001; Paugh, Qu et al. 2010). Indeed, the high frequency of loss of 17p in the brainstem tumours indicates loss of the 17p arm is the mechanism for the loss of at least one copy of *p53* in this subset of tumours. In medulloblastoma loss of 17p is seen in up to 50% of samples with focal loss often seen at 17p13.2 (De Smaele, Di Marcotullio et al. 2004). The gene *KCTD11*, located at 17p13.2 has been recently identified as a suppressor of Hedgehog (HH) signalling which is mainly involved in embryonic patterning and tissue differentiation (De Smaele, Di Marcotullio et al. 2004). The expression of KCTD11 is normally restricted to embryonal development and neurogenesis and loss of *KCTD11* may lead to deregulation of the HH pathway and therefore promote tumour proliferation (De Smaele, Di Marcotullio et al. 2004). 17p

loss was seen in 4/13 (31%) brainstem tumours and just 1/25 (4%) non-brainstem tumour and so appears to be associated with infratentorial tumours although sample numbers are not high enough for this to be significant. Interesting, 17p loss is associated with medulloblastoma but not with supratentorial CNS PNETs.

14q loss was seen in 4/13 (31%) brainstem tumours but only 1/25 non-brainstem tumour (4%). Interestingly, the non-brainstem glioma with loss of 17p was the same non-brainstem sample with loss of 14q. This sample, HGG30, is a GBM located in the thalamus. A recent report by Zarghooni et al also saw 17p loss and 14q loss associated with paediatric brainstem tumours compared to non-brainstem high grade gliomas (Zarghooni, Bartels et al. 2010).

Loss of 13q was seen in 11% of samples in this study which is notably lower than the loss of 13q in 35% samples as reported recently by Paugh et al, but is still amongst the most common arm aberrations (Paugh, Qu et al. 2010). 13q14.2 is the location of the *RB1* gene, a well characterised tumour suppressor gene that has been implicated in paediatric brain tumours including gliomas. RB1 was the first tumour suppressor gene identified, and loss of RB1 function is the cause of retinoblastoma (King 2000). The majority of adult HGG have disruption of the RB pathway, frequently due to loss of *RB1* (see section 1.5.3). Disruption of the RB pathway is thought to be associated with the marked increase in cell proliferation seen in the transformation from low grade to high grade glioma in adults (Ohgaki 2005; Wong, Tsang et al. 2006).

Loss of 16q was seen in 13% tumours and has also been reported lost in CNS PNETs and medulloblastoma (Lo, Rossi et al. 2007; Pfister, Remke et al. 2007). 16q is the location of a number of potential tumour suppressor genes including *WWOX* (16q23.3-24.1) which had been implicated in a variety of cancers (Ramos and Aldaz 2006; Hezova, Ehrmann et al. 2007; Jenner, Leone et al. 2007). *WWOX* is involved in inducing apoptosis and is known to regulate the WNT pathway (Ramos and Aldaz 2006).

Loss of 22q is seen in 13% of tumours in this study and is the location of the tumour suppressor gene *NF2* (22q12.2). *NF2* mutations are associated with neurofibromatosis type 2, a syndrome characterised by tumours of the CNS. NF2 is highly expressed during embryonic development whilst in adults expression is localised to nerves, Schwann cells and the meninges (Evans 2009). Neurofibromatosis type 2 is associated with schwannomas, meningiomas and ependymomas but not HGG, whilst sufferers of neurofibromatosis type 1 can develop HGG and brainstem gliomas (see section 1.3.1).

CHAPTER 6

FOCAL GENOMIC CHANGES

6.1 Identifying aberrant regions

Oligo array CGH data was analysed using Agilent's 'CGH Analytics' software, version 3.5.14. (Agilent Technologies) The data was analysed in a variety of ways using CGH Analytics. The software allows for visual analysis down to the probe level and also generates gene lists for small aberrant regions, individual samples and for the most commonly gained and lost genes across the sample set.

Although CGH Analytics is able to generate summary gene lists from the data, the poor quality DNA used on this study meant some areas of certain chromosomes were consistently noisy. Therefore, when gene lists were generated through the program the most commonly aberrant genes were those in persistently noisy areas, i.e. telomeric regions and chromosome 19. Because of this a visual analysis of each chromosome of every sample was performed in CGH Analytics using the chromosome view and gene view display. This visual analysis allows for a closer look at the log2ratios of the probes in regions that have been called 'aberrant' by the software to see if the aberration is real. If an aberrant region was deemed to be 'real' through visual analysis, a small gene list was generated for that region. All these small gene lists were collated to give a final gene list. This list, together with information on the function of the genes from Pubmed, was used to create a final gene list for further study.

Table 6.1: Regions of Gain/Loss identified in CGH Analytics.

Chromosome Region	Genes of Interest in Region	Gain	Loss
1p36	*CDC42, WNT4*		2
1q22	*CLK2*	1	
1q42	*WNT3A, ARF1*	2	
2p24.1	*MYCN*	2	
2p24-22	*MTA3, SIX2/3, MAP4K3, RAB10, CAD*		1
2q12	*MAP4K4,AFF3, REV1*	1	1
3q25	*NMD3*		3
4q11-13	*PDGFRA, KIT, CLOCK*	3	
4q13.2	*UGT2B15, UGT2B17*		2
6p21	*TAP1, TAP2*	3	1
6q26-27	*QKI, PACRG*	1	
7p15	*HOXA1-13*	1	
7q36	*CDK55, MLL3*	1	
8p11.23	*ADAM3A*		6
8p23	*MSRA, MFHAS1*		1
9p22	*CDKN2A, CDKN2B, MTAP*		4
10q11.22	*ANXA8*	1	
11q13	*CCND1, FGF3, FGF4*	13	1
11q13.4	*RSF1, PAK1, WNT11*	1	
12q13	*CDK4*	3	
13q22	*KLF12, MYCBP2*		1
16p12.2	*ARHGAP17, PRKCB, PALB2*		1
17q21.2	No genes in region		1
20p21.1	*FLRT3*		1

Genes highlighted in red were used for validation studies.

6.1.1 Gene List

The genes from the aberrant regions that will be target for further study are displayed in Table 6.2 below:

Table 6.2: Gene list generated by analysis in CGH Analytics.

Chromosome	**Gene**	**Deletion (% samples)**	**Gain (% samples)**
chr2	*MYCN*	0	5
chr4	*PDGFRA*	0	8
chr6	*QKI*	0	3
chr8	*ADAM3A*	15	0
chr9	*CDKN2A*	10	0
chr9	*CDKN2B*	10	0
chr11	*CCND1*	0	33
chr11	*FGF3*	0	33
chr12	*CDK4*	0	8

6.2 Visual Analysis in CGH Analytics

6.2.1 Amplified regions

Four different regions of high level amplifications were seen across the 38 samples; 2p24.1 (*MYCN*), 4q12 (*PDGFRA* and *KIT*), 6q26-27(*QKI*) and 11q13 (*CCND1* and *FGF3*).

High level amplification of *MYCN* on 2p24.1 was seen in two samples, one brainstem glioma (HGG20) and one GBM (HGG15) (Figure 6.1).

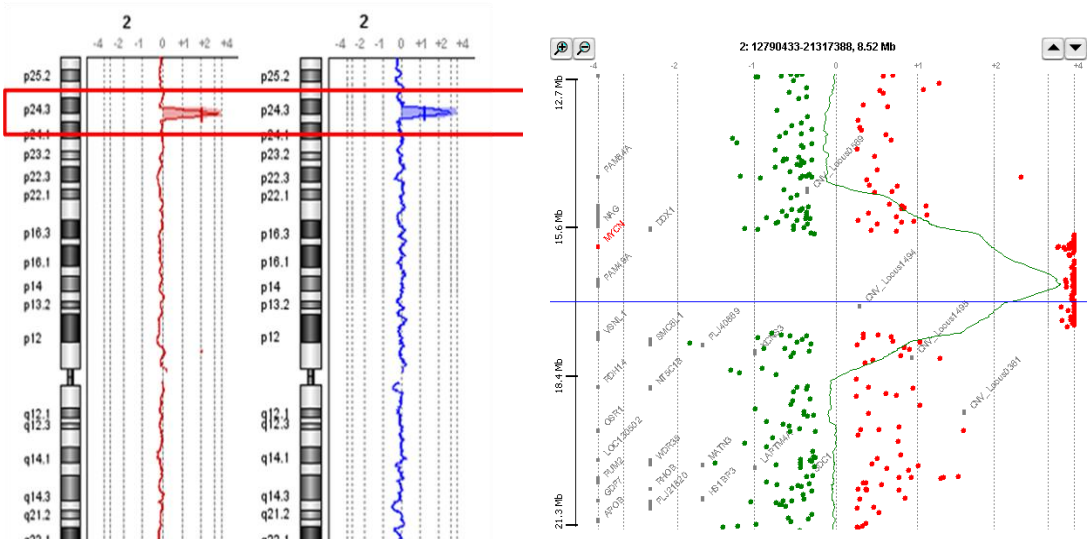

Figure 6.1: Chromosome views showing amplification of *MYCN* in samples HGG20 (left) and HGG15 (right). Gene view showing probes for amplified region to the far right of the zero line, indicating high level amplification.

Whilst HGG20 has a moderately good DLR spread, HGG15 is very noisy with a DLR spread of 1.03 and yet the amplification of *MYCN* is still clear.

Amplification of 4q was seen in 3 samples, although the size of the amplified region and therefore the genes involved varies between the samples (Figure 6.2).

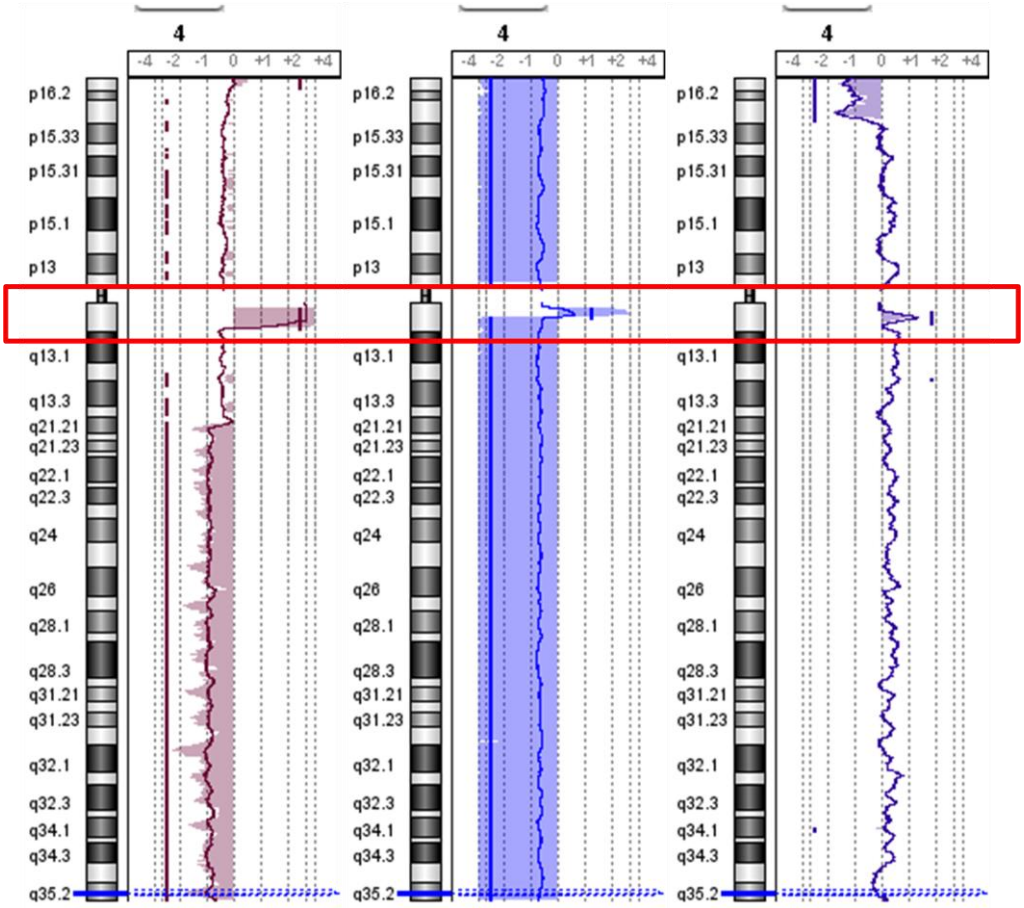

Figure 6.2: Amplification of *PDGFRA* in sample HGG20, HGG30 and HGG36 (left to right).

In sample HGG20 the region of high level amplification covers genes including *PDGFRA* and *KIT*. In HGG30 PDGFRA is amplified whilst *KIT* is not. HGG36 has low level amplification of both *PDGFRA* and *KIT*. Interestingly, in HGG20 and HGG30 *PDGFRA* amplification is seen alongside loss of the majority of 4q. Samples HGG20 and HGG36 are brainstem gliomas and HGG30 is a GBM.

Amplification at 6q26-27 is seen in just one sample, HGG20 (Figure 6.3). This high level amplification includes the gene *QKI* which is involved in RNA splicing and protein translation. *QKI* has also been implicated in oligodendrocyte formation and myelination in the CNS.

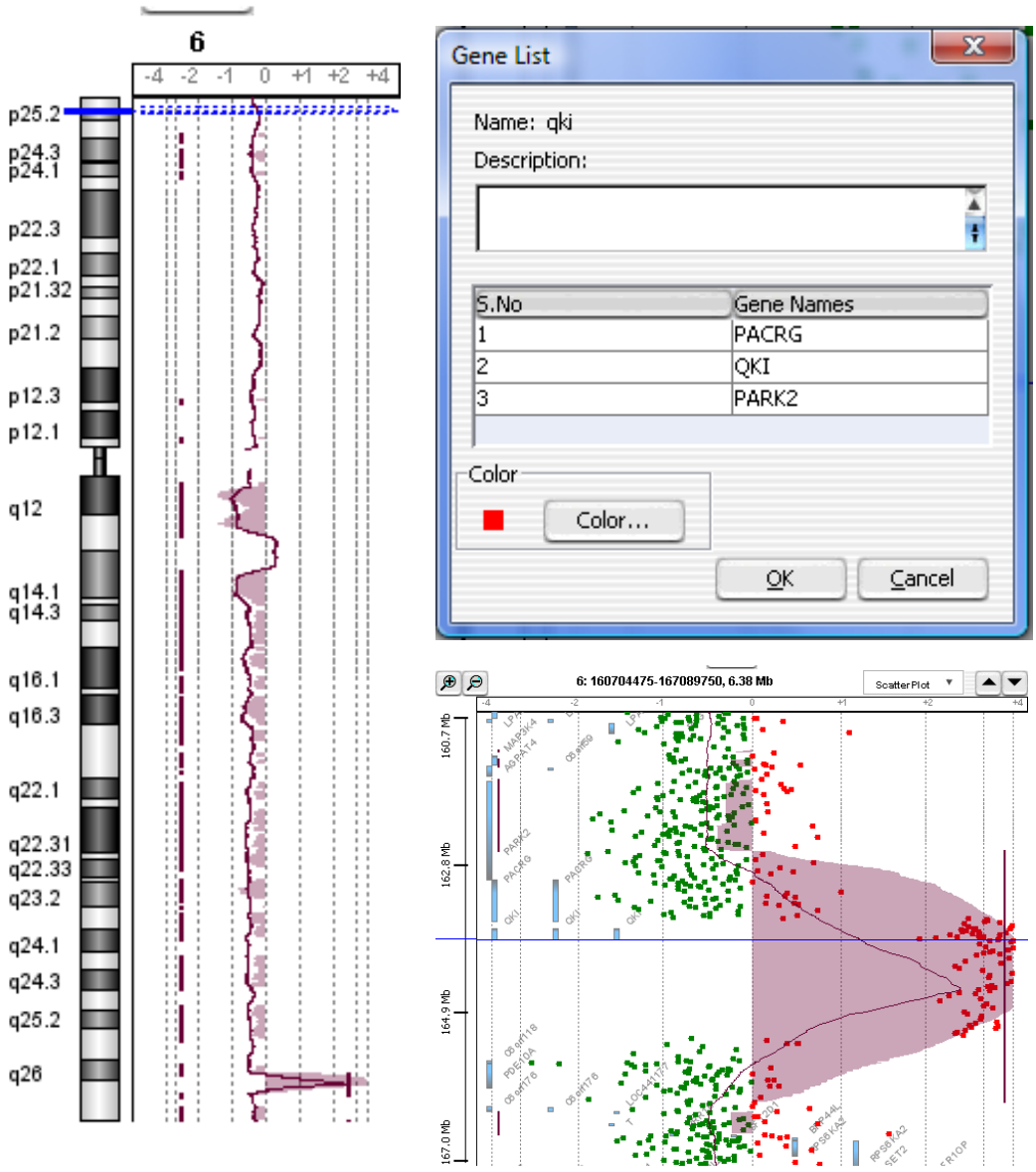

Figure 6.3: Chromosome view of chromosome 6 of HGG20 showing loss of 6q with amplification at 6q26. The gene list shows three genes in the region including *QKI*. The gene view shows the probes in the amplified region to the far right of the zero line, indicating high level amplification.

This discrete high level amplification is seen in conjunction with the loss of the majority of 6q.

6.2.2 Gained regions

The most common small region of gain appears to be at 11q13. This region is shown as gained in 40% of samples (Figure 6.4).

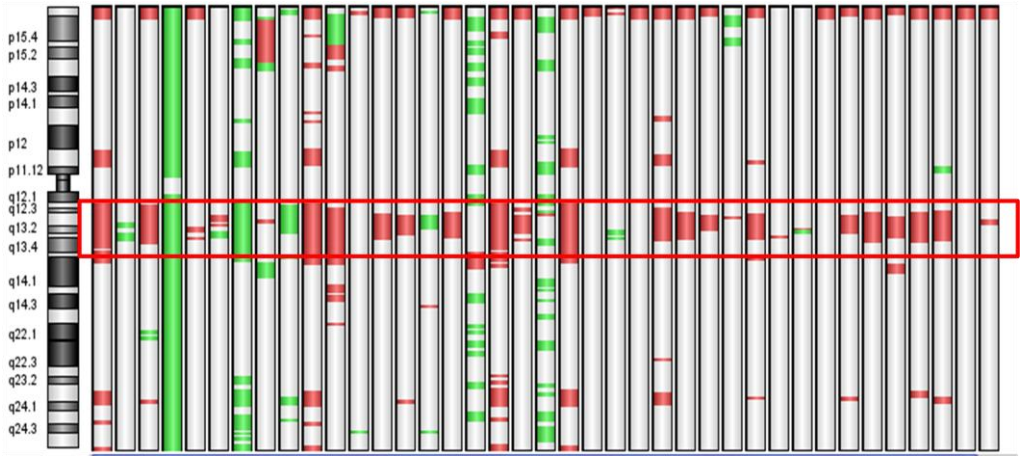

Figure 6.4: Chromosome 11 heatmap shows an apparent region of gain at 11q13 in 40% of samples.

This region contains the well characterised cell cycle control gene *CCND1* and various fibroblast growth factors (FGFs) including *FGF3* which is frequently over expressed in tumours and thought to be involved in malignant transformation and tumour progression. This region is noisy with the log2ratios on adjacent probes often varying widely. Therefore it is important to validate this gain as it is seen in so many samples.

One sample, HGG11, has an area of gain at 11q13 with a smaller focal region of amplification which includes *CCND1* and *FGF3* (Figure 6.5). This sample is a brainstem glioma.

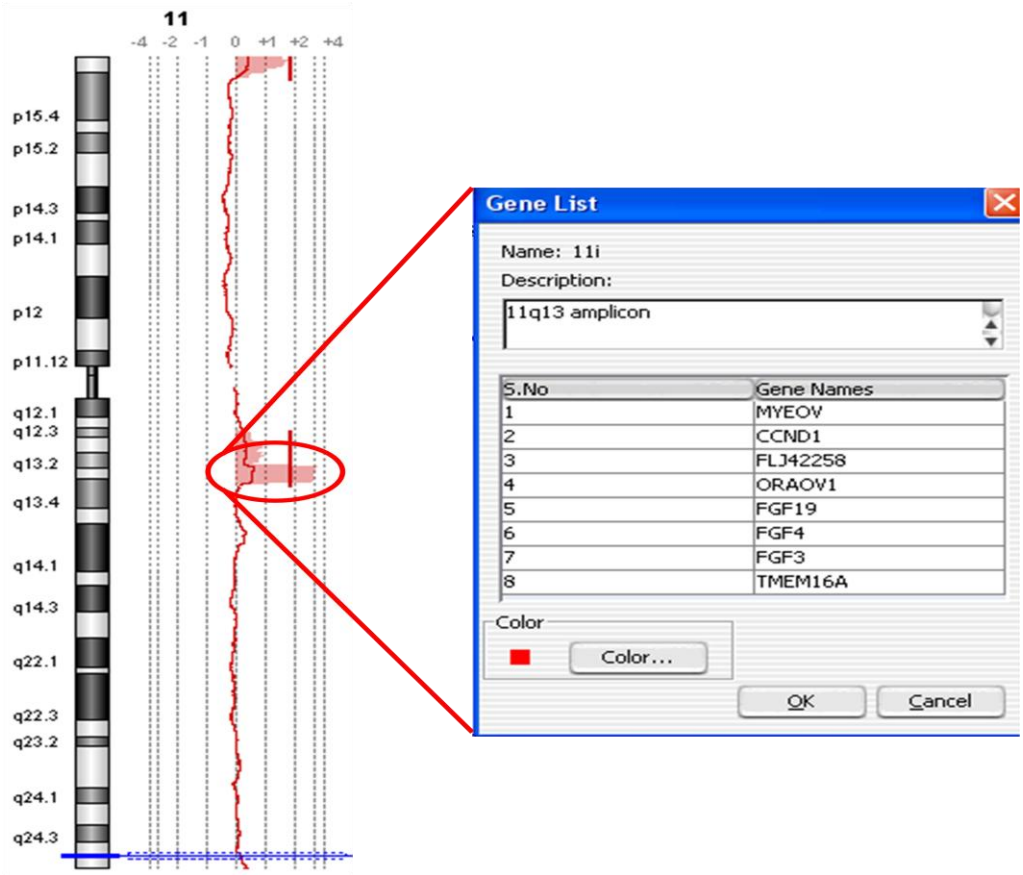

Figure 6.5: Amplification at 11q13 in sample HGG11 including *CCND1* and *FGF3*, *4* and *19*. CGH Analytics can generate a gene list for a specific aberrant region.

Three samples showed regions of gain on 12q (Figure 6.6). The gene showing the highest level of gain in this region was *CDK4*, a cyclin dependant kinase. All three aberration profiles are similar for chromosome 12, with the wavy moving aberration line often indicating areas of noise.

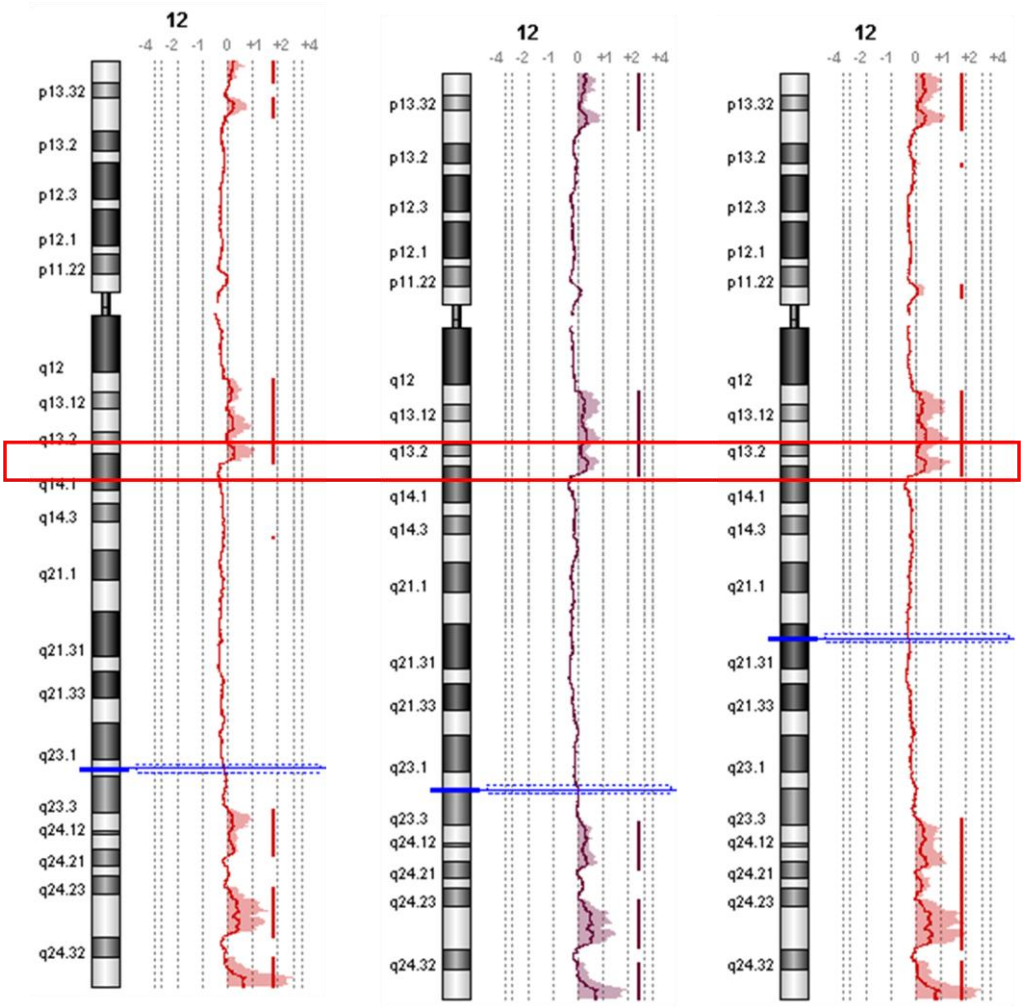

Figure 6.6: Samples HGG17, HGG18 and HGG25 all appear to have gain of CDK4, although the profiles are noisy.

6.2.3 Regions of loss

Loss of 9p21 is seen in four samples although the size of the deleted region is varied (Figure 6.7). 9p21 is the site of genes *CDKN2A* and *B*. *CDKN2A* is a well known tumour suppressor gene that is known to be deleted in a variety of tumour types. *CDKN2B* lies adjacent to *CDKN2A* on chromosome 9p, and is a cell growth regulator gene. *CDKN2A* and *CDKN2B* are frequently deleted together, as seen in these samples.

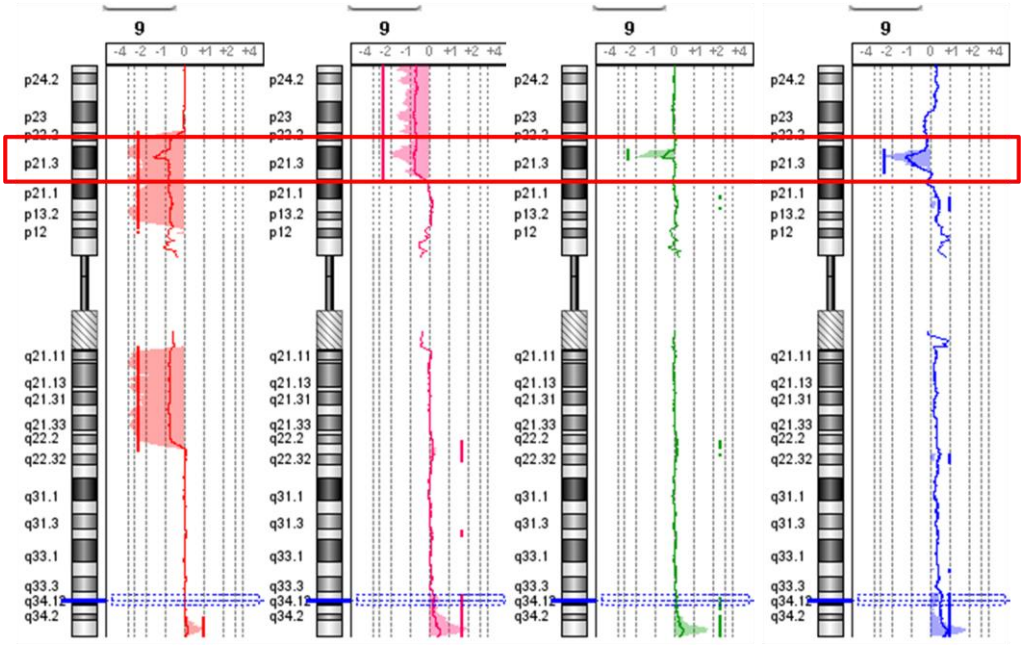

Figure 6.7: Chromosome view for HGG1, HGG4, HGG10 and HGG25 (left to right) with deletions of *CDKN2A* and *CDKN2B*.

The deleted region varies from almost all of 9p and some of 9q in HGG4 to a much more specific deletion seen in HGG25 involving just a handful of genes, including *CDKN2A* and *CDKN2B*.

The most discrete deletion in this data set is at 8p11.23. This deletion is seen in 6/38 samples, and the minimal deleted region covers probes on just one gene, *ADAM3A* (Figure 6.8).

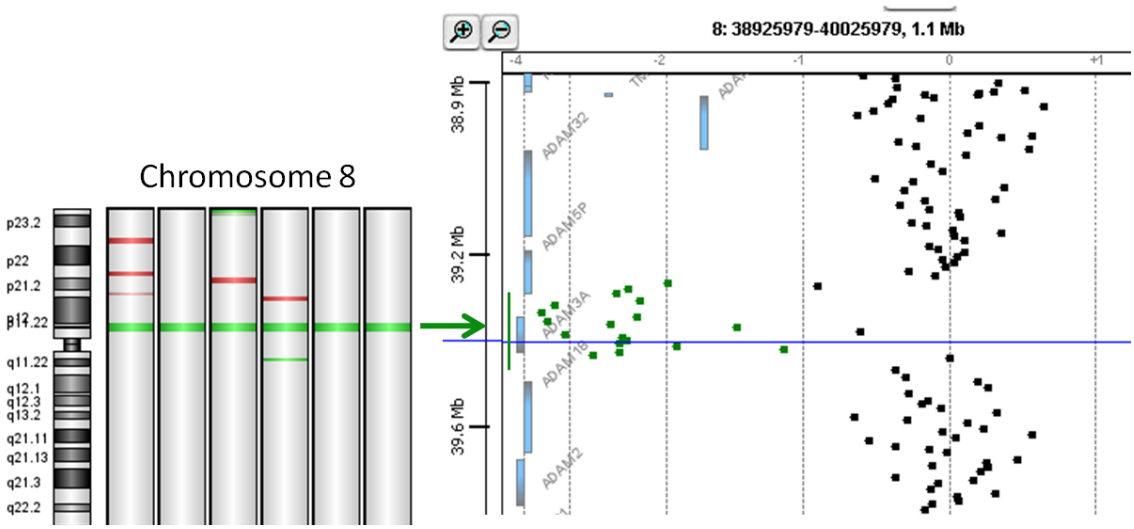

Figure 6.8: Deletion of *ADAM3A* represented by the green bands on the chromosome 8 summaries (left). The probes for the gene *ADAM3A* lie to the left of the centre line on the chromosome view (right), indicating loss.

ADAM3A is a member of the *ADAM* family of genes which are involved in cell to cell communication and adhesion.

There is one primary/recurrent pair in this study; HGG31 (primary) and HGG32 (recurrence). Both these tumours had no chromosome arm aberrations and very few focal aberrations. HGG31 and HGG32 had homozygous deletion at 8p11.23 and a small region of loss on 22q. No differences between the primary and recurrent sample were seen in this study.

6.2.4 Frozen DNA vs FFPE DNA

Corresponding frozen DNA from four of the FFPE samples in this study was analysed by aCGH to determine whether aberrations seen in the high quality frozen samples were replicated in the profiles of the poorer quality FFPE samples. The four frozen samples were not included as part of the overall analysis in this study. On the whole, the frozen/FFPE pairs demonstrated the same gains and losses although there were certain noisy regions in the FFPE samples where CGH Analytics identified false regions of gain, e.g. chromosome 19. This makes validation of genes identified

by aCGH with FFPE samples vital. Selected chromosomes from the FFPE and frozen samples of HGG30 are displayed in Figure 6.9.

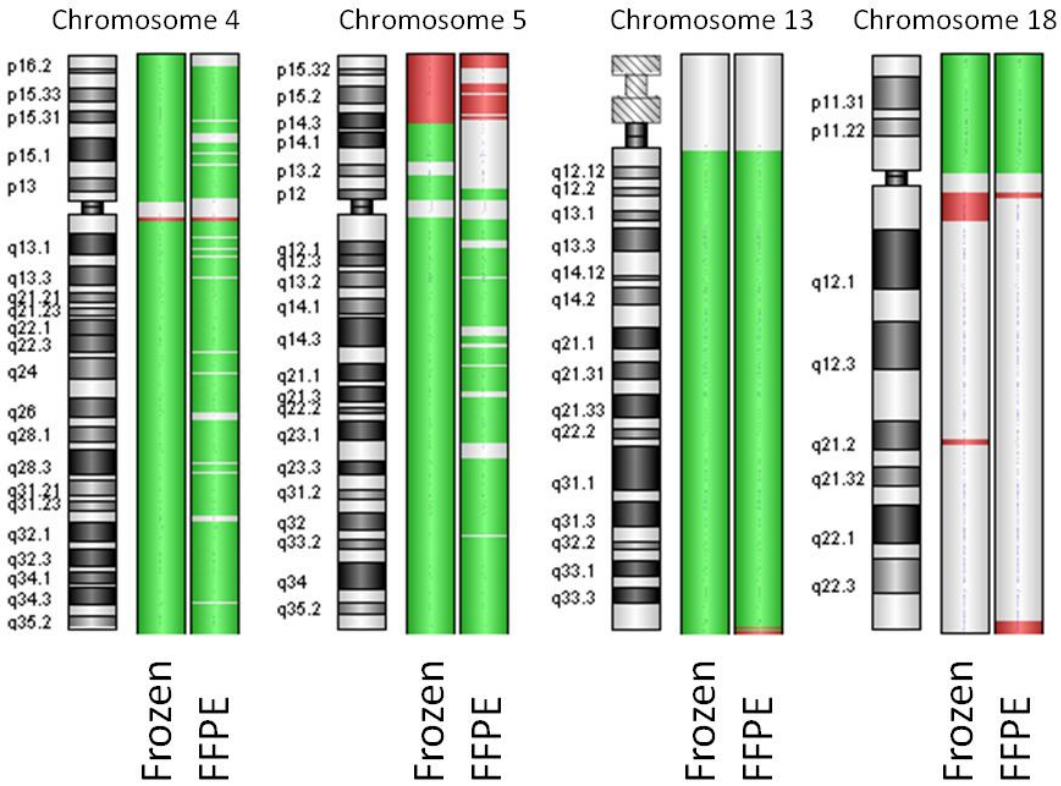

Figure 6.9: Chromosome views for Frozen and FFPE samples of HGG30. Aberrations are preserved in the FFPE sample, e.g. loss of chromosome 4 (green) with amplification at 4q13 (red), gain of ~50% 5p (red) with loss of the remainder of chromosome 5 (green), loss of chromosome 13 (green), and loss of 18p (green).

6.3 Discussion

The high resolution analysis of 38 FFPE pHGG samples by aCGH has identified focal regions of gains and loss. Comparisons between the 13 brainstem tumours compared to the 25 non-brainstem tumours led to the discovery of anatomical site associated aberrations that warrant further study.

Numerous gene and chromosome region aberrations were seen across the data set. There were four regions that showed amplification in one or more samples. Out of those four regions, amplification of 4q12 was the most frequent in 3/38 samples (8%). 4q12 contains the genes *PDGFRA* and *KIT* which have both been identified as aberrant in other cancers. Interestingly two out of the three samples with *PDGFRA* amplification are brainstem tumours and so 2/13 brainstem gliomas (15%) had amplification at 4q12.The PDGFRA protein is a growth factor receptor for the PDGF family. The PDGFs are mitogens that influence cells of mesenchymal origin by promoting the cell cycle and mitosis. Therefore, amplification of *PDGFRA* leading to high level expression of PDGFRA will promote high levels of cell proliferation consistent with high grade tumours. PDGFRA is a possible drug target in pHGG (see section 1.5.1). *KIT* is an oncogene which encodes a growth factor receptor protein. An increase in the number of growth factor receptors potentially means that more growth factors can be detected by the cell and so when *KIT* is amplified this may lead to increased cell proliferation.

MYCN amplification was seen in 2/38 (5%) samples and appeared to be the most highly amplified gene in this study according to aCGH data analysis (see fig. 6.1). Both samples with *MYCN* amplification were anaplastic astrocytomas. *MYCN* is highly amplified in aggressive neuroblastoma but has also been reported amplified in CNS PNETs, medulloblastoma and paediatric high grade gliomas, as well as non-brain tumours (Fruhwald, O'Dorisio et al. 2000; Pfister, Remke et al. 2009; Paugh, Qu et al. 2010). *MYCN*, an oncogene, is a member of the MYC family of transcription factors and so amplification leading to aberrant expression of the MYCN protein causes increased transcription of growth factors and in turn leads to

increased cell proliferation (Maris and Matthay 1999). Amplification of the gene *QKI* at 6q26-27 was seen in just one sample, HGG20. QKI proteins belong to a family of proteins that are involved in RNA splicing, protein translation and transport of RNA from the nucleus. QKI is also thought to play a role in oligodendrocyte differentiation and myelination (Bockbrader and Feng 2008). 6q26 has been identified as a fragile site. Fragile sites are specific regions that are susceptible to chromosome instability and are distributed throughout the genome (Durkin and Glover 2007). Fragile sites have been identified as the location of frequent chromosome rearrangements and deletions in cancer. Losses at 7q36 and 10q11.2 were also identified in this study, and both these locations have been shown to be fragile sites.11q13 was amplified in one sample, and contains the gene *CCND1* and a number of *FGF* genes. *CCND1* is a well characterised regulator of the cell cycle so amplification would promote the cell cycle and so cell proliferation. *FGF3*, *FGF4* and *FGF19* are all in this region. The FGFs are growth factors which promote cell cycle progression and so amplification of these genes could lead to increased cellular proliferation and tumour progression. (Schwertfeger 2009)

The focal deletion at 9p21 includes the well known tumour suppressor genes *CDKN2A* and *B* which have previously been reported lost in other types of paediatric brain tumour including CNS PNETs. (Pfister, Remke et al. 2007) *CDKN2A* and *B* are cyclin dependant kinase inhibitors which inhibit the cell cycle. Therefore, loss of *CDKN2A* and *B* could lead to uncontrolled cell proliferation. Interestingly, *CDKN2A* and *B* loss was only seen in four GBMs that are all supratentorial tumours. None of the brainstem gliomas or other infratentorial tumours in the oligo aCGH study showed loss of *CDKN2A* and *B*. Our group has recently reported loss of *CDKN2A* and *B* is seen in supratentorial CNS PNETs but not in medulloblastoma, suggesting further studies are needed to determine whether this genetic abnormality is restricted to supratentorial tumours.

The most common focal deletion seen in this study was a small region of loss at 8p11 that was seen in 6/38 samples and has not been previously found in adult or paediatric high grade gliomas in high resolution studies using the Affymetrix SNP

platforms (Paugh, Qu et al. 2010; Qu, Jacob et al. 2010). This is likely due to the lack of probes for this particular gene on the Affymetrix 500K and 250K platforms.

The minimal deleted region across these six samples is a discrete deletion of the gene *ADAM3A*. Very little is known about the function of this gene in humans, although *ADAM3A* has been shown to be vital to sperm binding and migration in mice (Yamaguchi, Muro et al. 2009). *ADAM3A* is a member of the *ADAM* family of genes which are involved in cell to cell communication and adhesion (Wolfsberg, Straight et al. 1995). Certain *ADAM* family genes are thought to be involved in neurogenesis whilst others have been implicated in cancer (Mochizuki and Okada 2009; Seniski, Camargo et al. 2009).

The frequency and specificity of the deletion at 8p11 in this sample set makes this focal region, and specifically *ADAM3A*, an interesting target for possible future study. However, 8p11.23 has been identified as a copy number variable region (CNV) in the human genome. CNVs are widespread throughout the human genome in healthy individuals and are thought to include around 12% of the whole human genome (Kuiper, Ligtenberg et al. 2010). Some CNVs are associated with diseases, including cancer, whilst many CNVs have unknown clinical significance. As matched constitutional blood was unavailable for the samples used in this study it is possible that the loss seen at 8p11.23 is a CNV that may be also present in healthy individuals. However, this deletion was seen at a higher frequency (16%) than may be expected for a non-pathogenic CNV.

Three members of the Wnt family of genes were identified in the original gene list; *Wnt3a*, *Wnt4* and *Wnt11*. *Wnt3a* lies within a CNV in the human genome. The Wnt gene family encodes a range of signalling proteins that are involved in embryonic patterning and other developmental processes. The Wnt pathway regulates many developmental processes including cell proliferation, cell migration and cell fate (Giunta 2009). As the Wnt pathway has such a diverse range of targets ands effects, loss of control of the pathway can have dire consequences.

The Wnt signalling cascade has been widely implicated in oncogenesis in a variety of cancers. *Wnt4* encodes a signalling protein involved in sex determination and has been implicated in abnormal proliferation of cells in breast carcinoma. *Wnt3a* has also been implicated in breast cancer studies. *Wnt11* encodes a protein involved in

the development of bones, lungs and kidneys and has been implicated in prostate cancer. Aberrant Wnt pathway activation has previously been reported in medulloblastoma (Zurawel, Chiappa et al. 1998; Koch, Waha et al. 2001).

A cluster of homeobox (HOX) genes (*HOXA1-13*) was seen gained at 7p15 in one sample. 7p15 has been identified as a CNV. HOX genes encode for a family of transcription factors involved in embryonic patterning at specific time points during development (Shah and Sukumar 2010). The genes *HOXA1-13* encode for transcriptions factors involved in the regulation or morphogenesis and differentiation of cells. *HOXA1-6* encode proteins that are involved in the development of the hindbrain along the anterior-posterior axis. A fusion between *HOXA9* and the gene *NUP98* has been identified in myeloid leukaemia. *HOXA10* encodes a protein involved in haematopoietic differentiation, whilst both *HOXA10* and *HOXA11* play role in female fertility and uterine development.

Deregulation of *Hox* gene expression has been widely implicated in oncogenesis (Shah and Sukumar 2010). Hox genes control organogenesis pathways that can become deregulated and lead to uncontrolled cell proliferation. Alterations on Hox gene expression can also maintain a more primitive cell phenotype by suppressing differentiation of cells and activating anti-apoptotic pathways.

Transporter associated with antigen processing 1 *(TAP1)* and Transporter associated with antigen processing 2 *(TAP2)* (6p21) were seen gained in three samples. *TAP1* and *TAP2* encode proteins of the ATP-binding cassette (ABC) transporter family involved in transport of molecules in and out of cells. The proteins encoded by these genes are involved in multidrug resistance.

5/38 (13%) samples in this study did not have any whole arm or focal aberrations according to the aCGH analysis. This indicates that epigenetic changes and mutations are important in these tumours. Subsets of balanced tumours have also been seen in studies of ependymoma and CNS PNETs (Dyer, Prebble et al. 2002; Natrajan, Williams et al. 2006).

CHAPTER 7

VALIDATION OF aCGH

7.1 Quantitative Real Time PCR (qPCR)

7.1.1 Primers

qPCR is a techniques to measure copy number of a gene using specifically designed primers for the gene of interest. A control gene is also required to give a 'normal' result that the gene of interest can be compared to. In this study, the gene *PPIA* was chosen as the normal control as it had in normal copy number in all samples according to the aCGH results. A further nine genes of interest that were identified as being most highly amplified or most commonly gained/lost were validated.

Primers were designed using PrimerBlast (NCBI) and ordered from Operon (Eurofins MWG Operon, London, UK).

Table 7.1: qPCR primers.

Gene	**Primer**	**Primer Sequence**	**Primer Length (bp)**	**Product Length (bp)**
CCND1 (exon 1)	Forward	CTGTGCTGCGAAGTGGAAAC	20	
CCND1 (exon 1)	Reverse	GGACCTCCTTCTGCACACAT	20	142
PDGFRA (exon 4)	Forward	AGTCAGGGGAAACGATTGTG	20	
PDGFRA (exon 4)	Reverse	AGCCATTGCACGTTTTGAG	19	111
CDK4 (exon 1)	Forward	CCCTTGATCTGAGAATGGCT	20	
CDK4 (exon 1)	Reverse	CCATTGGGGACTCTCACACT	20	139
CDKN2A (exon 2)	Forward	TCAGGTAGCGCTTCGATTCT	20	
CDKN2A (exon 2)	Reverse	GGCTCCTCATTCCTCTTCCT	20	132
CDKN2B (exon 2)	Forward	GCGGATTTCCAGGGATATTT	20	
CDKN2B (exon 2)	Reverse	CACCAGGTCCAGTCAAGGAT	20	105
MYCN (exon 2)	Forward	CGCTACAGCCCTGCTTCTAC	20	
MYCN (exon 2)	Reverse	GGCAGCAGCTCAAACTTCTT	20	103
QKI (exon 1)	Forward	GGGAAATGGAAACGAAGGAG	20	
QKI (exon 1)	Reverse	TTGAAGATCCCGCAGAAGTT	20	109
FGF3	Forward	AGATAACGGCAGTGGAGGTG	20	
FGF3	Reverse	TGGACTCACCGAAGCATAGA	20	104
ADAM3A	Forward	AGCCTCATTGCCTTTCACAT	20	
ADAM3A	Reverse	TTTCTGTGGACCTTTTTGGC	20	125
PPIA (exon 4)	Forward	ATGCTGGACCCAACACAAAT	20	
PPIA (exon 4)	Reverse	TAGTGTTTGTTCCGTTCCCC	20	132

7.1.2 Optimisation of qPCR with FFPE DNA

Ideally, high quality DNA is used for qPCR. FFPE DNA is often highly fragmented and degraded which can cause problems with primer binding and the production of the PCR product. 10ng of DNA from frozen tissue is used as a standard. A concentration gradient PCR experiment was set up to determine the optimal amount of FFPE DNA to use in qPCR. The DNA quantities used were 100 ng, 50 ng, 25 ng and 12.5 ng.

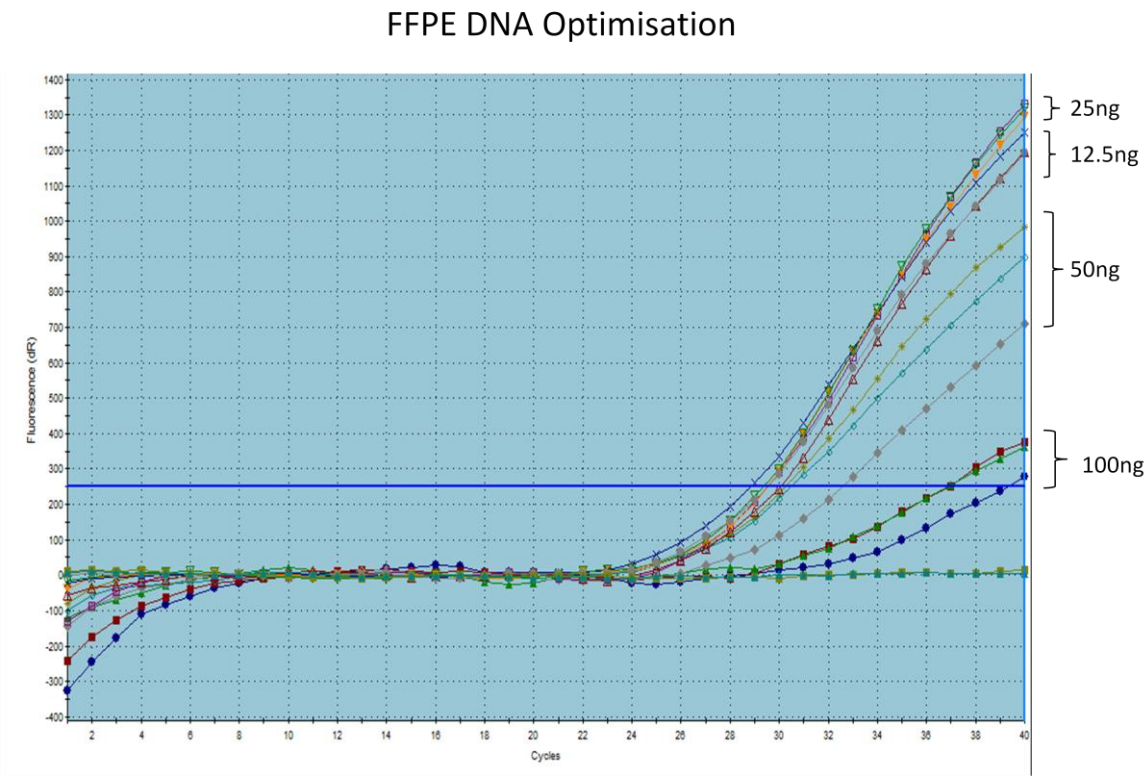

Figure 7.1: Amplification curves from optimisation of FFPE DNA for qPCR.

The x axis of the amplification graph displays the number of PCR cycles and the y axis displays the fluorescence. 25 ng and 12.5 ng of FFPE gave clean amplification curves, with 25 ng giving the most consistent result. Therefore, 25 ng of FFPE DNA was used for each qPCR reaction.

Unfortunately, the DNA for some samples analysed by aCGH was depleted and so unavailable for validation studies. A number of samples were used for qPCR but

consistently failed to give any result so were also unusable for validation. 21 samples had DNA available and worked with qPCR. Many of these 21 samples only had small quantities of DNA available for validation and therefore only select samples were used to validate each gene. Each qPCR is performed in triplicate.

7.1.3 Control Gene Primers

PPIA was the control gene used for all the qPCR reactions. Temperature gradient PCR showed the optimal temperature for these primers is 58^{o}C. The efficiency of the *PPIA* primers was calculated in the MxPRO software (Stratagene) from a concentration gradient using a control DNA. As these primers were used as a control for every target gene the efficiency of these primers was re-calculated after each set of experiments was completed to make sure the efficiency was accurate.

The derived copy number was calculated by multiplying the 'Fold change' from the Pfaffl equation by two. The 'aCGH Copy Number' is derived from the log2ratio values given to each probe on the array. The log2ratios from all the probes in the gene of interest were averaged and converted into a copy number.

7.2 Results of qPCR

CCND1

CCND1 was seen gained in ~40% of samples in the aCGH results, however the area of chromosome 11 where *CCND1* is located was prone to noise and therefore validation of this gain is important. The temperature gradient PCR had shown that the *CCND1* primers work optimally at 58^{o}C.

An efficiency of 91.5% was calculated from the concentration gradient standard curve. The Pfaffl equation was used to calculate fold change.

Table 7.2: qPCR results for *CCND1*.

Sample	Gene	aCGH Copy Number	Fold change	Derived Copy Number
HGG11	*CCND1*	21.2	5.3	10.6
HGG17	*CCND1*	5.2	1.3	2.6
HGG22	*CCND1*	3.8	1.1	2.2
HGG28	*CCND1*	2.8	1.5	3.0
HGG10	*CCND1*	3.4	1.3	2.6
HGG7	*CCND1*	3.6	0.9	1.9
HGG32	*CCND1*	3.0	0.7	1.5
HGG36	*CCND1*	1.0	0.4	0.7

Whilst qPCR has confirmed the amplification in sample HGG11 and the deletion in samples HGG36 it has failed to validate gain of *CCND1* in HGG17 and HGG22 which had been suggested by aCGH. All samples which had copy number 2 for *CCND1* in the aCGH data have normal copy numbers by qPCR.

FGF3

FGF3 is located at 11q13, the same region as *CCND1*. Gain of *FGF3* was seen in around 40% samples.

Table 7.3: qPCR results for FGF3.

Sample	Gene	aCGH Copy Number	Fold change	Derived Copy Number
HGG17	*FGF3*	9.8	1.5	3.0
HGG18	*FGF3*	12.2	1.7	3.4
HGG11	*FGF3*	13.0	8.9	17.8
HGG7	*FGF3*	2.2	1.0	2.0
HGG31	*FGF3*	1.6	1.0	2.0
HGG25	*FGF3*	2.2	1.4	2.8

The gains of *FGF3* in HGG17 and HGG18 were confirmed by qPCR as was the amplification of *FGF3* in HGG11. The three samples with normal copy number of *FGF3* according to aCGH also have normal copy number according to qPCR.

PDGFRA

Amplification of *PDGFRA* was seen in three samples in the aCGH results; HGG20, HGG30 and HGG36. HGG20 and HGG30 showed high level amplification whilst HGG36 showed low level amplification. The efficiency of the *PDGFRA* primers was shown to be 92.4%.

Table 7.4: qPCR results for *PDGFRA*.

Sample	Gene	aCGH Copy Number	Fold change	Derived Copy Number
HGG30	*PDGFRA*	6.4	6.9	13.8
HGG20	*PDGFRA*	17.2	13.9	27.8
HGG36	*PDGFRA*	3.8	2.7	5.4
HGG3	*PDGFRA*	2.2	0.9	1.9
HGG24	*PDGFRA*	2.2	1.4	2.7
HGG32	*PDGFRA*	2.0	1.1	2.2
HGG7	*PDGFRA*	2.0	0.8	1.6
HGG10	*PDGFRA*	2.0	1.0	2.0

The amplification of *PDGFRA* in HGG20 and HGG30 has been validated. Sample HGG36 has a derived copy number of 5.4 which is a gain rather than an amplification (> copy number 6). The five samples which showed a normal copy number of *PDGFRA* by aCGH all show a normal copy number by qPCR.

CDK4

The aCGH results showed three samples, HGG17, 18 and 30, having gain of *CDK4*, although all three samples had a noisy chromosome 12 with a wavy moving average line. The efficiency of the *CDK4* primers was calculated as 103% and the temperature gradient showed the optimal temperature to be 58^{o}C.

Table 7.5: qPCR results for *CDK4*.

Sample	Gene	aCGH Copy Number	Fold change	Derived Copy Number
HGG17	*CDK4*	6.4	0.8	1.6
HGG18	*CDK4*	9.2	0.9	1.8
HGG30	*CDK4*	5.0	1.6	3.2
HGG4	*CDK4*	1.8	1.4	2.8

qPCR validated gain in just 1/3 samples with the other two samples showing a normal copy number by qPCR. It was concluded that these two gains were not real and were due to noise on chromosome 12.

CDKN2A and *CDKN2B*

These two genes are often seen deleted together in a range of tumour types although they have separate functions. Both genes will be analysed by qPCR to show the correlation between the copy numbers of these genes.

Four samples, HGG1, HGG4, HGG10 and HGG25 showed deletions of *CDKN2A* and *CDKN2B*. *CDKN2A* primers were shown to have an optimal annealing temperature of 58^{o}C and an efficiency of 94.5%.

Table 7.6: qPCR results for *CDKN2A*.

Sample	Gene	aCGH Copy Number	Fold change	Derived Copy Number
HGG25	*CDKN2A*	0.7	0.2	0.4
HGG4	*CDKN2A*	0.4	0.2	0.3
HGG10	*CDKN2A*	1.1	0.7	1.4
HGG1	*CDKN2A*	0.5	0.3	0.5
HGG32	*CDKN2A*	2.2	0.9	1.7
HGG26	*CDKN2A*	2.2	0.8	1.7
HGG31	*CDKN2A*	2.0	1.1	2.2
HGG3	*CDKN2A*	2.0	1.1	2.2

Samples HGG1, HGG4 and HGG25 showed homozygous deletions by qPCR, whilst HGG10 showed a heterozygous deletion. All four samples with a normal copy number in the aCGH data have a normal copy number by qPCR.

CDKN2B primers were shown to have an optimal annealing temperature of 58^{o}C and an efficiency of 92.9%.

Table 7.7: qPCR results for *CDKN2B*.

Sample	Gene	aCGH Copy Number	Fold change	Derived Copy Number
HGG25	*CDKN2B*	0.9	0.2	0.4
HGG4	*CDKN2B*	0.4	0.2	0.3
HGG10	*CDKN2B*	1.1	0.7	1.5
HGG1	*CDKN2B*	0.9	0.4	0.8
HGG3	*CDKN2B*	2.4	1.1	2.2
HGG31	*CDKN2B*	2.4	1.2	2.4
HGG7	*CDKN2B*	2.4	1.0	1.9

Sample HGG25 and HGG4 show homozygous deletions whilst HGG10 show a heterozygous deletion. HGG1 has a derived copy number of 0.78 which also indicates a homozygous deletion as the value is less than 1. All three samples which had normal copy number according to aCGH also have a normal copy number by qPCR.

CDKN2A and *B* are often lost together, as is seen in these four samples.

Table 7.8: Correlation of *CDKN2A* and *CDKN2B* loss.

Sample	*CDKN2A* Derived Copy Number	*CDKN2B* Derived Copy Number
HGG25	0.36	0.4
HGG4	0.34	0.32
HGG10	1.38	1.48
HGG1	0.5	0.78
HGG31	2.2	2.4
HGG3	2.2	2.2

10% of samples demonstrated loss of *CDKN2A* and *B* although interestingly none of the 13 brainstem gliomas in the study had loss of *CDKN2A* or *B*.

MYCN

High level amplification of *MYCN* was seen in two samples in the aCGH results, and one sample showed gain. *MYCN* primers showed an optimal annealing temperature of 58^{o}C and an efficiency of 90.2%.

Table 7.9: qPCR results for *MYCN*.

Sample	Gene	aCGH Copy Number	Fold change	Derived Copy Number
HGG20	*MYCN*	27.8	36.2	72.4
HGG15	*MYCN*	14.0	7.8	15.6
HGG26	*MYCN*	3.5	3.0	6.0
HGG17	*MYCN*	2.0	1.3	2.6
HGG3	*MYCN*	2.2	1.4	2.8
HGG7	*MYCN*	2.0	1.4	2.8

MYCN amplification is confirmed in HGG20 and HGG15 and gain of *MYCN* is confirmed in HGG26. The three samples which showed normal copy number of *MYCN* by aCGH have all shown normal copy number by qPCR.

QKI

Amplification of the gene *QKI* was seen in just one sample, HGG20. Temperature gradient PCR showed that the optimal temperature for the *QKI* primers was 58^{o}C and the efficiency of the primers was calculated as 95.8%.

Table 7.10: qPCR results for *QKI*.

Sample	Gene	aCGH Copy Number	Fold change	Derived Copy Number
HGG20	*QKI*	15.0	9.6	19.2
HGG3	*QKI*	2.2	1.3	2.6
HGG37	*QKI*	2.0	1.6	3.2
HGG11	*QKI*	1.8	1.3	2.6

The amplification of *QKI* in HGG20 was validated by qPCR. Two of the normal samples from aCGH analysis showed normal copy number for *QKI* by qPCR, but one sample that had a normal copy number in aCGH analysis showed gain by qPCR.

ADAM3A

Deletion of *ADAM3A* was the most common focal deletion seen in the aCGH data with 15% of samples showing deletion of *ADAM3A*. Optimal annealing temperature for the *ADAM3A* primers was shown to be 58^{o}C and the efficiency of the primers was calculated as 90%.

Table 7.11: qPCR results for *ADAM3A*.

Sample	Gene	aCGH Copy Number	Fold change	Derived Copy Number
HGG4	*ADAM3A*	0.5	0.1	0.3
HGG32	*ADAM3A*	0.3	0.0	0.0
HGG28	*ADAM3A*	0.5	0.0	0.0
HGG22	*ADAM3A*	0.2	0.0	0.0
HGG7	*ADAM3A*	2.0	0.9	1.8
HGG8	*ADAM3A*	2.0	0.9	1.7
HGG3	*ADAM3A*	3.6	2.2	4.4
HGG10	*ADAM3A*	2.0	1.2	2.4

Four samples which showed loss of *ADAM3A* by aCGH were validated by qPCR. All four samples showed homozygous loss with samples HGG28 and HGG22 not even registering a Ct value showing a complete loss of *ADAM3A*. Four samples that had normal copy number for *ADAM3A* in the aCGH data were validated by qPCR. Three of these samples showed normal copy number by qPCR, however one sample showed a low level gain.

7.3 FISH

Fluorescence in situ hybridisation (FISH) is a technique used to measure copy number of chromosomal regions, ranging from whole arms to single genes. 10 high grade glioma tissue microarrays (TMAs) were available for this study with ~150 high grade glioma samples across the TMAs in triplicate. There are 26 brainstem gliomas on the TMAs, including 10 of the 13 brainstem tumours analysed by aCGH. The amount of 'scorable' samples on the TMA varies in each experiment due to differences in core loss, auto-fluorescence, and how successfully the FISH has worked with a particular probe set.

7.3.1 Gain of 1q

Gain 1q was the most common aberration seen in this study in the aCGH analysis (40% samples). 1q FISH was performed on all high grade glioma TMAs using 1q25 SpectrumGreen probe (green) and a 1p36 SpectrumOrange control probe (red) (Vysis LSI 1p36/LSI 1q25 Dual colour probe, Abbott Technologies).

41 samples were scorable for 1q FISH. 12 of the 41 scorable samples were analysed by aCGH and only two of the 41 samples were brainstem gliomas. 11/41 (27%) samples had gain of 1q. Of those 11 samples seven were GBM, two AA and two GBM of the brainstem. Sample HGG35 had gain of 1q and loss of 1p, as seen in the aCGH analysis (Figure 7.2).

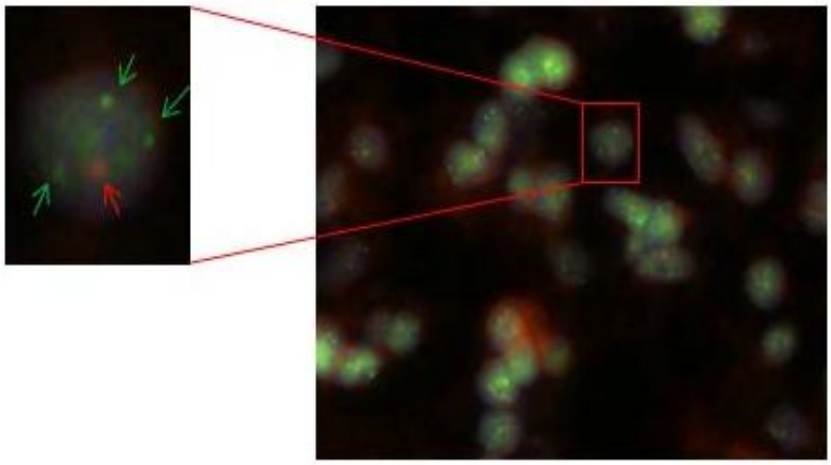

Figure 7.2: 1q FISH on sample HGG35. Three copies of 1q are visible (green probe) but only one copy of 1p (red probe).

7.3.2 Amplification of *MYCN*

MYCN amplification was seen in 5% samples in the aCGH analysis, and was the highest level amplification seen. A *MYCN* (2p24) specific PlatinumBright550 probe (red) plus a *LAF* (2q11) PlatinumBright495 control probe (green) was used to FISH all TMAs. (Poseidon Repeat Free *MYCN* & *LAF* Control Probe, Kreatech).

80 samples on the TMAs were scorable for *MYCN* FISH. Of those 80 samples, four samples had amplification of *MYCN* (figure 7.3) including the two samples with *MYCN* amplification that were analysed by aCGH (HGG20 and HGG15).

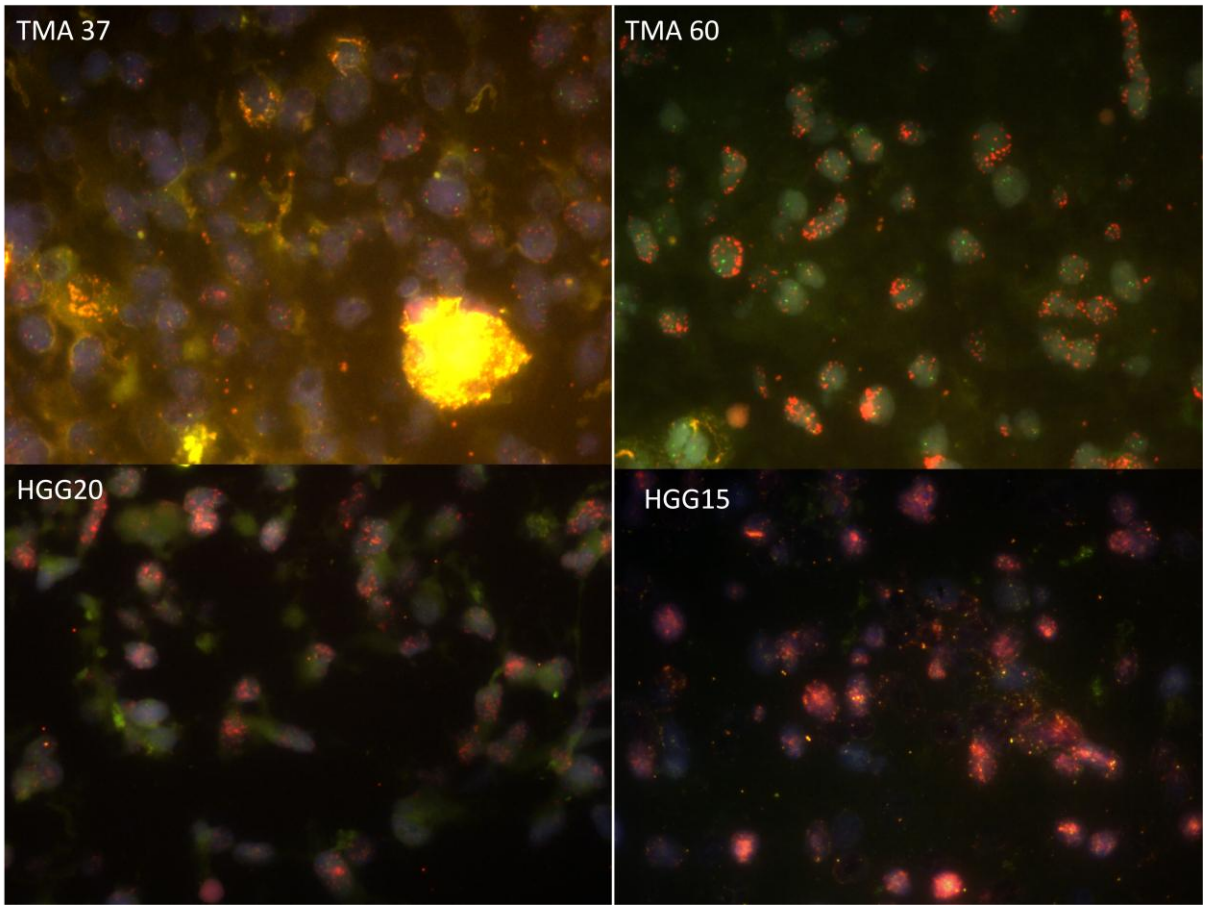

Figure 7.3: TMA37, TMA60, HGG20 and HGG15 all displayed amplification of *MYCN* by FISH. FISH has validated the amplification of *MYCN* in samples HGG20 and HGG15 seen in the aCGH data (red probe is *MYCN*, green probe is control).

It is impossible to count copy number for *MYCN* in any of these four samples as the high copy number makes it very difficult to distinguish between each separate probe signal (Figure 7.3).

Sample HGG20 is a brainstem glioma whilst sample HGG15, TMA37 and TMA60 are all anaplastic astrocytomas. No GBMs demonstrated amplification of *MYCN*. Fisher's exact test was used to show that *MYCN* amplification was significantly associated with anaplastic astrocytomas in this dataset (p=0.03).

One sample, HGG2, demonstrated amplification of *LAF4*, the control probe target on 2q. High level gain of *LAF4* in HGG2 was seen in the aCGH data (Figure 7.4).

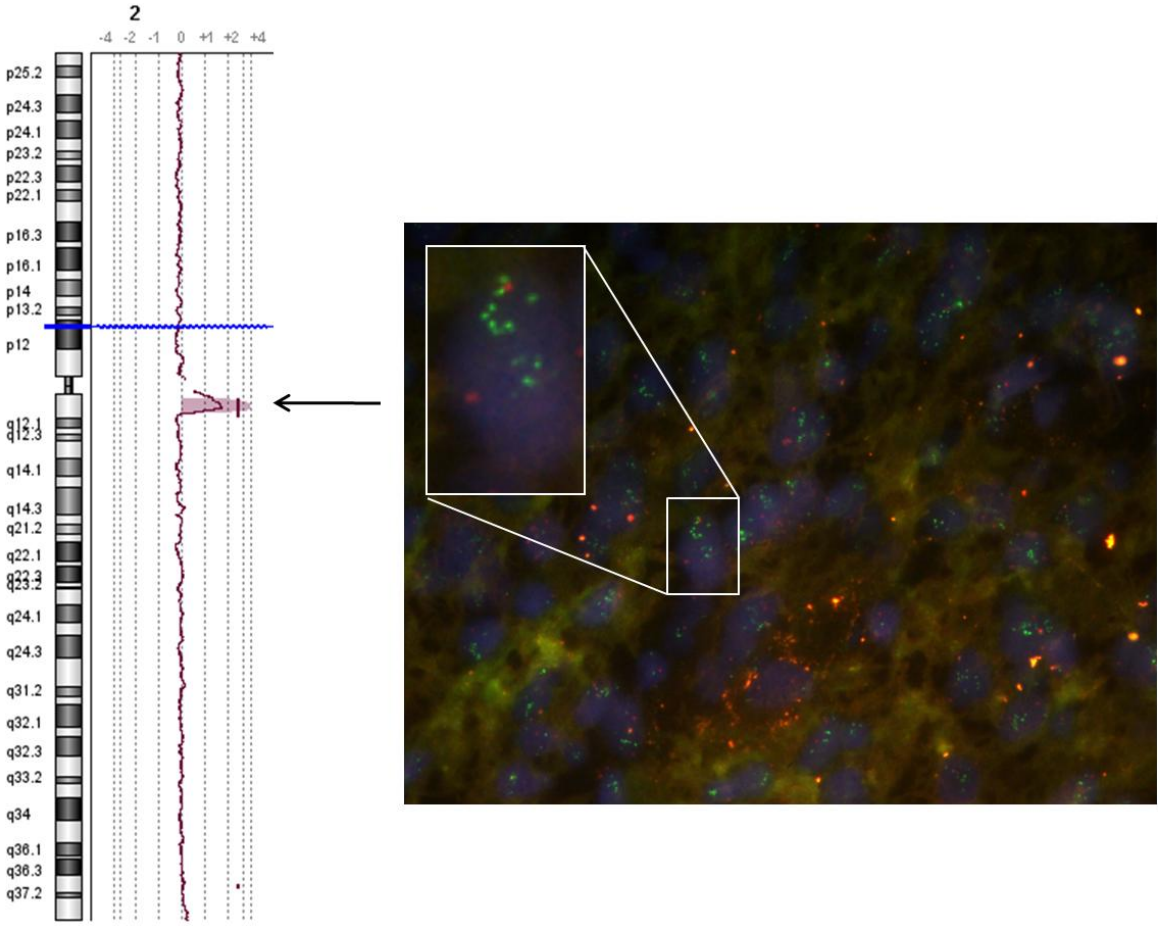

Figure 7.4: Chromosome view of chromosome 2 from sample HGG2 showing gain at 2q12. *LAF4* FISH confirms amplification of *LAF4* (green probe) in sample HGG2.

Sample HGG2 is a GBM but the patient had previously had radiation treatment for acute lymphoblastic leukaemia (ALL). The *LAF4* gene is associated with ALL.

7.3.3 Loss of *p16*

Loss of *CDKN2A* and *CDKN2B* (9p21) was seen in 10% samples by aCGH. FISH was performed across all TMAs using *p16* (9p21) PlatinumBright550 probe (red) and 9q21 PlatinumBright495 (green) control probe (Figure 7.5).

There were 61 scorable samples across the TMAs. 21/61 samples were infratentorial tumours including five brainstem gliomas, 28/61 were supratentorial tumours, 3/61 were spinal tumours and for nine tumours the location was unknown. 39 of the scorable samples were GBM, 11 AA, five brainstem gliomas, four AO, one APX and one CNS PNET that had been originally diagnosed as a high grade glioma.

Out of the 61 samples, three had heterozygous loss of *p16* and five had homozygous loss of *p16*, although two of the samples with homozygous loss were from two surgeries on the same tumour. Interestingly, all the tumours with loss of *p16* were supratentorial GBMs, occurring in the cerebral lobes. None of the 21 scorable infratentorial samples on the TMAs showed loss of *p16*, the same result seen in the aCGH data.

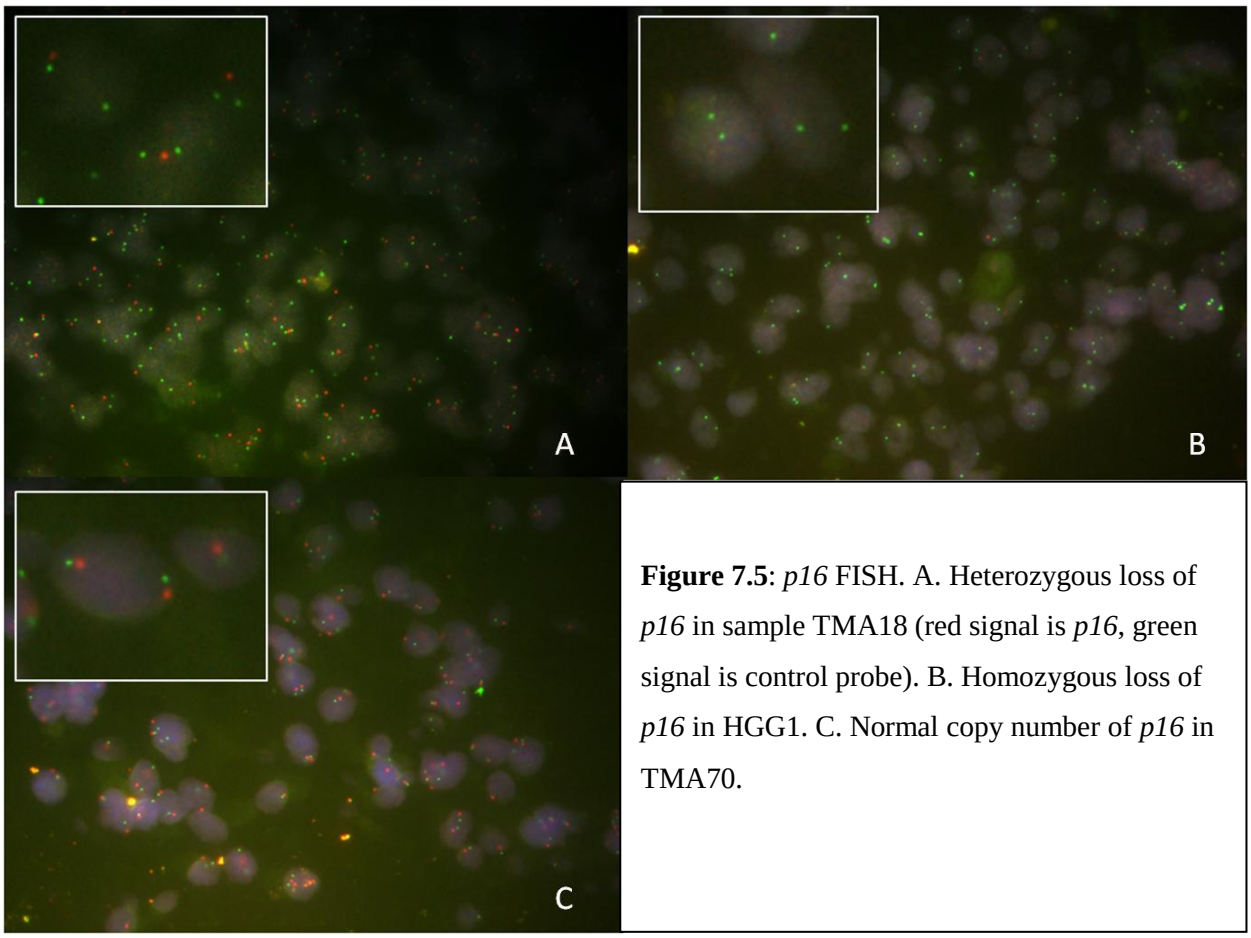

Figure 7.5: *p16* FISH. A. Heterozygous loss of *p16* in sample TMA18 (red signal is *p16*, green signal is control probe). B. Homozygous loss of *p16* in HGG1. C. Normal copy number of *p16* in TMA70.

7.3.4 Amplification of *PDGFRA*

PDGFRA FISH was performed on five of the high grade glioma TMAs as part of a separate study. There were 45 scorable samples (27 GBM, 7 AA, 3 AO and 8 brainstem tumours) across the five TMAs with six samples showing amplification of *PDGFRA*. Of the six samples with *PDGFRA* amplification, two were brainstem gliomas, two were GBMs and two AAs. 13% (6/45) of samples demonstrated amplification of *PDGFRA* by FISH whilst only 8% (3/38) samples showed amplification of *PDGFRA* by aCGH.

7.4 Immunohistochemistry

Immunohistochemistry (IHC) was performed on the high grade glioma TMAs to look at the expression of the MYCN, CDKN2B and PDGFRA proteins.

7.4.1 MYCN IHC

MYCN IHC was carried out to determine whether the level of MYCN expression in those samples that showed amplification of MYCN by aCGH or FISH was higher than those samples without *MYCN* amplification. MYCN IHC was performed on all HGG TMAs and 81 samples were scorable across the TMAs. Of those 81 samples, 67 were negative for MYCN expression and 14 samples were positive for MYCN expression. Five of the 14 samples had previously shown normal copy number of *MYCN* indicating a different mechanism of overexpression in these samples. No *MYCN* copy number data was available for the remaining five samples with overexpression of *MYCN*, and so the mechanism of overexpression is undefined. All four samples which demonstrated amplification of *MYCN* were positive for MYCN expression (Figure 7.6).

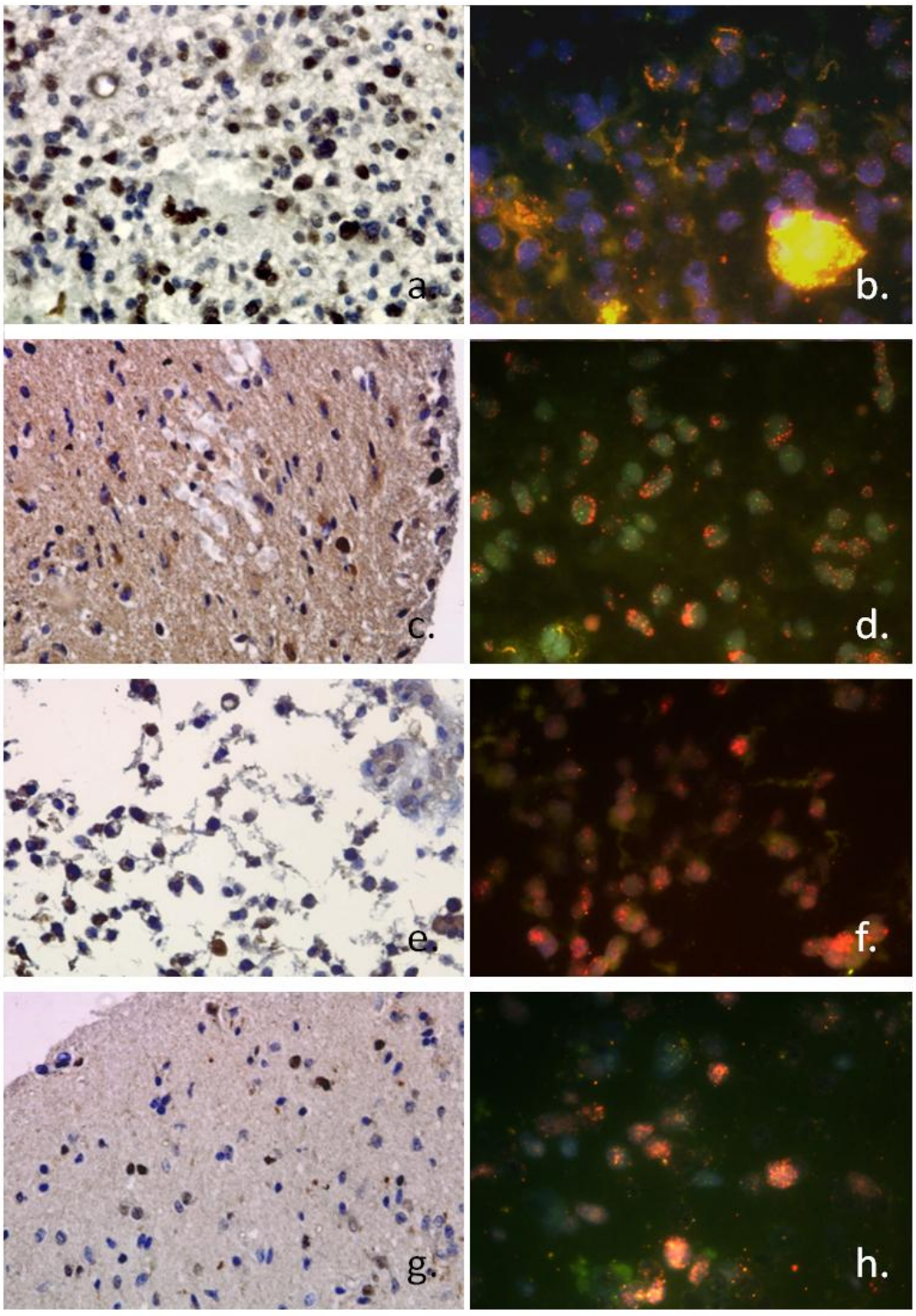

Figure 7.6: a. MYCN IHC with high level expression in sample TMA37 **b.** FISH showing amplification of *MYCN* in sample TMA37 **c.** MYCN IHC with high level expression in sample TMA60 **d.** FISH showing amplification of *MYCN* in sample TMA60 **e**. MYCN IHC with high level expression in sample HGG20 **f**. FISH showing amplification of *MYCN* in sample HGG20 **g**. MYCN IHC with high level expression in sample HGG15 **h**. FISH showing amplification of *MYCN* in sample HGG15.

7.4.2 CDKN2B IHC

CDKN2B IHC was performed to investigate levels of expression of CDKN2B in samples with normal *CDKN2B* copy number compared to those samples with loss of one or both copies of *CDKN2B*, as shown in previous experiments. CDKN2B IHC was performed on all HGG TMAs and 93 samples were scorable. 38/93 samples were negative for CDKN2B expression, 35 samples showed low level expression of CDKN2B and 20 samples showed high level expression of CDKN2B (Figure 7.7).

Out of the 93 samples scorable for IHC, four samples had shown homozygous loss of *CDKN2B* in previous experiments. All four samples were negative for expression of CDKN2B. 2/93 samples had previously shown heterozygous loss of *CDKN2B*. One of these samples was negative for CDKN2B expression and the other sample showed low level expression of CDKN2B.

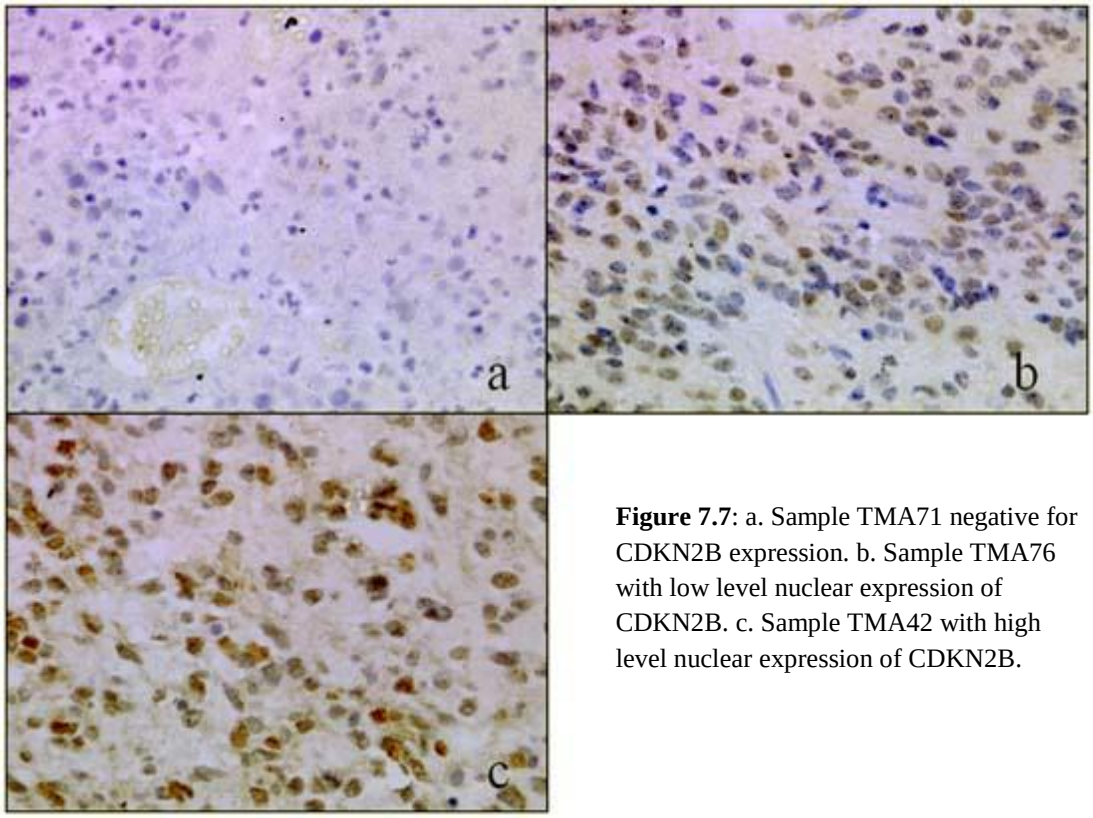

Figure 7.7: a. Sample TMA71 negative for CDKN2B expression. b. Sample TMA76 with low level nuclear expression of CDKN2B. c. Sample TMA42 with high level nuclear expression of CDKN2B.

Of the 38 samples negative for CDKN2B expression, five were infratentorial tumours and 33 were supratentorial tumours. Of the 55 samples positive for

CDKN2B expression, 46 had location data available. 30/46 were supratentorial and 16/46 infratentorial. Therefore, around half the supratentorial tumours were negative and around half were positive, whilst a quarter of infratentorial tumours were negative and ¾ were positive. This comparison between CDKN2B expression in supratentorial and infratentorial tumours is statistically significant (p = 0.03).

7.4.3 PDGFRA IHC

PDGFRA IHC was performed across all HGG TMAs (Figure 7.8). 101 samples were scorable for PDGFRA expression. Of those 101 samples, 75 samples were negative for PDGFRA expression, 12 samples showed weak expression of PDGFRA and 14 samples showed strong expression of PDGFRA.

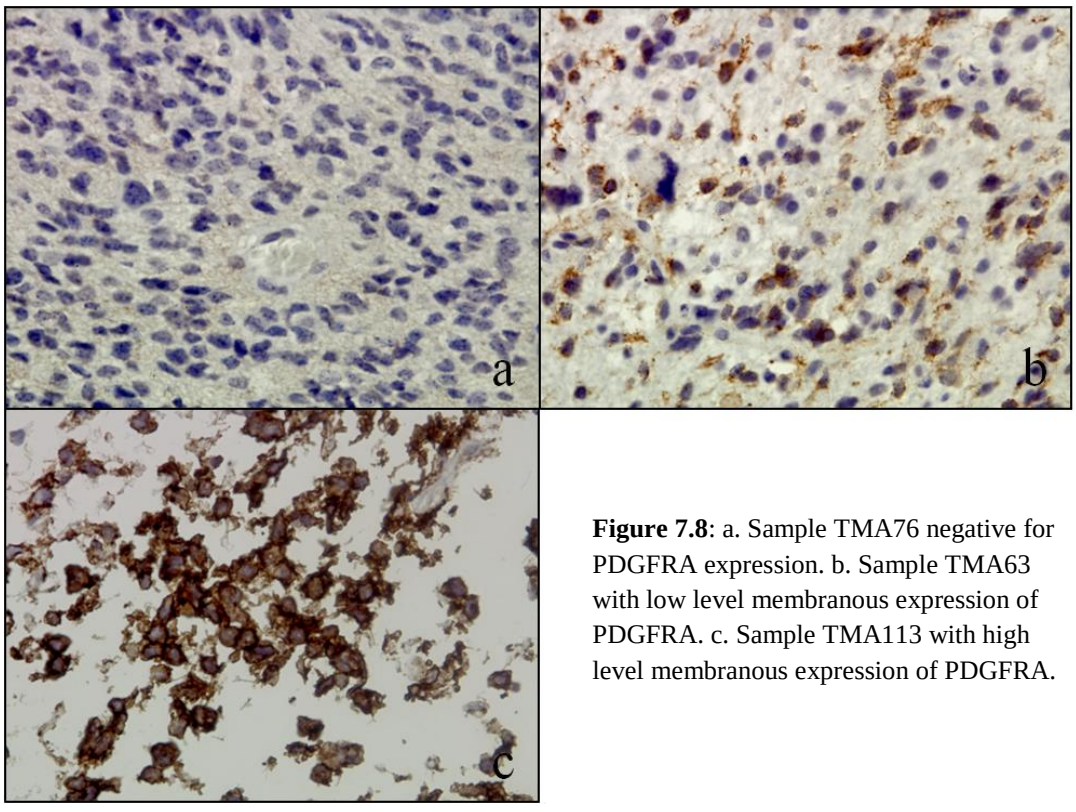

Figure 7.8: a. Sample TMA76 negative for PDGFRA expression. b. Sample TMA63 with low level membranous expression of PDGFRA. c. Sample TMA113 with high level membranous expression of PDGFRA.

Four of the scorable samples on the TMA had previously demonstrated amplification or high level gain either by aCGH or by FISH as part of a separate study. Of these

four samples, three showed high expression of PDGFRA whilst the other sample appeared to be negative for expression of PDGFRA.

7.5 Discussion

In a study where the starting DNA material was degraded DNA isolated from FFPE samples, validation is especially important. The optimal quantity of FFPE DNA was shown to be 25 ng for qPCR, which is higher than that of frozen DNA. This is as expected due to the fragmentation of the FFPE DNA. Several tumour samples repeatedly failed to work in a qPCR reaction probably due to the degraded nature of the DNA. This, in addition to the DNA for many samples having been depleted by aCGH, made it important to carefully select which of the available samples to use for validation, and how many samples to use for each gene.

Despite concerns regarding the quality of the DNA the majority of the genes selected for further study were validated, with the qPCR results confirming those seen in the aCGH data. However, the gains of *CCND1* and *CDK4* seen in the aCGH data failed to validate. Both these genes were in noisy regions on chromosome 11 and 12 respectively. The gain of 11q13 was seen in around 40% samples and the size of the apparent region of gain was similar in all samples. The two samples that were used for *CCND1* qPCR were the two samples which appeared to have the highest level of *CCND1* gain in the aCGH data, excluding the sample with amplification. These two samples both gave a normal derivative copy number by qPCR. However, *FGF3* which is in the same region and was also seen gained in the aCGH data did validate by qPCR. Unfortunately, the DNA for samples with gain at 11q13 was limited and only two samples that showed gain by aCGH could be validated. The fact *FGF3* validated and *CCND1* did not may indicate that the gain of *FGF3* is real and because the region is noisy CGH Analytics has called a larger region as gained than is actually gained. Another explanation could be that only part of the *CCND1* gene is gained and that the primers were designed to target a region of the gene that wasn't gained. Because of the lack of DNA available for these samples it is not possible to do further qPCR experiments on this sample set.

Gain of 1q was the most common whole chromosome arm aberration seen in the aCGH study (22%). The 1q FISH showed a very similar level of 1q gain with 11/41 (27%) samples having gain of 1q. Gain of 1q has been previously reported as commonly gained in paediatric high grade glioma, as well as other paediatric brain tumours. It is not known why 1q is gained at such high frequencies in these tumours or the effect on the behaviour of the tumour as a result. It was shown in the aCGH data that the whole of 1q was gained as opposed to just regions of 1q as sometimes seen in other tumours, e.g. paediatric ependymoma (Dyer, Prebble et al. 2002).

High level *MYCN* amplification was seen in 5% tumours in the aCGH study. 4/80 samples showed amplification of *MYCN* by FISH with two of those samples being the two samples identified as having *MYCN* amplification by aCGH. Interestingly, three out of the four tumours with *MYCN* amplification were anaplastic astrocytomas with the other sample being a brainstem glioma. Amplification of this oncogene has been associated with poor prognosis in other tumour types including neuroblastoma (Tonini, Boni et al. 1997). However none of the grade IV GBMs in this study showed amplification of *MYCN*. *MYCN* amplification was shown to be significantly associated with anaplastic astrocytomas (p=0.03). More cases need to be studied to further explore the relationship between *MYCN* amplification and anaplastic astrocytoma.

Loss of *p16* (*CDKN2A* and *B*) was seen in 10% samples by aCGH, and all of those samples were supratentorial GBMs. In the FISH experiment 8/61 samples showed loss of either one or two copies of p16. As seen in the aCGH data, all eight samples showing loss at *p16* were supratentorial GBMS. No infratentorial tumours, including brainstem tumours, showed loss at *p16*. This would indicate different mechanisms or different pathways being disrupted in supratentorial and infratentorial tumours. The association of *CDKN2A/B* with supratentorial high grade gliomas has not been previously reported. Unfortunately the numbers in this study were insufficient for the association of *CDKN2A/B* loss with supratentorial GBMs to be significant. However, the differential expression of CDKN2B between supratentorial and infratentorial tumours, shown using IHC, is statistically significant (p = 0.03).

The FISH for *PDGFRA* was performed as part of a separate study. 3/39 samples analysed by aCGH showed amplification of *PDGFRA*. In the FISH study 6/45 showed amplification of *PDGFRA*, which is always twice the frequency seen in the aCGH study. However, the frequency of *PDGFRA* amplification in the FISH data is closer to the frequency previously reported in other studies. It may be that the probes on the aCGH arrays are not correctly designed to detect some of the *PDGFRA* amplifications.

IHC across TMAs allows efficient screening of a large sample set for expression of a target protein. IHC for expression of MYCN, CDKN2B and PDGFRA was performed for this study. MYCN IHC showed expression in those samples with MYCN amplification and low level or negative MYCN expression in all other samples. Whilst MYCN IHC was as expected, CDKN2B IHC proved harder to interpret. However, all samples that had homozygous loss of CDKN2B and had expression data available from IHC showed negative expression of CDKN2B.

CHAPTER 8

FINAL DISCUSSION

8.0 Final discussion

Original hypotheses;

- Paediatric and adult high grade glioma have different genetic causes.
- High grade glioma occurring in the brainstem are genetically distinct from high grade glioma in the cerebrum.
- High grade glioma occurring in children over 3 years old are genetically distinct from those tumours occurring in children under 3 years old.

The aim of this study was to use DNA isolated from formalin fixed brain tumour samples to facilitate the identification of aberrant regions and genes that would lead to diagnostic and prognostic markers for paediatric high grade glioma. Formalin fixed tumour samples is a resource which is only now starting to be exploited in cancer research. A large number of FFPE blocks are available for many types of cancer and so high throughput genomic techniques which can allow for the degraded nature of FFPE DNA will open up a whole new sample set. This is vitally important for tumours that are rare or that only small samples can be taken from, such as brainstem tumours.

In this study, only around half the FFPE blocks from which DNA isolation was attempted provided DNA of sufficient quality and quantity for oligo aCGH. However, new DNA isolation techniques are being developed all the time and so this number can only improve. The quality of the isolated DNA varied widely and although multiplex PCR gave an indication of how degraded the DNA was, the results of the PCR were often not as clear as hoped. A handful of samples failed to label in the preparation for aCGH probably due to the poor quality of the DNA. Since this study was completed, Agilent Technologies have released a new labelling kit specifically for use with FFPE DNA which uses non-enzymatic labelling to overcome the problems of DNA fragmentation. The new labelling method is based on Kreatech's Universal Linkage System (Stretton Scientific, Stretton, UK) and

involves the binding of a platinum complex, labelled with either Cy-3 or Cy-5, directly to the N7 position of guanine bases in the DNA (De Witte 2007). This direct method labels independently of fragment length which makes it ideal for poor quality FFPE DNA. If this new kit had been available to be used in this study may be even less samples would have failed the labelling step.

38 FFPE samples were run on Agilent 244K oligo arrays with mixed results ranging from very clean, precise genomic profiles to messy, difficult to interpret profiles. The Agilent guidelines for array quality are stringent and not designed for this type of research. The majority of arrays in this study failed most of the QC thresholds that Agilent has set and yet aberrations in the majority of these samples, both whole arm aberrations and regions, were clearly visible. This illustrates that a change in attitude may be required towards using low quality samples, and that although the data maybe noisy and take more time to analyse useful data can be produced from even the poorest samples.

The oligo aCGH results described a heterogeneous sample set with widespread chromosome arm gains and losses, and many other regional aberrations. Gain of 1q was the most common arm aberration, and is also seen in other paediatric brain tumours. Why gain of 1q is such a frequent event in these tumours, and indeed other paediatric cancers, is as yet unknown. Loss of 10q was also frequent with 10q being the location of the tumour suppressor *PTEN* which is lost in up to 80% adult high grade gliomas (Paugh, Qu et al. 2010). Overall, more regions of gain were seen than regions of loss across all the samples. Amplification of genes *PDGFRA, KIT, MYCN, QKI* and *CCN D1* was seen at varying frequencies, with amplification of *PDGFRA* being the most common amplification. There were several focal regions of loss including loss of *CDKN2A* and *B* and loss at 8p11.

Homozygous loss at 8p11.23 was seen in 16% of high grade gliomas and has not been previously reported in adult or paediatric high grade gliomas. The minimal deleted region is of the gene *ADAM3A.* The *ADAM* (A Disintegrin And

Metalloproteinase) family of genes are widely expressed and have many potential functions relating to cell to cell communication and adhesion. Little is known about *ADAM3A* and it is listed on PubMed as a pseudogene and has been reported as non-functional in humans (Grzmil, Kim et al. 2001). However, a number of other papers have described a role for *ADAM3A* in spermatogenesis and fertilisation. (McLaughlin, Frayne et al. 2001) The *ADAM* family of genes have functions relating to cell to cell communication and adhesion and several other members of the *ADAM* gene family have been implicated in cancer. Notable examples include overexpression of *ADAM28* in lung and breast carcinomas (Mochizuki and Okada 2009) and loss of expression of *ADAM23* in breast tumours correlating with increasing grade (Seniski, Camargo et al. 2009) (Costa, Verbisck et al. 2004). *ADAM17* has been shown to be involved in EGFR regulation, and overexpression of *ADAM17* in astrocytes promotes an increase in cell proliferation and invasion (Katakowski, Jiang et al. 2009). This novel homozygous deletion of *ADAM3A* merits further study. 8p11.23 has been identified as a CNV and as matched somatic DNA was not available for the samples in this study it is important to note that this deletion could be a somatic CNV. It would be interesting to look at the expression of *ADAM3A,* possibly by IHC on HGG TMAs, to see if *ADAM3A* is being expressed in samples without deletion of *ADAM3A*.

Using FISH on FFPE tissue microarrays is a fast, efficient way of screening a high number of samples at once for a specific aberration, and as shown in this study can be very successful. Constructing TMAs allows FFPE samples, including those that maybe do not have enough tissue available for DNA isolation, to be analysed by methods such as FISH and IHC. FISH was used in this study to confirm the frequency of 1q gain, *MYCN* amplification and *CDKN2A* and *B* loss in paediatric gliomas, and indeed the frequency of these aberrations was almost identical in the aCGH data and the FISH data.

In addition to confirming the frequencies of the aberrations, FISH also allowed some further conclusions to be made. Loss of *CDKN2A* and *B* occurred in 10% samples in the aCGH analysis, and the size of the deleted region varied between these samples

from a small discrete deletion to loss of over half the 9p chromosome arm. *CDKN2A* and *CDKN2B* are well characterised tumour suppressors that are known to be deleted in other types of paediatric brain tumours and other cancers, including adult high grade gliomas. *CDKN2A* and *CDKN2B* loss was only seen in supratentorial GBMs in the aCGH data and the *p16* FISH across a larger sample set showed the same result; there was no loss of *CDKN2A* and *CDKN2B* in any infratentorial tumours including brainstem tumours, only in supratentorial GBMs. This may point to a cell of origin effect as seen in ependymoma (Taylor, Poppleton et al. 2005). Deletion of *CDKN2A/B* in 24% of paediatric high grade glioma has been previously reported (Paugh, Qu et al. 2010). In this study deletion of *CDKN2A/B* was seen in 10% samples by aCGH and 13% samples by FISH. Unfortunately, the number of samples in this study was insufficient for the relationship between *CDKN2A*/*B* loss and supratentorial GBMs to be significant. However, differential expression of CDKN2B in infratentorial and supratentorial tumours was shown to be significant by IHC ($p = 0.03$). The results of methylation analysis of *CDKN2A* and *CDKN2B* in these tumours would be interesting and mutation analysis could also be performed to further investigate this site-associated aberration.

MYCN amplification was seen in one anaplastic astrocytoma and one brainstem tumour in the aCGH data. The FISH results confirmed both these amplifications and showed a further two samples with *MYCN* amplification, both of which were anaplastic astrocytomas. *MYCN* amplification was shown to be significantly associated with anaplastic astrocytomas ($p=0.03$). *MYCN* is highly amplified in neuroblastoma but has also been reported amplified in CNS PNETs, medulloblastoma and paediatric high grade gliomas, as well as non-brain tumours. *MYCN* is a proto-oncogene and part of the MYC transcription factor family and amplification is often associated with poor outcome in other tumour types, (Tonini, Boni et al. 1997) so it is interesting that *MYCN* amplification is seen in AAs and not the more aggressive grade IV GBMs. A larger cohort of samples, particularly larger numbers of AAs, would need to be analysed either by FISH or by microarray analysis to further establish this relationship.

The lack of *p16* loss in infratentorial tumours and the absence of *MYCN* amplification in any of the GBMs analysed are both interesting results that could be further investigated in future projects.

A small sub-group of tumours (13%) appeared to have balanced genomes by aCGH analysis. This has also been seen in other paediatric tumours including ependymoma, CNS PNETs and Wilms' Tumours (Dyer, Prebble et al. 2002; Natrajan, Williams et al. 2006). The lack of copy number changes indicates that these tumours may be driven purely by mutations or by epigenetic mechanisms. Methylation and expression studies may provide further insight into this subset of tumours. Methylation analysis is currently being carried out on a cohort of pHGG tumours including some tumours with balanced genomes. This methylation data combined with expression data will expand our understanding of balanced tumours and allow further insight into pHGG as a whole.

The quantity and quality of the DNA isolated from the FFPE samples was the limiting factor in this study. Some samples were completely used for aCGH, whilst others were depleted or of insufficient quality for qPCR. This meant that validation studies had to be carefully planned and were not as extensive as they might have been if more DNA had been available. Real time quantitative PCR (qPCR) proved to work successfully with the majority of remaining FFPE DNA samples once the technique had been optimised for FFPE DNA. Samples that repeatedly failed to work with qPCR were those that had given the noisiest aCGH profiles and so the failure was most likely due to the poor quality of these samples. On the whole, those genes that were chosen for validation validated well. However, the high frequency of *CCND1* gain failed to validate although the results for *FGF3* which is adjacent to *CCND1* were more encouraging. This region on 11q13 was a noisy region across the whole sample set and this shows the importance of validation when using degraded DNA.

8.1 Original Hypotheses

Paediatric and adult high grade glioma have different genetic causes.

The findings in this study have shown that paediatric and adult high grade gliomas represent two different genetic entities that are distinguished by differences in copy number changes. The most obvious difference is the increased frequency gain of 1q in paediatric high grade glioma compared to adult tumours. Gain of 1q is commonly seen in paediatric brain tumours including CNS PNETs, ependymoma and high grade glioma. In this study 21% of high grade gliomas demonstrated gain of 1q by aCGH whilst only 9% of adult high grade gliomas have been reported to have gain 1q (TCGA 2008). A recent study by Bax et al found gain of 1q in 12/63 (19%) of paediatric high grade glioma samples. Combining data from this study with that of Bax et al reveals 20/101 (20%) paediatric high grade gliomas have gain of 1q compared to 17/189 (9%) of adult tumours. This is statistically significant ($p = 0.03$). 23% of brainstem tumours have gain of 1q which is comparable to the level of gain seen in other paediatric high grade glioma. Gain of 1q has been associated with poorer outcome in other paediatric brain tumours (Mendrzyk, Korshunov et al. 2006).

PARP-1 has been highlighted as a gene of interest on 1q in a recent brainstem glioma study by Zarghooni et al, although no focal gain of *PARP-1* was seen in this study (Zarghooni, Bartels et al. 2010). Zarghooni et al carried out IHC on a limited number of samples and saw a correlation between gain of *PARP-1* (as part of 1q gain) and increased PARP-1 expression (Zarghooni, Bartels et al. 2010). PARP-1 is a possible drug target and so further investigation of this PARP-1 expression should be carried out. PARP-1 IHC could be performed across HGG TMAs to look for a correlation between 1q gain and increased PARP-1 expression.

Loss of 10q is seen in 16% of all high grade glioma samples and only 1/13 brainstem gliomas in this study, which is notably lower than 35% loss of 10q previously reported in paediatric high grade glioma (Paugh, Qu et al. 2010). Loss of 10q is the most common whole arm aberration in adult GBM (80%) which includes loss of

PTEN (10q23). *PTEN* is a tumour suppressor which negatively regulates the Akt signalling pathway and *PTEN* loss or mutation is seen in many cancers (Maher, Furnari et al. 2001). The lack of 10q loss in this cohort may indicate a different mechanism of loss or that different pathways are involved in these paediatric tumours.

Amplification of *PDGFRA* is seen more frequently in paediatric high grade gliomas compared with adults, and has recently been reported as occurring at a frequency of ~15% in adults and ~25% in paediatric high grade gliomas (Paugh, Qu et al. 2010). This study has shown amplification of *PDGFRA* in just 2/38 (5%) high grade gliomas with an additional sample showing high level gain of *PDGFRA*. *PDGFRA* is a possible target for therapy in the subset of paediatric high grade glioma with *PDGFRA* amplification.

Expression of PDGFRA has been shown to correlate with malignant grade in pHGG, with high expression being associated with malignant histology (WHO grades III and IV) (Thorarinsdottir, Santi et al. 2008). Amplification of *PDGFRA* has recently been reported in 12% of Grade III and 17% of grade IV pHGG tumours in a large recent series based on high resolution copy number and expression profiling (Paugh, Qu et al. 2010). Similar levels of focal amplification are reported in this study based on the aCGH and IHC data. In the study by Paugh et al amplification of *PDGFRA* was found at a significantly higher frequency (50%) in irradiation induced childhood and adolescent HGG (Paugh, Qu et al. 2010). This later finding might explain the relatively high frequency of PDGFRA expression reported in a brainstem glioma study by Zarghooni et al, as 82% of their cohort was analysed post treatment (Zarghooni, Bartels et al. 2010).

Consistent with this possibility is that amplification of *PDGFRA* in adult tumours is associated with a secondary GBM (Toepoel, Joosten et al. 2008), although the time course for the latter is likely longer. Further studies of the role of PDGFRA in childhood and adolescent HGG are needed to understand the influence of treatment

on *PDGFRA* amplification and to determine whether this TRK receptor is a conditional target for therapy in the subset of pHGG with *PDGFRA* amplification.

No amplification of *EGFR* was seen in the 38 paediatric high grade glioma samples, where as *EGFR* amplification is the most common focal amplification in adult high grade gliomas (Maher, Furnari et al. 2001).

Four focal regions of amplification were seen across this data set compared to 27 different sites of amplification identified in a dataset of 97 adult high grade glioma samples by metaphase CGH (Mohapatra, Bollen et al. 1998). Moreover, a sub-group of pHGG tumours (13%) have balanced genomes by aCGH analysis. This has also been seen in other paediatric brain tumours including ependymoma and CNS PNETs (Dyer, Prebble et al. 2002; Natrajan, Williams et al. 2006). In our series of pHGG this was not defined by young age at diagnosis as for ependymoma (Dyer, Prebble et al. 2002). This important difference in the number of genomic imbalances and regions of amplification in adults and children may reflect the development of the tumour in a narrower time frame / developmental window. It might also be that other mechanisms are important in the pathogenesis of these tumours and suggests that relatively fewer mutations may be required to initiate the disease if these arise within a specific developmental period.

High grade glioma occurring in the brainstem are genetically distinct from other high grade gliomas.

The brainstem gliomas in this study demonstrated many of the same aberrations as the other high grade tumours in the study e.g. *PDGFRA* amplification, *MYCN* amplification, 1q gain. As a group the brainstem gliomas were as heterogeneous as the other high grade gliomas and displayed many of the same aberrations. One difference between the brainstem tumours and the other high grade tumours was the lack of *CDKN2A* and *B* loss in the brainstem tumours. Similar findings were recently

reported in a study by Zarghooni et al (Zarghooni, Bartels et al. 2010). However, since *CDKN2A* and *B* loss was seen only in supratentorial GBMs it may be that high grade gliomas should be grouped into supratentorial and infratentorial rather than brainstem and non-brainstem. Interestingly, loss of *CDKN2A* and *B* has been reported in supratentorial CNS PNETs but not in infratentorial medulloblastoma (Pfister, Remke et al. 2007). The differential loss of *CDKN2A/CDKN2B* depending on tumour location may point to a cell of origin effect as seen in ependymoma (Taylor, Poppleton et al. 2005). This finding merits further study.

Loss of 14q was seen in 4/13 (31%) brainstem tumours and only 1/25 non-brainstem tumours (4%). In a recent study, Zarghooni et al also identified 14q loss as being more common in DIPG (Zarghooni, Bartels et al. 2010). Loss of 17p was seen in 4/13 (31%) brainstem tumours and only 1/25 non-brainstem tumours. Zarghooni et al also reported 17p loss associated with paediatric DIPG compared to non-brainstem high grade gliomas (Zarghooni, Bartels et al. 2010). Combining data from this study and that of Zarghooni et al reveals 11/24 (46%) DIPG had loss of 17p whilst only 3/36 (8%) of non-brainstem tumours had loss of 17p, which is statistically significant ($p = 0.02$). Interestingly, loss of 17p is seen in up to 50% of infratentorial medulloblastoma but is rarely seen in supratentorial CNS PNETs (De Smaele, Di Marcotullio et al. 2004). This site related difference in the frequency of 17p loss and 14q loss deserves further study. 17p and 14q FISH could be performed across HGG TMAs to further investigate the relationship between loss of these chromosome arms and brainstem gliomas.

Loss of 10q was seen in only 8% of brainstem tumours compared to 18% of high grade gliomas overall in this study. Loss of 10q is the location of a number of tumour suppressors, most notably *PTEN* which is implicated in adult high grade glioma. The lack of 10q loss in brainstem gliomas may indication a different mechanism of tumour suppressor loss in these tumours, or that different pathways are involved.

Zarghooni et al identified a number of genes involved in DNA repair pathways as being lost in brainstem gliomas compared to supratentorial high grade gliomas (Zarghooni, Bartels et al. 2010). Loss of some of these DNA repair pathway genes was seen in this study as part of whole arm deletions, e.g. 17p (*RPA1* and *MYH1*, 14q (*MNAT1* and *RAD51L1*) and 1p (*MSH4*). However, losses of other DNA repair pathway genes identified by Zarghooni were not seen in this study (*GTF2H3, LIG4, XRCC4, XRCC5, MLH1, BRCA1, BRCA2, RAD50, DUT, PMS1*) (Zarghooni, Bartels et al. 2010). Importantly their cohort included just two pre-treatment samples compared to ten pre-treatment brainstem samples in this study suggesting that treatment with DNA damaging agents such as radiotherapy and temozolomide may be responsible for the loss of DNA repair pathway genes and possibly other genetic aberrations.

It has previously been shown that diagnostic biopsy of diffuse brainstem glioma is relatively safe (Cartmill and Punt 1999) and this study demonstrates that pre treatment tumour tissue, even small samples from biopsy, can generate high quality biological information on which to base future strategies. Therefore, it is important that brainstem gliomas are biopsied to allow further studies into these devastating tumours.

High grade glioma occurring in children over three years old are genetically distinct from those tumours occurring in children under three years old.

At the start of this study one aim was to look at the genetic differences between children diagnosed with a high grade glioma under the age of three and those diagnosed over the age of three. Unfortunately, the majority of the samples in this study were from children over three although some samples were missing clinical information and so age at diagnosis was unknown. This group of samples is very important as the underlying biology is thought to be different to that of tumours occurring in children over three.

The oligo aCGH on FFPE high grade samples was part of a larger study to comprehensively map the genetic profiles of these tumours. By performing aCGH on DNA isolated from FFPE high grade glioma samples many aberrations were discovered across the sample set. The results of this study, combined with SNP data, methylation data and expression data and will hopefully lead to a wider understanding of the genetic profiles of paediatric high grade glioma. If complete clinical information can be gathered for these samples and all the data pulled together then hopefully diagnostic or prognostic targets can be teased out for these complex, heterogeneous tumours.

This study involved the high-throughput analysis of the largest ever cohort of brainstem gliomas (13) plus 25 non-brainstem pHGG. Although the tissue used in this study was FFPE tissue which presents problems with DNA quality, and therefore quality of array data produced, the results of this study have still provided interesting and novel data on these rare tumours. When the DNA isolation and aCGH was performed for this study there were very few protocols and kits being produced by companies specifically for FFPE tissue. Over the past few years the interest in using FFPE tissue for high-throughput techniques has led to the development of DNA isolation methods and array protocols specifically for FFPE DNA. If these had been available for this study then results may have been less noisy and less complex to analyse. However, the data from this study is still useful and has shown novel aberrations as well as confirming aberrations and frequencies of aberrations seen in the few other studies of pHGG.

BIBLIOGRAPHY

Abdel-Rahman, W. M. (2008). "Genomic instability and carcinogenesis: an update." Curr Genomics **9**(8): 535-541.

Affymetrix (2006). www.affymetrix.com.

Alcantara Llaguno, S., J. Chen, et al. (2009). "Malignant astrocytomas originate from neural stem/progenitor cells in a somatic tumor suppressor mouse model." Cancer Cell **15**(1): 45-56.

Baruchel, S., J. R. Sharp, et al. (2009). "A Canadian paediatric brain tumour consortium (CPBTC) phase II molecularly targeted study of imatinib in recurrent and refractory paediatric central nervous system tumours." Eur J Cancer **45**(13): 2352-2359.

Bockbrader, K. and Y. Feng (2008). "Essential function, sophisticated regulation and pathological impact of the selective RNA-binding protein QKI in CNS myelin development." Future Neurol **3**(6): 655-668.

Boland, C. R. and A. Goel (2010). "Microsatellite instability in colorectal cancer." Gastroenterology **138**(6): 2073-2087 e2073.

Boyd, K. P., B. R. Korf, et al. (2009). "Neurofibromatosis type 1." J Am Acad Dermatol **61**(1): 1-14; quiz 15-16.

Broniscer, A. and A. Gajjar (2004). "Supratentorial high-grade astrocytoma and diffuse brainstem glioma: two challenges for the pediatric oncologist." Oncologist **9**(2): 197-206.

Brown, K. W., F. Power, et al. (2008). "Frequency and timing of loss of imprinting at 11p13 and 11p15 in Wilms' tumor development." Mol Cancer Res **6**(7): 1114-1123.

Cairncross, J. G., K. Ueki, et al. (1998). "Specific genetic predictors of chemotherapeutic response and survival in patients with anaplastic oligodendrogliomas." J Natl Cancer Inst **90**(19): 1473-1479.

Cartmill, M. and J. Punt (1999). "Diffuse brain stem glioma. A review of stereotactic biopsies." Childs Nerv Syst **15**(5): 235-237; discussion 238.

Carvalho, B., E. Ouwerkerk, et al. (2004). "High resolution microarray comparative genomic hybridisation analysis using spotted oligonucleotides." J Clin Pathol **57**(6): 644-646.

Catteau, A., W. H. Harris, et al. (1999). "Methylation of the BRCA1 promoter region in sporadic breast and ovarian cancer: correlation with disease characteristics." Oncogene **18**(11): 1957-1965.

Chan, T., S. Yuen, et al. (1999). "Germline hMSH2 and differential somatic mutations in patients with Turcot's syndrome. Genes Chromosomes Cancer 25:75-81, 1999." Genes Chromosomes Cancer **26**(3): 273.

Choux, M., DiRocco, C., Walker, M.L., Hockley, A.D. (2000). Pediatric Neurosurgery, Churchill Livingstone.

Costa, F. F., N. V. Verbisck, et al. (2004). "Epigenetic silencing of the adhesion molecule ADAM23 is highly frequent in breast tumors." Oncogene **23**(7): 1481-1488.

Cowell, J. K., S. Matsui, et al. (2004). "Application of bacterial artificial chromosome array-based comparative genomic hybridization and spectral karyotyping to the analysis of glioblastoma multiforme." Cancer Genet Cytogenet **151**(1): 36-51.

De Smaele, E., L. Di Marcotullio, et al. (2004). "Chromosome 17p deletion in human medulloblastoma: a missing checkpoint in the Hedgehog pathway." Cell Cycle **3**(10): 1263-1266.

De Witte, A., Lea-Chou, E., Collins, J. (2007). Copy Number Analysis of Archival FFPE Tumor Samples

by Oligo Array CGH. A. Technologies.

Dong, S., E. Wang, et al. (2001). "Flexible use of high-density oligonucleotide arrays for single-nucleotide polymorphism discovery and validation." Genome Res **11**(8): 1418-1424.

Duffner, P. K., J. P. Krischer, et al. (1996). "Treatment of infants with malignant gliomas: the Pediatric Oncology Group experience." J Neurooncol **28**(2-3): 245-256.

Durkin, S. G. and T. W. Glover (2007). "Chromosome fragile sites." Annu Rev Genet **41**: 169-192.

Dyer, S., E. Prebble, et al. (2002). "Genomic imbalances in pediatric intracranial ependymomas define clinically relevant groups." Am J Pathol **161**(6): 2133-2141.

Epstein, F. (1985). "A staging system for brain stem gliomas." Cancer **56**(7 Suppl): 1804-1806.

Esteller, M., J. Garcia-Foncillas, et al. (2000). "Inactivation of the DNA-repair gene MGMT and the clinical response of gliomas to alkylating agents." N Engl J Med **343**(19): 1350-1354.

Evans, D. G. (2009). "Neurofibromatosis type 2 (NF2): a clinical and molecular review." Orphanet J Rare Dis **4**: 16.

Fanton, C. P., M. McMahon, et al. (2001). "Dual growth arrest pathways in astrocytes and astrocytic tumors in response to Raf-1 activation." J Biol Chem **276**(22): 18871-18877.

Faury, D., A. Nantel, et al. (2007). "Molecular profiling identifies prognostic subgroups of pediatric glioblastoma and shows increased YB-1 expression in tumors." J Clin Oncol **25**(10): 1196-1208.

Fellermann, K., D. E. Stange, et al. (2006). "A chromosome 8 gene-cluster polymorphism with low human beta-defensin 2 gene copy number predisposes to Crohn disease of the colon." Am J Hum Genet **79**(3): 439-448.

Freeman, C. R. and J. P. Farmer (1998). "Pediatric brain stem gliomas: a review." Int J Radiat Oncol Biol Phys **40**(2): 265-271.

Fruhwald, M. C., M. S. O'Dorisio, et al. (2000). "Gene amplification in PNETs/medulloblastomas: mapping of a novel amplified gene within the MYCN amplicon." J Med Genet **37**(7): 501-509.

Garinis, G. A., G. P. Patrinos, et al. (2002). "DNA hypermethylation: when tumour suppressor genes go silent." Hum Genet **111**(2): 115-127.

Giunta, S. (2009). "A gust of WNT: analysis of the canonical WNT pathway." Acta Biomed **80**(3): 187-199.

Godard, S., G. Getz, et al. (2003). "Classification of human astrocytic gliomas on the basis of gene expression: a correlated group of genes with angiogenic activity emerges as a strong predictor of subtypes." Cancer Res **63**(20): 6613-6625.

Grzmil, P., Y. Kim, et al. (2001). "Human cyritestin genes (CYRN1 and CYRN2) are non-functional." Biochem J **357**(Pt 2): 551-556.

Halatsch, M. E., U. Schmidt, et al. (2006). "Epidermal growth factor receptor inhibition for the treatment of glioblastoma multiforme and other malignant brain tumours." Cancer Treat Rev **32**(2): 74-89.

Hamilton, S. R., B. Liu, et al. (1995). "The molecular basis of Turcot's syndrome." N Engl J Med **332**(13): 839-847.

Hargrave, D., U. Bartels, et al. (2006). "Diffuse brainstem glioma in children: critical review of clinical trials." Lancet Oncol **7**(3): 241-248.

Hegi, M. E., A. C. Diserens, et al. (2005). "MGMT gene silencing and benefit from temozolomide in glioblastoma." N Engl J Med **352**(10): 997-1003.

Hemmati, H. D., I. Nakano, et al. (2003). "Cancerous stem cells can arise from pediatric brain tumors." Proc Natl Acad Sci U S A **100**(25): 15178-15183.

Herr, A., R. Grutzmann, et al. (2005). "High-resolution analysis of chromosomal imbalances using the Affymetrix 10K SNP genotyping chip." Genomics **85**(3): 392-400.
Hezova, R., J. Ehrmann, et al. (2007). "WWOX, a new potential tumor suppressor gene." Biomed Pap Med Fac Univ Palacky Olomouc Czech Repub **151**(1): 11-15.
Holland, E. C., W. P. Hively, et al. (1998). "A constitutively active epidermal growth factor receptor cooperates with disruption of G1 cell-cycle arrest pathways to induce glioma-like lesions in mice." Genes Dev **12**(23): 3675-3685.
Hu, J., J. C. Pang, et al. (2002). "High-resolution genome-wide allelotype analysis identifies loss of chromosome 14q as a recurrent genetic alteration in astrocytic tumours." Br J Cancer **87**(2): 218-224.
Inazawa, J., J. Inoue, et al. (2004). "Comparative genomic hybridization (CGH)-arrays pave the way for identification of novel cancer-related genes." Cancer Sci **95**(7): 559-563.
Iwama, T. (2001). "Somatic mutation rate of the APC gene." Jpn J Clin Oncol **31**(5): 185-187.
Jallo, G. I., A. Biser-Rohrbaugh, et al. (2004). "Brainstem gliomas." Childs Nerv Syst **20**(3): 143-153.
Jenner, M. W., P. E. Leone, et al. (2007). "Gene mapping and expression analysis of 16q loss of heterozygosity identifies WWOX and CYLD as being important in determining clinical outcome in multiple myeloma." Blood **110**(9): 3291-3300.
Johnson, N. A., R. A. Hamoudi, et al. (2006). "Application of array CGH on archival formalin-fixed paraffin-embedded tissues including small numbers of microdissected cells." Lab Invest **86**(9): 968-978.
Jones, P. A. and D. Takai (2001). "The role of DNA methylation in mammalian epigenetics." Science **293**(5532): 1068-1070.
Katakowski, M., F. Jiang, et al. (2009). "Tumorigenicity of cortical astrocyte cell line induced by the protease ADAM17." Cancer Sci **100**(9): 1597-1604.
King, R. (2000). Cancer Biology, Pearson Education Limited.
Koch, A., A. Waha, et al. (2001). "Somatic mutations of WNT/wingless signaling pathway components in primitive neuroectodermal tumors." Int J Cancer **93**(3): 445-449.
Korkolopoulou, P., K. Kouzelis, et al. (1998). "Expression of retinoblastoma gene product and p21 (WAF1/Cip 1) protein in gliomas: correlations with proliferation markers, p53 expression and survival." Acta Neuropathol (Berl) **95**(6): 617-624.
Kramm, C. M., S. Wagner, et al. (2006). "Improved survival after gross total resection of malignant gliomas in pediatric patients from the HIT-GBM studies." Anticancer Res **26**(5B): 3773-3779.
Kreiger, P. A., Y. Okada, et al. (2005). "Losses of chromosomes 1p and 19q are rare in pediatric oligodendrogliomas." Acta Neuropathol (Berl) **109**(4): 387-392.
Kuiper, R. P., M. J. Ligtenberg, et al. (2010). "Germline copy number variation and cancer risk." Curr Opin Genet Dev **20**(3): 282-289.
Lo, K. C., M. R. Rossi, et al. (2007). "Genome wide copy number abnormalities in pediatric medulloblastomas as assessed by array comparative genome hybridization." Brain Pathol **17**(3): 282-296.
Louis, D. N., H. Ohgaki, et al. (2007). WHO Classification of Tumours of the Central Nervous System. Lyon, IARC.
Magdinier, F., S. Ribieras, et al. (1998). "Down-regulation of BRCA1 in human sporadic breast cancer; analysis of DNA methylation patterns of the putative promoter region." Oncogene **17**(24): 3169-3176.
Maher, E. A., F. B. Furnari, et al. (2001). "Malignant glioma: genetics and biology of a grave matter." Genes Dev **15**(11): 1311-1333.
Maris, J. M. and K. K. Matthay (1999). "Molecular biology of neuroblastoma." J Clin Oncol **17**(7): 2264-2279.

Martens, T., Y. Laabs, et al. (2008). "Inhibition of glioblastoma growth in a highly invasive nude mouse model can be achieved by targeting epidermal growth factor receptor but not vascular endothelial growth factor receptor-2." Clin Cancer Res **14**(17): 5447-5458.

Mauffrey, C. (2006). "Paediatric brainstem gliomas: prognostic factors and management." J Clin Neurosci **13**(4): 431-437.

McGillicuddy, L. T., J. A. Fromm, et al. (2009). "Proteasomal and genetic inactivation of the NF1 tumor suppressor in gliomagenesis." Cancer Cell **16**(1): 44-54.

McLaughlin, E. A., J. Frayne, et al. (2001). "Do fertilin beta and cyritestin play a major role in mammalian sperm--oolemma interactions? A critical re-evaluation of the use of peptide mimics in identifying specific oocyte recognition protiens." Mol Hum Reprod **7**(4): 313-317.

Mendrzyk, F., A. Korshunov, et al. (2006). "Identification of gains on 1q and epidermal growth factor receptor overexpression as independent prognostic markers in intracranial ependymoma." Clin Cancer Res **12**(7 Pt 1): 2070-2079.

Mendrzyk, F., A. Korshunov, et al. (2006). "Isochromosome breakpoints on 17p in medulloblastoma are flanked by different classes of DNA sequence repeats." Genes Chromosomes Cancer **45**(4): 401-410.

Mochizuki, S. and Y. Okada (2009). "ADAM28 as a target for human cancers." Curr Pharm Des **15**(20): 2349-2358.

Mohapatra, G., A. W. Bollen, et al. (1998). "Genetic analysis of glioblastoma multiforme provides evidence for subgroups within the grade." Genes Chromosomes Cancer **21**(3): 195-206.

Mulhern, R. K., T. E. Merchant, et al. (2004). "Late neurocognitive sequelae in survivors of brain tumours in childhood." Lancet Oncol **5**(7): 399-408.

Nalin Gupta, A. B., Daphne Haas-Kogan. (2004). Pediatric CNS Tumors, Springer.

Napolioni, V. and P. Curatolo (2008). "Genetics and molecular biology of tuberous sclerosis complex." Curr Genomics **9**(7): 475-487.

Natrajan, R., R. D. Williams, et al. (2006). "Array CGH profiling of favourable histology Wilms tumours reveals novel gains and losses associated with relapse." J Pathol **210**(1): 49-58.

Ohgaki, H. (2005). "Genetic pathways to glioblastomas." Neuropathology **25**(1): 1-7.

Ohgaki, H. and P. Kleihues (2007). "Genetic pathways to primary and secondary glioblastoma." Am J Pathol **170**(5): 1445-1453.

Packer, R. J. (1999). "Brain tumors in children." Arch Neurol **56**(4): 421-425.

Paugh, B. S., C. Qu, et al. (2010). "Integrated molecular genetic profiling of pediatric high-grade gliomas reveals key differences with the adult disease." Journal of Clinical Oncology **In press**.

Perry, J., A. Chambers, et al. (2007). "Gliadel wafers in the treatment of malignant glioma: a systematic review." Curr Oncol **14**(5): 189-194.

Pfister, S., M. Remke, et al. (2009). "Outcome prediction in pediatric medulloblastoma based on DNA copy-number aberrations of chromosomes 6q and 17q and the MYC and MYCN loci." J Clin Oncol **27**(10): 1627-1636.

Pfister, S., M. Remke, et al. (2007). "Supratentorial primitive neuroectodermal tumors of the central nervous system frequently harbor deletions of the CDKN2A locus and other genomic aberrations distinct from medulloblastomas." Genes Chromosomes Cancer **46**(9): 839-851.

Pollack, I. F., S. D. Finkelstein, et al. (2001). "Age and TP53 mutation frequency in childhood malignant gliomas: results in a multi-institutional cohort." Cancer Res **61**(20): 7404-7407.

Pomeroy, S. L., P. Tamayo, et al. (2002). "Prediction of central nervous system embryonal tumour outcome based on gene expression." Nature **415**(6870): 436-442.

Primrose, S. B., Twyman, R.M., Old, R.W. (2001). Principles of Gene Manipulation, Blackwell Science.

Qu, H. Q., K. Jacob, et al. (2010). "Genome-wide profiling using single-nucleotide polymorphism arrays identifies novel chromosomal imbalances in pediatric glioblastomas." Neuro Oncol **12**(2): 153-163.

Ramos, D. and C. M. Aldaz (2006). "WWOX, a chromosomal fragile site gene and its role in cancer." Adv Exp Med Biol **587**: 149-159.

Redon, R., S. Ishikawa, et al. (2006). "Global variation in copy number in the human genome." Nature **444**(7118): 444-454.

Reilly, K. M., D. A. Loisel, et al. (2000). "Nf1;Trp53 mutant mice develop glioblastoma with evidence of strain-specific effects." Nat Genet **26**(1): 109-113.

Rickert, C. H., R. Strater, et al. (2001). "Pediatric high-grade astrocytomas show chromosomal imbalances distinct from adult cases." Am J Pathol **158**(4): 1525-1532.

Rieber, J., M. Remke, et al. (2009). "Novel oncogene amplifications in tumors from a family with Li-Fraumeni syndrome." Genes Chromosomes Cancer **48**(7): 558-568.

Rosenfeld, A., R. Listernick, et al. (2009). "Neurofibromatosis type 1 and high-grade tumors of the central nervous system." Childs Nerv Syst.

Rutka, J. T., M. Murakami, et al. (1997). "Role of glial filaments in cells and tumors of glial origin: a review." J Neurosurg **87**(3): 420-430.

Samadani, U. and K. D. Judy (2003). "Stereotactic brainstem biopsy is indicated for the diagnosis of a vast array of brainstem pathology." Stereotact Funct Neurosurg **81**(1-4): 5-9.

Schinkel, A. H. (1999). "P-Glycoprotein, a gatekeeper in the blood-brain barrier." Adv Drug Deliv Rev **36**(2-3): 179-194.

Schwertfeger, K. L. (2009). "Fibroblast growth factors in development and cancer: insights from the mammary and prostate glands." Curr Drug Targets **10**(7): 632-644.

Scotting, P. J., D. A. Walker, et al. (2005). "Childhood solid tumours: a developmental disorder." Nat Rev Cancer **5**(6): 481-488.

Seniski, G. G., A. A. Camargo, et al. (2009). "ADAM33 gene silencing by promoter hypermethylation as a molecular marker in breast invasive lobular carcinoma." BMC Cancer **9**: 80.

Shah, N. and S. Sukumar (2010). "The Hox genes and their roles in oncogenesis." Nat Rev Cancer **10**(5): 361-371.

Simon, M., G. Koster, et al. (1999). "Functional evidence for a role of combined CDKN2A (p16-p14(ARF))/CDKN2B (p15) gene inactivation in malignant gliomas." Acta Neuropathol (Berl) **98**(5): 444-452.

Singh, S. and P. B. Dirks (2007). "Brain tumor stem cells: identification and concepts." Neurosurg Clin N Am **18**(1): 31-38, viii.

Soni, D., J. A. King, et al. (2005). "Genetics of glioblastoma multiforme: mitogenic signaling and cell cycle pathways converge." J Clin Neurosci **12**(1): 1-5.

Stiller, C. A. (2004). "Epidemiology and genetics of childhood cancer." Oncogene **23**(38): 6429-6444.

Stroink, A. R., H. J. Hoffman, et al. (1986). "Diagnosis and management of pediatric brain-stem gliomas." J Neurosurg **65**(6): 745-750.

Sung, T., D. C. Miller, et al. (2000). "Preferential inactivation of the p53 tumor suppressor pathway and lack of EGFR amplification distinguish de novo high grade pediatric astrocytomas from de novo adult astrocytomas." Brain Pathol **10**(2): 249-259.

Suzuki, T., M. Maruno, et al. (2004). "Genetic analysis of human glioblastomas using a genomic microarray system." Brain Tumor Pathol **21**(1): 27-34.

Tamarin, R. (2002). Principles of Genetics, McGraw-Hill.

Taylor, M. D., H. Poppleton, et al. (2005). "Radial glia cells are candidate stem cells of ependymoma." Cancer Cell **8**(4): 323-335.

TCGA (2008). "Comprehensive genomic characterization defines human glioblastoma genes and core pathways." Nature **455**(7216): 1061-1068.

Thorarinsdottir, H. K., M. Santi, et al. (2008). "Protein expression of platelet-derived growth factor receptor correlates with malignant histology and PTEN with survival in childhood gliomas." Clin Cancer Res **14**(11): 3386-3394.

Toepoel, M., P. H. Joosten, et al. (2008). "Haplotype-specific expression of the human PDGFRA gene correlates with the risk of glioblastomas." Int J Cancer **123**(2): 322-329.

Tonini, G. P., L. Boni, et al. (1997). "MYCN oncogene amplification in neuroblastoma is associated with worse prognosis, except in stage 4s: the Italian experience with 295 children." J Clin Oncol **15**(1): 85-93.

van Beers, E. H., S. A. Joosse, et al. (2006). "A multiplex PCR predictor for aCGH success of FFPE samples." Br J Cancer **94**(2): 333-337.

Vescovi, A. L., R. Galli, et al. (2006). "Brain tumour stem cells." Nat Rev Cancer **6**(6): 425-436.

Waller, C. F. (2010). "Imatinib mesylate." Recent Results Cancer Res **184**: 3-20.

Warr, T., S. Ward, et al. (2001). "Identification of extensive genomic loss and gain by comparative genomic hybridisation in malignant astrocytoma in children and young adults." Genes Chromosomes Cancer **31**(1): 15-22.

Wolfsberg, T. G., P. D. Straight, et al. (1995). "ADAM, a widely distributed and developmentally regulated gene family encoding membrane proteins with a disintegrin and metalloprotease domain." Dev Biol **169**(1): 378-383.

Wong, K. K., Y. T. Tsang, et al. (2006). "Genome-wide allelic imbalance analysis of pediatric gliomas by single nucleotide polymorphic allele array." Cancer Res **66**(23): 11172-11178.

Yamaguchi, R., Y. Muro, et al. (2009). "Disruption of ADAM3 impairs the migration of sperm into oviduct in mouse." Biol Reprod **81**(1): 142-146.

Zarghooni, M., U. Bartels, et al. (2010). "Whole-Genome Profiling of Pediatric Diffuse Intrinsic Pontine Gliomas Highlights Platelet-Derived Growth Factor Receptor {alpha} and Poly (ADP-ribose) Polymerase As Potential Therapeutic Targets." J Clin Oncol.

Zhao, X., C. Li, et al. (2004). "An integrated view of copy number and allelic alterations in the cancer genome using single nucleotide polymorphism arrays." Cancer Res **64**(9): 3060-3071.

Zurawel, R. H., S. A. Chiappa, et al. (1998). "Sporadic medulloblastomas contain oncogenic beta-catenin mutations." Cancer Res **58**(5): 896-899.

APPENDIX

Sample: HGG1 CCLG Centre: Nottingham

Diagnosis: GBM

Genomic Overview of Aberrations (DLR Spread: 0.61)

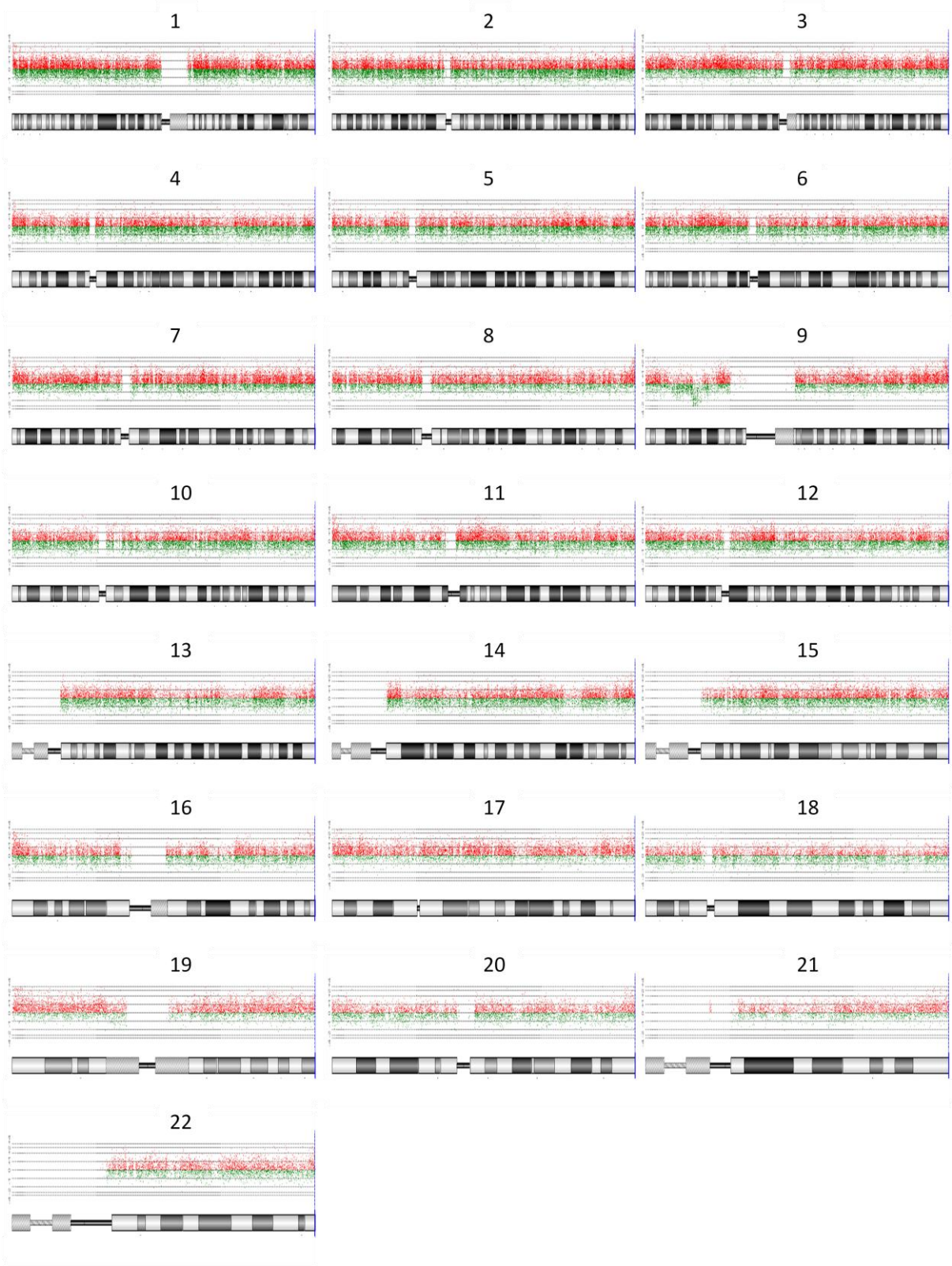

Sample: HGG2 CCLG Centre: Nottingham

Diagnosis: GBM

Genomic Overview of Aberrations (DLR Spread: 0.56)

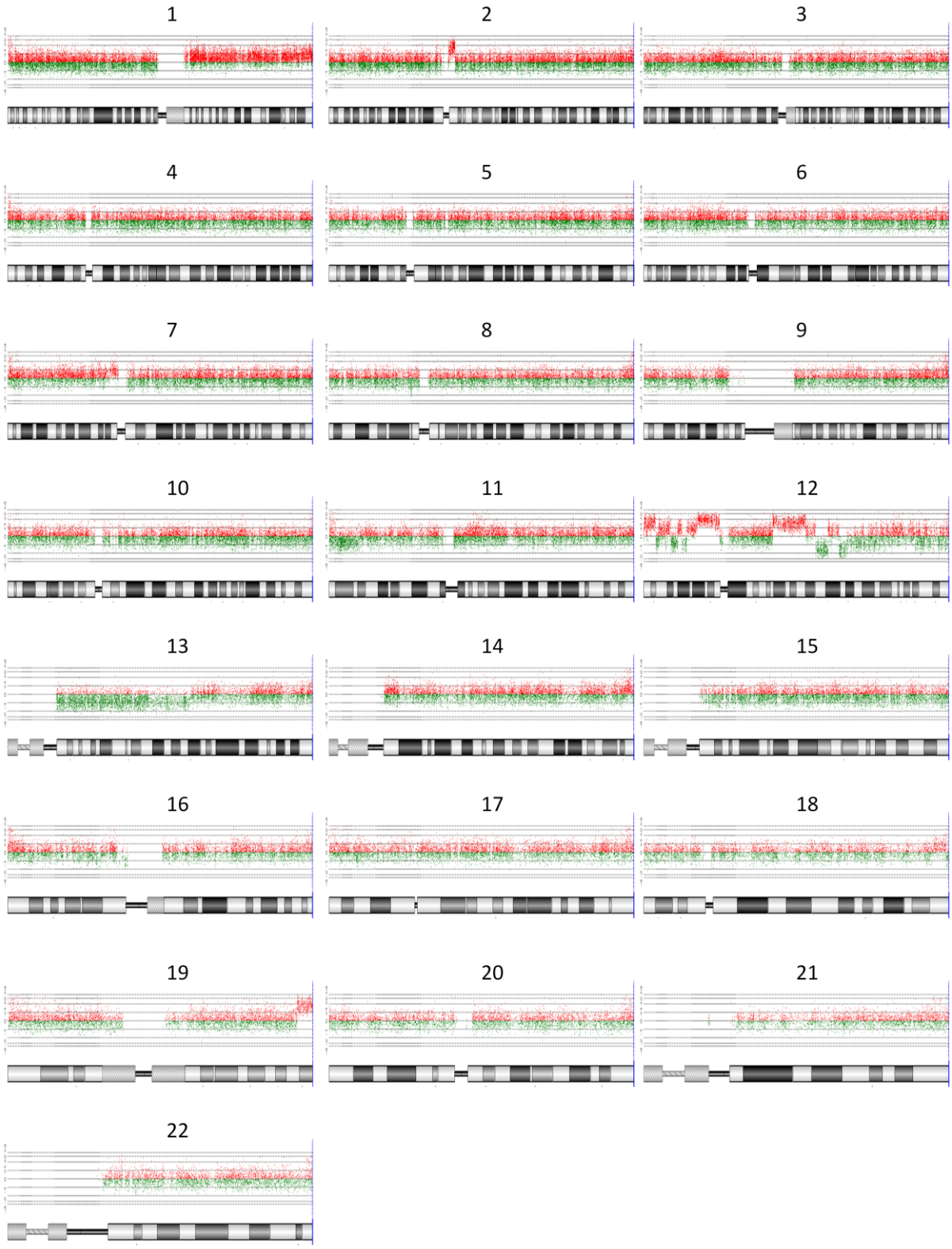

Sample: HGG3 CCLG Centre: Nottingham

Diagnosis: GBM

Genomic Overview of Aberrations (DLR Spread: 0.37)

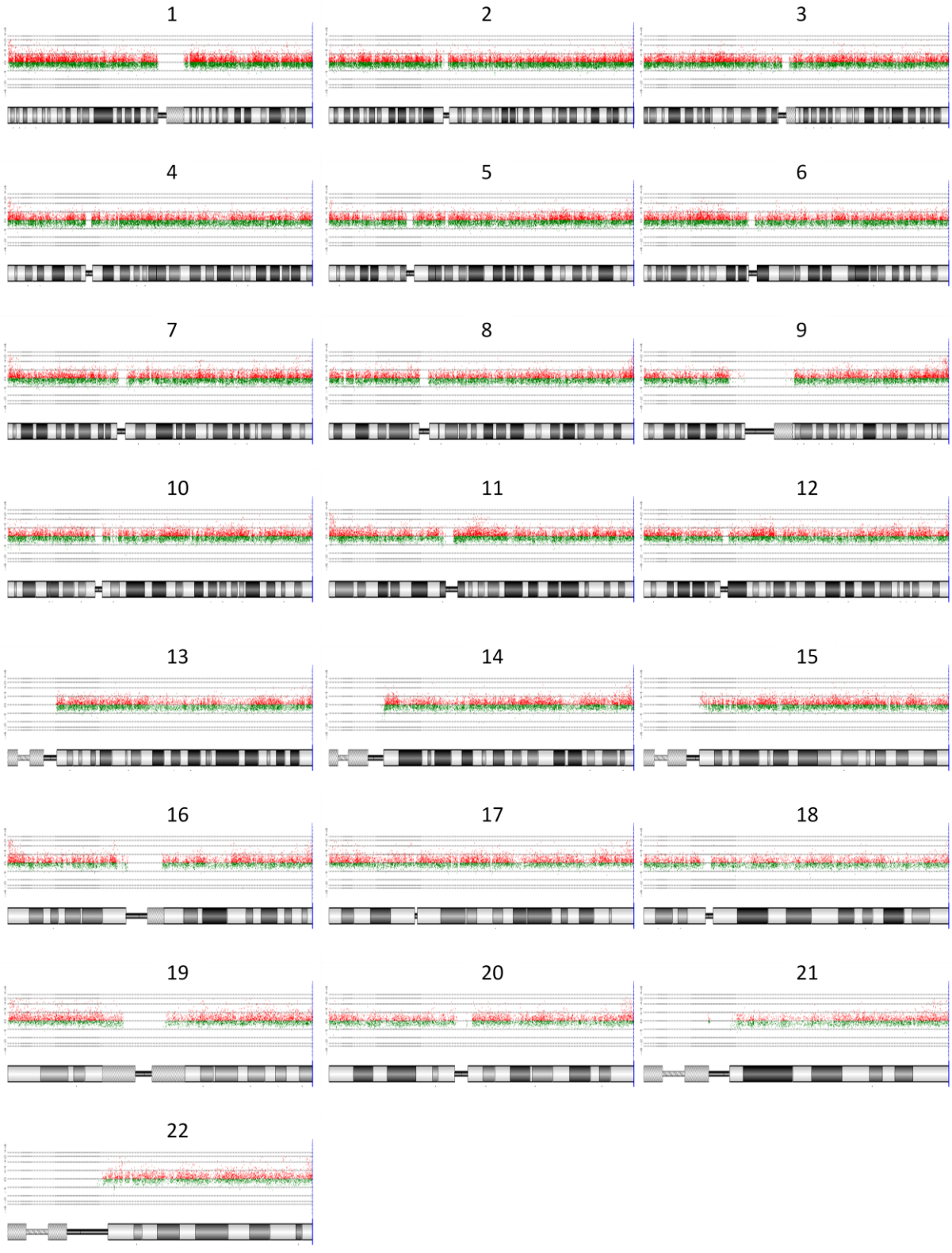

Sample: HGG4 CCLG Centre: Nottingham

Diagnosis: GBM

Genomic Overview of Aberrations (DLR Spread: 0.30)

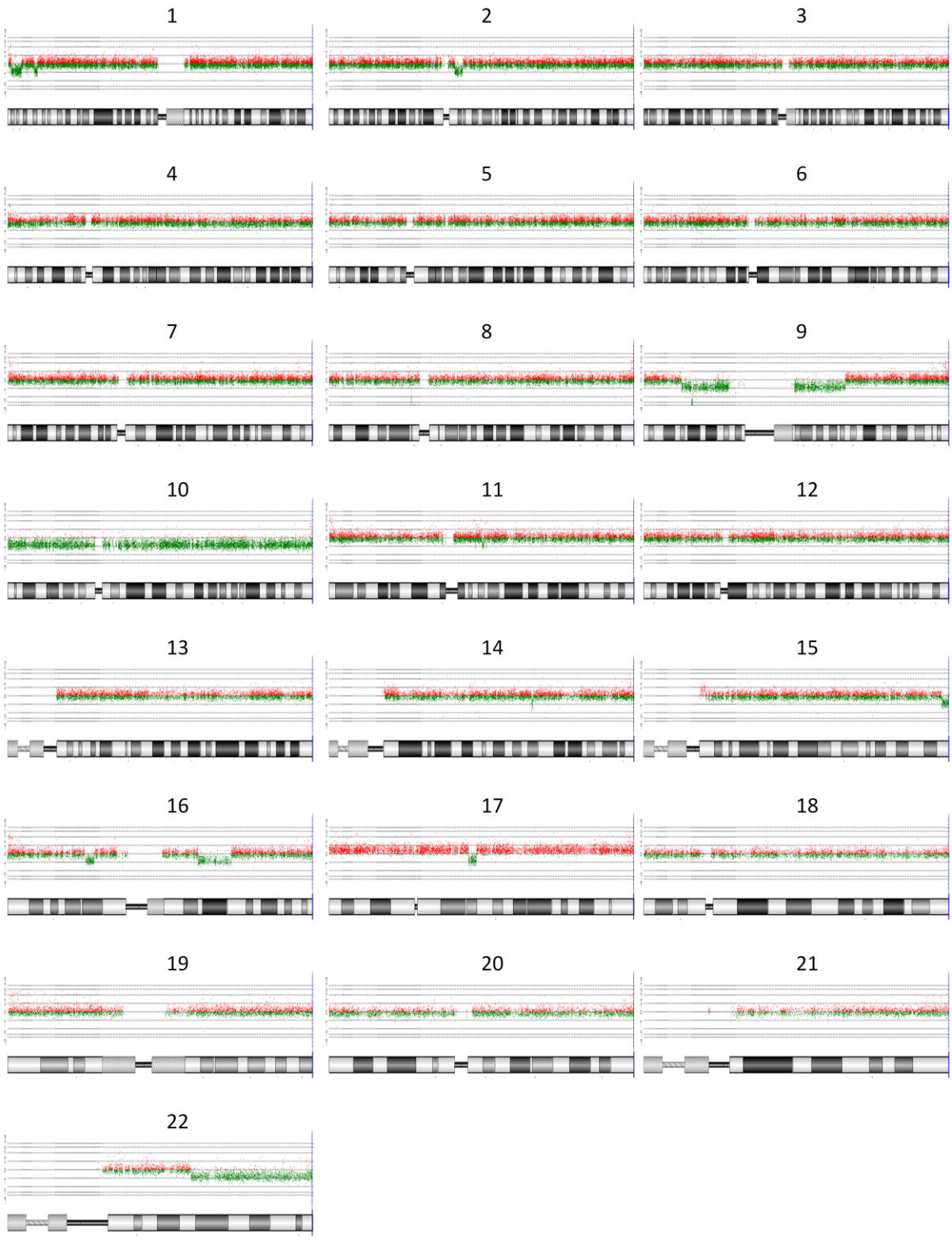

Sample: HGG5 CCLG Centre: Nottingham

Diagnosis: GBM

Genomic Overview of Aberrations (DLR Spread: 0.82)

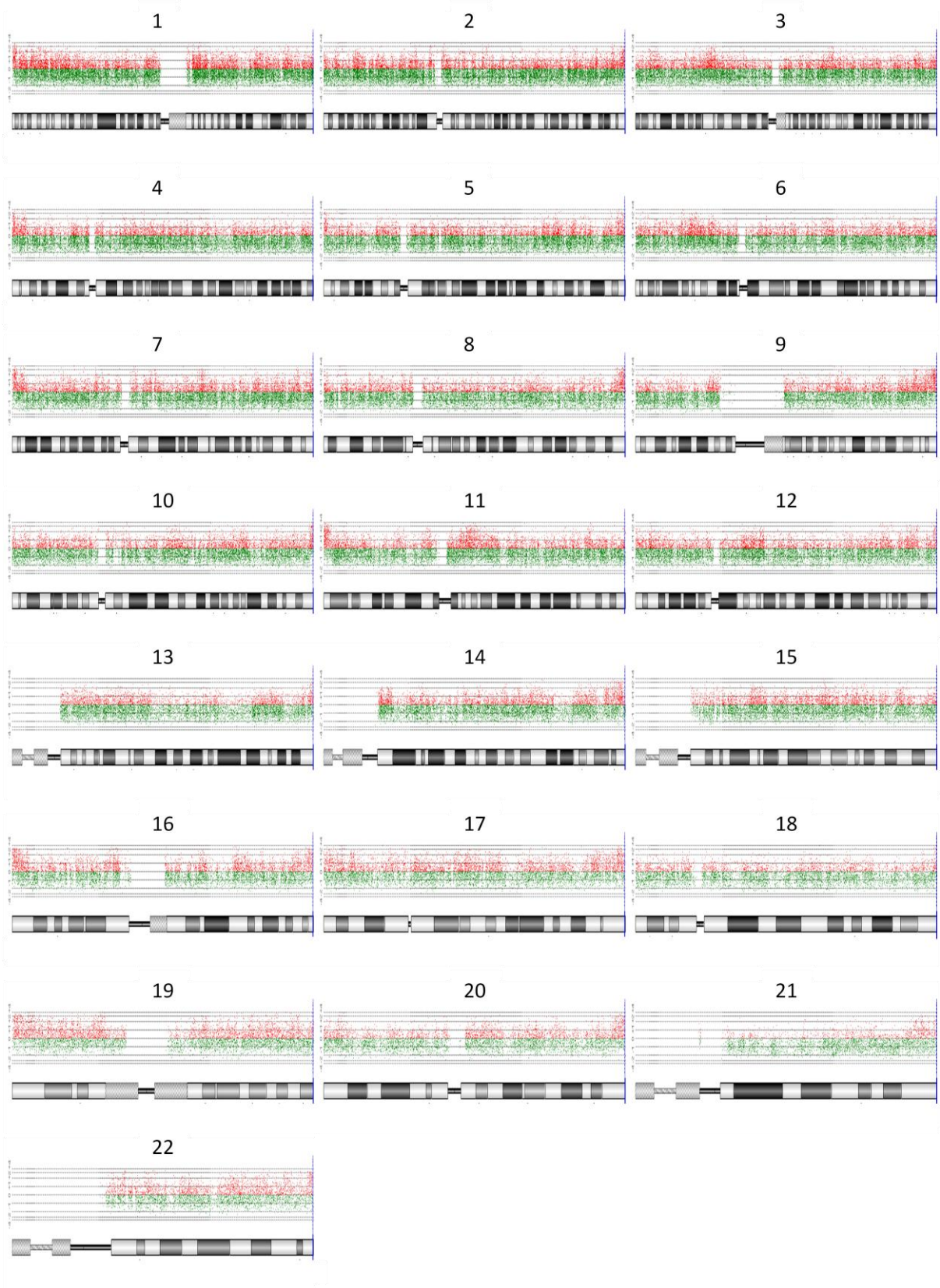

Sample: HGG6 CCLG Centre: Nottingham

Diagnosis: GBM

Genomic Overview of Aberrations (DLR Spread: 0.63)

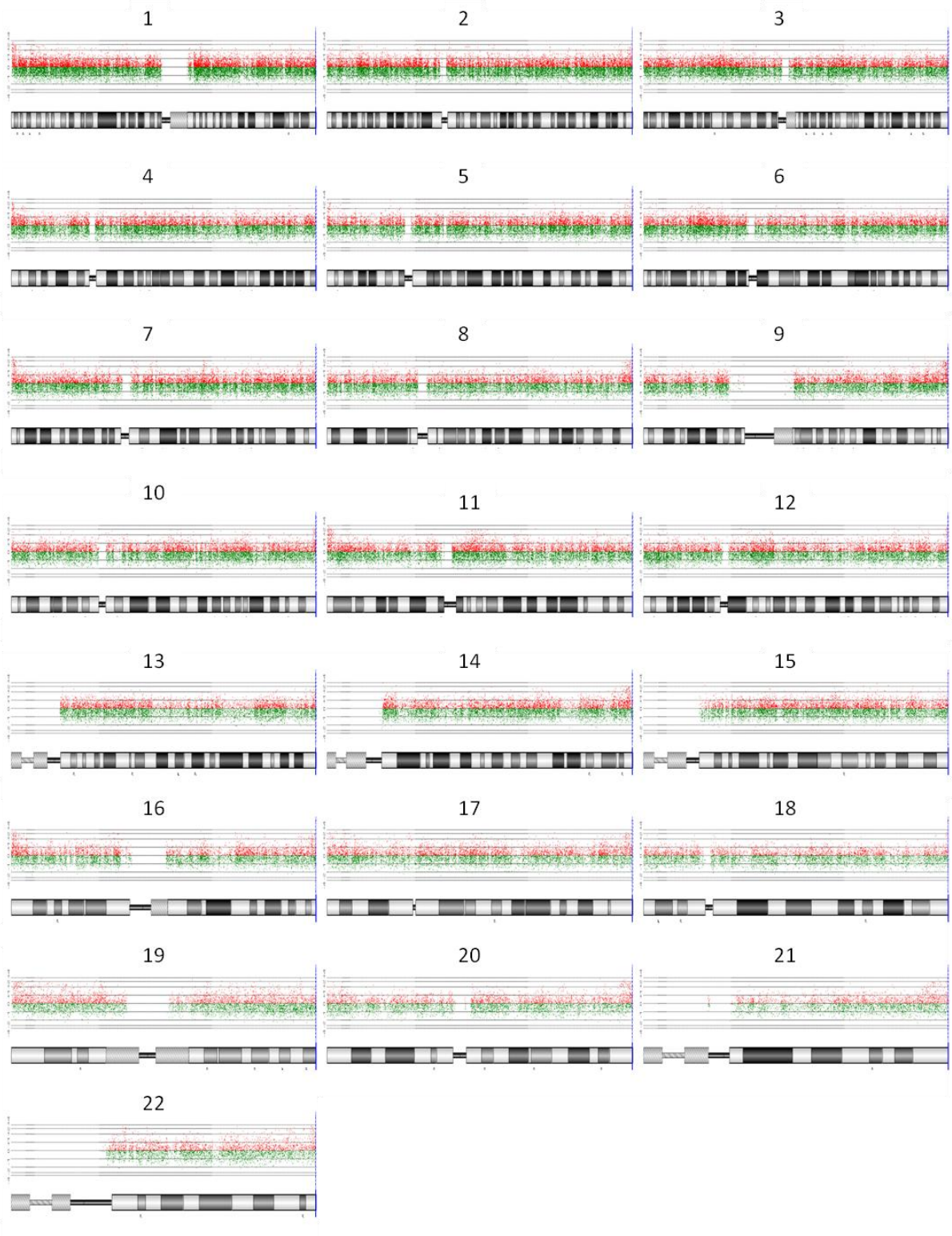

Sample: HGG7 CCLG Centre: Nottingham

Diagnosis: DIPG (GBM)

Genomic Overview of Aberrations (DLR Spread: 0.32)

Sample: HGG8 CCLG Centre: Nottingham

Diagnosis: GBM

Genomic Overview of Aberrations (DLR Spread: 0.39)

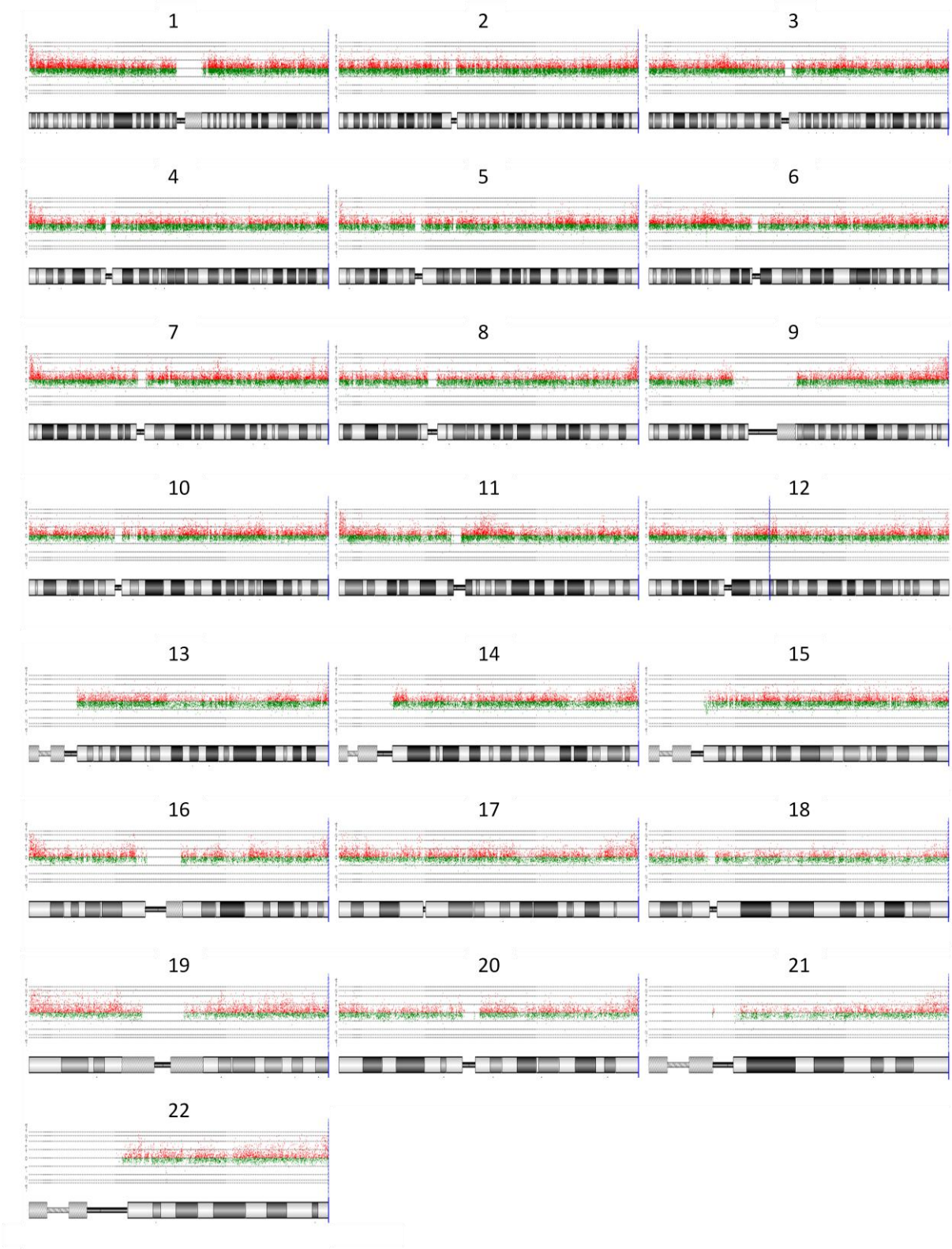

Sample: HGG9 CCLG Centre: Nottingham

Diagnosis: DIPG (LGA)

Genomic Overview of Aberrations (DLR Spread: 0.50)

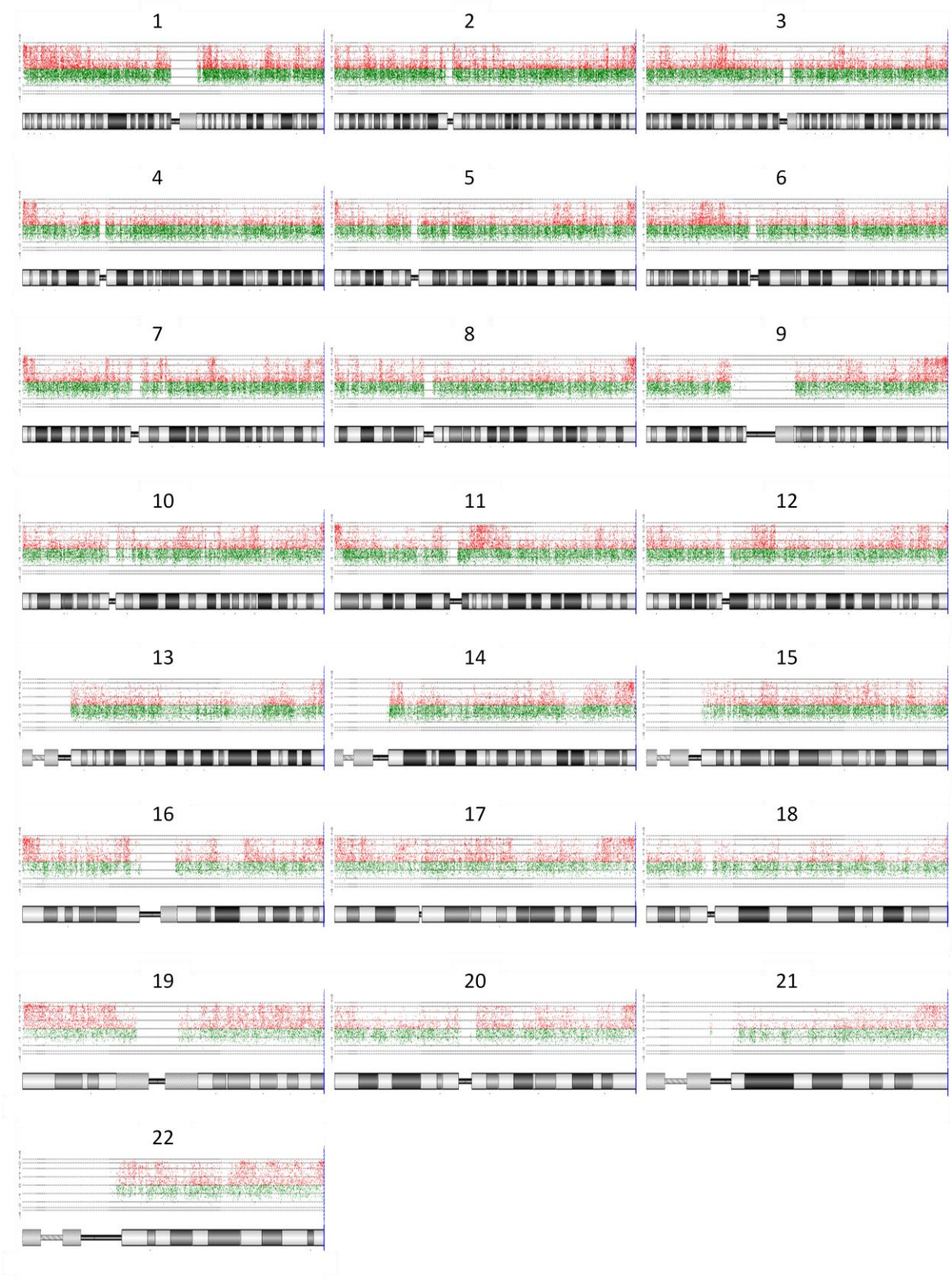

Sample: HGG10 CCLG Centre: Nottingham

Diagnosis: GBM

Genomic Overview of Aberrations (DLR Spread: 0.36)

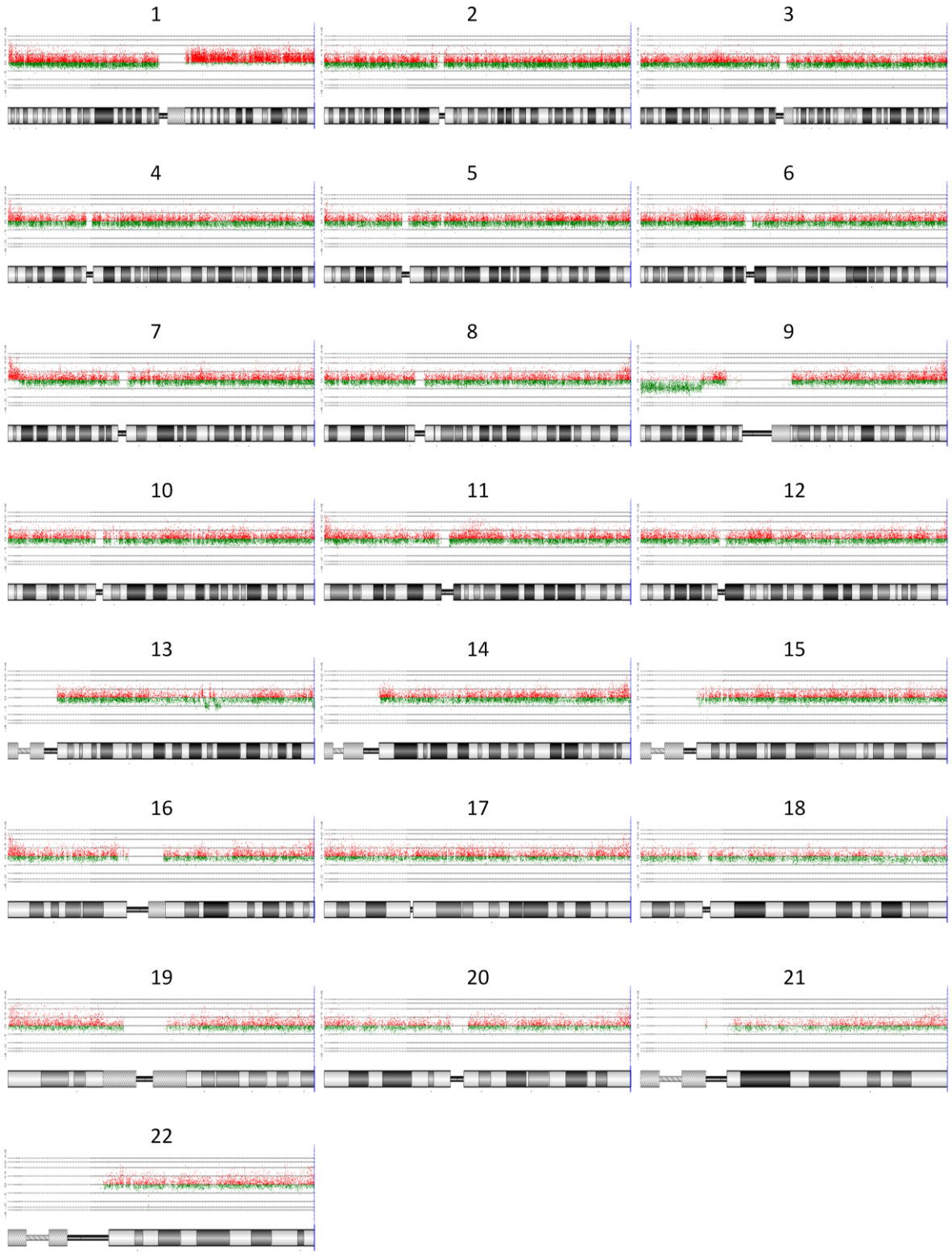

Sample: HGG11 CCLG Centre: Nottingham

Diagnosis: DIPG (GBM)

Genomic Overview of Aberrations (DLR Spread: 0.70)

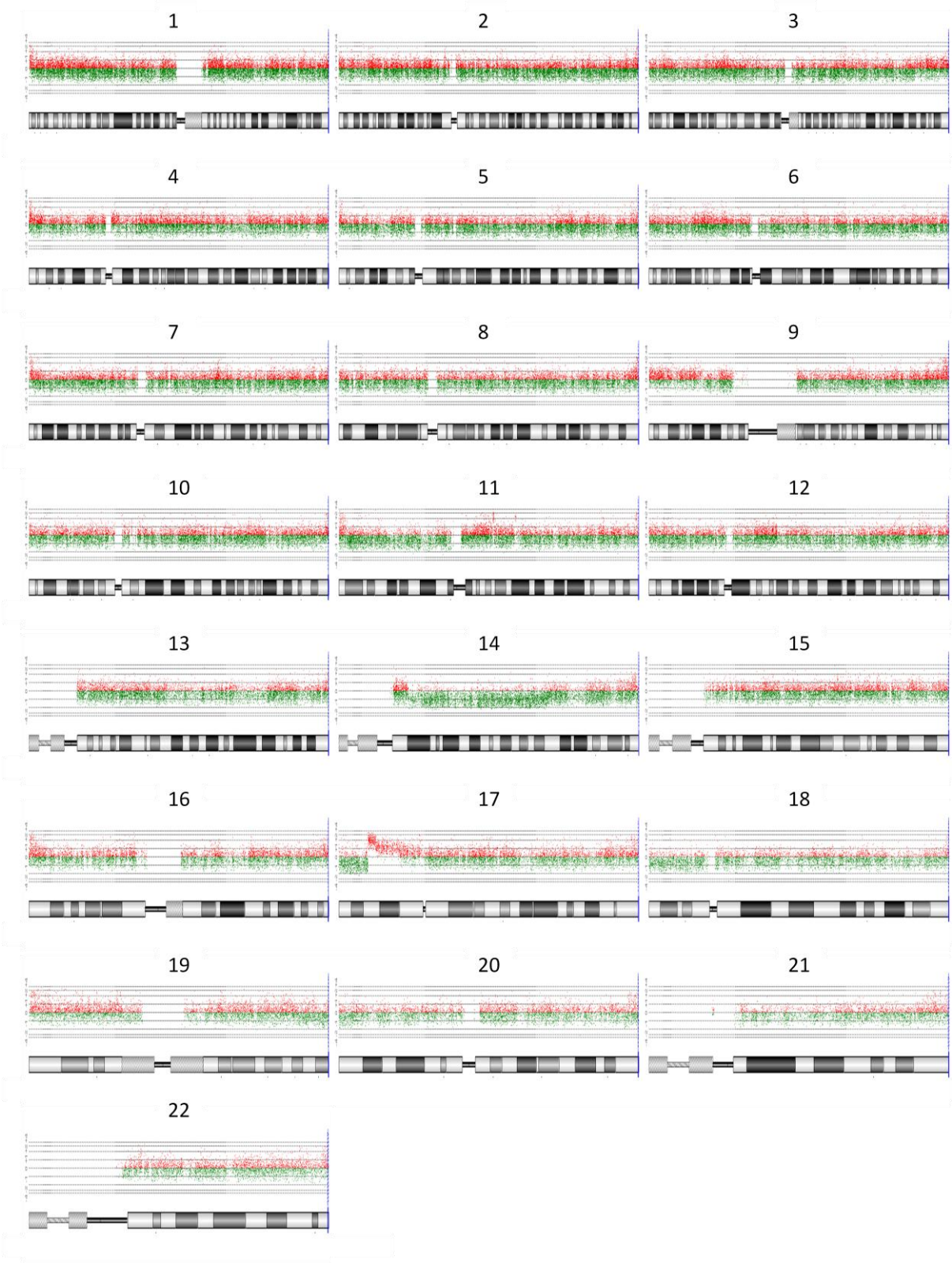

Sample HGG11: FROZEN

Genomic Overview of Aberrations (DLR Spread: 0.31)

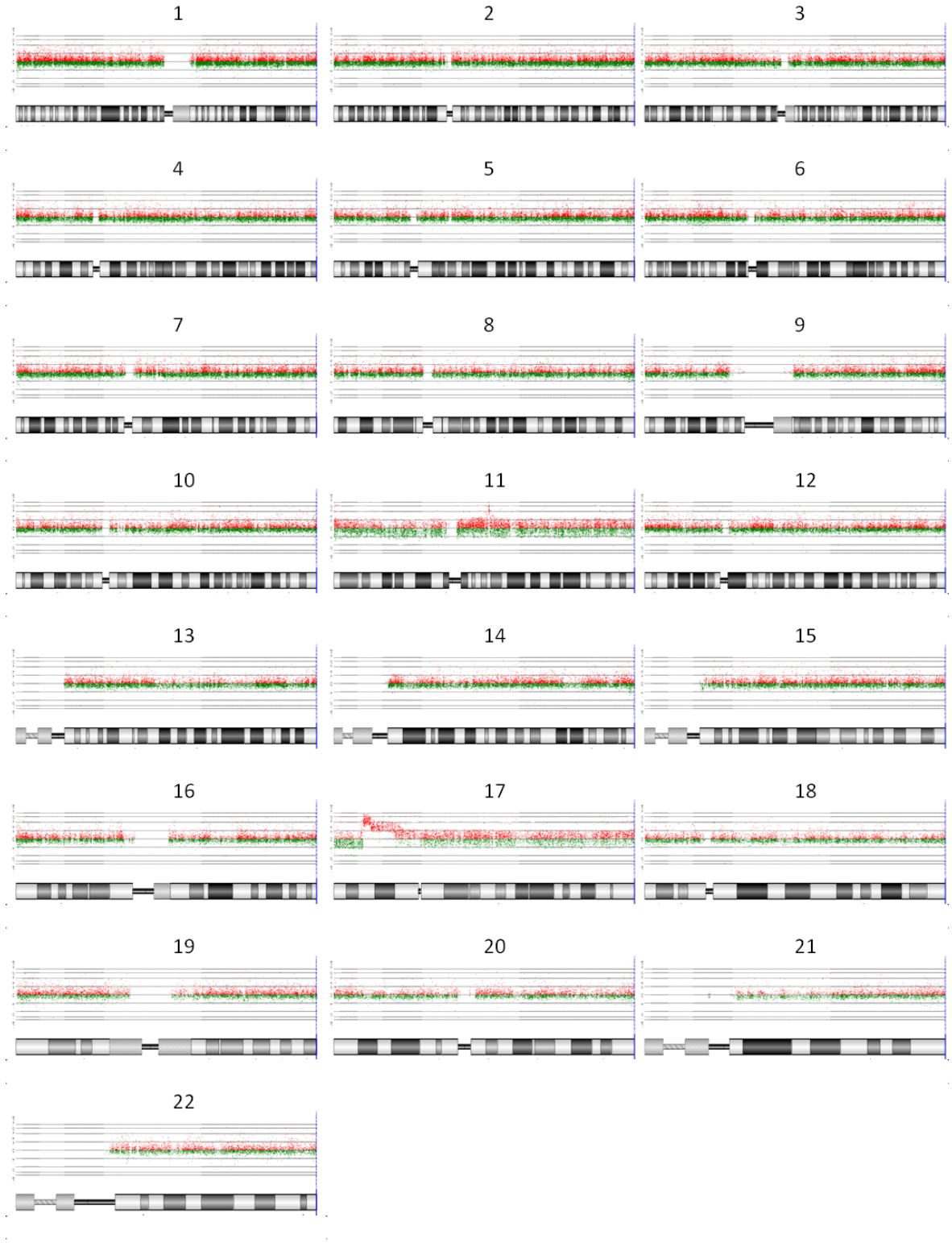

Sample: HGG12 CCLG Centre: Nottingham

Diagnosis: AA

Genomic Overview of Aberrations (DLR Spread: 0.57)

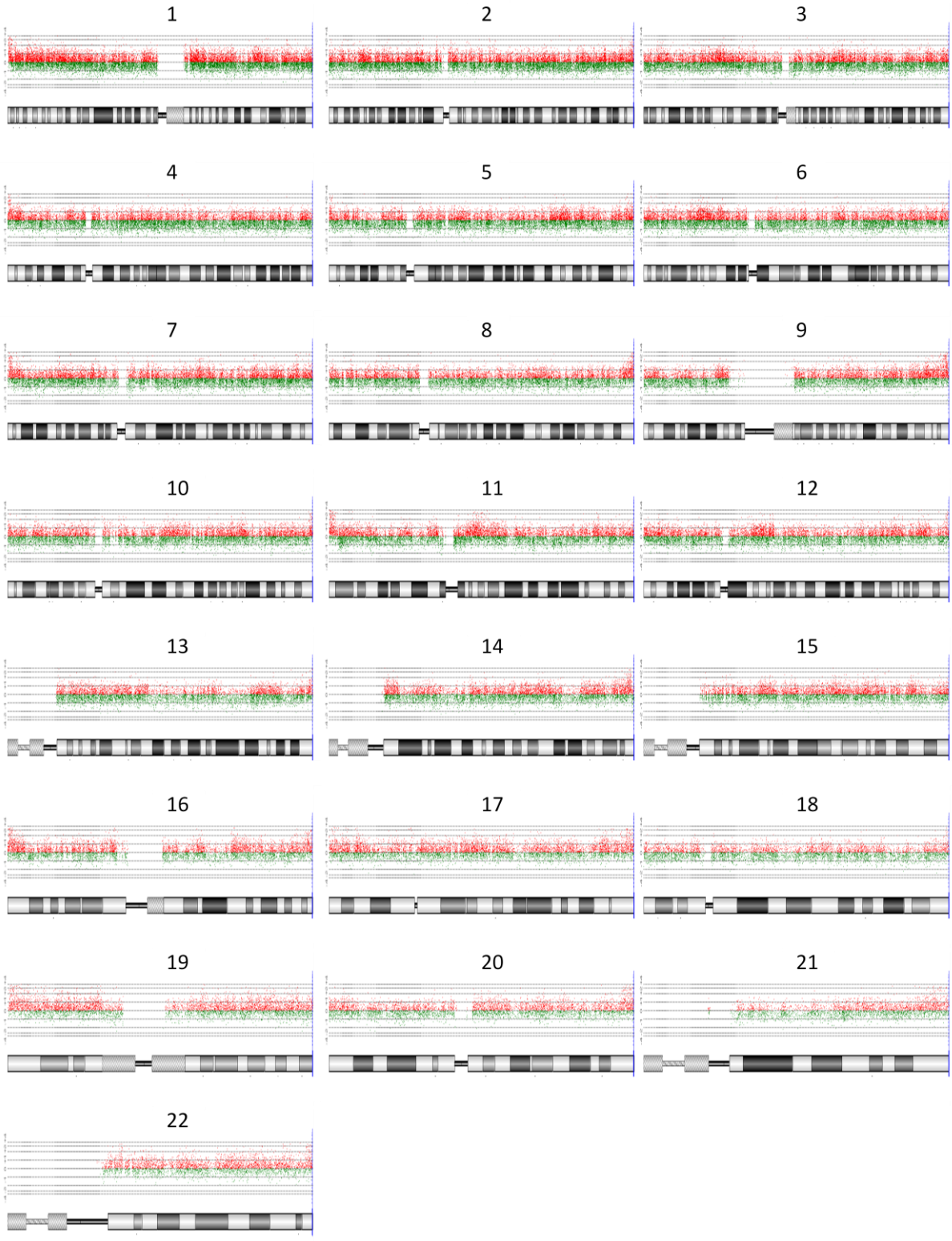

Sample: HGG13 CCLG Centre: Nottingham

Diagnosis: DIPG (GBM)

Genomic Overview of Aberrations (DLR Spread: 0.90)

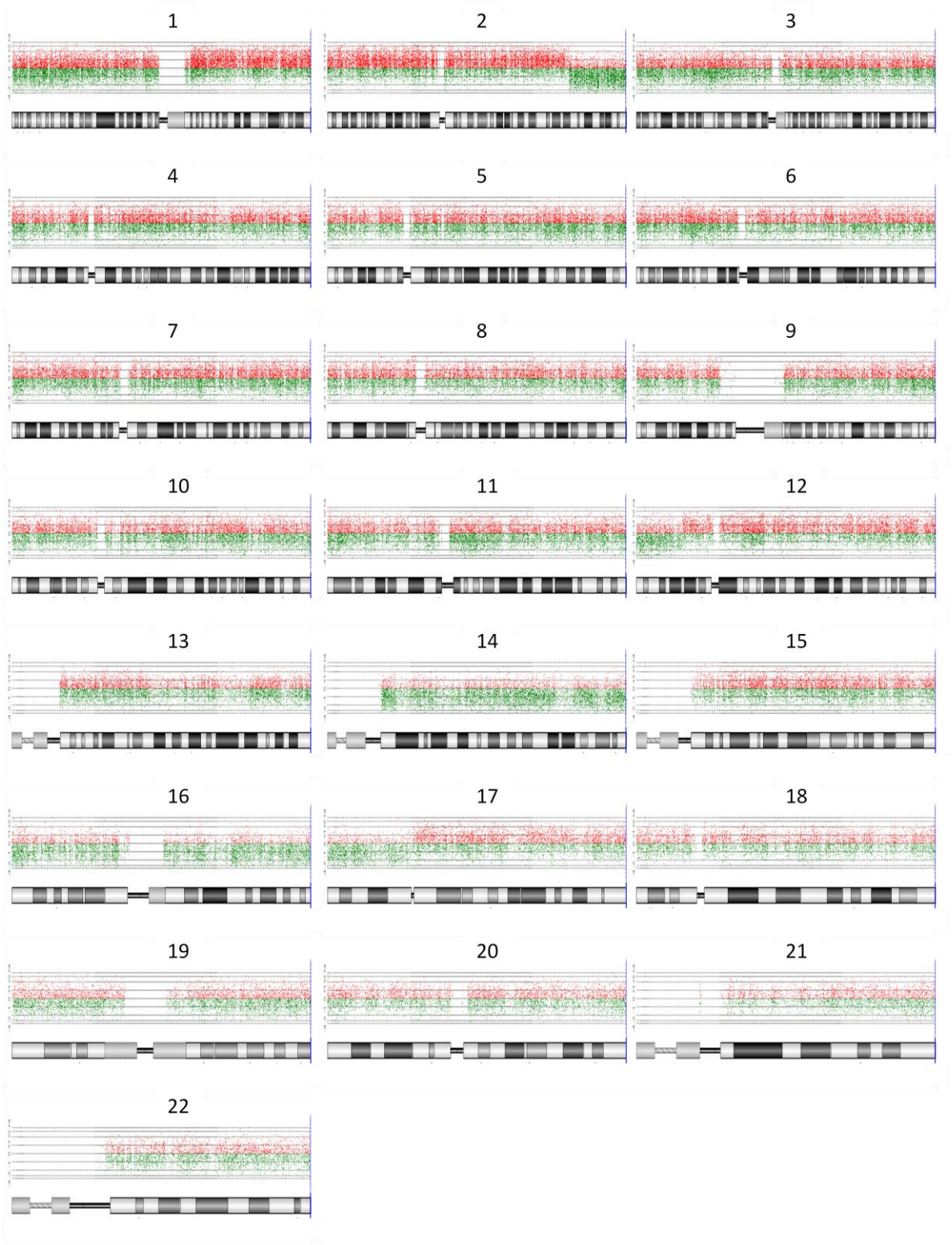

Sample: HGG14 CCLG Centre: Nottingham

Diagnosis: DIPG (GBM)

Genomic Overview of Aberrations (DLR Spread: 0.91)

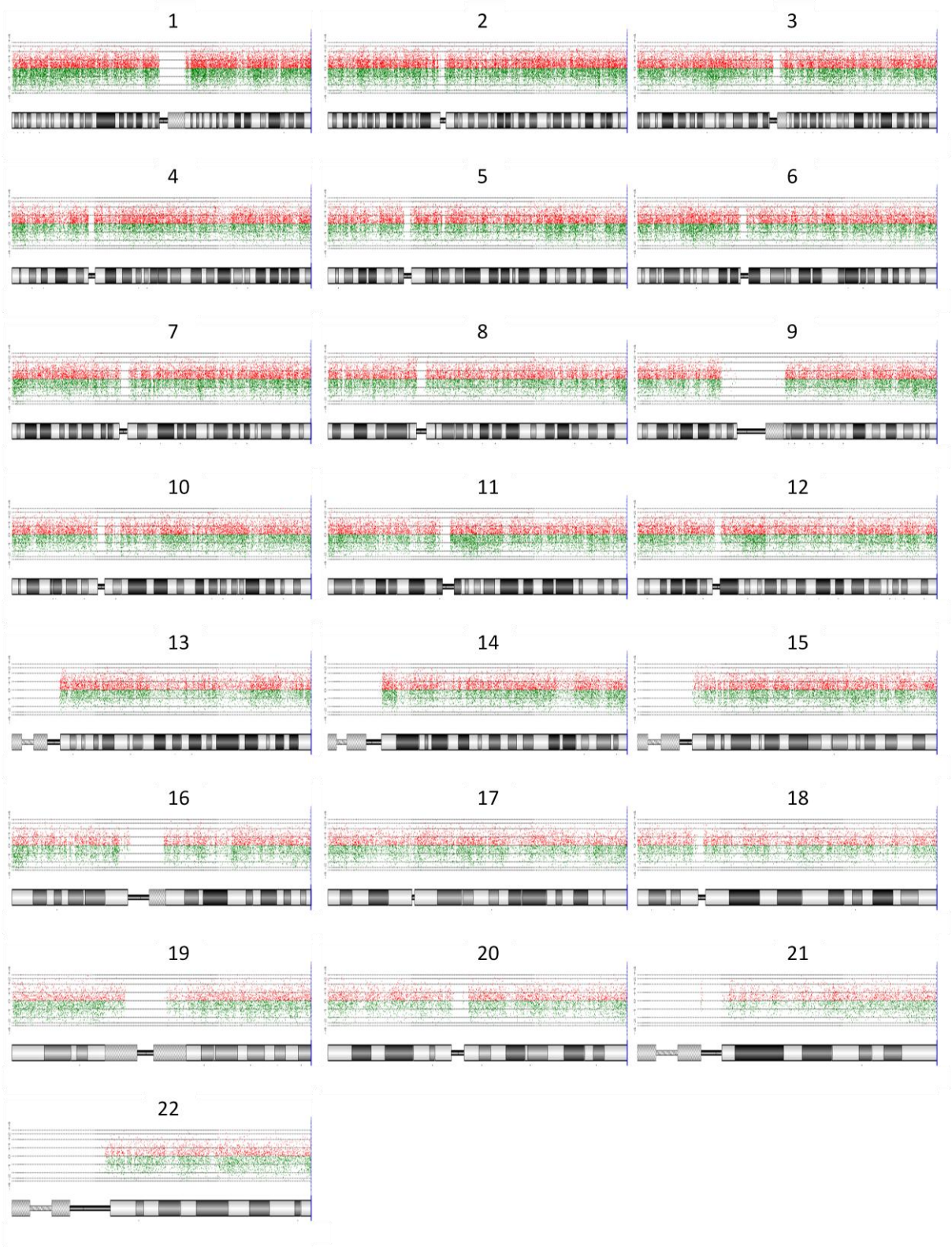

Sample: HGG15 CCLG Centre: Nottingham

Diagnosis: AA

Genomic Overview of Aberrations (DLR Spread: 1.03)

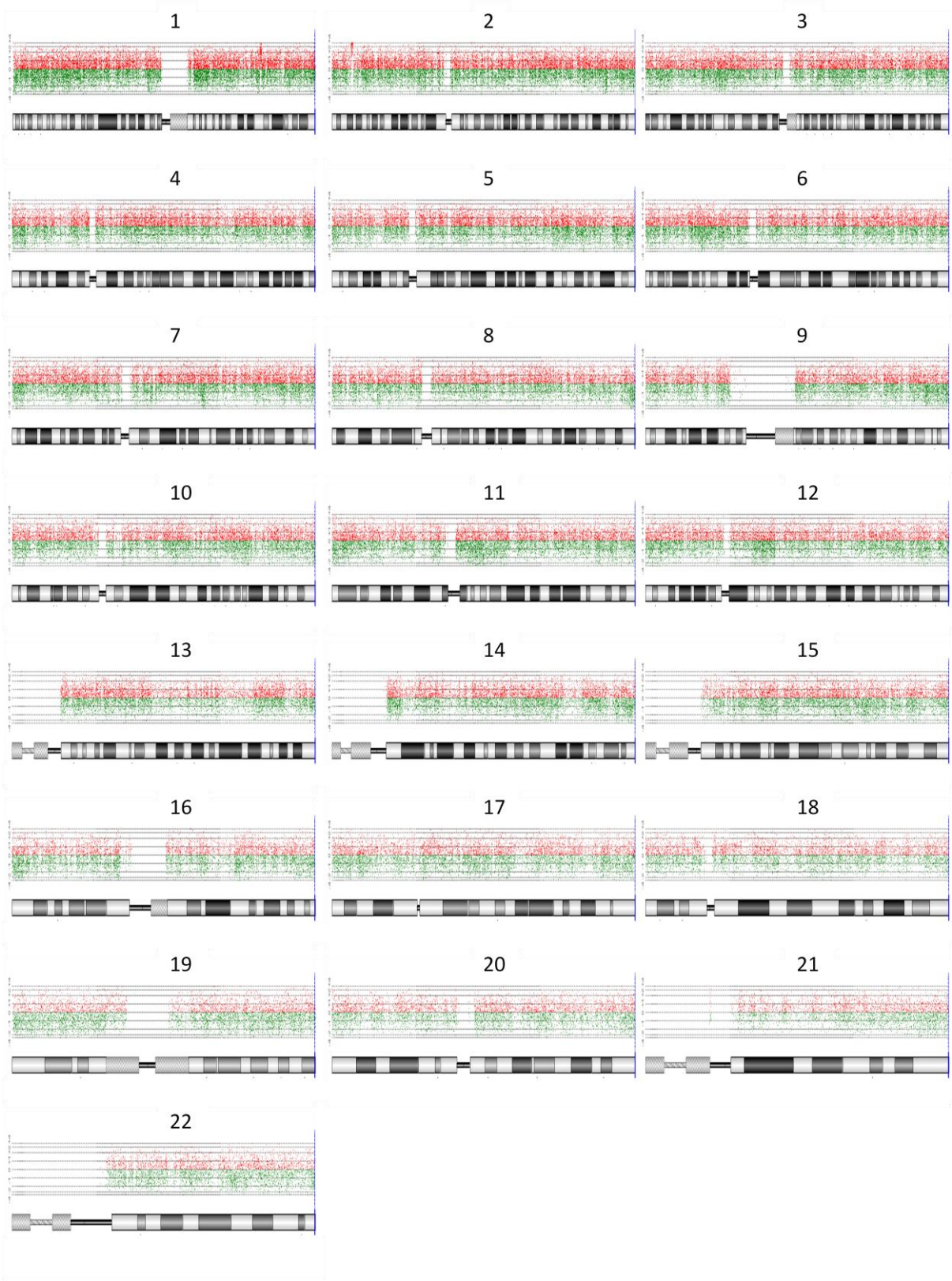

Sample: HGG16 CCLG Centre: Nottingham

Diagnosis: AO

Genomic Overview of Aberrations (DLR Spread: 0.54)

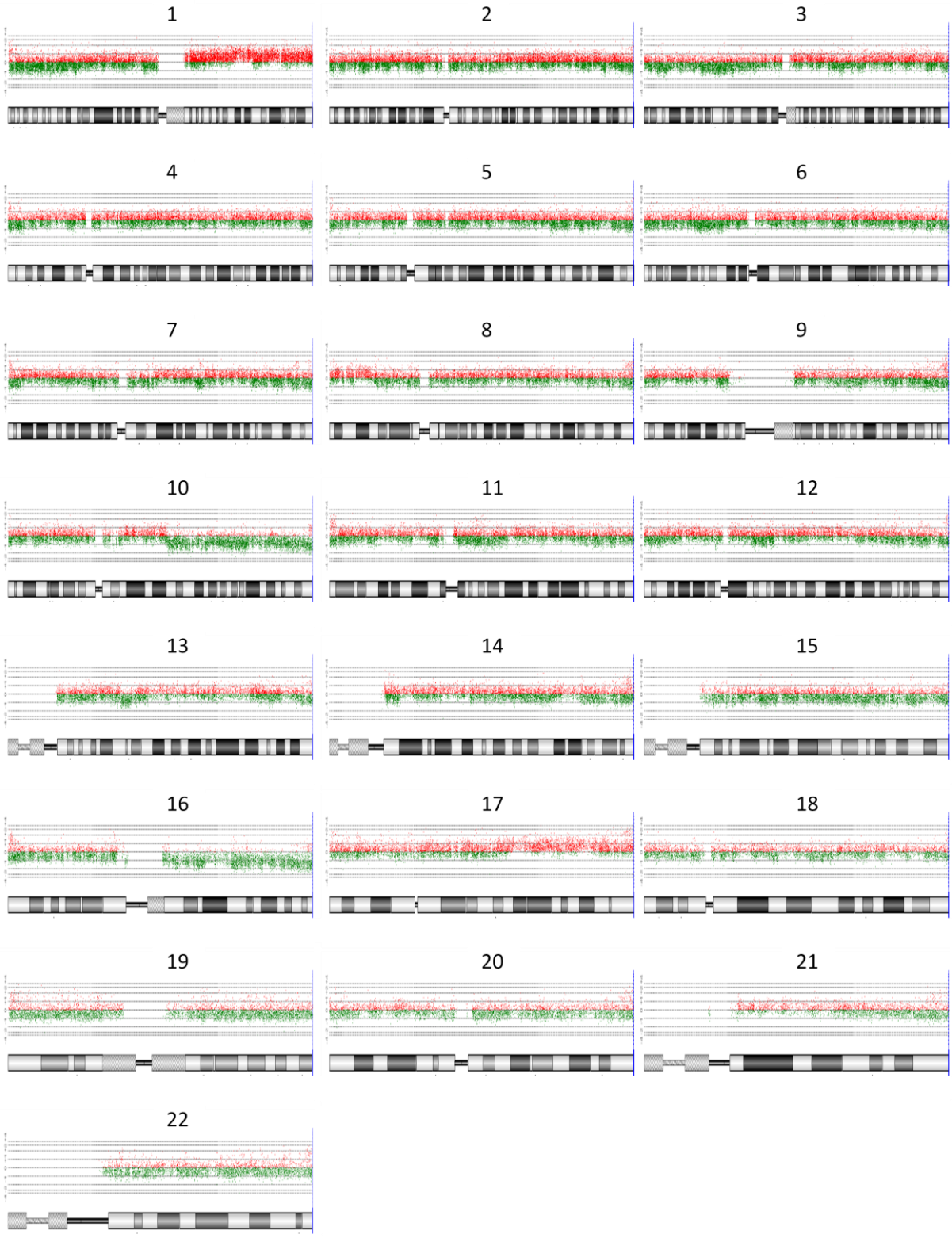

Sample HGG16: FROZEN

Genomic Overview of Aberrations (DLR Spread: 0.40)

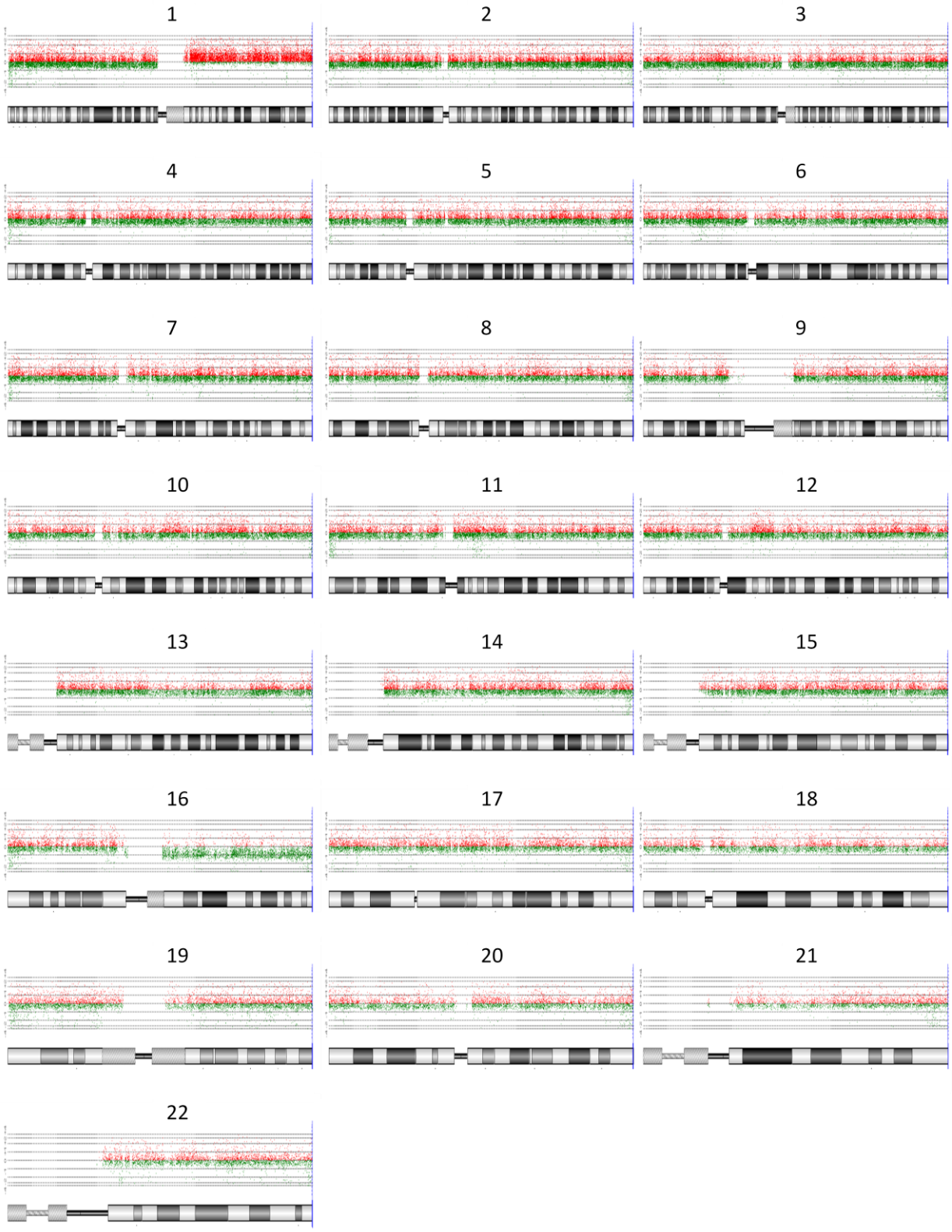

Sample: HGG17 CCLG Centre: Newcastle

Diagnosis: GBM

Genomic Overview of Aberrations (DLR Spread: 0.47)

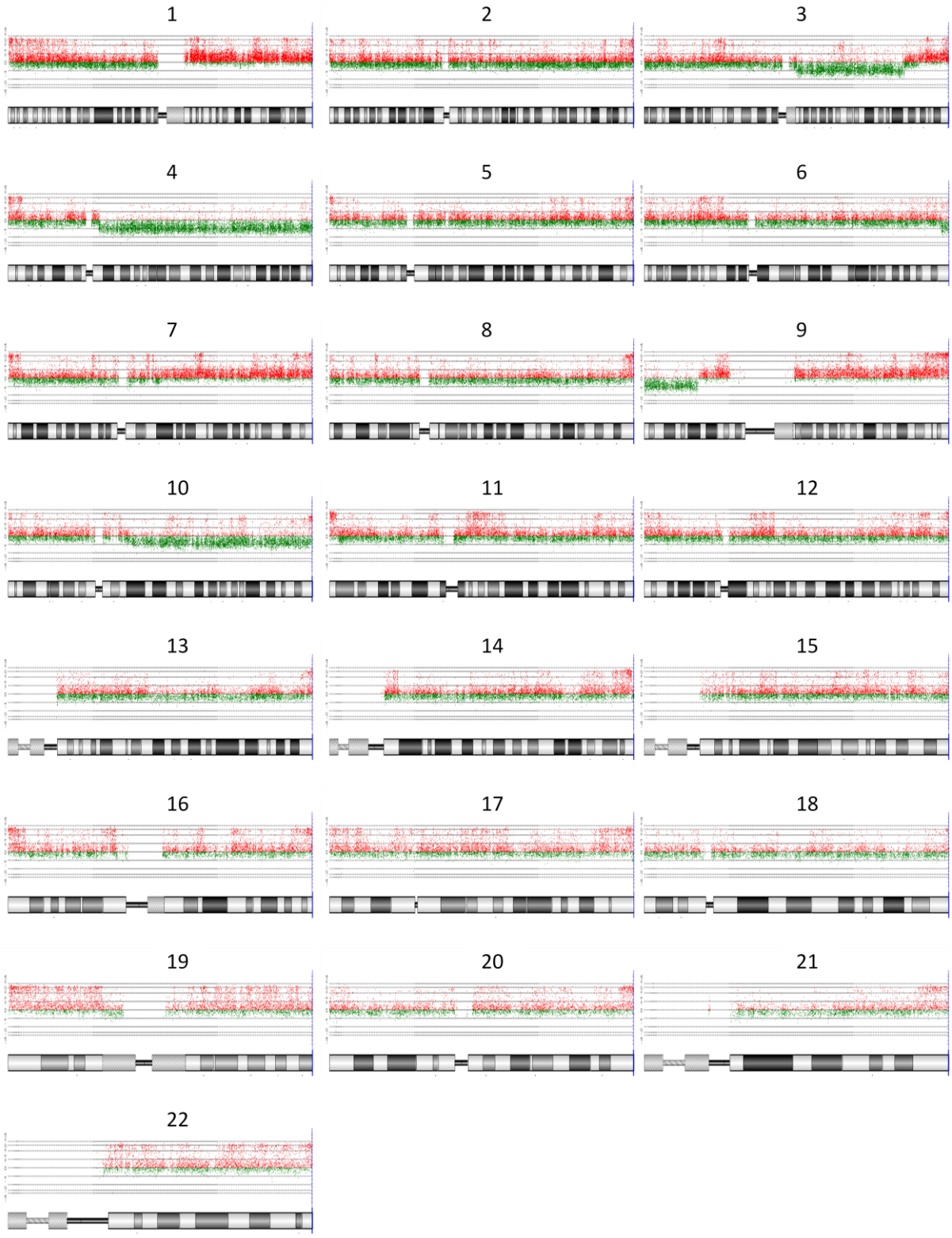

Sample: HGG18 CCLG Centre: Newcastle

Diagnosis: GBM

Genomic Overview of Aberrations (DLR Spread: 0.70)

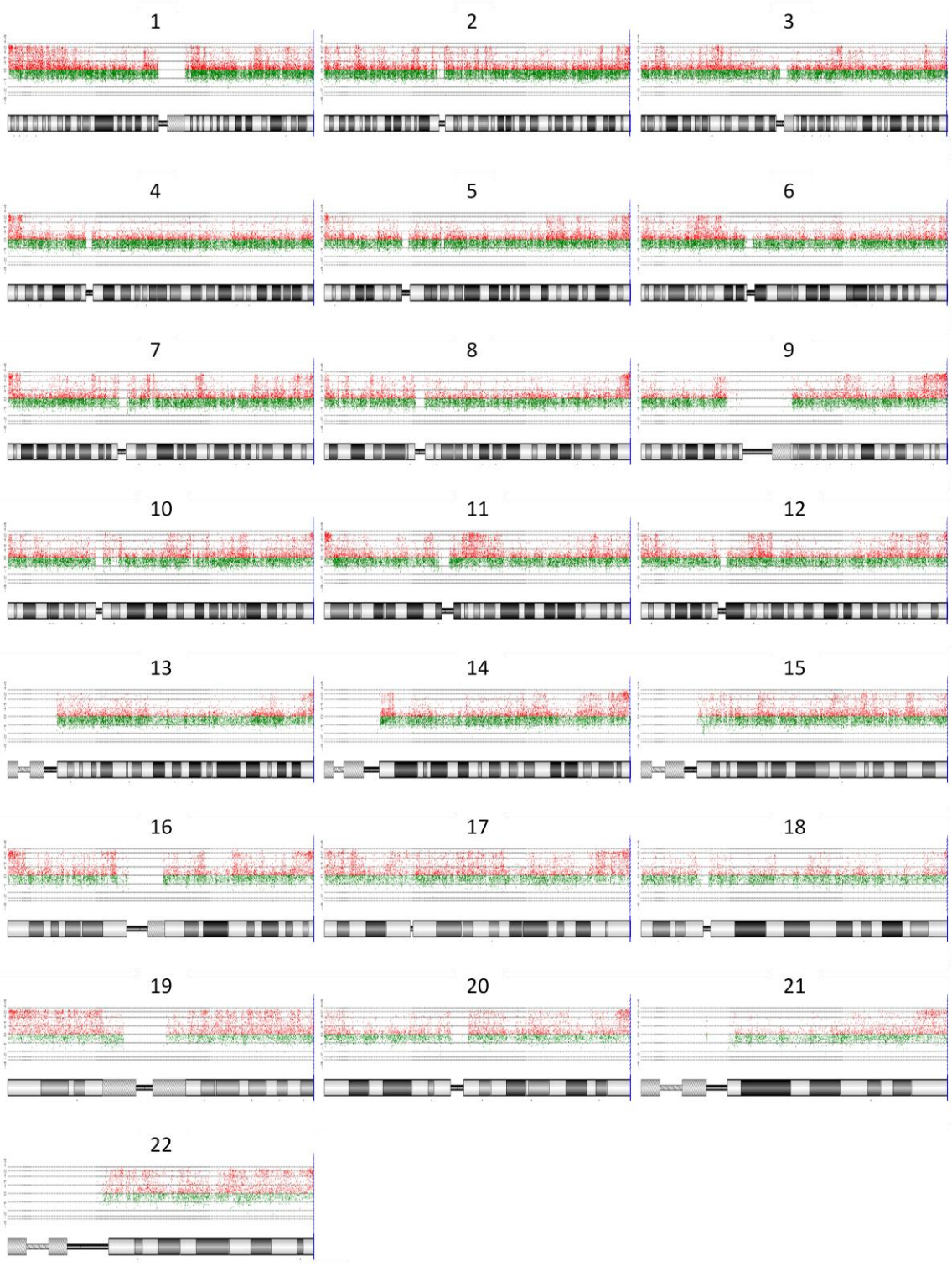

Sample: HGG19 CCLG Centre: Newcastle

Diagnosis: DIPG (GBM)

Genomic Overview of Aberrations (DLR Spread: 0.61)

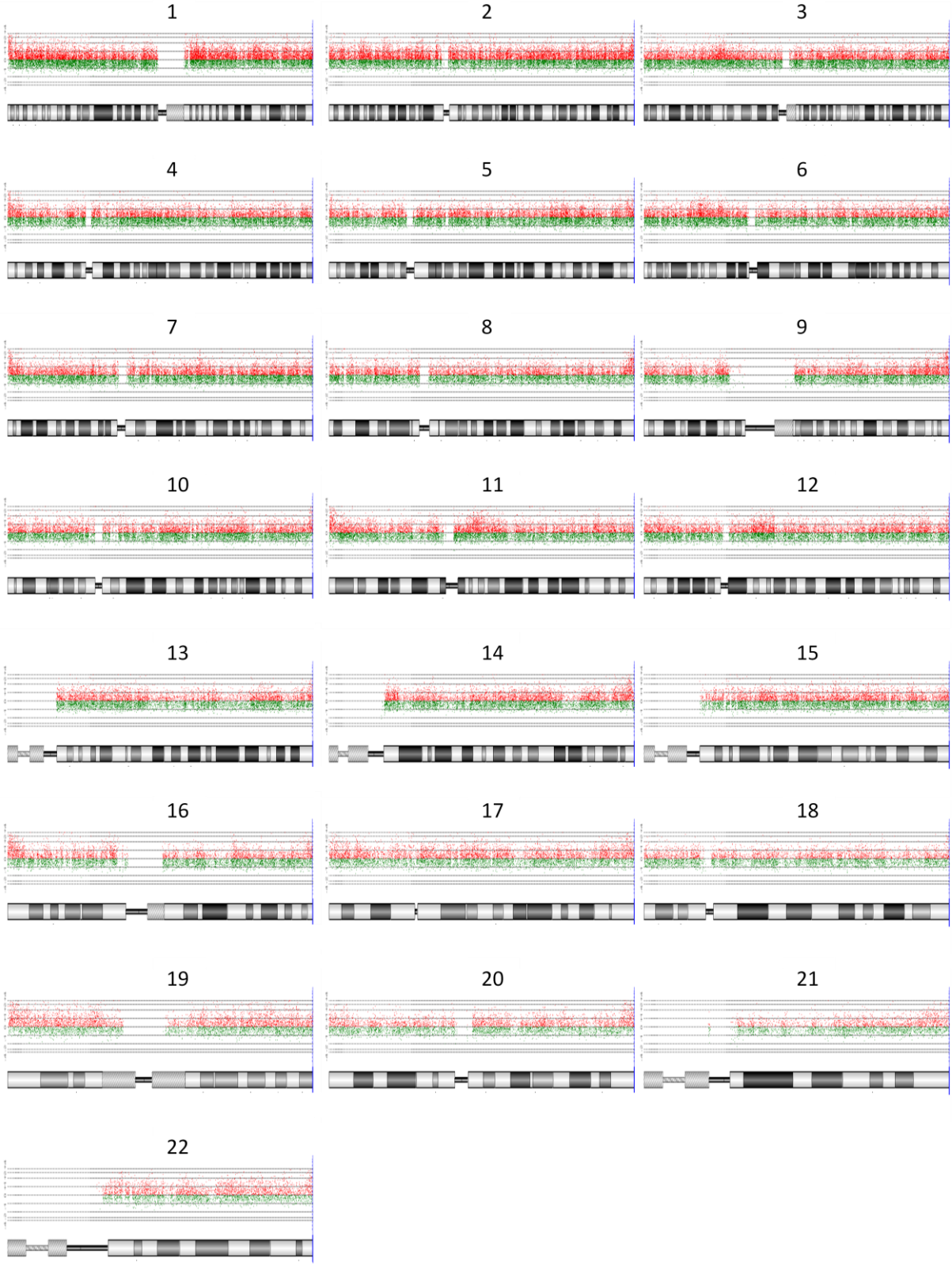

Sample: HGG20 CCLG Centre: Newcastle

Diagnosis: DIPG (GBM)

Genomic Overview of Aberrations (DLR Spread: 0.51)

Sample: HGG21 CCLG Centre: Newcastle

Diagnosis: DIPG (GBM)

Genomic Overview of Aberrations (DLR Spread: 0.43)

Sample: HGG22 CCLG Centre: Liverpool

Diagnosis: GBM

Genomic Overview of Aberrations (DLR Spread: 0.39)

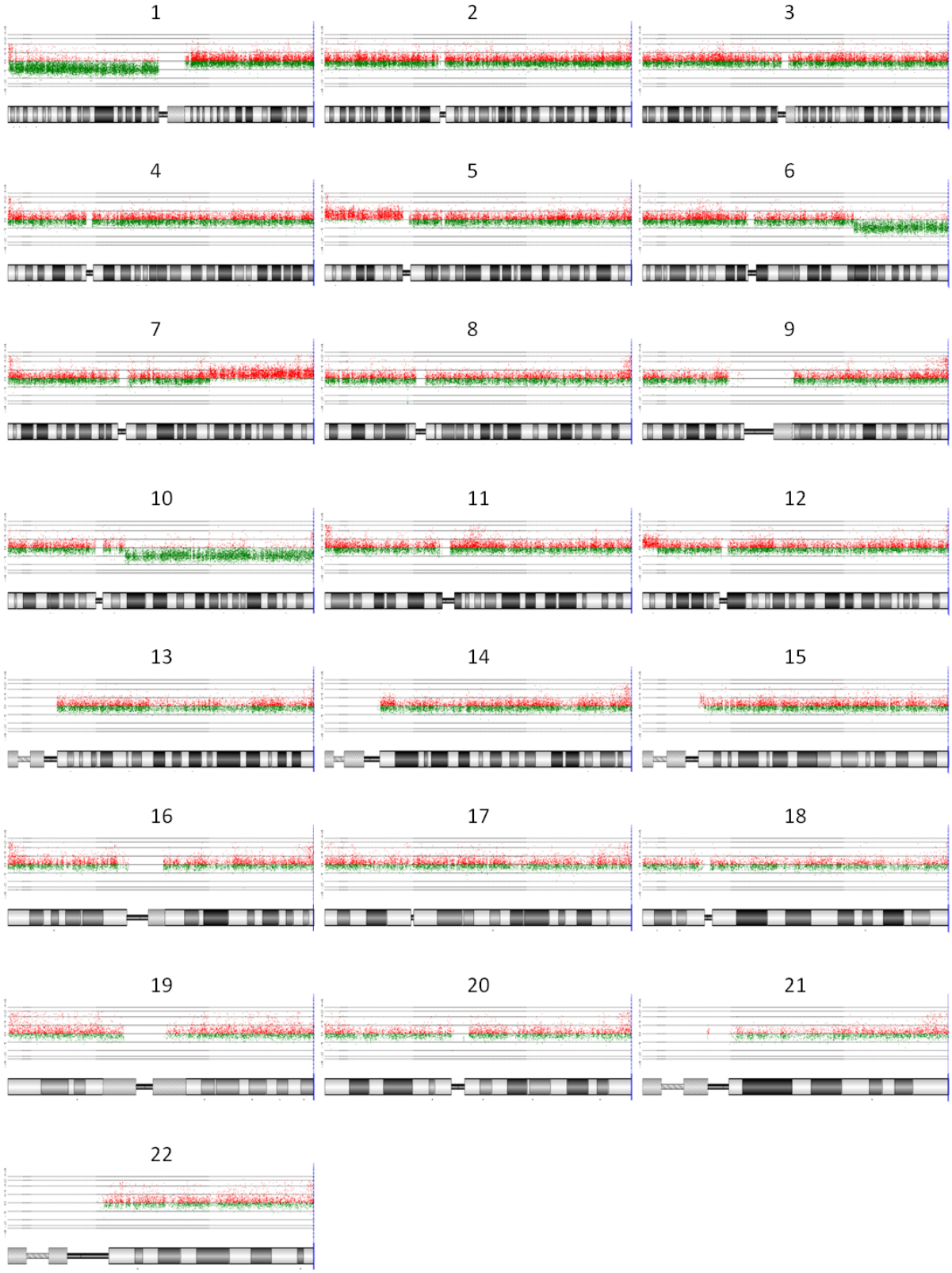

Sample: HGG23 CCLG Centre: Liverpool

Diagnosis: GBM

Genomic Overview of Aberrations (DLR Spread: 0.35)

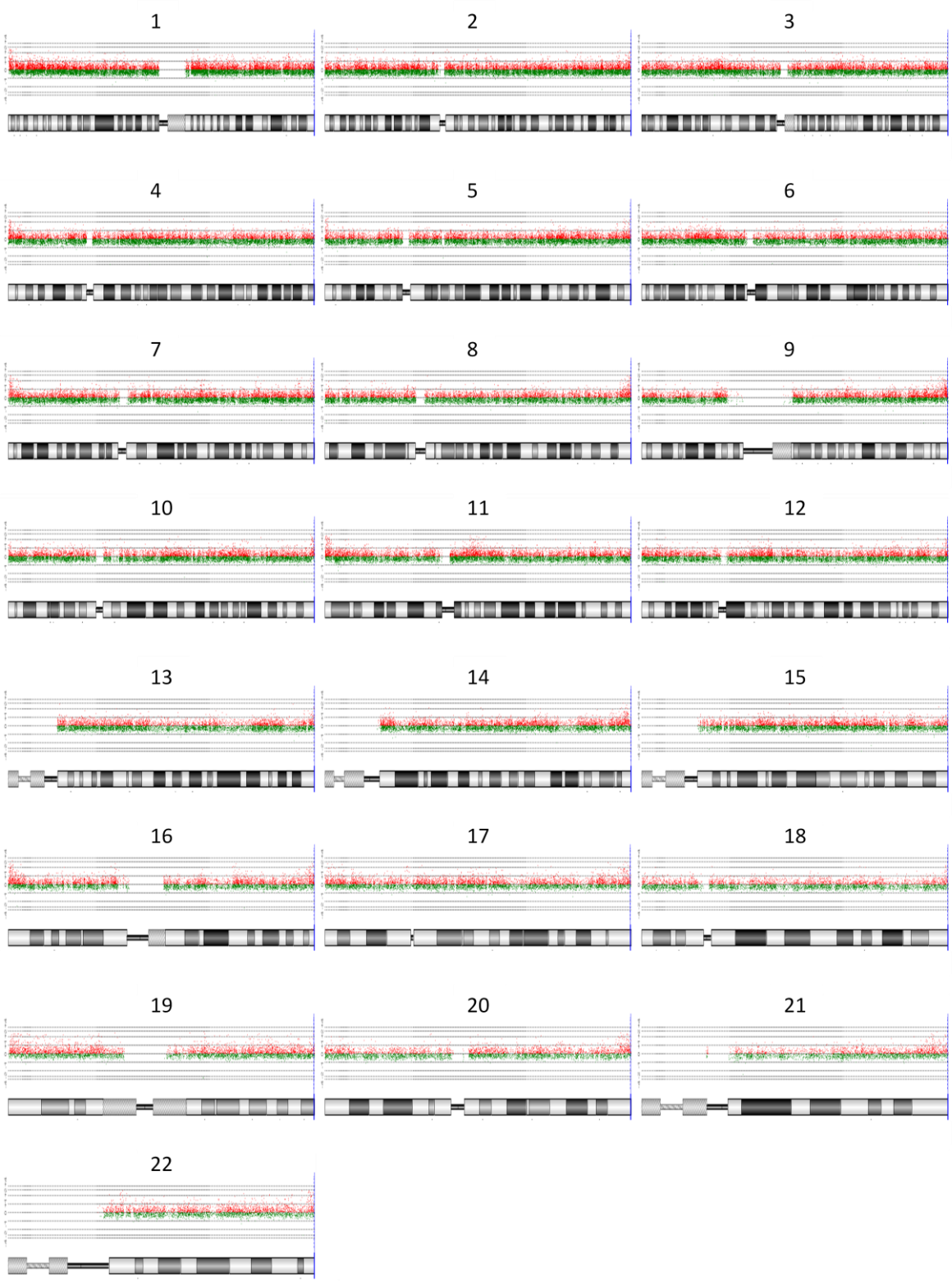

Sample: HGG24 CCLG Centre: Liverpool

Diagnosis: AA

Genomic Overview of Aberrations (DLR Spread: 0.33)

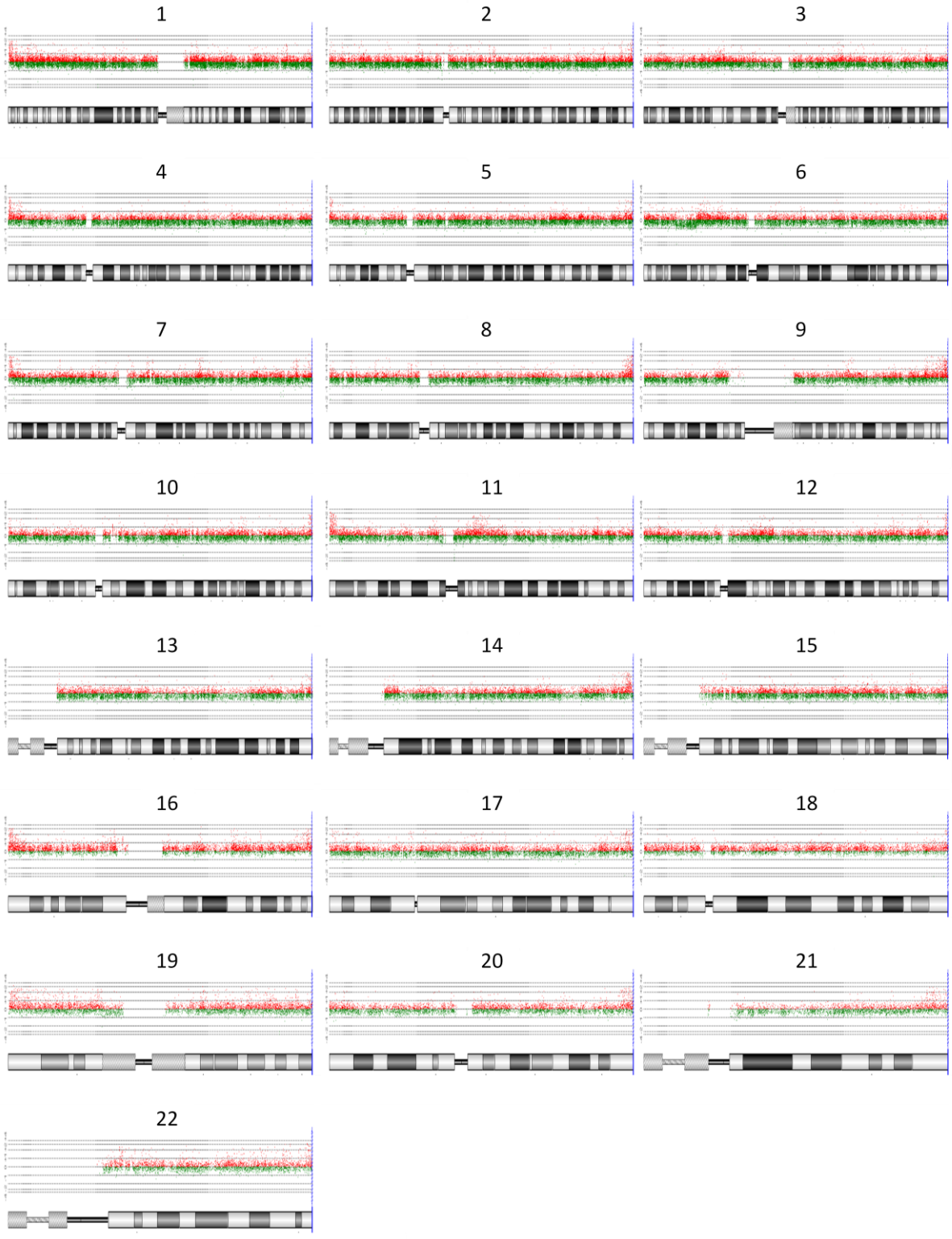

Sample: HGG25 CCLG Centre: Liverpool

Diagnosis: GBM

Genomic Overview of Aberrations (DLR Spread: 0.41)

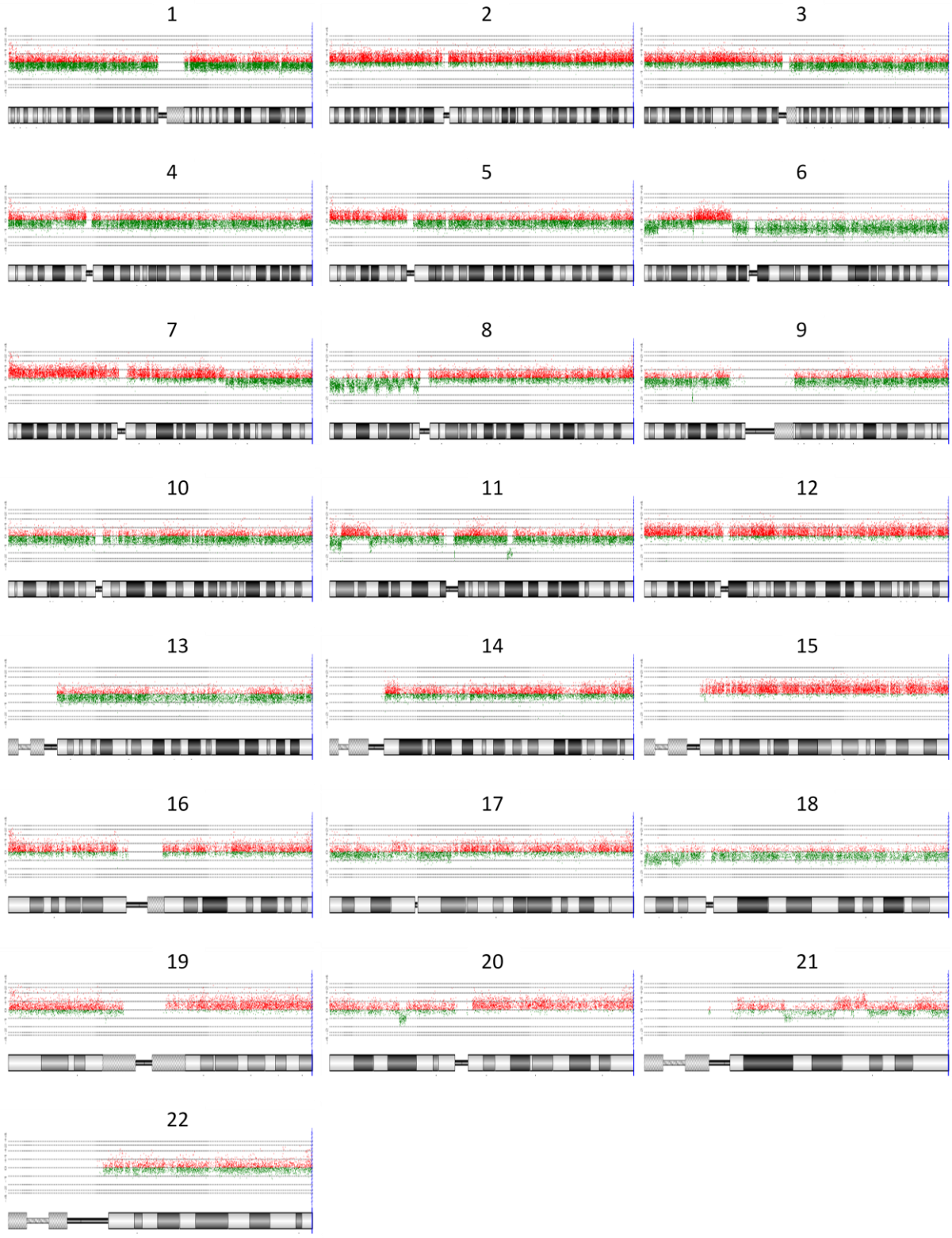

Sample: HGG26 CCLG Centre: Liverpool

Diagnosis: AO

Genomic Overview of Aberrations (DLR Spread: 0.43)

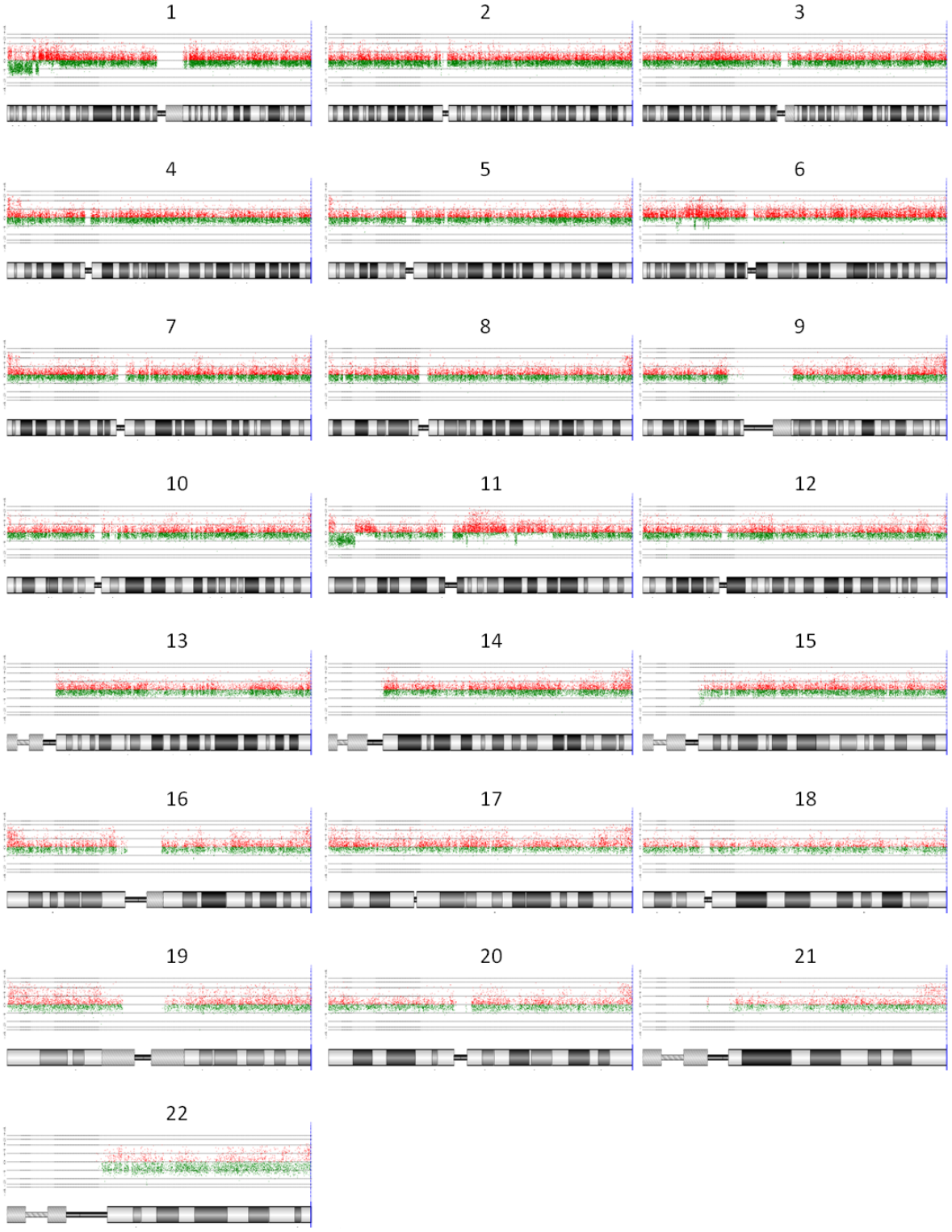

Sample: HGG27 CCLG Centre: Cardiff

Diagnosis: AO

Genomic Overview of Aberrations (DLR Spread: 0.62)

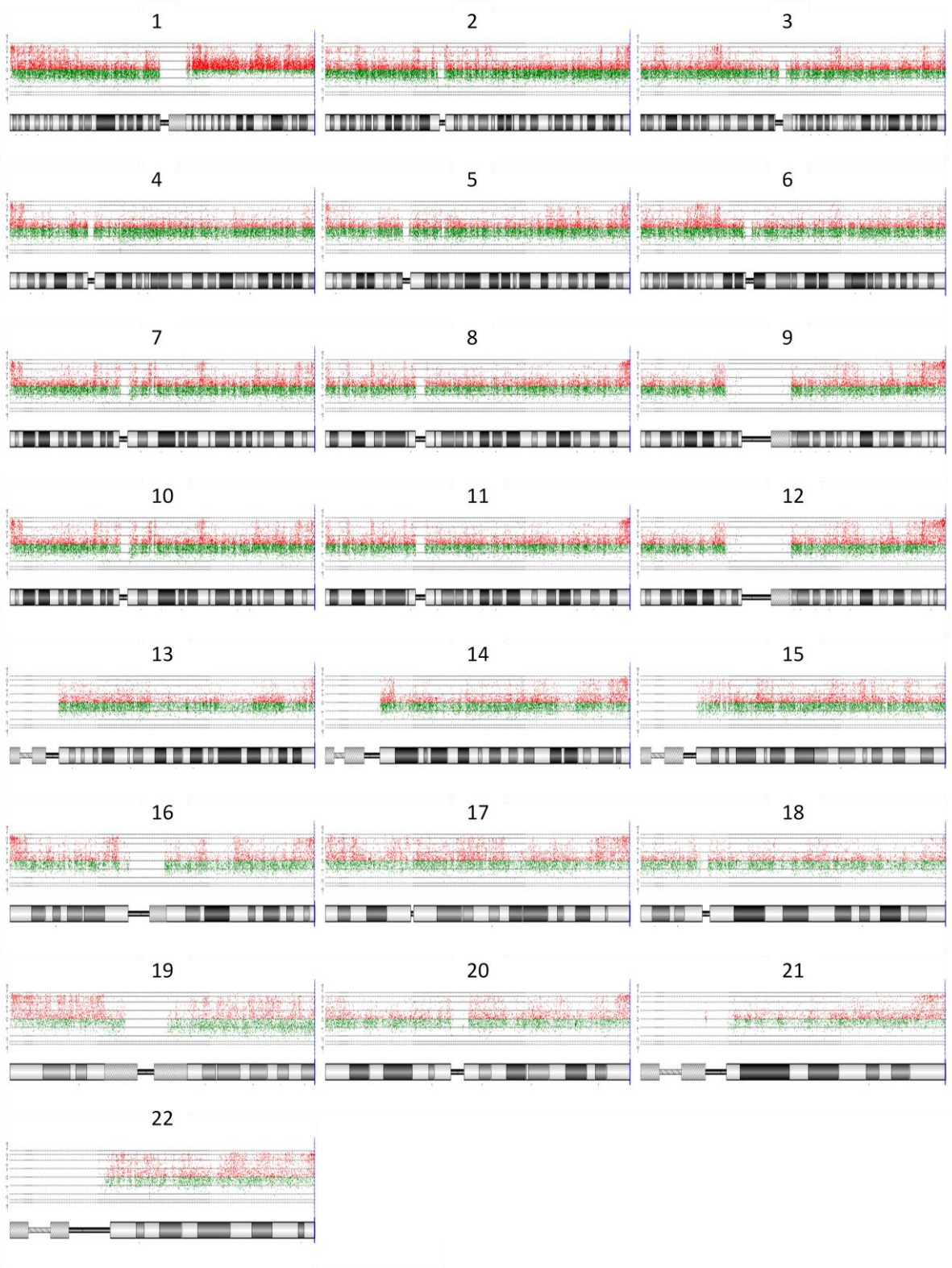

Sample: HGG28 CCLG Centre: Birmingham

Diagnosis: DIPG (GBM)

Genomic Overview of Aberrations (DLR Spread: 0.34)

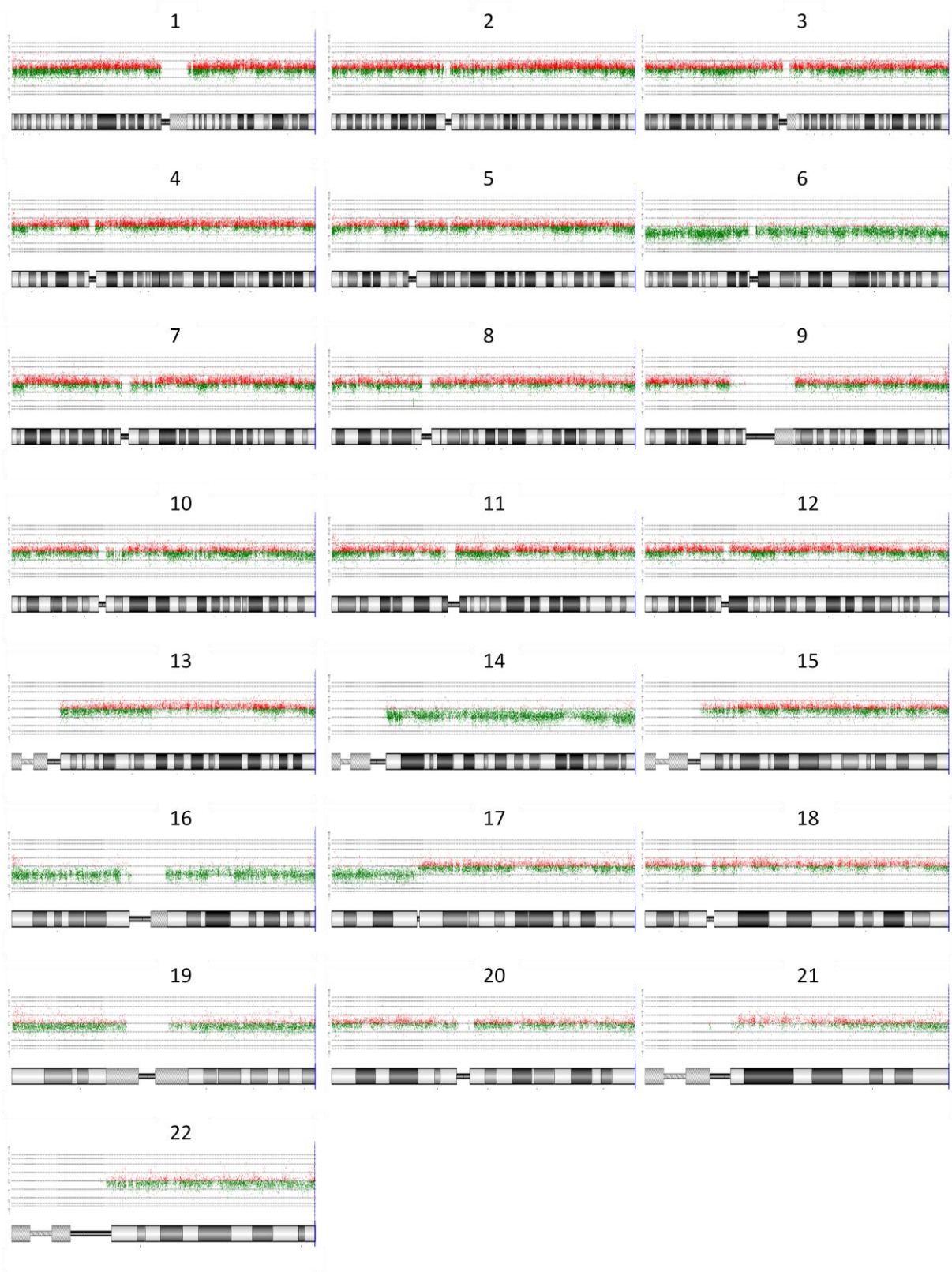

Sample: HGG29 CCLG Centre: Birmingham

Diagnosis: GBM

Genomic Overview of Aberrations (DLR Spread: 0.71)

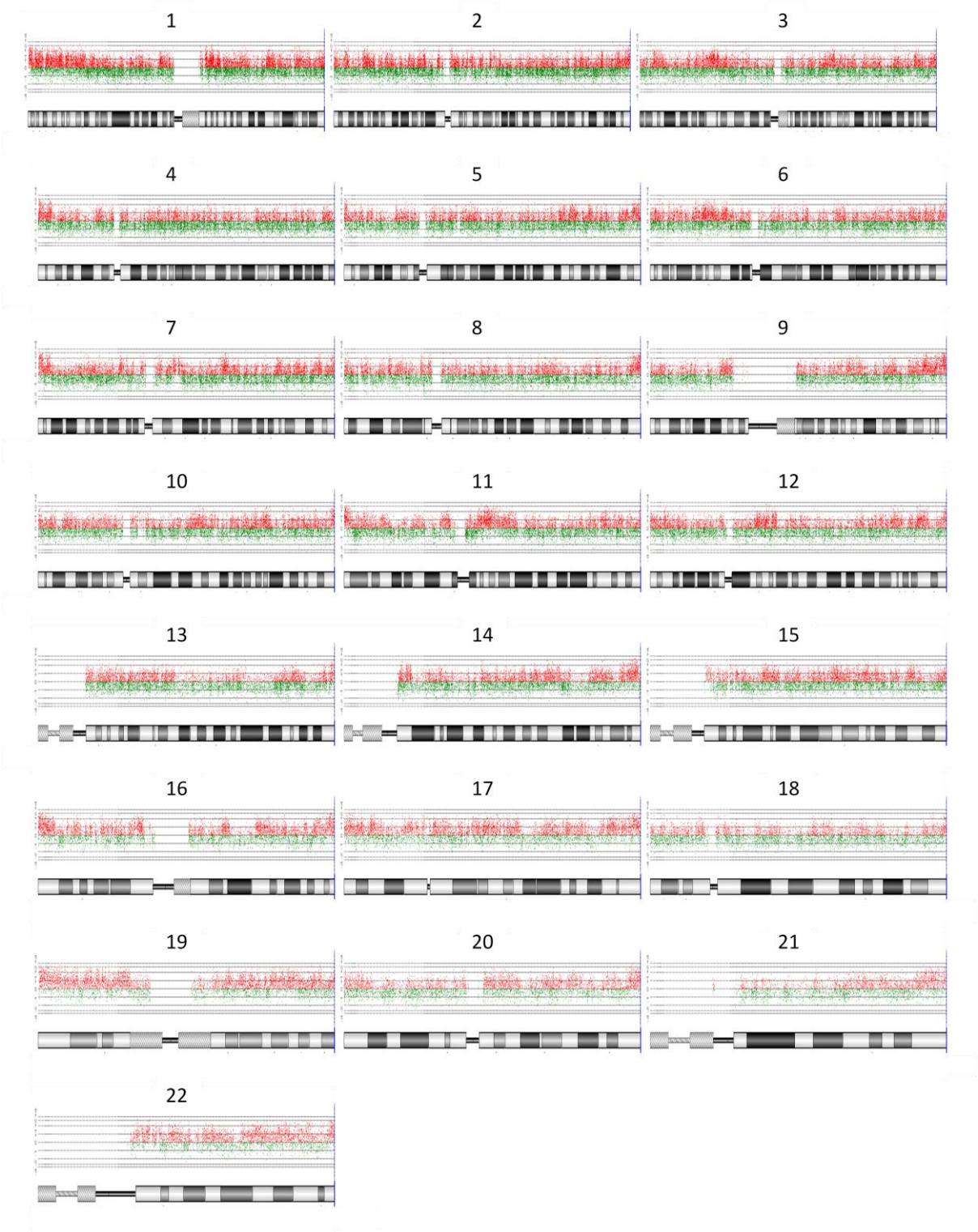

Sample: HGG30 CCLG Centre: Birmingham

Diagnosis: GBM

Genomic Overview of Aberrations (DLR Spread: 0.46)

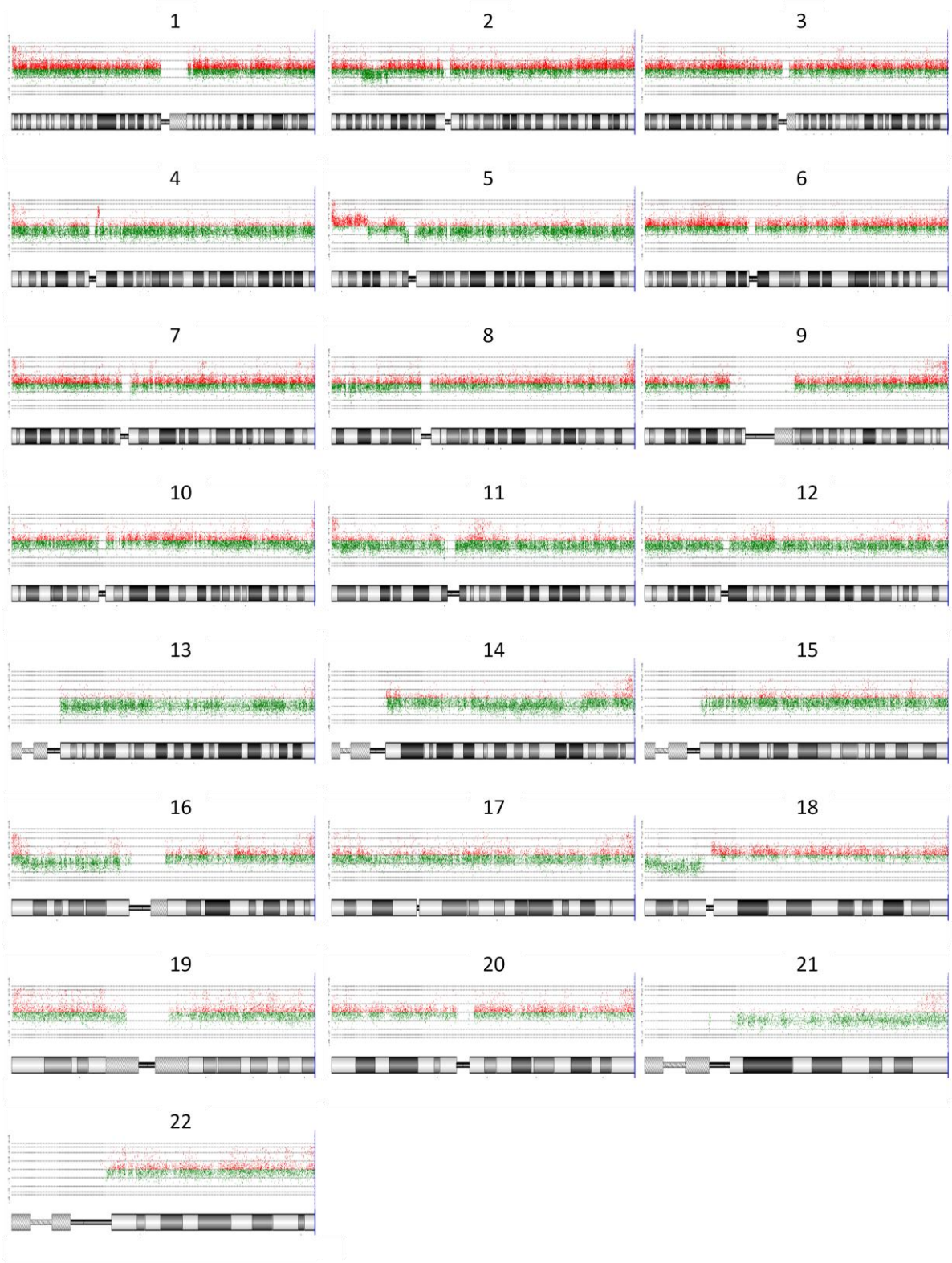

Sample HGG30: FROZEN

Genomic Overview of Aberrations (DLR Spread: 0.17)

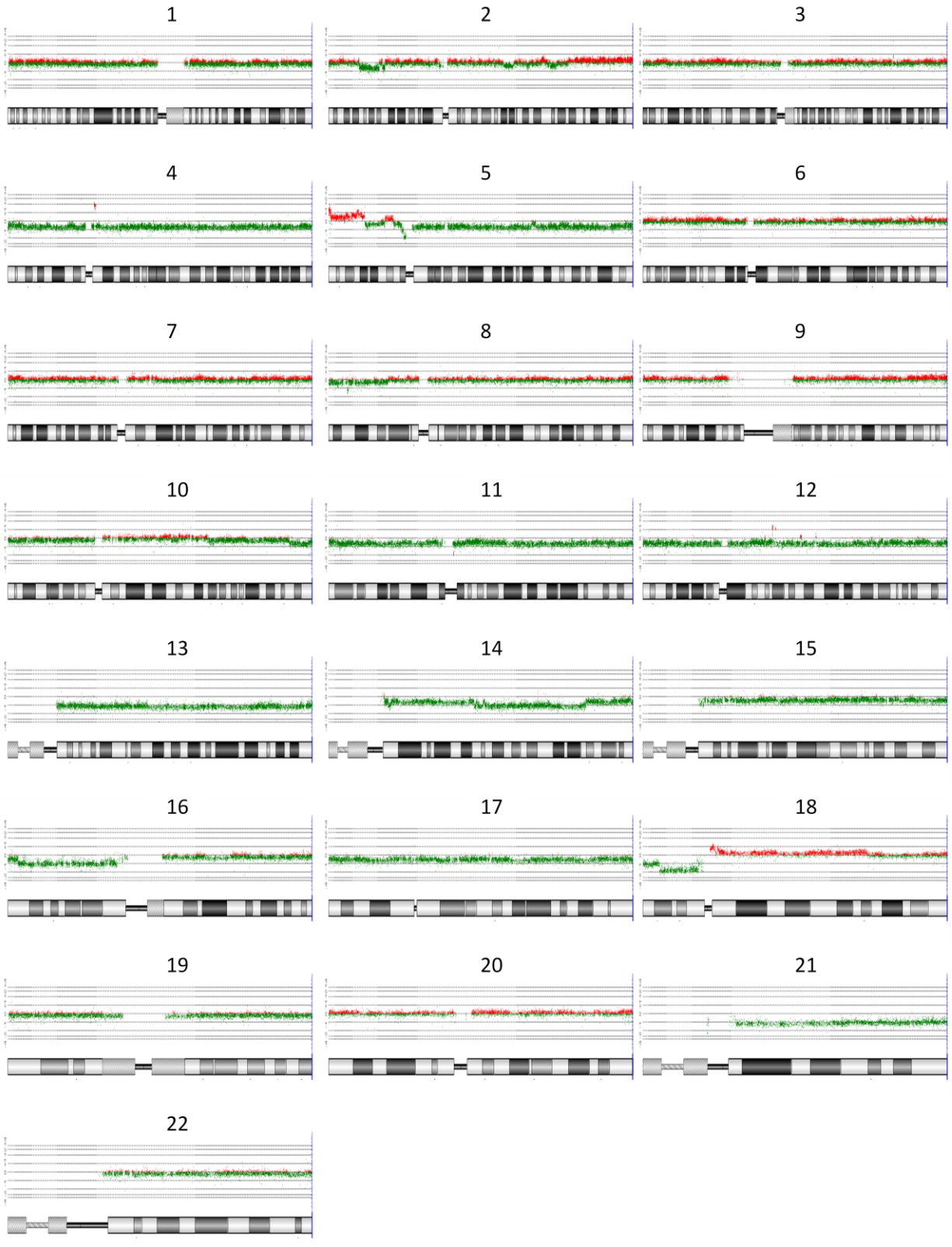

Sample: HGG31 CCLG Centre: Birmingham

Diagnosis: GBM

Genomic Overview of Aberrations (DLR Spread: 0.47)

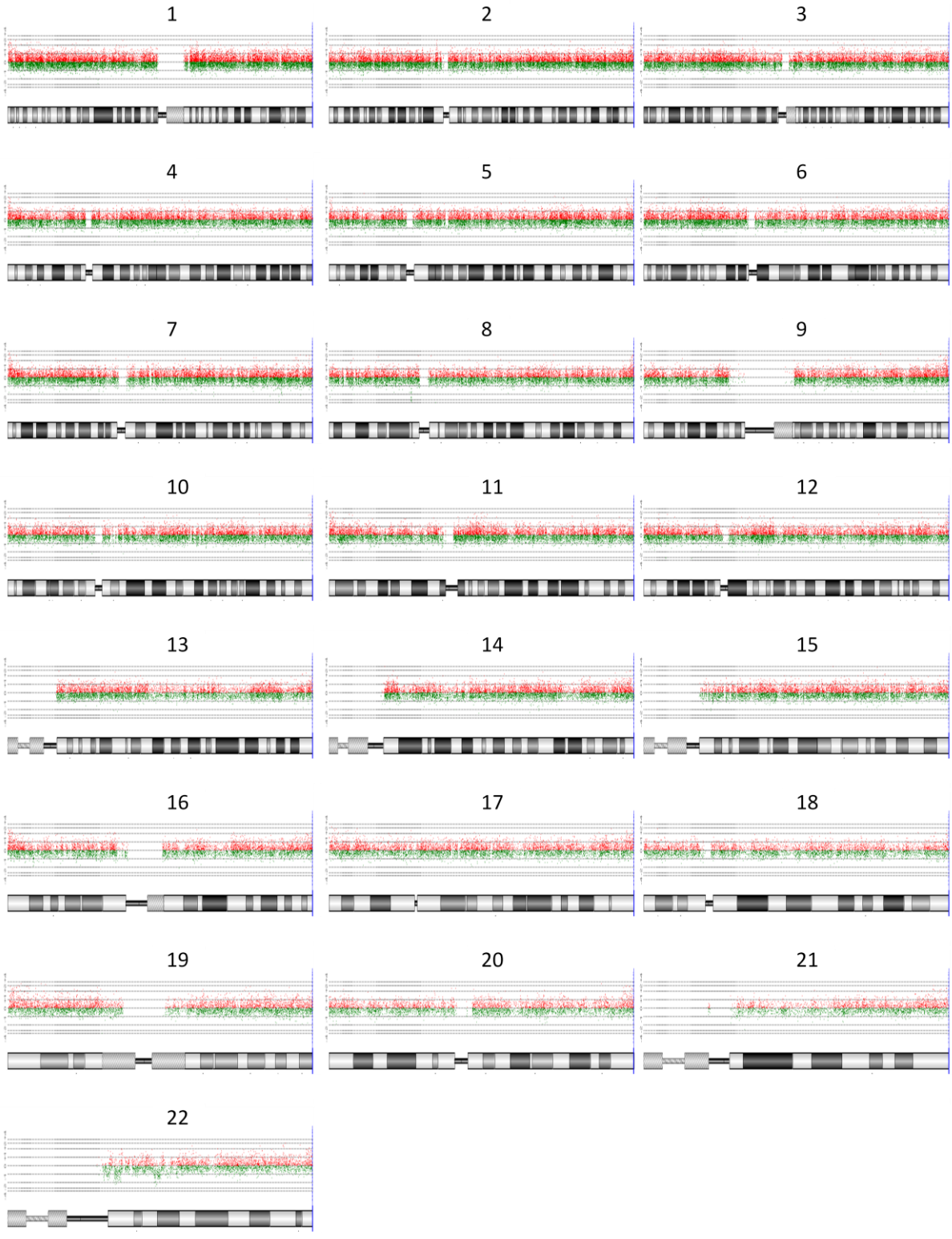

Sample: HGG32 CCLG Centre: Birmingham

Diagnosis: GBM

Genomic Overview of Aberrations (DLR Spread: 0.38)

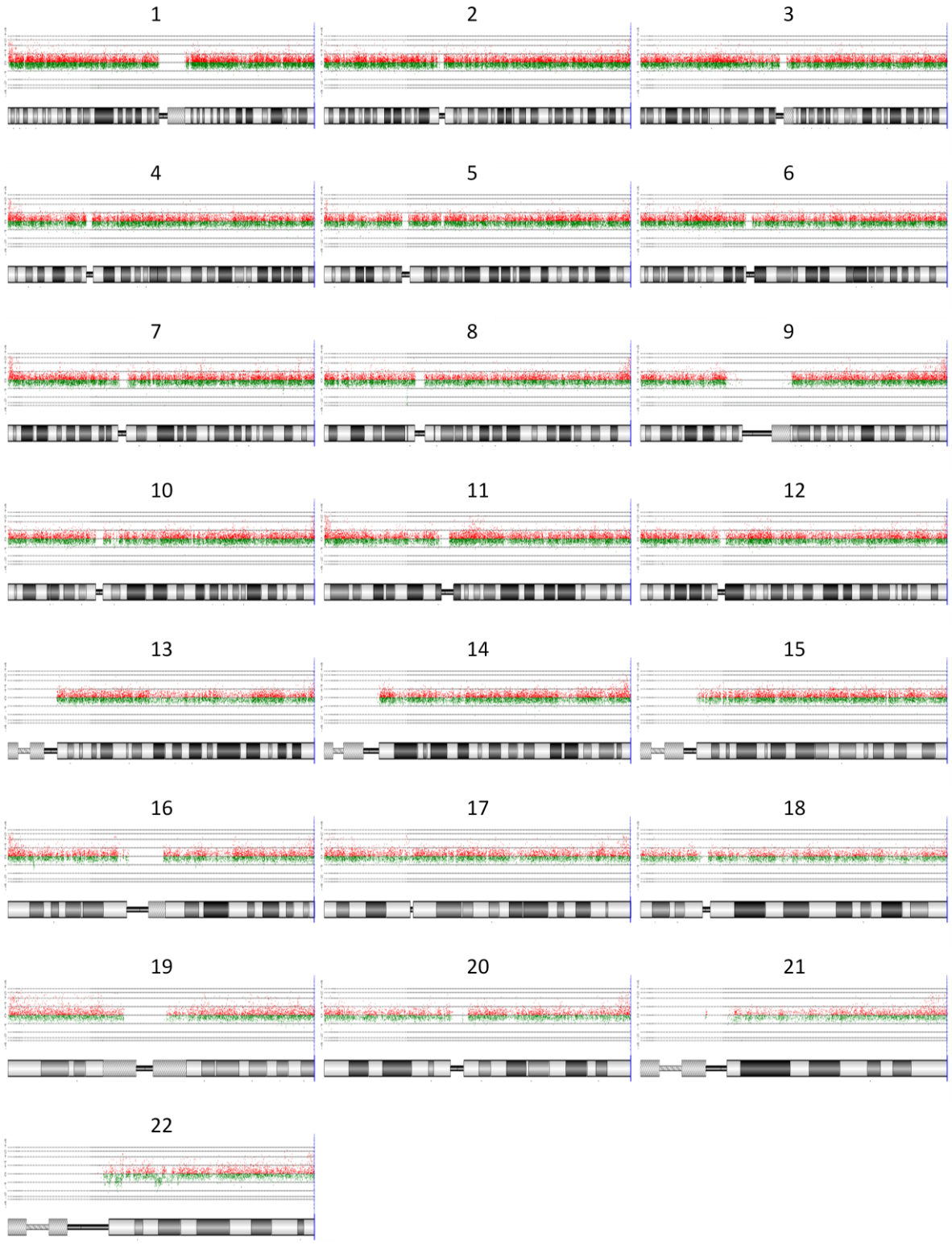

Sample: HGG33 CCLG Centre: Birmingham

Diagnosis: GBM

Genomic Overview of Aberrations (DLR Spread: 0.63)

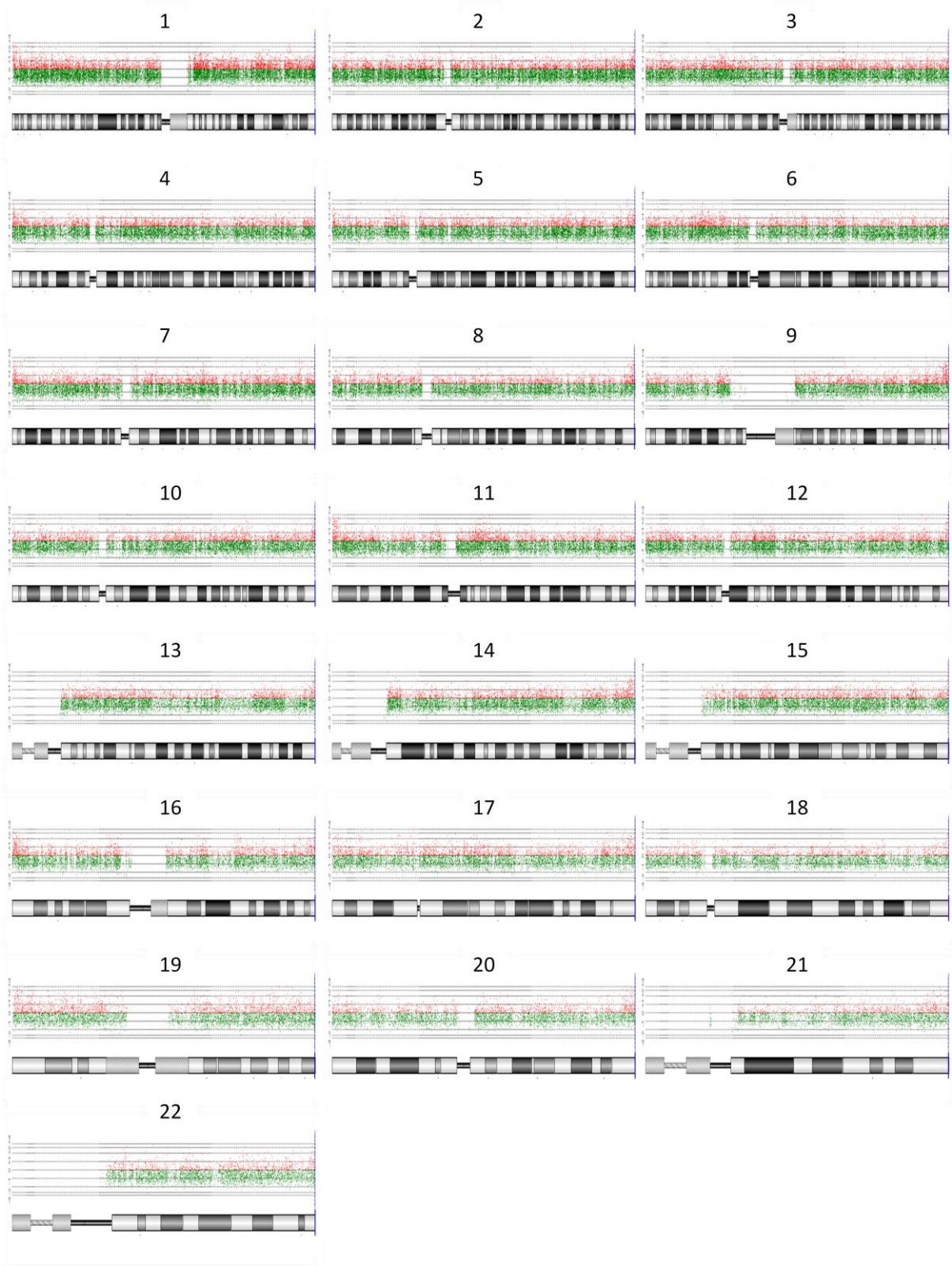

Sample HGG33: FROZEN

Genomic Overview of Aberrations (DLR Spread: 0.38)

Sample: HGG34 CCLG Centre: Birmingham

Diagnosis: GBM

Genomic Overview of Aberrations (DLR Spread: 0.40)

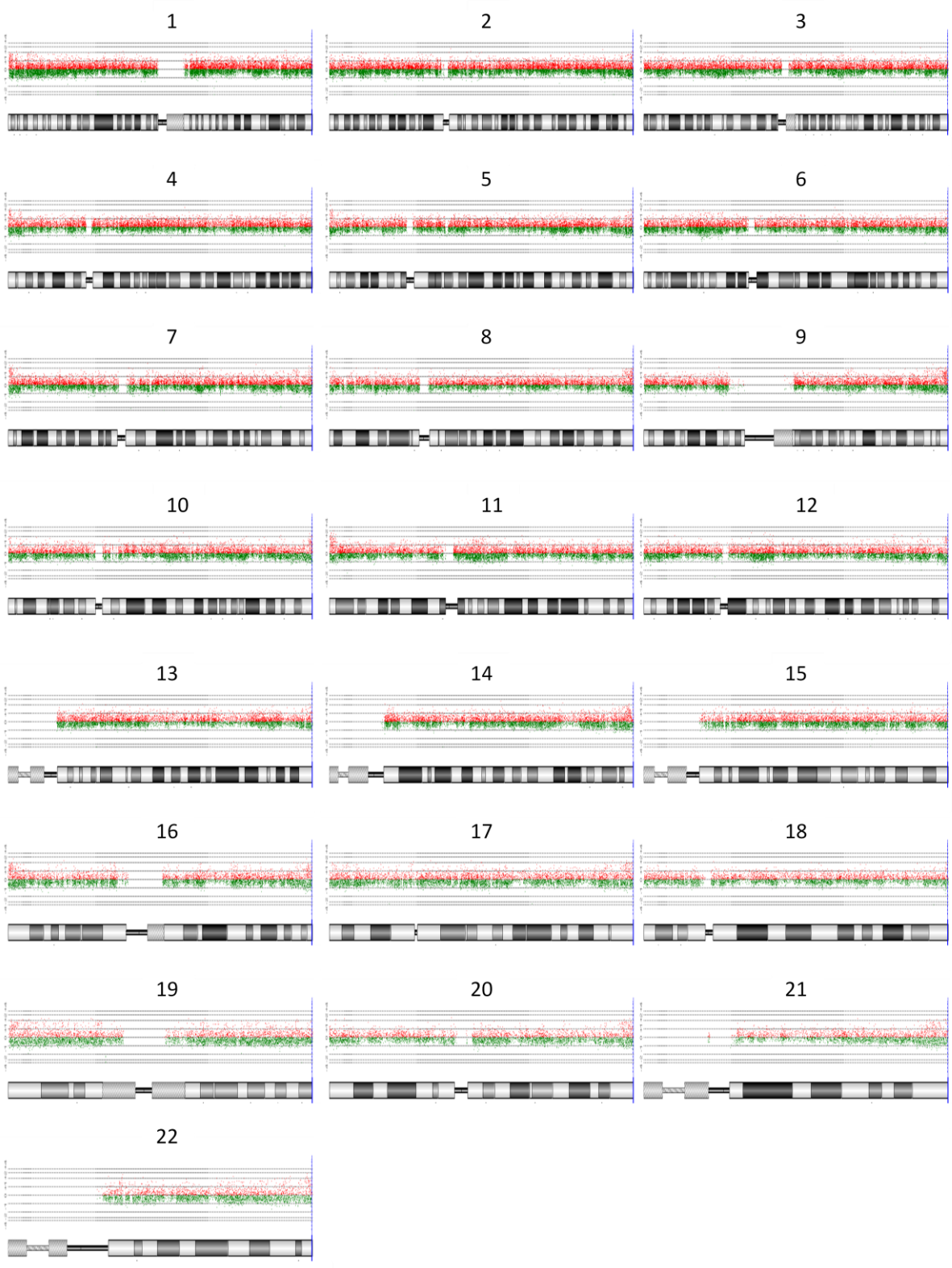

Sample: HGG35 CCLG Centre: Birmingham

Diagnosis: DIPG (GBM)

Genomic Overview of Aberrations (DLR Spread: 0.61)

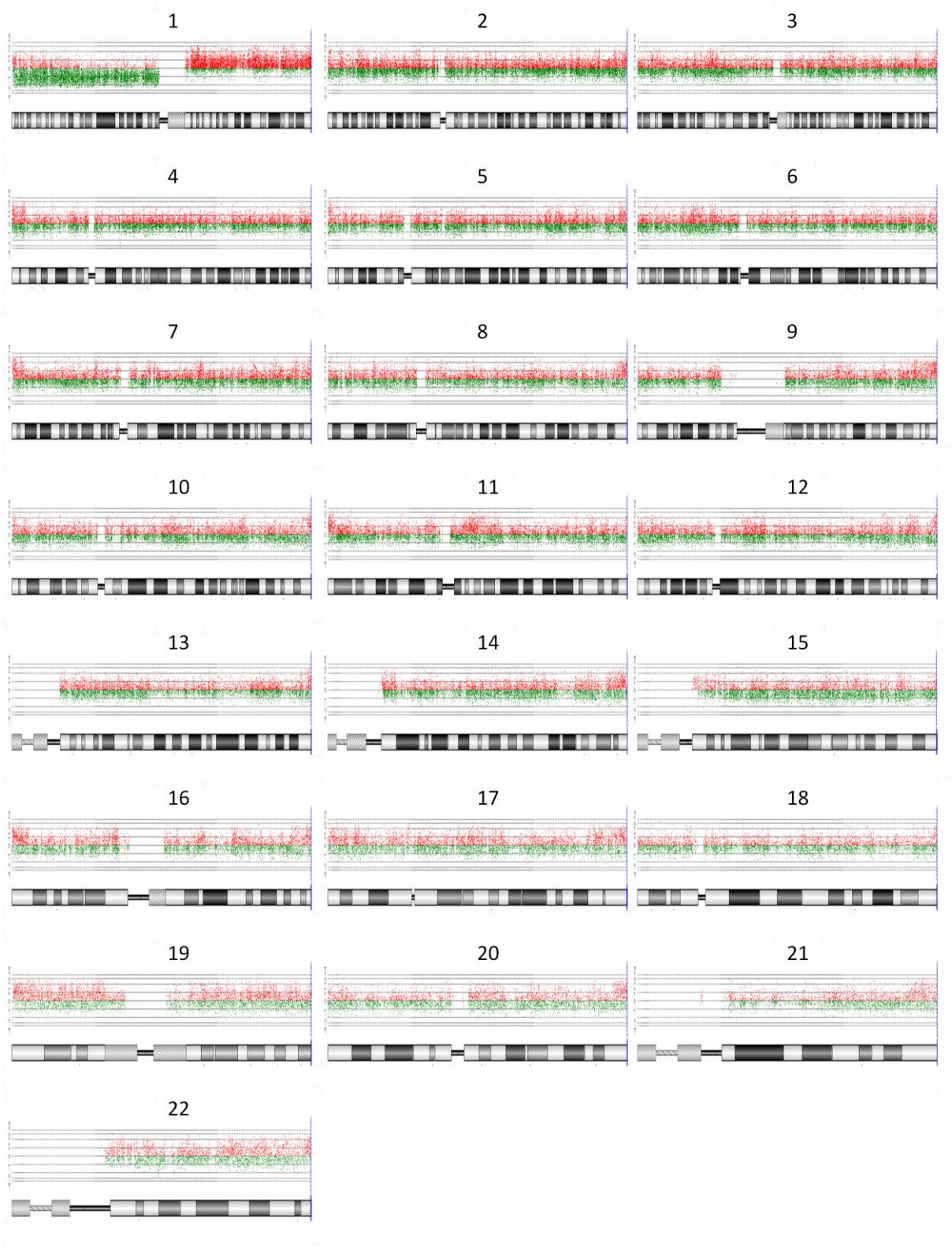

Sample: HGG36 CCLG Centre: Birmingham

Diagnosis: DIPG (GBM)

Genomic Overview of Aberrations (DLR Spread: 1.02)

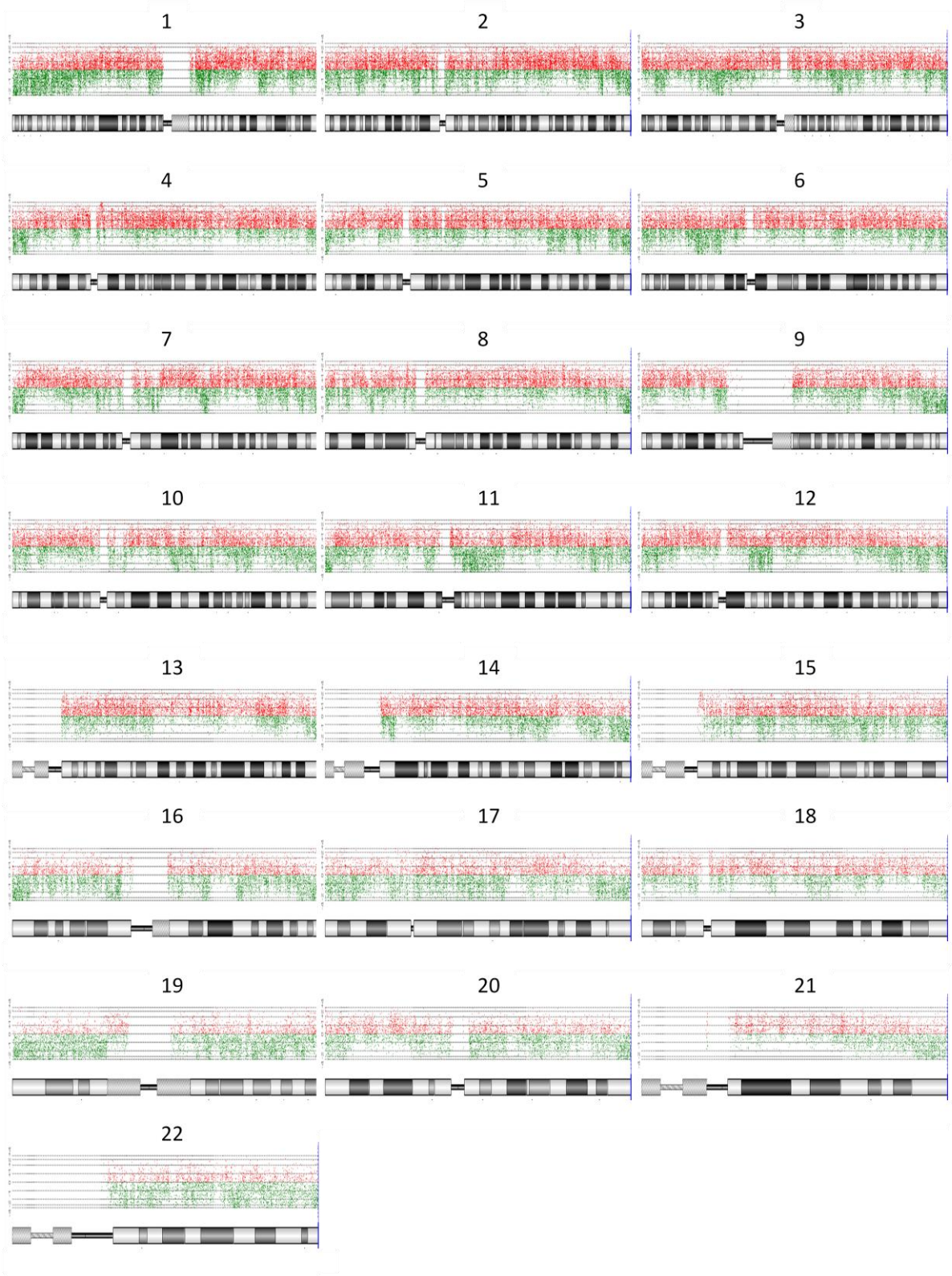

Sample: HGG37 CCLG Centre: Edinburgh

Diagnosis: DIPG (GBM)

Genomic Overview of Aberrations (DLR Spread: 0.54)

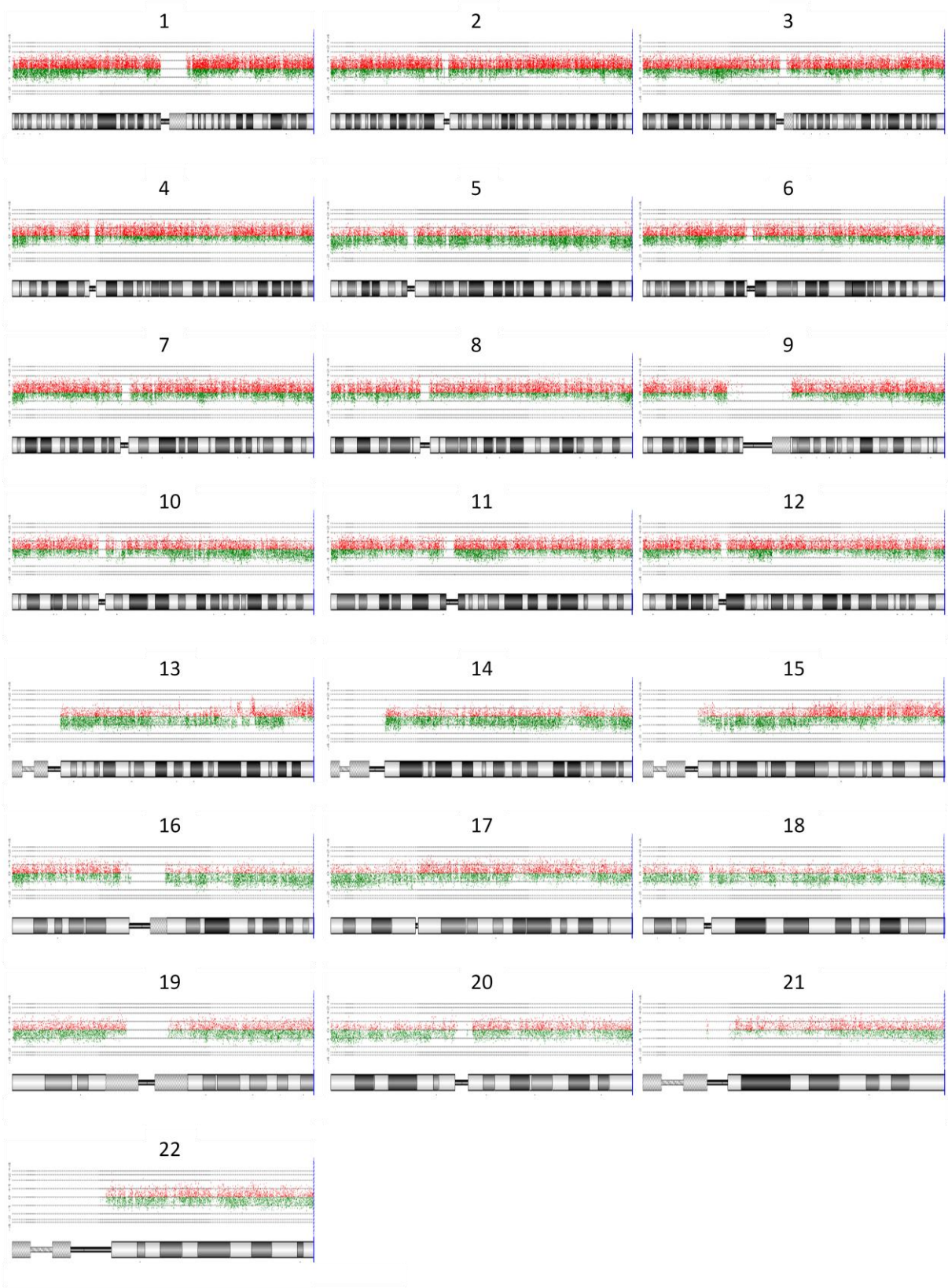

Sample: HGG38 CCLG Centre: Edinburgh

Diagnosis: DIPG (GBM)

Genomic Overview of Aberrations (DLR Spread: 0.80)